

FINAL TECHNICAL REPORT

May 7, 2010 to August 28, 2015

Rapid Deployment of Engineered Solutions for Environmental Problems

Date submitted:

August 28, 2015

Principal Investigator:

Leonel E. Lagos, Ph.D., PMP®

Florida International University Collaborators:

Yelena Katsenovich, Ph.D.

Ravi Gudavalli, Ph.D.

Vasileios Anagnostopoulos, Ph.D.

Hilary Emerson, Ph.D.

FIU Graduate Research Assistant

DOE Fellows

Prepared for:

U.S. Department of Energy

Office of Environmental Management

Under Cooperative Agreement # DE-EM0000598



Applied Research Center

FLORIDA INTERNATIONAL UNIVERSITY

FIU STUDENTS DIRECTLY SUPPORTING DOE EM PROJECTS

DOE Fellows from the DOE-FIU Science & Technology Workforce Development Program as well as FIU Graduate Research Assistants provide direct support to DOE EM projects around the complex. The following DOE Fellows and FIU Graduate Research Assistants supported the soil and groundwater research tasks and contributed to the Year End Report for the Hanford and Savannah River Sites under FIU Project 2:

DOE Fellow: Paola Sepulveda-Medina

Mentor: Yelena Katsenovich

Project Task: Effect of U(VI) and Bicarbonate on Cell Viability (Hanford)

DOE Fellows: Claudia Cardona, Robert Lapierre

Mentor: Yelena Katsenovich

Project Task: Sequestering Uranium at the Hanford 200 Area Vadose Zone by In Situ Subsurface pH Manipulation Using NH₃ Gas (Hanford)

DOE Fellow: Christian Pino

Mentors: Ravi Gudavalli, Hilary Emersion

Project Task: Evaluation of Ammonia Fate and Biological Contributions During and After Ammonia Injection for Uranium Treatment

DOE Fellow: Hansell Gonzalez

Mentors: Yelena Katsenovich, Vasileios Anagnostopoulos

Project Task: Sorption Properties of Humate Injected into the Subsurface System (SRS)

DOE Fellow: Christian Pino

Mentor: Ravi Gudavalli

Project Task: Synergistic Effects of Silica and Humic Acid on U(VI) Removal (SRS)

DOE Fellow: Christine Wipfli

Mentor: Vasileios Anagnostopoulos

Project Task: FIU's Support for Groundwater Remediation at SRS F/H –Area

DOE Fellow: Aref Shehadeh

Mentor: Yelena Katsenovich

Project Task: Monitoring of U(VI) Bioreduction after ARCADIS Demonstration at F-Area (SRS)

FIU Graduate Research Assistant: Sandra Herrera

Mentors: Yelena Katsenovich, Vasileios Anagnostopoulos

Project Task: Investigation on Microbial Meta-Autunite Interactions - Effect of Bicarbonate (Hanford)

A complete list of DOE Fellows supporting the DOE EM research efforts can be found in the Year End Report for Project 5, section 8, “DOE Fellows Directly Supporting DOE EM Projects” on pages 57-58.

Addendum:

This document represents one (1) of five (5) reports that comprise the Year End Reports for the period of May 17, 2014 to August 28, 2015 prepared by the Applied Research Center at Florida International University for the U.S. Department of Energy Office of Environmental Management (DOE-EM) under Cooperative Agreement No. DE-EM0000598.

The complete set of FIU's Year End Reports for this reporting period includes the following documents and is available at the DOE Research website for the Cooperative Agreement between the U.S. Department of Energy Office of Environmental Management and the Applied Research Center at Florida International University (<http://doeresearch.fiu.edu>):

Project 1: Chemical Process Alternatives for Radioactive Waste
Document number: FIU-ARC-2015-800000393-04b-237

Project 2: Rapid Deployment of Engineered Solutions for Environmental Problems
Document number: FIU-ARC-2015-800000438-04b-228

Project 3: Remediation and Treatment Technology Development and Support
Document number: FIU-ARC-2015-800000439-04b-232

Project 4: Waste and D&D Engineering and Technology Development
Document number: FIU-ARC-2015-800000440-04b-229

Project 5: DOE-FIU Science & Technology Workforce Development Initiative
Document number: FIU-ARC-2015-800000394-04b-090

Each document will be submitted to OSTI separately under the respective project title and document number as shown above.

DISCLAIMER

This report was prepared as an account of work sponsored by an agency of the United States government. Neither the United States government nor any agency thereof, nor any of their employees, nor any of its contractors, subcontractors, nor their employees makes any warranty, express or implied, or assumes any legal liability or responsibility for the accuracy, completeness, or usefulness of any information, apparatus, product, or process disclosed, or represents that its use would not infringe upon privately owned rights. Reference herein to any specific commercial product, process, or service by trade name, trademark, manufacturer, or otherwise does not necessarily constitute or imply its endorsement, recommendation, or favoring by the United States government or any other agency thereof. The views and opinions of authors expressed herein do not necessarily state or reflect those of the United States government or any agency thereof.

TABLE OF CONTENTS

Project 2 Overview	1
Technical Progress From FIU Year 1 To FIU Year 4	4
Task 1 Summary - Investigation On Microbial-Meta-Autunite Interactions: Effect Of Bicarbonate.....	4
Task 2 Summary - Effect Of Bicarbonate On The Dissolution Of Meta-Autunite.....	5
Task 3 Summary - Uranium (VI) Stabilization In The Hanford Site Vadose Zone (200 Area) Sediment Utilizing In Situ Calcite Mineral	6
Rapid Deployment of Engineered Solutions to Environmental Problems (FIU Year 5).....	8
Executive Summary	8
Introduction	10
Task 1: Sequestering Uranium at the Hanford 200 Area by In Situ Subsurface pH Manipulation using Ammonia (NH ₃) Gas	12
Subtask 1.1: Sequestering Uranium at the Hanford 200 Area Vadose Zone by In Situ Subsurface pH Manipulation Using NH ₃ Gas	12
Subtask 1.1: Introduction.....	12
Subtask 1.1: Material and Methods	14
Subtask 1.1: Results and Discussion	17
Subtask 1.1: Future Work.....	27
Subtask 1.1: Acknowledgements.....	28
Subtask 1.1: References.....	28
Subtask 1.1.1: Characterization of New Uranium-Bearing Samples	30
Subtask 1.1.1: Introduction.....	30
Subtask 1.1.1: Materials and Methods.....	31
Subtask 1.1.1: Results and Discussion	34
Subtask 1.1.1: Future Work.....	37
Subtask 1.1.1: Acknowledgements.....	38
Subtask 1.1.1: References.....	38
Subtask 1.2: Investigation on Microbial Meta-Autunite Interactions - Effect of Bicarbonate .	39
Task 1.2: Introduction.....	39

Task 1.2: Materials and Methods	40
Task 1.2: Results and Discussion	42
Task 1.2: Future Work.....	54
Task 1.2: Acknowledgment.....	54
Task 1.2: References.....	54
Task 2.0: Remediation Research and Technical support for Savannah River Site.....	57
Subtask 2.1: Sodium Silicate Treatment For U(VI) Bearing Groundwater At F/H Area At Savannah River Site	57
Subtask 2.1: Introduction.....	57
Subtask 2.1: Materials and Methods.....	58
Subtask 2.1: Results and Discussion	61
Subtask 2.1: Future Work.....	72
Subtask 2.1: Acknowledgements.....	72
Subtask 2.1: References.....	73
Subtask 2.1.1: Carryover FIU's support for groundwater remediation at SRS F/H Area-Synergetic interactions between humic acid and colloidal silica for the removal of uranium	74
Subtask 2.1.1: Introduction.....	74
Subtask 2.1.1: Materials and Methods.....	75
Subtask 2.1.1: Results and Discussion	77
Subtask 2.1.1: Future Work.....	86
Subtask 2.1.1: Acknowledgements.....	86
Subtask 2.1.1: References.....	86
Subtask 2.2: Monitoring of U (VI) Bioreduction after ARCADIS Demonstration at F-Area ..	88
Subtask 2.2: Introduction.....	88
Subtask 2.2: Methodology	88
Subtask 2.2: Results and Discussion	94
Subtask 2.2: Future Work.....	105
Subtask 2.2: Acknowledgements.....	106
Subtask 2.3: The Sorption Properties of the Humate Injected Into the Subsurface System ...	106
SUBTASK 2.3: Introduction	106

Subtask 2.3: Methodology	108
Subtask 2.3: Results and Discussion	112
Subtask 2.3: Future Work	122
Subtask 2.3: Acknowledgements	122
Subtask 2.3: References	122
Task 3.0: Evaluation of ammonia fate and biological contributions during and after ammonia injection for uranium treatment	128
Task 3.1: Investigation on NH ₃ Partitioning In Bicarbonate-Bearing Media	128
Task 3.1: Introduction	128
Task 3.1: Current Experimental Protocol	128
Task 3.1: Discussion	129
Task 3.1: Future Work	141
Task 3.1: References	144
APPENDICES	145

LIST OF FIGURES

Figure 1. Isopiestic chamber to conduct solubility experiments; aluminum block with holes to hold nickel crucibles.	14
Figure 2. Analytical balance weighing covered crucible.....	14
Figure 3. Isopiestic chamber to conduct solubility experiments connected to the acquisition system.	15
Figure 4. Changes of water activities vs. molality for LiCl and CaCl ₂ standards.	18
Figure 5. Osmotic coefficient for multicomponent samples as a function of water activities, a_w , using LiCl as a standard.....	20
Figure 6. Osmotic coefficient for multicomponent samples as a function of water activities, a_w , using CaCl ₂ as a standard.....	20
Figure 7. Water activities against molalities for the multicomponent samples using CaCl ₂ standard.	21
Figure 8. Osmotic coefficient vs. molalities for the multicomponent samples using CaCl ₂ standard.....	22
Figure 9. Aluminum block to fit crucible cups.	23
Figure 10. The underside of the chamber plate.....	23
Figure 11. The full assembly of the isopiestic chamber with crucibles inside.	24
Figure 12. Drawing of the isopiestic chamber final assembly.....	24
Figure 13. Fabricated new isopiestic chambers to continue the solubility experiments.....	25
Figure 14. A new isopiestic chamber set up in the FIU-ARC radiation laboratory.....	25
Figure 15. SEM image showing the crystalline uranium phases of interest.....	30
Figure 16. Comparisons of the XRD patterns for uranium bearing precipitates with nitratine (left) and cejkaite (right)	31
Figure 17. TEM suspensions undergoing sonication to disperse solids	33
Figure 18. Example component input for geochemical modeling software	34
Figure 19. TEM images of sample fragments attached to carbon mesh of TEM micro-grid	35
Figure 20. Selective area electron diffraction pattern for detected crystalline phase	35
Figure 21. Changes in pH associate with increasing dissolved NH_4^+	36
Figure 22. Speciation changes for uranyl-carbonate species with increasing pH (by NH_4 increase)	37
Figure 23. Petri dish with grown culture of <i>Shewanella oneidensis</i> MR1.....	40
Figure 24. Fresh culture of <i>Shewanella oneidensis</i> MR1 grown in liquid LB media.....	41
Figure 25. Experimental bottles placed in incubator-shaker at 20°C for autunite dissolution studies.	42

Figure 26. Concentration of U (VI) released from autunite to the aqueous phase before inoculation with <i>Shewanella oneidensis</i> .	44
Figure 27. Uranium (VI) released into the aqueous phase as a function of time in bicarbonate-free solution.	45
Figure 28. Uranium (VI) released into the aqueous phase as a function of time in 3 mM bicarbonate media solution.	45
Figure 29. Uranium (VI) released in the aqueous phase as function of time under two different bicarbonate concentrations: 5 and 10 mM.	46
Figure 30. Concentration of calcium detected in the aqueous phase as a function of time in different bicarbonate concentrations: 0, 3, 5 and 10 mM.	47
Figure 31. Concentration of phosphorous released in the aqueous phase as a function of time in different bicarbonate concentrations: 0, 3, 5 and 10 mM.	47
Figure 32. Bacterial growth in the sample amended with 10 mM and inoculated with bacteria.	48
Figure 33. Bacterial contamination in the control samples with no-bicarbonate and amended with 10 mM bicarbonate.	48
Figure 34. Clear plates with no evidence of contamination; samples were taken from control bottles amended with 3 mM and 5 mM of bicarbonate.	49
Figure 35. 20-mL glass scintillation vial prepared with media amended with KHCO_3 and autunite mineral.	49
Figure 36. Sampling schedule before and after inoculation.	50
Figure 37. Sacrificial vials inside the anaerobic glove box, prepared to conduct the autunite biodissolution experiment.	50
Figure 38. Water bath with dilutions for calibration curve.	51
Figure 39. Calibration curve for protein analysis.	52
Figure 40. Correlation between cell density of <i>Shewanella oneidensis</i> MR1 and protein content.	52
Figure 41. Correlation between cell density of <i>Shewanella oneidensis</i> MR1 and protein content based on amended protocol.	53
Figure 42. Image of live cells on the left and dead cells on the right.	54
Figure 43. Schematic representation of sequential filtration experimental procedure	60
Figure 44. Monitoring of pH as a function of time for batch samples of SRS soil and synthetic groundwater.	61
Figure 45. Percent removal of U(VI) from aqueous phase as a function of sodium silicate concentration added in the sample. Data were recorded after 3 days of equilibration	63
Figure 46. Speciation diagram for the conditions of Savannah River Site synthetic groundwater amended with 0.5 mg L ⁻¹ U(VI) and 60 mg L ⁻¹ . The solubility of atmospheric CO ₂ has been included. Note: “c” stands for crystalline	64

Figure 47. U(VI) distribution between different phases as a function of time for treatment with 70 ppm sodium silicate.	65
Figure 48. U(VI) distribution between different phases as a function of time for treatment with 80 ppm sodium silicate.	65
Figure 49. U(VI) distribution between different phases as a function of time for treatment with 90 ppm sodium silicate.	66
Figure 50. Percentage of Si removed from the aqueous phase as a function of time for treatment with different sodium silicate concentrations.	67
Figure 51. Schematic depiction of polymer equilibrium of silicate solutions.	67
Figure 52. Iron concentration in the aqueous phase as a function of sodium silicate addition for unfiltered and filtered through 0.45 μ m filters samples.	68
Figure 53. SEM images of the surface of 0.45 μ m filters.....	69
Figure 54. EDS spot analysis of the amorphous particle shown in Figure 53 on the left.....	69
Figure 55. SEM/EDS analysis of the “spongy” background.....	70
Figure 56. SEM/EDS area analysis, including the amorphous particles and the “spongy” layer (0.45 μ m filters).....	70
Figure 57. SEM image and EDS analysis of 0.2 μ m filter.....	71
Figure 58. Monitoring of pH evolution for batch samples comprised of SRS soil and synthetic groundwater containing 0.5 mg L ⁻¹ U(VI), spiked with different sodium silicate concentrations.....	72
Figure 59. Experimental setup.	76
Figure 60. Shaker and centrifuge experimental setup.....	77
Figure 61. Silica removal at 50 ppm.	81
Figure 62. Uranium (VI) removal at 50 ppm HA.	81
Figure 63. Uranium (VI) removal in unfiltered at 50 ppm HA.	84
Figure 64. Uranium (VI) removal at 50 ppm HA Unfiltered.....	84
Figure 65. Uranium (VI) removal at 10 ppm HA Unfiltered.....	85
Figure 66. Uranium (VI) removal at 50 ppm HA Unfiltered.....	86
Figure 67. No. 80, 180 μ m sieve.....	89
Figure 68. Basal medium with 500 ppm sulfate, basal medium, and molasses.....	89
Figure 69. Batch 1 samples (12 bottles with orange caps).	90
Figure 70. Microcosm Batch 2 samples.....	91
Figure 71. Anaerobic chamber used for microcosm experiments.	92
Figure 72. Amorphous sample holder with F-Area sediment to be placed into XRD instrument.....	93
Figure 73. Bruker 5000D XRD instrument.....	93
Figure 74. Perkin Elmer Optima 7300 ICP-OES.....	94

Figure 75. Fungal growth in Batch 1 sample.....	95
Figure 76. Batch 1, Set 1 pH evolution.....	96
Figure 77. Batch 1, Set 2 pH evolution.....	96
Figure 78. Batch 1, Set 3 pH evolution.....	97
Figure 79. Batch 1, Set 4 pH evolution.....	97
Figure 80. Batch 2 samples pH evolution.....	98
Figure 81. Background sample vs. quartz.....	100
Figure 82. Background sample vs. montmorillonite.....	100
Figure 83. Background sample vs. goethite.....	100
Figure 84. Background sample vs. kaolinite.....	100
Figure 85. Set 1 vs. siderite and pyrite.....	101
Figure 86. Set 2 vs. siderite and pyrite.....	101
Figure 87. Set 3 vs. siderite and pyrite.....	101
Figure 88. Set 4 vs. siderite and pyrite.....	101
Figure 89. Set 1 vs. siderite and pyrite.....	102
Figure 90. Set 2 vs. siderite and pyrite.....	102
Figure 91. Set 3 vs. siderite and pyrite.....	102
Figure 92. Set 4 vs. siderite and pyrite.....	102
Figure 93. Set 1 vs. siderite and pyrite.....	103
Figure 94. Set 2 vs. siderite and pyrite.....	103
Figure 95. Set 3 vs. siderite and pyrite.....	103
Figure 96. Set 4 vs. siderite and pyrite.....	103
Figure 97. Soil humic acid structure proposed by Schulten and Schnitzer.	107
Figure 98. Huma-K black powder/shiny flakes.	107
Figure 99. Samples coated with Gold/Palladium for SEM/EDS analysis	108
Figure 100. Setup for the Potentiometric Titration	109
Figure 101. Centrifuge tube with sediment and humate solution	110
Figure 102. Shaker table with samples.	111
Figure 103. Samples centrifugation.	111
Figure 104. UV-Vis spectrophotometer.....	111
Figure 105. SEM Image and EDS Elemental Analysis of Huma-K.....	112
Figure 106. SEM Image and Elemental Analysis of SRS sediment coarse fraction via EDS	113
Figure 107. SEM Image and Elemental Analysis of SRS sediment fine fraction via EDS	113

Figure 108. Differential potentiometric curve of Huma-K.....	114
Figure 109. Differential potentiometric curve of SRS sediments and Quartz sand standard	115
Figure 110. FTIR spectrum of Huma-K	116
Figure 111. FTIR spectrum of SRS sediment fine fraction	116
Figure 112. FTIR spectrum of Kaolinite.....	117
Figure 113. Spectra of Huma-K.....	118
Figure 114. Kinetic Experiment of Huma-K.	119
Figure 115. Sorption Experiment of Huma-K at pH 4.....	121
Figure 116. Sorption Experiment of Huma-K at different pH values.....	122
Figure 117. Comparison of triplicate measurements of conductivity changes in 3 mM, 30 mM, 60 mM and 100 mM HCO_3^- solutions with respect to the volume of NH_3 gas injected	130
Figure 118. Comparison of triplicate measurements of pH in 3 mM, 30 mM, 60 mM and 100 mM HCO_3^- solutions with respect to the volume of NH_3 gas injected	131
Figure 119. Comparison of the conductivity ($\mu\text{S}/\text{cm}$) with respect to injection volume of NH_3 (g) for variable bicarbonate suspensions with a linear fit including data from triplicate experiments for each bicarbonate concentration	132
Figure 120. Comparison of the change in conductivity ($\mu\text{S}/\text{cm}$) with respect to injection volume of NH_3 (g) for variable bicarbonate suspensions with a linear fit for each dataset (including triplicate experiments)	133
Figure 121. Comparison of measured (<i>open circles</i>) conductivity ($\mu\text{S}/\text{cm}$) with respect to injection volume of NH_3 (g) for variable bicarbonate suspensions with a model prediction from PHREEQC software (USGS, <i>lines</i>) with error bars based on triplicate experiments.....	134
Figure 122. Comparison of initial, experimental pH in triplicate experiments at 3 mM, 30 mM, 60 mM and 100 mM HCO_3^- concentration to equilibrium pH of open and closed HCO_3^- systems at constant ionic strength (0.2 M) via Visual Minteq.	136
Figure 123. Comparison of triplicate experiments injecting NH_3 gas into 3 mM, 30 mM, 60 mM, and 100 mM HCO_3^- solutions versus aqueous NH_3 in mol/L incorporated into the sample versus injection gas volume	137
Figure 124. Comparison of triplicate experiments injecting NH_3 gas into 3 mM, 30 mM, 60 mM and 100 mM HCO_3^- solutions versus aqueous NH_3 in mol/L incorporated into the sample versus pH.....	138
Figure 125. Ammonium (NH_3) and ammonia (NH_4^+) concentrations in pure/dilute H_2O at 25°C and gas partial pressure of 1 atm partial pressure of NH_3 (g) with respect to pH for a system open to the gas phase	139
Figure 126. Ammonium (NH_3) and ammonia (NH_4^+) concentrations in pure/dilute H_2O at 25°C with respect to pH for a closed system	139
Figure 127. Comparison of recovery of NH_3 in the aqueous phase with respect to total gas mass injected, Note: one outlier is not shown.....	141

Figure 128. Diagram of apparatus used for experiments described by Mackay, Note: previous equipment was utilized in experiments by Lee et al. (Mackay 1979, Lee, Mukherjee et al. 2013)	143
Figure 129. Proposed equipment for the experimental setup of the NH ₃ (g) stripping experiments (Pyrex 31760-BO)	144

LIST OF TABLES

Table 1. Sample Composition.....	16
Table 2. Reference and Multicomponent Samples - Weights, Solute Content, and Molalities at the Beginning of Experiment.....	17
Table 3. Values for water activities, a_w , and osmotic coefficients, ϕ , for CaCl_2 and multicomponent samples	19
Table 4. Values for water activities, a_w , and osmotic coefficients, ϕ , for LiCl and multicomponent samples	19
Table 5. Initial Weights and Molality Calculations for Standards NaCl and CaCl_2	26
Table 6. Stock Solution & Synthetic Pore Water Concentrations for Sample Preparation	32
Table 7. Concentrations of Primary Constituents	32
Table 8. Extraction Experiment Solid-to-Liquid Ratios	33
Table 9. Uranium Content of Suspension Extractions.....	33
Table 10. Average d-spacings as determined by diffraction pattern analysis.....	36
Table 11. U(VI) Concentrations in the aqueous phase under all conditions studied.....	43
Table 12. Uranium distribution in different phases in samples amended with 70, 80 and 90 mg L ⁻¹ sodium silicate for a 9 day period.	66
Table 13. Experimental Matrix with Amount of Components	76
Table 14. Analytical Results for pH 3	78
Table 15. Analytical Results for pH 4	78
Table 16. Analytical Results for pH 5	79
Table 17. Analytical Results for pH 6	79
Table 18. Analytical Results for pH 7	79
Table 19. Analytical Results for pH 8	80
Table 20. Major Uranium species with respect to pH	82
Table 21. Uranium (VI) removal at 50 ppm HA.	83
Table 22. Batch 1 Sample Composition	90
Table 23. pH Monitoring Data.....	91
Table 24. Batch 2 Samples Composition.....	92
Table 25. Batch 1 Samples pH Evolution.....	95
Table 26. Batch 2 Samples pH Evolution.....	98
Table 27. ICP-OES Data for Batch 1 and Batch 2.....	105
Table 28. Average Fe concentration for Batch 1 and 2 Combined.....	105

Table 29. Kinetic Order Reaction Models	119
Table 30. Theoretical buffering capacity (in mol/L per pH unit of change) for variable bicarbonate solutions based on initial experiment pH	135

PROJECT 2 OVERVIEW

Past practices of waste disposal operations allowed radioactive waste discharges to retention basins, trenches, or cribs where the waste percolated into the soil. These leakages influenced the vadose zone sediments by creating a potential source for groundwater contamination and risk to receptors, those who will use these groundwater resources down gradient, through water uptake from contaminated wells or discharge to surface water.

The Rapid Deployment of Engineered Solutions for Environmental Problems (Project 2) focuses on providing assistance to Hanford's and Savannah River Site (SRS) environmental cleanup in the areas of soil and groundwater. During FIU Year 5 (FY14), FIU ARC worked on three tasks, providing research support on uranium contamination and remediation at the Hanford Site and SRS:

Two subtasks were carryout for Task 1 on Hanford Site related research:

Subtask 1.1: Sequestering Uranium at the Hanford 200 Area Vadose Zone by In Situ Subsurface pH Manipulation Using NH₃ Gas

The technology under consideration to control U(VI) mobility at Hanford is a manipulation of soil pH via ammonia gas injection by creation of alkaline conditions in the uranium-contaminated soil. This technology allows the transformation of mobile uranium species to lower solubility precipitates that are stable in the natural environment (Szecsody et al., 2012). However, there is a need for a better understanding of the stability of the U-bearing precipitates created in the soil as a result of ammonia gas remedial actions. This information would help to accurately predict the mobility of U(VI) in the post-treated vadose zone soil.

The purpose of this subtask was to conduct isopiestic measurements to quantify mineral solubility for the unsaturated vadose zone conditions. This method is considered very accurate, helping to make more realistic predictions of solid phases' deliquescence behavior in vadose zone environments. Experimental data are scarce for uranium-bearing multicomponent mixtures. Experimental studies also continued for mineralogical and morphological characterization of NH₃-treated U(VI)-bearing solids precipitated from the solution mixture containing major pore water cations and ions that could be present in pore water from mineral phase dissolution. Analytical design of experiment methods were reviewed and applied prior to sample preparation in order to ensure the statistical significance of the data produced. To accomplish this, a set of samples was prepared by following the same sample preparation procedures as previously but the concentration of U(VI) was increased up to 500 ppm. The increase in uranium concentration can help to increase the atomic percentage of U(VI) in the sample composition and the probability of a successful identification of uranium phases by means of XRD. This research is still on-going and requires preparation of new samples to continue identification of solid phases. The drafted proposal for access to the Environmental Molecular Sciences Laboratory (EMSL) was review by PNNL contacts prior become familiar with the project and theory behind it.

Currently, two graduate students are involved in this research, including DOE Fellow Robert Lapierre, working towards a master's thesis and DOE Fellow Claudia Cardona, a Ph.D. candidate, working towards her Ph.D. dissertation.

Subtask 1.2: Investigation on Microbial-Meta-Autunite Interactions - Effect of Bicarbonate and Calcium Ions

Experiments were conducted to investigate the effect of facultative microorganisms (e.g., *Shewanella Oneidensis* MR-1) on the dissolution of autunite mineral in the presence of the bicarbonate ions. Experiments were conducted using inoculated and control samples in oxygen-restricted conditions and sampled at certain time intervals over the period of 4-5 months. Another set of sacrificial samples was prepared and sampling is currently on-going to investigate for uranium biorelease from autunite mineral and account for cells viability, protein analysis and changes in mineral and bacterial cells surface morphology and composition over the course of experiments. This research is a thesis topic of the graduate student Sandra Herrera.

Task 2. Remediation Research and Technical Support for Savannah River Site

Three subtasks were carryout for the Task 2 on SRS groundwater remediation studies:

Subtask 2.1: FIU's support for groundwater remediation at SRS F/H Area

The F/H Area Seepage Basins located in the center of SRS received approximately 1.8 billion gallons of acidic waste solutions (pH from 3.2 to 5.5) contaminated with a variety of radionuclides and dissolved metals. The acidic nature of the basin waste solutions caused the mobilization of metals and radionuclides, resulting in contaminated groundwater plumes. The primary focus of this investigation is uranium (VI), which is a key contaminant of concern in the basin's groundwater.

The purpose of this subtask is to investigate whether a base solution of dissolved silica can be used to replace the carbonate base and evaluate the potential use of sodium silicate for uranium removal from the aqueous phase. The experiments can suggest if the silica solution has sufficient alkalinity to restore the pH of the treatment zone as well as removing U(VI) from the aqueous phase through precipitation or co-precipitation with Si. This study involves the speciation modeling by means of geochemical software and SEM/EDS analysis of precipitates.

The carry-over subtask for this task explored the effect of the higher humic acid (HA) concentrations up to 50 ppm on the synergetic interactions between U(VI) ions, colloidal silica and HA under oxidized conditions. The study also investigated the influence of HA and Si on the sorption of U(VI) onto sediments collected from the F/H Area. The experimental matrix was similar as for the study conducted last year using 10 ppm of HA.

An undergraduate student DOE Fellow Christine Wipfli is involved in this research.

Subtask 2.2: Monitoring of U(VI) bioreduction after ARCADIS demonstration at F-Area

This investigation was focusing on microcosm experiments using SRS sediments augmented with molasses and sulfate. The study was aiming to determine whether forms of reduced iron such as siderite and pyrite would arise in the reducing zone and if any mineralogical changes occurred in sediments during the re-oxidation period. The study utilized mineralogical analysis via XRD and measured changes in ferrous iron and sulfate before and after molasses addition. An undergraduate student DOE Fellow Aref Shehadeh is involved in this research.

Subtask 2.3: The sorption properties of the humate injected into the subsurface system.

Savannah River National Lab has been testing an unrefined, low cost humic substance known as Huma-K as an amendment that can be injected into contaminant plumes to enhance sorption of Uranium and Sr-90. Humic substances are important ion exchange and metal-complexing ligand, carrying a large number of functional groups with high complexing capacity that can greatly affect the mobility behavior of actinides in natural systems. The purpose of this task was to conduct batch sorption experiments to investigate for Huma-K sorption on SRS sediments at different pH values and investigate for sorption kinetics at pH 4. This research is still on-going focusing on the kinetics of Huma-K sorption at different pH values and sediments characterization studies. DOE Fellow Hansell Gonzalez, a Ph.D. student, is supporting this task.

Task 3: Evaluation of ammonia fate and biological contributions during and after ammonia injection for uranium treatment

This task is focusing on the physical mechanisms associated with the fate of ammonia after injection into the unsaturated subsurface. These tests can identify and quantify factors controlling the relative rate of NH_3 gas partitioning at different temperatures and the effect of bicarbonate ions with concentration up to 100mM on this process. This study explores mechanisms of potential importance using controlled laboratory systems to complement efforts underway at PNNL. This year experimental results suggested that the equilibrium partitioning may or may not be different with the variable bicarbonate solutions, but the buffering capacity has a significant impact on the amount of $\text{NH}_3(\text{g})$ required for this remediation technique. FIU is planning alterations in the experimental design to further elucidating the effect of variable bicarbonate concentrations on $\text{NH}_3(\text{g})$ partitioning. A recent graduate a DOE Fellow Christian Pino was supporting this task. A new Ph.D. student, DOE Fellow, Silvina Di Pietro, was admitted to the program to continue research on this task.

TECHNICAL PROGRESS FROM FIU YEAR 1 TO FIU YEAR 4

TASK 1 SUMMARY - INVESTIGATION ON MICROBIAL-META-AUTUNITE INTERACTIONS: EFFECT OF BICARBONATE

This study investigated the role of bacteria on the stability of autunite precipitates created as a result of the tripolyphosphate remediation technology and studied the microbial effect on the uranium release from autunite solid phases in bicarbonate rich environments. The study was conducted in mixed reactors comprised of autunite powder, media solution and bacteria and in a bacteria-autunite non-contact mode, employing culture ware with inserts. The *Arthrobacter* G975 and G968 strains, which roughly accounted for up to 25% of subsurface isolates, was used in the experiments. The uranyl release from autunite prior to the *Arthrobacter* G975 strain inoculation in mixed reactors was increased by a factor of 1.5 ± 0.6 - 62.6 ± 27.0 compared to the no-bicarbonate control. After bacteria inoculation, U(VI) measured in the reactors increased 7.5 ± 3.9 - 1.4 ± 0.1 fold when compared to the corresponding bicarbonate-bearing controls at a steady-state. A diminishing trend on the effect of bacteria on autunite leaching was observed as bicarbonate concentrations were increased in the solution. In non-contact autunite biodissolution, the steady-state maximum concentrations of U(VI) detected were 1.0 ± 0.7 - 4.6 ± 3.11 fold higher than the abiotic control without the bicarbonate amendment. After bacteria inoculation, U(VI) concentrations increased 0.5 ± 0.3 - 3.2 ± 1.4 fold compared to U(VI) concentration at steady-state prior to inoculation. The data suggests that bacteria is responsible for autunite dissolution and is able to influence U(VI) leaching while are not in direct contact with the mineral. The aqueous concentrations of U(VI), P, and Ca released during the dissolution of autunite were non-stoichiometric over the range of experimental conditions. SEM analysis revealed biofilms on the surface of the autunite particles that apparently produce unique physiochemical conditions leading to U(VI) dissolution.

Visual MINTEQ was applied to evaluate the aqueous speciation and saturation state of the solutions with respect to key minerals and aqueous phases. The predicted saturation indices suggested that the biotic system would become saturated with respect to various calcium phosphates and to calcite at 10 mM HCO_3^- . However, the system would remain under-saturated with respect to all potential U(VI) minerals except Na-autunite. Our results confirmed that *Arthrobacter* sp. G975 can effectively remove soluble U(VI) ions from aqueous solutions. The U(VI) biouptake obtained by conducting a 2^2 factorial design experiment was shown to be in the 83-90% range for the aqueous solutions at equilibrium with CO_2 atmospheric pressure.

Kinetics data analysis confirmed that the process follows a pseudo second-order kinetics model ($R^2 > 0.991$). It was conclusively proven that bicarbonate ions affect the sorption behaviors of U(VI). The maximum biosorption capacity of U(VI) ions in the studied U(VI) concentration range at 25°C by *Arthrobacter* sp. G975 was observed at 154.7 ± 60.6 , 42.4 ± 10.8 , 20.6 ± 6.5 , and 5.5 ± 8.0 mg/g for 0, 0.5, 2.5, 5 mM bicarbonate-bearing solutions, respectively. The incremental increase in aqueous bicarbonate concentrations exponentially reduced the U(VI) microbial uptake compared to values obtained in carbonate-free SGW. Experimental data indicates that increasing bicarbonate concentrations to 0, 0.5, 2.5 and 5 mM reduced the maximum U(VI) uptake by 0%, $72 \pm 13\%$, $87 \pm 7\%$ and $96 \pm 5\%$, respectively. The linear isotherm models produced a higher correlation coefficient with the experimental data than the Freundlich and Langmuir adsorption models. Despite the large biosorption capacity, there is experimental evidence to

suggest that not all uranium is adsorbed by the cell surface; it is also accumulated inside the cell. In the presence of bicarbonate, when highly soluble and mobile carbonate complexes dominate the aqueous speciation of U(VI), the viability of cells treated with a high concentration of U(VI) was noted to increase.

AFM was used to investigate qualitative and quantitative changes on microbial cell surfaces when the cells interact with the uranyl ion. Our quantitative results show the ability to capture the surface phenomenon for three different strains of *Arthrobacter* sp. It was found that the level of precipitation is not uniform across the cell membrane and it also differs from strain to strain. Roughness analysis shows that an increase in the uranium concentration does not have any significant effect on cell surface roughness for all strains ($P > 0.012$). The force spectroscopy results reveal an exponential decay relationship between the adhesion force and the concentration of uranium added to the growth media. Each strain has a unique adhesion force parameter ($P < 0.001$) that decreases as the uranium concentration is increased. Further, force spectroscopy results indicate that the cell membrane adhesion properties change due to chemical interactions with various concentrations of uranium.

In addition, this study concluded that the low uranium tolerant strain, *Arthrobacter* strain G968, can accelerate the release of uranium from autunite in the presence of bicarbonate through biodissolution of both natural Ca-autunite and synthetic Na-autunite, in conditions mimicking the arid and semiarid subsurface environments of the western U.S.

TASK 2 SUMMARY - EFFECT OF BICARBONATE ON THE DISSOLUTION OF META-AUTUNITE

This task was primarily concentrated on the autunite mineral dissolution experiments in the presence of bicarbonate ions. Uranium is one of the two most common radionuclides in the groundwater at 91 waste sites at 18 U.S. Department of Energy (DOE) facilities within the United States. Activities related to the nuclear energy and weapons production at the Hanford Site have resulted in widespread uranium contamination of subsurface environments, which accounts for 202,703 kg of uranium. Phosphate is one of the most important components in the uranium geochemical cycle; uranium has a high affinity for forming strong and stable complexes with phosphate among oxygen-containing ligands. The presence of phosphate in groundwater can limit the mobility of the uranyl cation (UO_2^{2+}) in the subsurface due to the formation of sparingly insoluble advanced secondary uranyl-phosphate minerals during the oxidized weathering of primary UO_2 deposits. Even small quantities of phosphate present in the groundwater can promote the formation of autunite group minerals, $\text{X}_{3-n}^{(n)+}[(\text{UO}_2)_2(\text{PO}_4)_2] \cdot x\text{H}_2\text{O}$, that can persist under intense weathering conditions over a geologic period of time.

In oxidizing groundwater conditions, hydrogen carbonate (known as bicarbonate) and carbonate anions are an important complexing agent for U(VI), forming several strong soluble complexes with the uranyl ion (UO_2^{2+}); UO_2CO_3^0 , $\text{UO}_2(\text{CO}_3)_2^{2-}$, and $\text{UO}_2(\text{CO}_3)_3^{4-}$ are predominant species at a $\text{pH} > 4$. Aqueous carbonate, equilibrated with a groundwater CO_2 pressure of 10^{-2} to $10^{-3.5}$ atm in the CO_2 open system, is considered one of the key variables affecting the dissolution of actinides and facilitating uranium desorption reactions from soil and sediments, thus increasing uranium mobility in natural waters. The purpose of this study was to investigate the effects of bicarbonate solutions (0.0005-0.003 M) on the uranium rate of release from synthetic Na meta-autunite and to quantify the kinetic rate law parameters of the dissolution process. This was

accomplished through a series of dissolution experiments conducted via a single-pass flow-through (SPFT) reactor using TRIS (tris hydroxymethyl aminomethane) buffered bicarbonate solutions over a range of pH and temperature variations. Such experiments are essential to predict and understand the long-term effects of bicarbonate on the uranium release from Na-autunite and the fate and transport of uranium in the subsurface.

The study evaluated the rate of dissolution of Na-autunite under low bicarbonate concentrations ranging from 0.0005 to 0.003 M, pH ranging from 6 to 11 and temperature variations from 5 to 60°C via single-pass flow-through cell experiments to obtain the geochemical parameters that affect uranium mobility in the subsurface.

The uranium rate of release from Na-autunite was found directly correlated to increasing concentrations of bicarbonate solutions. The bicarbonate ions in the solution form negatively charged soluble complexes with uranium, which are highly mobile in subsurface environments. Results from these experiments showed that the rate of uranium release increased with an increase in the bicarbonate concentration at low pH values. However, as the pH of the system increased, the effect of bicarbonate faded due to the prevailing pH effect. The rate of uranium release increased from 1.90×10^{-12} to 2.64×10^{-10} ($\text{mol m}^{-2} \text{s}^{-1}$) at 23°C in the pH range and bicarbonate concentrations tested. The geochemical modeling data from Visual MINTEQ predicted that, at low pH, the uranium release was controlled by the formation of $(\text{UO}_2)_3(\text{PO}_4)_2(\text{s})$, which became under-saturated at higher pH, effectively increasing the overall uranium release rate.

The activation energy values were unaffected by temperature and bicarbonate concentration variations but were strongly dependent on pH conditions. The activation energy averaged 29.94 kJ mol^{-1} and 26.87 kJ mol^{-1} for pH 6 and 7, respectively. In the pH range 8-11, activation energies ranged from 15.6 to 13.1 kJ mol^{-1} . Geochemical modeling suggested that uranyl speciation is strongly dependent on pH and the concentration of carbonate ions in the solution. At high pH, the mineral surface is saturated with carbonate uranyl complexes that accelerate the release of U(VI) ions out of the autunite structure. The calculated theoretical and experimental values of U(VI) rate of release differ within a $\pm 10\%$ error range.

The information collected in this study has provided an additional understanding of the bicarbonate effect on the uranium rate of release from Na-autunite. Data from Na-autunite dissolution experiments were incorporated into the Hanford model that simulates the application of polyphosphate injection technology to determine if the treatment is a feasible solution for uranium remediation at the 300 Area of the Hanford Site.

TASK 3 SUMMARY - URANIUM (VI) STABILIZATION IN THE HANFORD SITE VADOSE ZONE (200 AREA) SEDIMENT UTILIZING IN SITU CALCITE MINERAL

The groundwater beneath the 200 Area has been reported to contain some of the hazardous and radioactive contaminants that are similar to the chemicals stored in the tank farm, thus indicating contaminant migration from the vadose zone.

Vadose zone soil/sediment in the 200 Area is reported to contain natural calcite minerals (calcium carbonate) in abundance. Several studies have reported the affinity of uranium to form complexes with calcite or its constituents-carbonate/calcium (Kitano and Oomori 1971, Russel et al. 1994, Sturchio et al. 1998, Kelly et al. 2003, and Joseph et al. 2011). Three of the complexes

have been reported for uranium and carbonate (uranyl carbonate): rutherfordine, UO_2CO_3 ; blatonite, $\text{UO}_2\text{CO}_3 \cdot \text{H}_2\text{O}$; and joliotite, $\text{UO}_2\text{CO}_3 \cdot n\text{H}_2\text{O}$, $n \sim 2$. There are other complexes that include both carbonate and calcite, such as wyartite, $\text{Ca}(\text{CO}_3)\text{U}^{5+}(\text{UO}_2)_2\text{O}_4(\text{OH})(\text{H}_2\text{O})_7$; zellerite, $\text{Ca}(\text{UO}_2)(\text{CO}_3)_2(\text{H}_2\text{O})_5$; liebigite, $\text{Ca}_2(\text{UO}_2)(\text{CO}_3)_3(\text{H}_2\text{O})_{11}$; and sharpite, $\text{Ca}(\text{UO}_2)_6(\text{CO}_3)_5(\text{OH})_4(\text{H}_2\text{O})_6$, to mention a few. In addition, uranium can co-precipitate with calcite in the Hanford vadose zone sediment.

This task involved adsorption experiments of uranium on the Hanford sediments and a study on calcite dissolution and its influence on the adsorption process. The adsorption coefficient for uranium in the Hanford sediment (with very low organic content) was found in the order of $24 \times 10^{-3} \text{ mL/g}$ at pH 9.0. The study also showed reduced sorption when supplemented with calcite crystals at all pH levels tested in this study (5.5, 7.5, and 9.0). Based on these observations, it was concluded that the uranium migration can be rapid in the sediment rich in soluble calcite. Also, the low adsorption coefficient for uranium in the sediments may imply that the soil has a lower ability to retain uranium. In this context, calcite-based technology for uranium stabilization needs a cautious approach so as to prevent uranium transport and maximize its stability in the vadose zone sediment.

RAPID DEPLOYMENT OF ENGINEERED SOLUTIONS TO ENVIRONMENTAL PROBLEMS (FIU YEAR 5)

Executive Summary

This project focuses on providing assistance to Hanford's and SRS environmental cleanup in the areas of soil and groundwater. The purpose of the research activities in FIU Year 5 were to examine the solubility properties and deliquescence behavior of uranium-free precipitates mimicking solid phases possibly created after *in situ* subsurface pH manipulation using ammonia gas. A progressive increase in the relative humidity of salt mixtures placed in the isopiestic system allowed the samples to obtain water activities and osmotic coefficients values in the conditions most closely mimicking the unsaturated vadose zone environment. Experimental studies also continued for mineralogical and morphological characterization of NH_3 -treated U(VI)-bearing solids precipitated from the solution mixture containing major pore water cations and ions that could be present in pore water from mineral phase dissolution. FIU explored transmission electron microscope (TEM) analysis to obtain diffraction patterns for polycrystalline mineral phases and prepared samples with an elevated uranium concentration of 500 ppm for the subsequent SEM/EDS and XRD analysis. Another line of research was dedicated to microbial autunite dissolution studies in the presence of facultative *Shewanella Oneidensis* MR-1 cells. Experiments were conducted in mixed bottles under oxygen-restricted and anaerobic conditions via sacrificial vials. The latter experiments are still in progress for sampling and chemical analysis, cell protein content and cell viability in the presence of facultative *Shewanella Oneidensis* MR-1. Another line of research related to the Hanford Site 200 Area was conducted to investigate total $\text{NH}_3/\text{NH}_4^+$ in the aqueous phase after the injection of 5% NH_3 (95% N_2) in the solutions amended with 100 mM, 60 mM, 30 mM and 3 mM HCO_3^- . This research is still on-going; however, the current report includes initial results for measured $\text{NH}_3/\text{NH}_4^+$ in the solution after ammonia gas injection, speciation modeling (using Visual Minteq) results, statistical analysis and a literature review to provide recommendations for the design of future experiments to investigate the partitioning of $\text{NH}_3/\text{NH}_4^+$ in laboratory systems.

Experiments were conducted for the F/H Area at SRS to investigate whether dissolved sodium silicate solutions have enough alkalinity to replace the carbonate base being used to correct the acidic nature of the contaminated sediments. This investigation also evaluated the synergy between Si and humic acid on the removal of U(VI) from the treatment zone. Humic substances (HS) are a major component of soil organic matter that usually account for 50-80% of the organic carbon in the soil or sediment. They are known for their excellent binding capacity for metals. This unique structure allows HS to play a part in the ion exchange and complexation reactions forming stable complexes with heavy metals and actinides. These reactive features of HS make them to be a strong candidate for remediation efforts to reduce the mobility of uranium (VI) in the subsurface. The study was conducted using batch reactors and post-reacted sediments will be evaluated for surface morphology and composition. Experiments were also extended to investigate whether contaminants remain sequestered after the ARCADIS demonstration at the F-Area. To promote the formation of ferrous iron solid phases, the media solution was amended with sulfate. This is particularly important since the remediation strategy chosen by ARCADIS relies on changing the geochemical conditions in a direction that is opposite of their natural evolution. Chemical analysis and characterization of solid phases doesn't show the presence of

ferrous iron phases, which might suggest that the method isn't sustainable for application to treat the SRS acidic soil.

Detailed task descriptions and deliverables and milestones can be found in the Project Technical Plan.

Introduction

Nuclear weapon production activities at the Department of Energy (DOE) Hanford and SRS Sites generated millions of gallons of radioactive wastes that were initially allowed to be stored in retention basins, trenches, or cribs where the waste percolated into the soil. These leakages influenced the vadose zone sediments contaminating soil and groundwater. At Hanford, the greatest concern is the radioactive waste storage tanks, 67 of which are known or suspected to be leaking radioactive waste. There is a growing concern that elevated uranium concentrations could slowly migrate downward, creating a risk of higher U concentrations reaching the groundwater and then entering the Columbia River along the shoreline. Similar concerns exist about possible contamination of the Savannah River in South Carolina. DOE is responsible for the remediation of contamination at sites involved in the past production of nuclear weapons. Therefore, the number of environmental challenges that DOE is facing is tremendous with enormous associated costs for cleanup activities. Thus, the goal of the remediation efforts at Hanford and SRS is rapid deployment of engineering solutions to assist with environmental cleanup of the contaminated soil and groundwater, seeking to reduce the potential for radionuclide mobility in the subsurface. Uranium (VI) is a key contaminant of concern at Hanford and SRS Sites. Due to the potential threat on human health, the U.S. Environmental Protection Agency (USEPA) has set a maximum contaminant level of 30 µg/L for uranium concentration in groundwater (USEPA 2001). Once released in the subsurface, uranium species persist in the environment and can have toxic effects on living organisms. In addition, the uranyl ion has a varying tendency towards complexation with other chemicals and is greatly affected by aquifer characteristics such as pH, redox status, ligand (silicate, carbonate, sulfate, phosphate, and dissolved carbon) concentrations, and aluminum-oxide and iron-oxide mineral concentrations. Therefore, *in situ* stabilization of uranium without changing its oxidation state can sequester mobile uranyl species, converting them to less mobile uranium. In this regard, *in situ* stabilization of uranium by ammonia gas injection for remediation of the Hanford Site vadose zone or applications of humic acid for the remediation of the SRS F/H Area groundwater has gained popularity as potential remediation methods to reduce uranium concentrations in pore and groundwater.

Additional research is necessary to understand the effect of various environmental factors on the behavior of U(VI) in vadose zone sediments and groundwater under Hanford Site and SRS conditions before implementation of those methods for soil and groundwater remediation.

Based on the results of this investigation, Project 2 has accomplished the following in FIU Year 5 (2014-2015):

- Completed a progress report on microcosm studies prepared with SRS sediments augmented with molasses and sulfate (January 2015).
- Completed a progress report on the solubility measurements via the isopiestic method (February 2015).
- Completed a progress report on batch experiments prepared with SRS sediments, colloidal Si and higher HA concentration up to 50 ppm (carryover scope) (March 2014).
- Completed a progress report on sorption properties of the humate injected into the subsurface system (April 2014).
- Published a manuscript in the Research in Microbiology Journal: Sepulveda-Medina, P., Y. Katsenovich, V. Musaramthota, M. Lee, B. Lee, R. Dua, L. Lagos (2015) The effect of

uranium on bacterial viability and cell surface morphology using atomic force microscopy in the presence of bicarbonate ions, *Research in Microbiology*. 166, 5, 419–427.

- Published a manuscript in the *Journal of Environmental Radioactivity*: Sepulveda-Medina, P., Y. Katsenovich, D.M. Wellman, L.E. Lagos (2015). The effect of bicarbonate on the microbial dissolution of autunite mineral in the presence of gram-positive bacteria, *Journal of Environmental Radioactivity*. 144, 77–85.
- Presented an overview to DOE HQ/Site POCs of the project progress and accomplishments.
- Presented research results at the Waste Management 2015 (WM2015) Conference (March 2015).
 - The Influence of Humic Acid and Colloidal Silica on the Sorption of U(VI) onto SRS Sediments Collected from the F/H Area (15499). Hansell Gonzalez, Yelena Katsenovich, Miles Denham, Ravi Gudavalli, Leonel Lagos (Oral presentation).
 - Monitoring of U(VI) Bioreduction After ARCADIS Demonstration at Savannah River Site F-Area (Student poster), Aref Shehadeh (DOE Fellow).
 - Sodium Silicate Treatment for Uranium (VI) Bearing Groundwater Systems at F/H Area at Savannah River Site (Student poster), Christine Wipfli (DOE Fellow). The winner of the student poster competition
 - Use of XRF to Characterize Pre-Hanford Orchards in the 100-OL-1 Operable Unit (Student poster), Christian Pino (DOE Fellow).
 - Study of an Unrefined Humate Solution as a Possible Remediation Method for Groundwater Contamination (Student poster). Hansell Gonzalez Raymat (DOE Fellow).
 - Characterization of the Uranium-Bearing Products of the Ammonia Injection Remediation Method. (Student poster), Robert Lapierre (DOE Fellow).
 - A Study of Autunite Dissolution in the Presence of *Shewanella Oneidensis* MR1 and Different Bicarbonate Concentrations (Student poster), Sandra Herrera Landaez (DOE Fellow).
- DOE Fellow Christian Pino graduated with BS degree in chemistry.

TASK 1: SEQUESTERING URANIUM AT THE HANFORD 200 AREA BY IN SITU SUBSURFACE PH MANIPULATION USING AMMONIA (NH₃) GAS

Subtask 1.1: Sequestering Uranium at the Hanford 200 Area Vadose Zone by In Situ Subsurface pH Manipulation Using NH₃ Gas

Subtask 1.1: Introduction

Remediation of radionuclides residing in the Hanford Site vadose zone (VZ) is a challenging task due to the depth of the contaminants, which makes it difficult to reach with near-surface remediation techniques. Uranium is one of the key contaminants of the Hanford Site VZ. Uranyl carbonates are the predominant uranium (VI) aqueous species in Hanford's pore water and due to their high mobility are considered as a potential source of contamination for the underlying aquifer. So, in-situ remediation methods require sequestration of uranium in the subsurface to prevent further spreading of mobile uranium species. The technology under consideration to sequester U(VI) is a manipulation of soil pH via ammonia gas injection by creation of alkaline conditions in the uranium-contaminated soil. The soil pH manipulation causes uranium co-precipitation during mineralogical changes and the formation of uranium-bearing precipitates in the treated vadose zone soil. The injection of reactive gases such as NH₃ can reduce the potential for radionuclide mobility in the subsurface without water addition causing undesired downward migration of contaminants. This technology allows the transformation of mobile uranium species to lower solubility precipitates that are stable in the natural environment (Szecsody et al., 2012). The formation of a relatively insoluble mineral complex that integrates uranium is a desired outcome of the VZ remediation efforts at Hanford because the more immobile the contamination is, the less it will spread in the subsurface. However, there is a need for a better understanding of the stability of the U-bearing precipitates created in the soil as a result of ammonia gas remedial actions. This information would help to accurately predict the mobility of U(VI) in the post-treated vadose zone soil.

Traditionally, solubility measurements are conducted in batch experiments to measure the amount of solute that can be dissolved in a solvent until the system reaches equilibrium (Giammar et al., 2002; Rai et al., 2005; Gorman-Lewis et al., 2008). This method is better suited to measure solubility of minerals with respect to the groundwater saturated conditions; however, it doesn't allow accurately quantifying the solubility of minerals for the unsaturated vadose zone conditions. Evaluation of literature suggests that the isopiestic method can closely mimic the mineral deliquescence process, which refers to the formation of an aqueous solution by the absorption of water by hygroscopic salt minerals (Carroll et al., 2005). Thus, isopiestic measurements may be the most appropriate way to quantify mineral solubility for the unsaturated vadose zone conditions. This method is considered very accurate, helping to make more realistic predictions of contaminant fate and transport in vadose zone environments. Experimental deliquescence data are limited for mixed salts (Gruszkiewicz et al., 2007) and especially scarce for uranium-bearing multicomponent mixtures.

The tendency for solutes to deliquesce depends on their solubility and is influenced by the particular character of solute-solvent interactions described according to Raoult's law in vapor-pressure lowering ability. The basic features of the method include isothermal equilibration of

samples of known masses and known initial concentrations through a common vapor phase. In the closed system, the solvent is distilled isothermally from one crucible to another until each solution reaches the same chemical potential. All of the solutions at equal vapor pressure or isopiestic equilibrium have the same solvent activities. These conditions can be rewritten as $\ln a_s = \ln a_{ref}$. By equilibration, the samples with a standard of known solvent activities under the conditions of the experiment as a function of molality can be used to determine the solvent activity of another solution (Rard, 1985). If two or more solutions of different salts are in isopiestic equilibrium, the osmotic coefficient of a test solution, ϕ_x , is calculated from the reference solution, ϕ_{ref} , from the fundamental equation for isopiestic equilibrium:

$$\phi_s = \frac{v_{ref} m_{ref} \phi_{Rref}}{v_s m_s} \quad \text{Eq 1}$$

The water activities a_w of the reference solution can be calculated using the following equation:

$$\ln a_w = -0.001 v_s m_s M_w \phi_{ref} \quad \text{Eq 2}$$

Where v_s is the number of ions formed by the complete dissociation of one molecule of the reference standard, and for NaCl and KCl, $v=2$, M_w is molar mass of H_2O , and ϕ is the practical osmotic coefficient of the reference standard. Eq. 2 is defined for mixtures, as well as for single-salt solutions (Rard and Platford, 1991). The ratio $(\frac{m_{ref}}{m_s})$ is called the isopiestic ratio. The osmotic coefficient can be measured with 0.1%-0.3% accuracy at molalities down to 0.1 mol/kg. So, all solutions in the isopiestic chamber that are allowed to exchange solvent until isopiestic equilibrium is reached will have the same solvent activity with a value of $(\sum_i v_i m_i) \phi$.

Relative humidity, RH, is related to the activity of water through the partial pressure of water vapor as follows:

$$RH = p_w / p_w^o \quad \text{Eq 3}$$

Where p_w is the partial pressure of water vapor over an aqueous solution and p_w^o is the partial pressure of water vapor over pure water. The activity of water in aqueous solutions relates to its fugacity by equation (Rard and Clegg, 1997):

$$a_w = f_w / f_w^o \quad \text{Eq 4}$$

Where f_w is the fugacity of water vapor over an aqueous solution and f_w^o is the fugacity of water vapor over pure water. It is usually assumed that, in ambient temperature and moderate pressure, water vapor behaves ideally and the fugacities can be replaced by partial pressure (Reid et al., 1987):

$$f_w / f_w^o = p_w / p_w^o \quad \text{Eq 5}$$

yielding:

$$RH = a_w \quad \text{Eq 6}$$

The RH is commonly expressed as a percentage; thus $RH\% = 100 * a_w$.

This report summarizes initial results from isopiestic measurements of the deliquescence behavior of no- uranium multicomponent precipitates combined from major pore water constituents such as Na^+ , SiO_3^- , Al^+ , NO_3^- , K^+ , HCO_3^- , Ca^{2+} , and Cl^- .

Subtask 1.1: Material and methods

Rard and Platford (2000) presented detailed general descriptions of the isopiestic method with an emphasis on experimental aspects. In brief, the isopiestic apparatus used for the experiments was fabricated from a pressure pot and contained an aluminum heat-transfer block that has a good thermal conductivity, able to maintain a uniform temperature distribution inside the chamber (Figure 1).

The aluminum block contained fourteen holes drilled part way through to tightly hold the crucible cups containing standards and multicomponent precipitate samples. Isopiestic method procedures require for the isopiestic cups to be made of material that is chemically inert to the experimental solutions and have excellent thermal conductivity. In the experiments, 15-mL nickel cups were used; to avoid evaporation losses, tightly fitted light nickel lids were immediately added when the chamber was open. Then, the crucibles with lids were placed on balances for weighing. Metler Toledo analytical balances XS205DU with a precision of no less than 1×10^{-5} g were used for weighing the crucibles cups covered with lids (Figure 2).



Figure 1. Isopiestic chamber to conduct solubility experiments; aluminum block with holes to hold nickel crucibles.



Figure 2. Analytical balance weighing covered crucible.

The isopiestic method is a mostly gravimetric method that relies on the assumption that only one volatile component is present. The mass of the empty crucible along with the number of moles of electrolyte in each sample was accurately calculated. Therefore, any gains or losses in mass during isopiestic equilibration are only possible due to gains or losses of solvent. The observed changes in mass were used in the calculation of the solution molalities at isopiestic equilibrium (Rard and Platford, 2000).

Every time the system reached equilibrium, the isopiestic chamber was opened to weigh the samples. Then, when the chamber was re-closed, the air was evacuated until the pressure reached around 4.5 kPa (Blanco et al., 2006). After the gas is evacuated in a closed vessel, the volatile component is transported through the vapor phase until the solutions reach equilibrium. The

apparatus was equipped with a high accuracy pressure transducer with a range of 0-30 psia (Omega Engineering, Inc.) to provide a measurement of water vapor pressure, allowing for monitoring as the system approached equilibrium. The transducer was connected to the acquisition system to collect vapor pressure data. Labview code, used to record the direct vapor pressure measurements, was updated to show pressure in inches of mercury (in of Hg) and in Torr. The code was also modified to indicate when the system was under vacuum. The vessel was constantly kept in the environmental chamber to control a stable temperature of 25°C (Figure 3).



Figure 3. Isopiestic chamber to conduct solubility experiments connected to the acquisition system.

The reference standards were used to obtain osmotic coefficients for the low water activity values in the multicomponent salt systems. Stock solutions for standards were prepared by weight using deionized water from a Barnstead NANOpure water purification system or plasma grade water. Initially, the experiments were started with NaCl as a reference. Due to an inability to calculate water activities for the high molality values of NaCl, the experiment was extended to include two new reference standard solutions, calcium chloride (CaCl_2) and lithium chloride (LiCl), known for their high solubility. The most soluble is LiCl; its maximum molality to obtain an osmotic coefficient value for the water activity calculations is 19.219 mol/kg. The CaCl_2 and LiCl salts were “ultra dry” grade chemicals with metal-basis purities specified by Alfa Aesar as 0.99 and 0.995, respectively. Powdered salts were received sealed in argon-filled glass ampoules. Preparation of the reference solutions included breaking the glass ampoules and transferring their contents rapidly to polyethylene bottles containing weighed amounts of water. To avoid moisture, two samples of each reference standard solution were prepared in an anaerobic glove box. The masses of the reference standards were measured carefully to limit variations between

two identical standard samples: 0.04685g and 0.03465 g for CaCl_2 and 0.02548g and 0.02541g for LiCl .

The multicomponent precipitate samples prepared to measure a moisture-induced phase transformation from solid phase to solution and determine water activity and osmotic coefficient at the deliquescence point were combined from Na^+ , SiO_3^- , Al^+ , NO_3^- , K^+ , HCO_3^- , Ca^{2+} , and Cl^- ions. All of these elements are found in the pore water of the Hanford Site 200 Area and their concentrations used for the preparation of experimental mixtures were based on the characterization studies performed by Serne et al. (2008) on vadose zone sediments from borehole 299-E33-45 at the Hanford 200 Area. Uranium (VI) was not included in these experiments. Preparation of the samples started from the stock solutions made in deionized water (DIW) by dissolving preliminary dried in the oven $\text{Na}_2\text{SiO}_3 \cdot 9\text{H}_2\text{O}$, $\text{Al}(\text{NO}_3)_3 \cdot 9\text{H}_2\text{O}$, KHCO_3 , and $\text{CaCl}_2 \cdot 2\text{H}_2\text{O}$ salts into 50 mL vials. All multicomponent precipitate samples kept a constant ratio of $\text{Si}/\text{Al}=20$ by means of Si and Al concentrations of 100 mM and 5 mM, respectively. Bicarbonate concentrations used for the preparation of the solution mixture were 3 mM and 50 mM. Each bicarbonate concentration was combined with 0, 5, and 10 mM of calcium concentrations. The multicomponent solutions in the amount of 10 mL were prepared directly into the nickel crucibles by mixing the required stock solutions and DIW. The weights of the solutions were recorded using balances with an accuracy of 1×10^{-5} g. After mixing, all crucibles containing the multicomponent solutions were placed in an oven and dried at 40°C for at least 48h until a stable weight of dried precipitates was obtained. The concentrations of the stock solutions were maintained the same as in the previously conducted studies to investigate the effect of Si and Al concentration ratios on the removal of U(VI) in alkaline conditions. The amounts of each stock solution used in the preparation of six samples are presented in Table 1.

Table 1. Sample Composition

Crucible	Amount of Stock Solution and DIW (uL) $\text{Na}_2\text{SiO}_3 \cdot 9\text{H}_2\text{O} = 2368$ and $\text{Al}(\text{NO}_3)_3 \cdot 9\text{H}_2\text{O} = 1000$			
	Sample	KHCO_3	$\text{CaCl}_2 \cdot 2\text{H}_2\text{O}$	DIW
7	3 mM KHCO_3 , no Calcium	75	0	6657
8	50 mM KHCO_3 , no Calcium	1250	0	5382
9	3 mM KHCO_3 , 5 mM Calcium	75	20	6537
10	50 mM KHCO_3 , 5 mM Calcium	1250	20	5362
11	3 mM KHCO_3 , 10 mM Calcium	75	20	6537
12	50 mM KHCO_3 , 10 mM Calcium	1250	20	5362

The solute contents in each crucible were calculated as a summation of the total number of moles corresponding to the salt formula. In the experiments, ten nickel crucibles were used; two contained duplicate reference solutions of CaCl_2 , another two contained reference solutions of LiCl and six contained the multicomponent solids samples. Table 2 summarizes the compositions of the CaCl_2 and LiCl reference standards, solute contents, and initial molalities of the reference and experimental samples.

Table 2. Reference and Multicomponent Samples - Weights, Solute Content, and Molalities at the Beginning of Experiment

Cup #	Standard/Solute Multicomponent	Standard and Sample Weight (g)	Solute Content (Mm)	Pure Water in Sample (μl)	Initial Sample Molality mol/Kg
1	CaCl ₂	0.04685	0.42215	100	4.22
2	CaCl ₂	0.03465	0.31222	100	3.12
3	LiCl ₂	0.02548	0.60103	100	6.01
4	LiCl ₂	0.02541	0.59938	100	5.99
5	Na ₂ SiO ₃ + Al(NO ₃) ₃ + *KHCO ₃	0.19860	0.24206	0.13099	1.85
6	Na ₂ SiO ₃ + Al(NO ₃) ₃ + **KHCO ₃	0.23900	0.30433	1.15473	0.26
7	Na ₂ SiO ₃ + Al(NO ₃) ₃ + *KHCO ₃ + †CaCl ₂	0.20150	0.24216	0.17987	1.35
8	Na ₂ SiO ₃ + Al(NO ₃) ₃ + **KHCO ₃ + †CaCl ₂	0.24340	0.30443	0.16542	1.84
9	Na ₂ SiO ₃ + Al(NO ₃) ₃ + *KHCO ₃ + ††CaCl ₂	0.21020	0.24226	0.15091	1.61
10	Na ₂ SiO ₃ +Al(NO ₃) ₃ + **KHCO ₃ + ††CaCl ₂	0.25610	0.30453	0.18382	1.67

* 3 mM and ** 50 mM of KHCO₃† 5 mM and †† 10 mM of CaCl₂

Deliquescence behavior of multicomponent solids was studied by starting from uranium-free solid salt mixtures via a progressive increase in the relative humidity. It was achieved by incremental addition of 20-50 μL of DIW water to the standards, helping to increase the humidity of the system and find water activity values closer to the eutonic point, where the lowest relative humidity coexists with a liquid solution.

Subtask 1.1: Results and Discussion

This progress report presents the experimental results on solid-liquid transitions of the synthetic multicomponent precipitate samples prepared from synthetic porewater solutions mimicking conditions at the Hanford Site. Several parameters were taken into consideration for studying deliquescence behavior of dry solids with the most important being water activity and osmotic coefficients. Two samples were prepared for each standard, CaCl₂ and LiCl, and the osmotic coefficients (ϕ_{stand}) were estimated for each standard using an average value between the two samples. At each isopiestic measurement recorded, molalities of standards were interpolated from the literature data (Bert and Nuttall, 1977; and Hamer and Wu, 1972) to obtain their corresponding osmotic coefficients. The water activity (a_w) values for each standard were calculated as follows:

$$\ln a_w = (\sum_i v_i m_i) \phi \quad \text{Eq 7.}$$

The measured water activities of the LiCl-H₂O and CaCl₂ – H₂O against the standards molality values obtained throughout the isopiestic experiments are shown in Figure 4.

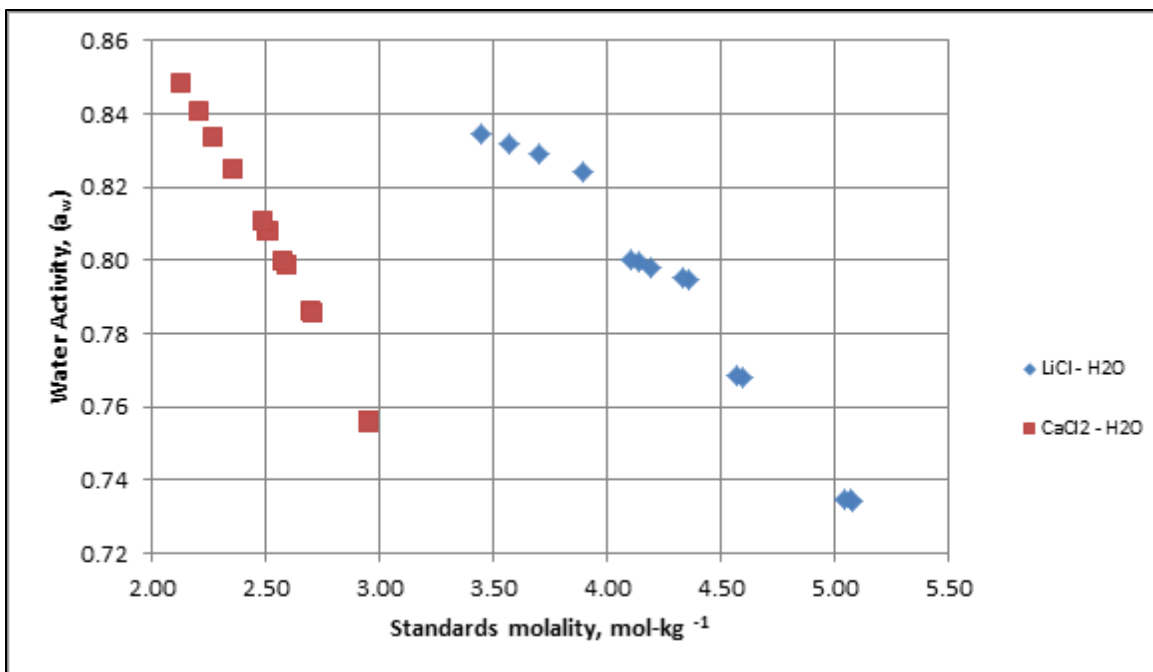


Figure 4. Changes of water activities vs. molality for LiCl and CaCL2 standards.

The standards values for molality, osmotic coefficient, and water activity calculated according to the Eq. 2 for each isopiestic measurement are presented in Table 3 and Table 4. The variation between water activity values obtained for the two standards, CaCl₂ and LiCl, was calculated as 1.4% (0.848 for CaCl₂ and 0.834 for LiCl). By the end of the experiments, crucibles with LiCl standards showed little corrosion spots inside the cups, which might have contributed to the difference in the osmotic coefficient values between the two standards. While the results for the water activities for both standards are in reasonable agreement, we consider that more accurate data were obtained with CaCl₂.

The molality of each multicomponent sample was calculated based on the solute content and water weight measurements. Then, the osmotic coefficients for multicomponent samples (ϕ) were calculated according to Eq.1. The water activities at equilibrium for all multicomponent samples were equal to the water activity of the standard at each isopiestic measurement recorded (Table 3 and Table 4).

Table 3. Values for water activities, a_w , and osmotic coefficients, ϕ , for CaCl_2 and multicomponent samples

$a_w \text{ CaCl}_2$	$\text{Na}_2\text{SiO}_3 + \text{Al}(\text{NO}_3)_3 + \text{KHCO}_3^*$	$\text{Na}_2\text{SiO}_3 + \text{Al}(\text{NO}_3)_3 + \text{KHCO}_3^{**}$	$\text{Na}_2\text{SiO}_3 + \text{Al}(\text{NO}_3)_3 + \text{KHCO}_3^* + \text{CaCl}_2^\dagger$	$\text{Na}_2\text{SiO}_3 + \text{Al}(\text{NO}_3)_3 + \text{KHCO}_3^* + \text{CaCl}_2^\dagger$	$\text{Na}_2\text{SiO}_3 + \text{Al}(\text{NO}_3)_3 + \text{KHCO}_3^* + \text{CaCl}_2^{\dagger\dagger}$	$\text{Na}_2\text{SiO}_3 + \text{Al}(\text{NO}_3)_3 + \text{KHCO}_3^* + \text{CaCl}_2^{\dagger\dagger}$	$\phi \text{ CaCl}_2$
0.786	1.485	1.820	3.499	2.462	2.803	2.961	1.652
0.798	1.436	1.861	3.424	2.426	2.727	2.929	1.607
0.800	1.303	1.755	3.336	2.331	2.643	2.902	1.602
0.808	1.319	1.803	3.199	2.341	2.585	2.951	1.573
0.808	1.300	1.814	2.470	2.229	2.489	2.881	1.575
0.811	1.259	1.811	1.852	2.235	2.428	2.910	1.564
0.825	1.380	2.050	1.953	2.407	2.592	3.141	1.515
0.834	1.475	2.405	2.084	2.770	2.819	3.566	1.483
0.840	1.587	2.645	2.192	3.029	2.978	3.894	1.458
0.848	1.682	2.985	2.266	3.377	3.193	4.328	1.429

* 3 mM and ** 50 mM of KHCO_3 † 5 mM and †† 10 mM of CaCl_2 **Table 4. Values for water activities, a_w , and osmotic coefficients, ϕ , for LiCl and multicomponent samples**

$a_w \text{ LiCl}$	$\text{Na}_2\text{SiO}_3 + \text{Al}(\text{NO}_3)_3 + \text{KHCO}_3^*$	$\text{Na}_2\text{SiO}_3 + \text{Al}(\text{NO}_3)_3 + \text{KHCO}_3^{**}$	$\text{Na}_2\text{SiO}_3 + \text{Al}(\text{NO}_3)_3 + \text{KHCO}_3^* + \text{CaCl}_2^\dagger$	$\text{Na}_2\text{SiO}_3 + \text{Al}(\text{NO}_3)_3 + \text{KHCO}_3^* + \text{CaCl}_2^\dagger$	$\text{Na}_2\text{SiO}_3 + \text{Al}(\text{NO}_3)_3 + \text{KHCO}_3^* + \text{CaCl}_2^{\dagger\dagger}$	$\text{Na}_2\text{SiO}_3 + \text{Al}(\text{NO}_3)_3 + \text{KHCO}_3^* + \text{CaCl}_2^{\dagger\dagger}$	$\phi \text{ LiCl}$
0.768	1.621	1.987	3.820	2.688	3.060	3.233	1.601
0.795	1.466	1.901	3.497	2.478	2.786	2.991	1.465
0.795	1.330	1.792	3.408	2.381	2.700	2.964	1.470
0.798	1.347	1.841	3.268	2.392	2.640	3.015	1.493
0.799	1.328	1.853	2.523	2.277	2.542	2.943	1.502
0.800	1.286	1.850	1.892	2.282	2.480	2.973	1.509
0.824	1.409	2.094	1.995	2.459	2.648	3.209	1.379
0.829	1.507	2.457	2.129	2.830	2.879	3.643	1.410
0.832	1.621	2.702	2.239	3.094	3.041	3.978	1.430
0.834	1.718	3.049	2.315	3.449	3.262	4.421	1.458

* 3 mM and ** 50 mM of KHCO_3 † 5 mM and †† 10 mM of CaCl_2

The graphical representation of the obtained results is given in Figure 5 and Figure 6. The phase changes are usually visible as breaks in the curve, representing the osmotic coefficient of the solution as a function of relative humidity (Gruskiewicz et al., 2007). In our case, it occurred for all experimental samples at water activity 0.81%, which correlates to the relative humidity of 81%.

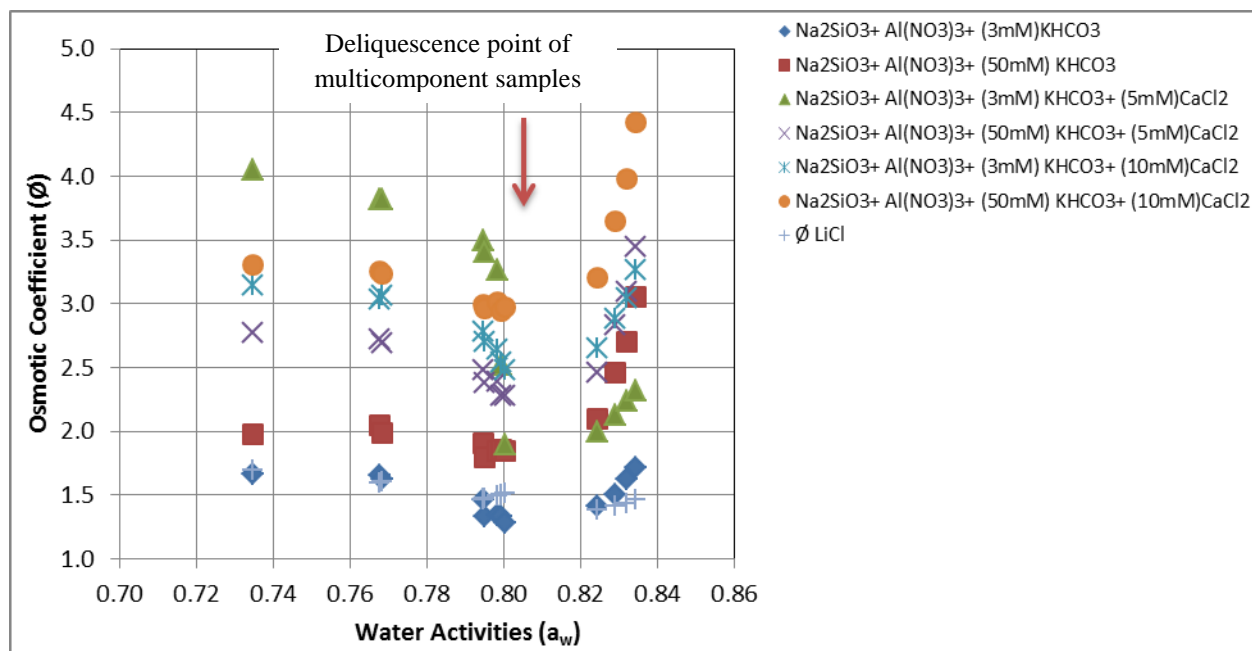


Figure 5. Osmotic coefficient for multicomponent samples as a function of water activities, a_w , using LiCl as a standard.

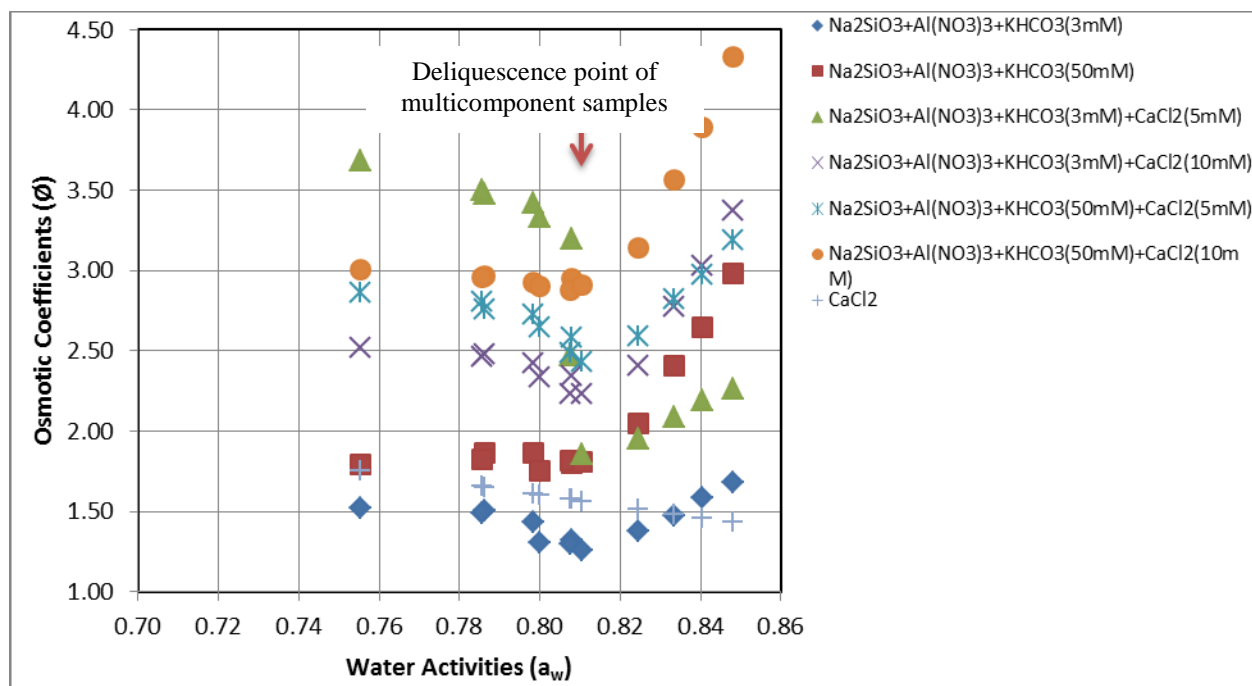


Figure 6. Osmotic coefficient for multicomponent samples as a function of water activities, a_w , using CaCl_2 as a standard.

All experimental water activities as a function of total molality for each multicomponent sample were plotted in Figure 7.

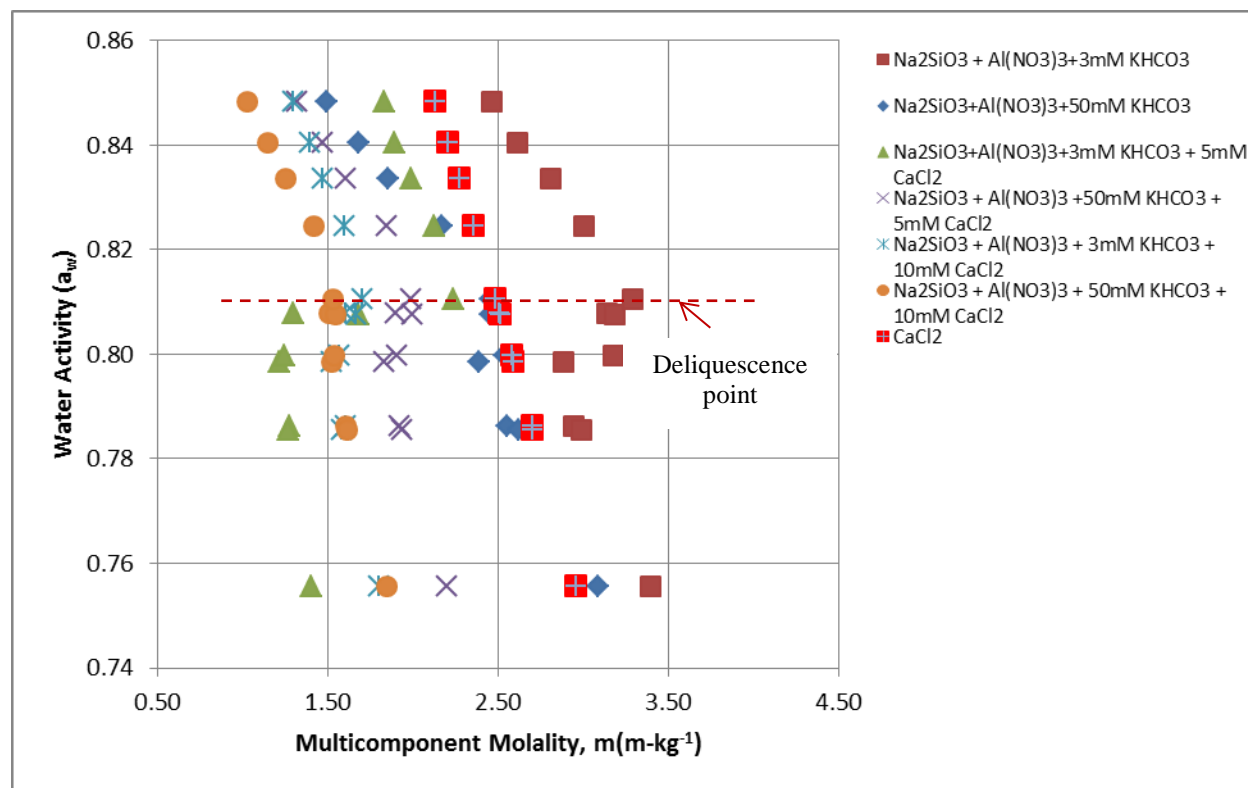


Figure 7. Water activities against molalities for the multicomponent samples using CaCl_2 standard.

The results show that the water activities for all multicomponent samples are similar and follow the same trend as the molality of the samples increased. There is some variability in the water activity data for a non-calcium sample comprised of 3 mM of bicarbonate [$\text{Na}_2\text{SiO}_3 + \text{Al}(\text{NO}_3)_3 + 3\text{mM KHCO}_3$]. However, starting from water activity value of 0.81, the visible break in the curve occurs for all samples. These results suggest that as humidity in the system increased, the deliquescence points for all multicomponent samples were obtained for $\text{RH} \geq 81\%$.

Figure 8 shows plots of the measured values of the osmotic coefficients against the molality of multicomponent samples. From Figure 8 it can be seen that as ϕ decreased with the increase in samples molality, a change in the slope indicates a possible solid–liquid transition. As an example, an arrow on Figure 8 represents the deliquescence point for the sample that contains $\text{Na}_2\text{SiO}_3 + \text{Al}(\text{NO}_3)_3 + 50\text{mM KHCO}_3$ and 10mM CaCl_2 . Similar changes in slope are visible for other sample compositions presented on Figure 8.

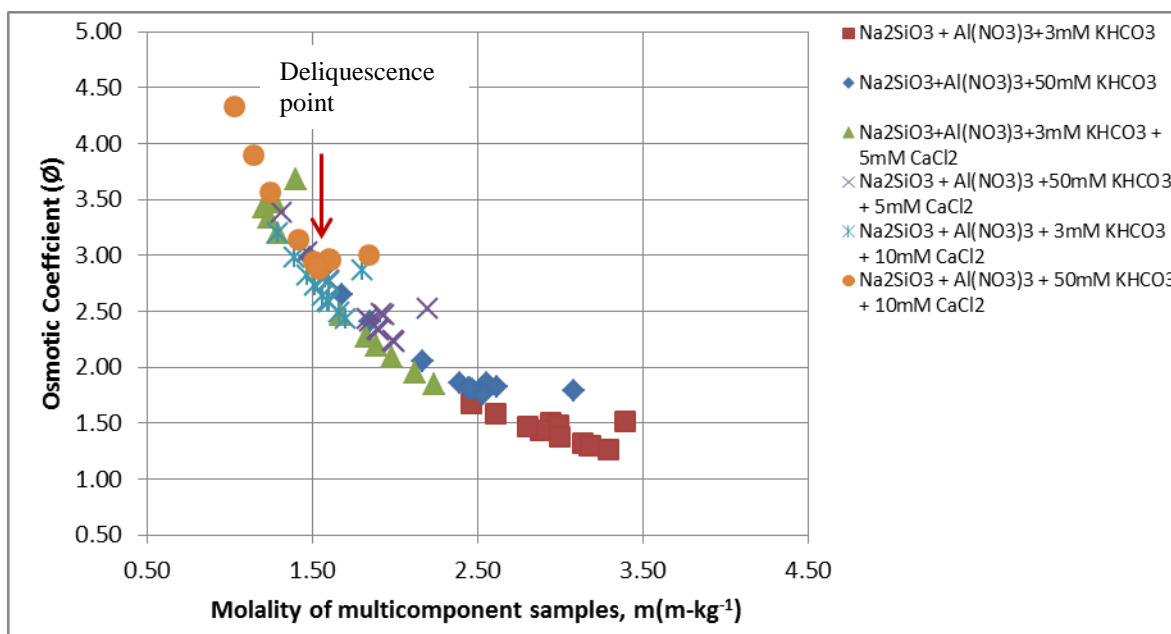


Figure 8. Osmotic coefficient vs. molalities for the multicomponent samples using CaCl_2 standard

The evaluation of the multicomponent samples indicated that the amount of sodium silicate comprises the major molar fraction for about 77-97%, depending on the samples' composition. It might be that the deliquescence behavior of the multicomponent precipitates is governed by the solubility of alkali silicate gel formed by the silicate ion polymerization reaction. The literature data on the deliquescence of polymerized silica is rather scarce and the isopiestic data can provide important insights on the solubility behavior of the multicomponent precipitates created in alkaline conditions as a result of the recrystallization of minerals due to ammonia gas injection in the subsurface. A sample of sodium silicate will be prepared in the next set to compare the solubility of dried silicate solids formed by the silicate ion polymerization with other multicomponent samples.

Fabrication of a new isopiestic chamber

The experiments performed with the isopiestic chamber fabricated from the commercially available pressure pot showed some limitations in the design. The chamber height was tall enough to hold an aluminum block with recessed holes to fit 15-mL crucibles. To reduce the weight of the chamber, the underside of the aluminum block was fabricated with slots, leaving some void space beneath the block. The block was tightly fit inside the chamber; however, it still has the possibility of accumulating water vapor in the voids on the underside of the aluminum block. To avoid this flaw in future experiments and to lower the weight of the chamber, a new design was initiated. In addition, decreasing the void spaces in the chamber and reducing the headspace above the crucibles cups would help to reach system equilibrium faster. Two identical chambers were designed from 6061 T6 aluminum to include 12 recesses for crucible cups in each vessel. The depth of each recess was designed the same (1.26 in) as in the previous chamber fabricated from the pressure pot. The distance between each row was determined by the dimensions of the nickel crucible lids. The negative rectangular boss was designed to house a sealing gasket of silicone with a shore durometer of 50A. The top and lateral port is for

degassing. The lateral port is threaded to receive a 1/4" male NPT thread to add a vacuum rated valve and a hose barb to connect to a vacuum line (Figure 9).

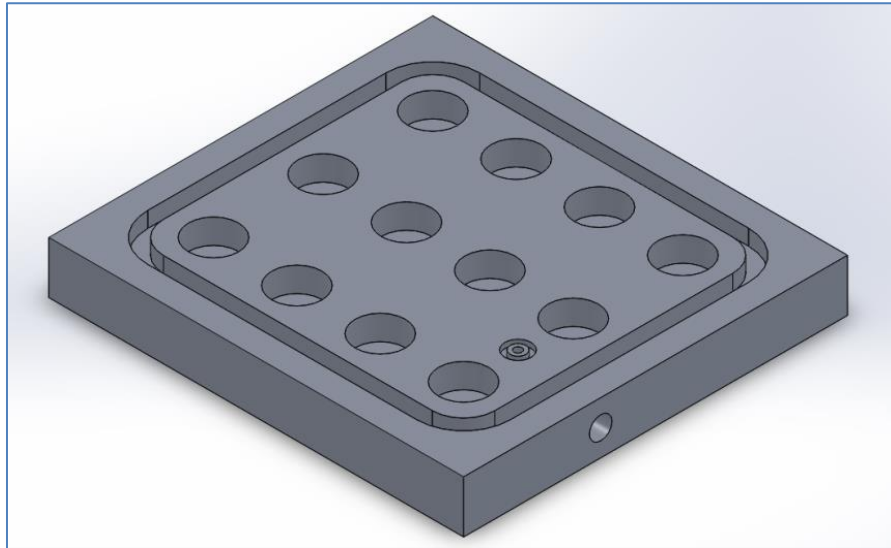


Figure 9. Aluminum block to fit crucible cups.

The underside of this plate consists of slots to reduce the overall weight and 1/4-20 threaded holes to mount the legs as seen in Figure 10.

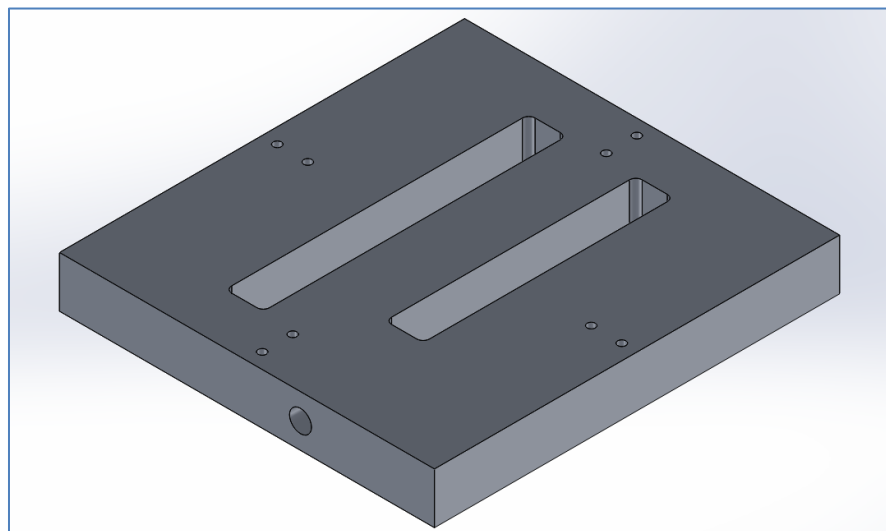


Figure 10. The underside of the chamber plate.

The design for the top required there to be a head space of about 2 cm above the lids of the crucibles. Since there will be a gasket to seal the chamber, the max height was set to 2 cm (0.787 in) and the minimum depth to about 1.86 cm (0.731 in) to prevent over compression of the gasket.

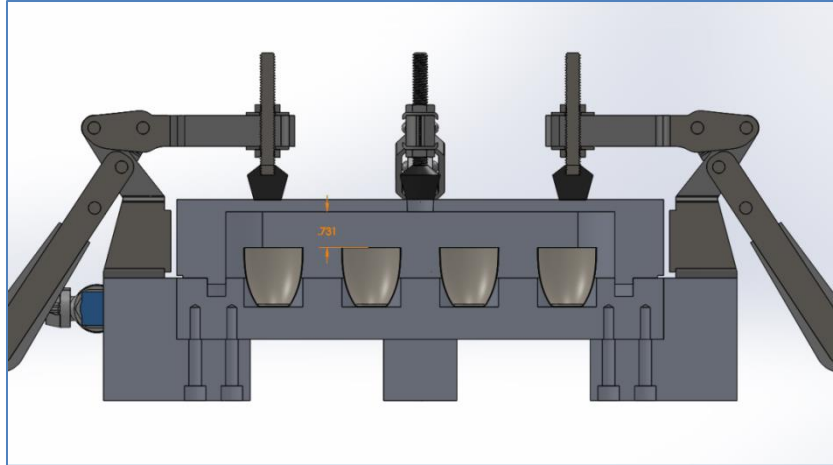


Figure 11. The full assembly of the isopiestic chamber with crucibles inside.

On the top of the lid, there is a $\frac{1}{4}$ NPT port for a gauge. On the bottom portion, there is a boss used to compress the gasket. Finally, for ease of closing the lid, toggle clamps were used and set on the legs as seen in Figure 11. The final assembly drawing is presented in Figure 12. The fabrication of the two new isopiestic chambers was completed and they were tested if they are properly sealed (Figure 13).

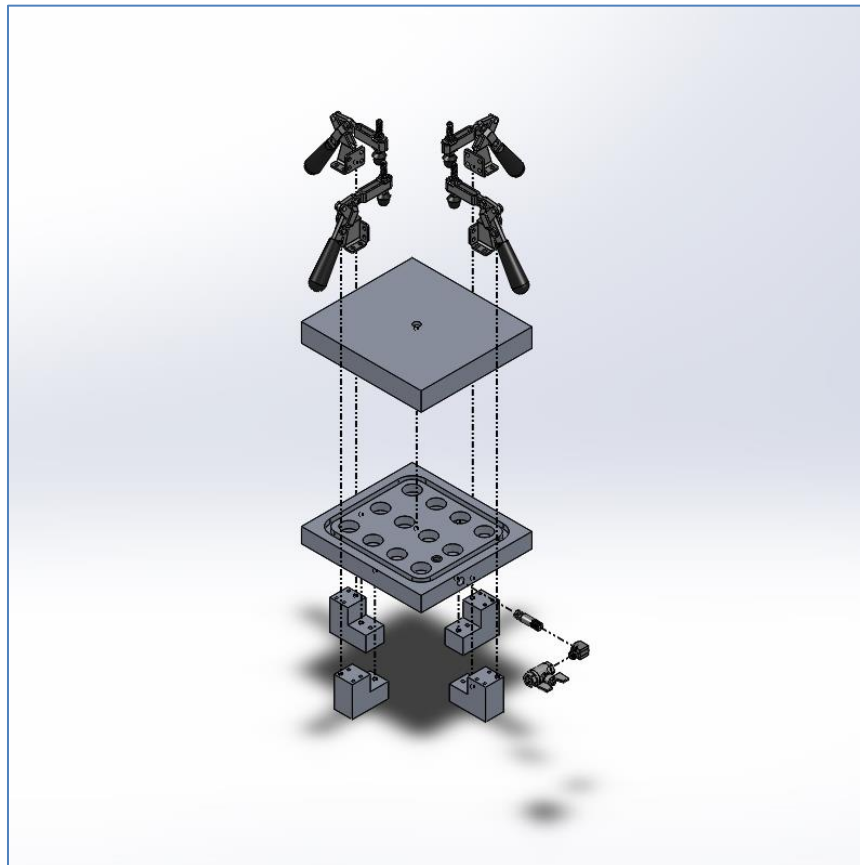


Figure 12. Drawing of the isopiestic chamber final assembly.

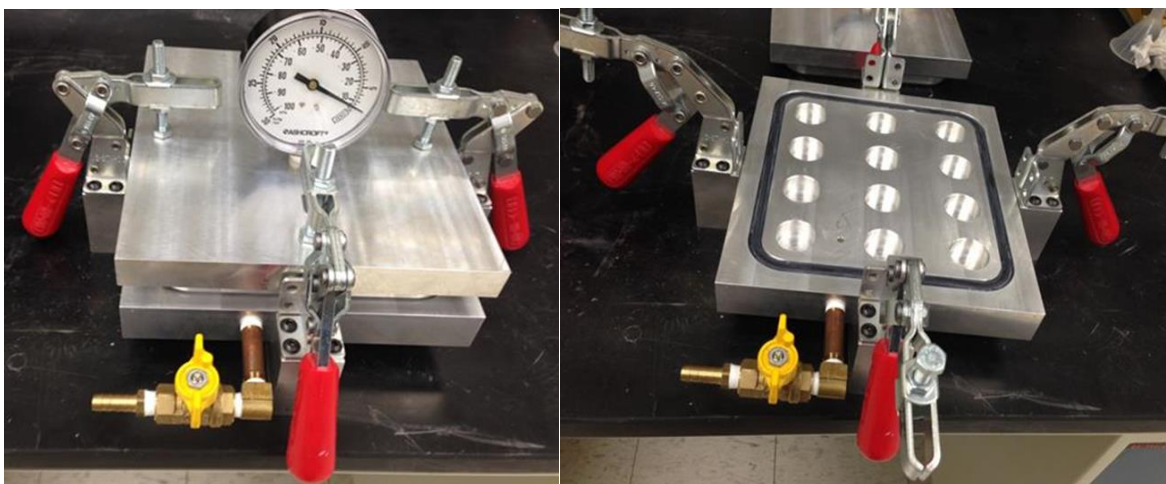


Figure 13. Fabricated new isopiestic chambers to continue the solubility experiments.

The new isopiestic chamber set-up that includes an environmental chamber, vacuum pump and balances was moved to the radiation lab to allow for the conduction of experiments with uranium-bearing samples (Figure 14).



Figure 14. A new isopiestic chamber set up in the FIU-ARC radiation laboratory.

Testing of a new isopiestic chamber set up

In order to evaluate the reliability of measurements obtained from a newly fabricated isopiestic chamber, two new reference standards, sodium (NaCl) and calcium chloride (CaCl_2), were

prepared and carefully weighed. Six samples of NaCl and three samples of CaCl₂ with varying weights were prepared from “ultra dry” grade chemicals. Then, each sample was amended with 20 uL of pure grade DIW and placed in the chamber. Table 5 presents information on the solute content in each crucible.

Table 5. Initial Weights and Molality Calculations for Standards NaCl and CaCl₂.

Crucible#	Standard Sample	Crucible + lid (g)	Standard Weight (g)	Solute Content (M)	Pure Water Added (g)	Crucible+lid + Standard (g)
13	NaCl	15.55070	0.15470	0.00265	0.0200	15.72540
15	NaCl	15.40052	0.23881	0.00409	0.0200	15.65933
20	NaCl	15.32886	0.41093	0.00703	0.0500	15.78979
21	NaCl	16.47894	0.85110	0.01456	0.0500	17.38004
22	NaCl	18.32013	1.53916	0.02634	0.0500	19.90929
23	NaCl	15.16116	2.36194	0.04042	0.0500	17.57310
24	CaCl ₂	16.90778	0.01763	0.00016	0.0200	16.94541
25	CaCl ₂	16.66326	0.05610	0.00051	0.0200	16.73936
26	CaCl ₂	19.63735	0.07249	0.00065	0.0200	19.72984

After equilibration and sample weighing, the obtained values of water activity (aw) for NaCl and CaCl₂ were compared with data published in the literature. Sample of standards were monitored for a period of three months with incremental increase in humidity levels in the system. This helped to determine if the system can achieve equilibrium and if the measurements for water activities and osmotic coefficients are reliable. This step is necessary to gauge the accuracy of isopiestic measurements using a new chamber prior to FIU starting to conduct experiments with U-bearing multicomponent solids samples. For each trial of sample weighing, osmotic coefficients and water activities were calculated at equilibrium conditions. Then, a specific water mass of 20-50 uL was added to each crucible before the chamber was closed to let the system equilibrate to a new humidity value.

The experimental molality measurements of the six NaCl samples in the system showed higher values than the NaCl isopiestic molality measurements available in the literature database. Therefore, the use of NaCl as reference to obtain the CaCl₂ experimental osmotic coefficients was not possible. The calculations for testing the reliability of the system were carried out using the three samples of CaCl₂, crucibles 24, 25, and 26. The molality of each solution was calculated based on the solute content and water weight measurements in each crucible. The osmotic coefficients of the CaCl₂ solution were calculated with the following Pitzer equation

$$\phi_{CaCl_2} = 1 - \frac{|z_{Ca} z_{Cl_2}| A_{\phi} I^{\frac{1}{2}}}{1 + b I^{\frac{1}{2}}} + \left(2 \frac{v_{Ca} v_{Cl_2}}{v} \right) m \left(\beta_{CaCl_2}^{(0)} + \beta_{CaCl_2}^{(1)} e^{-\alpha I^{\frac{1}{2}}} \right) + \left(2 \frac{v_{Ca} v_{Cl_2}}{v} \right) m^2 C_{CaCl_2}^{\phi} \quad \text{Eq 8}$$

In which ion strength I is given as

$$I = \frac{1}{2} \sum m_i z_i^2$$

The Debye-Huckel parameter A_ϕ was taken as 0.3915 at 25°C, b and α are the universal parameters generally considered to be 2 (kg-mol⁻¹)^{1/2}, the temperature dependent parameters Pitzer parameters $\beta_{CaCl_2}^{(0)}$, $\beta_{CaCl_2}^{(1)}$, and $C_{CaCl_2}^\theta$ are 0.31590, 1.61400, and -0.00034 respectively, taken from Pitzer, (1991); m_i is the molality of species i in the solution, and z_i is the valence of the species i . The calculated osmotic coefficients were compared to published data from Rard et al, (1997). This database includes isopiestic molality measurements in the range of 0.001 to 11 mol-kg⁻¹ for CaCl₂ (aq) at 25°C. The water activity (a_w) values were calculated by following Eq 2 and taken as a reference osmotic coefficient (ϕ_{ref}) calculated using the Pitzer Eq 8. The obtained osmotic coefficients (ϕ) and water activities (a_w) values of the CaCl₂ – H₂O system are shown in Table 6.

The relative percent error, Rel Err% was calculated by comparing the osmotic coefficient calculated using Pitzer Eq. 8 (ϕ^*) and the osmotic coefficient from the published data (ϕ^{**}) obtained by interpolating the database. The relative average relative percent error in the osmotic coefficient of CaCl₂ was 2.19% and the water activity standard deviation of CaCl₂ samples was 0.011. The water measurements suggested that water losses in the system due to sample weighing were in the range of 1.3-2.9%.

Table 6. Isopiestic Measurements for the CaCl₂ at 25°C

Crucible #	Solute Content (M)	Water Content (g)	Molality (m-k ⁻¹)	ϕ^* CaCl ₂	ϕ^{**} CaCl ₂	a_w	Rel Err ^a
24	0.00016	0.03859	4.1165	2.1780	2.2266	0.61596	0.0223
25	0.00051	0.11949	4.2305	2.2241	2.2726	0.60139	0.0218
26	0.00065	0.15238	4.2865	2.2465	2.1625	0.59426	0.0217

ϕ^* Pitzer Equation

ϕ^{**} Rard J and Clegg S., 1997

^aRelative Percent Error (Rel Err, %)= $|\phi^* - \phi^{**}| * 100/\phi^*$

Subtask 1.1: Future Work

Future work will focus on the deliquescence experiments using U-bearing solids. Two samples of a reference solution, CaCl₂, will be used to obtain values of osmotic coefficients and water activities for the experimental samples. FIU competed preparations of U-bearing samples to evaluate for solubility. Eight samples of 10 mL composed of Si-Al-Ca-HCO₃ and U(VI) have been prepared in tarred crucibles and kept at 35°C for drying. The concentration of U(VI) was kept constant in all samples as 2ppm. This concentration is similar to what was used in the earlier conducted study to investigate the effect of Si and Al concentration ratios on the removal of U(VI) in alkaline conditions by NH₃. The concentration of sodium silicate and aluminum was unchanged for all samples, 100 mM and 5 mM, respectively. Four samples were prepared with 3 mM bicarbonate and amended with 0 mM, 5 mM, 10 mM and 15 mM of calcium chloride. Another four samples were prepared with 50 mM of bicarbonate and amended with the same concentrations of calcium chloride as the 3 mM bicarbonate samples. All dried U-bearing multicomponent samples along with three CaCl₂ standards were placed in the isopiestic chamber. Chamber was sealed and degasses and left at 25°C in the environmental chamber.

The isopiestic chamber will be opened to weigh the samples when the system reaches equilibrium in order to investigate the deliquescence behavior of uranium-bearing multicomponent solids. The obtained results will be compared with the deliquescence data obtained for the study on U-free multicomponent solids.

Subtask 1.1: Acknowledgements

Funding for this research was provided by U.S. DOE cooperative agreement DE-EM0000598. We truly appreciate Dr. Mirosław Gruszkiewicz from ORNL for the valuable suggestions on these experiments. The isopiestic chamber was fabricated in ARC's machine shop with the support of engineers Amer Awwad and Jairo Crespo.

Subtask 1.1: References

- Blanko LH, Amadoa E, Avellaneda JA, 2006. Isopiestic determination of the osmotic and activity coefficients of dilute aqueous solutions of the series MeEt3NI to HepEt3NI at 298.15K. *Fluid Phase Equilibria* 249, 147–152.
- Carroll, Alai M, Craig L, Gdowski G, Hailey P, Nguyen AQ, Rard J, Staggs K, Sutton M, Wolery T, 2005. Chemical Environment at Waste Package Surfaces in a High-Level Radioactive Waste Repository. Lawrence Livermore National Laboratory, report UCRL-TR-212566.
- Giammar DE, and JG Hering, 2002. Equilibrium and Kinetic Aspects of Soddyite Dissolution and Secondary Phase Precipitation in Aqueous Suspension." *Geochimica Et Cosmochimica Acta*. 66,18 p.3235-3245.
- Gorman-Lewis D, Burns PC, Fein JB, 2008. Review of Uranyl Mineral Solubility Measurements. *J. Chem. Thermodynamics*, 40, p.335–352
- Gruszkiewicz MS, Palmer DA, Springer RD, Wang P, Anderko A, 2007. Phase Behavior of Aqueous Na–K–Mg–Ca–Cl–NO₃ Mixtures: Isopiestic Measurements and Thermodynamic Modeling. *J Solution Chem*, 36, p. 723–765
- Hamer, WJ and Yung-Chi Wu, 1972. Osmotic coefficients and mean activity coefficients of uni-univalent electrolytes in water at 25o C. *J. Phys. Chem Ref Data*, vol. 1, 4.
- Pitzer, K.S., 1991. 2nd ed. Activity Coefficients in Electrolyte Solutions, vol. I. CRC Press, Boca Raton, FL., pp. 75-153.
- Rai D, Xia Y, Rao L, Hess N J, Felmy A R, Moore DA, and McCready DE, 2005. Solubility of (UO₂)₃(PO₄)₂·4H₂O in H⁺-Na⁺-OH⁻-H₂PO₄⁻ -HPO₄²⁻ -PO₄³⁻ -H₂O and Its Comparison to the Analogous PuO₂⁺ 2 System. *Journal of Solution Chemistry* 34, 4. DOI: 10.1007/s10953-005-5216-4
- Rard J, 1985. Solubility determinations by the isopiestic method and application to aqueous lanthanide nitrate at 25°C. *Journal of Solution Chemistry*, 14, 7, p.457-471.
- Rard J and Platford R, 2000. Experimental method: isopiestic, Chapter 5 in Activity coefficients in the electrolyte solutions edited by K.Pitzer, CRC press, Boca Raton, Florida
- Rard JA and Platford R F, 1991. Experimental Methods: Isopiestic. In Activity Coefficients in Electrolyte Solutions, 2nd ed.; Pitzer, K. S., Ed.; CRC Press: Boca Raton, FL, Chapter 3.
- Rard, J. A., and Clegg, S. L., 1997. Critical Evaluation of the Thermodynamic Properties of Aqueous Calcium Chloride. *J. Chem. Eng. Data*, 42, 819–849.
- Reid, R.C., Prausnitz, J.M., and Poling, B.E., 1987. The properties of gases and liquids (4 th ed). New York, McGraw-Hill. Serne RJ, MJ Lindberg, SR Baum, GV Last, RE Clayton, KN

- Geiszler, GW Gee, VL LeGore, CF Brown, HT Schaef, RD Orr, MM Valenta, DC Lanigan, IV Kutnyakov, TS Vickerman, CW Lindenmeie, 2008. Characterization of Vadose Zone Sediment: Borehole 299-E33-45 Near BX-102 in the B-BX-BY Waste Management Area. 2002. PNNL-14083. Contract DE-AC06-76RL01830.
- Staples B. and Nuttall R, 1977. The activity and osmotic coefficients of aqueous calcium chloride at 298.15 K. J. Institute for Materials Research, National Bureau of Standards, Washington, DC 20234.
- Szecsody JE, Truex MJ, Zhong L, Johnson TC, Qafoku NP, Williams MD, Greenwood WJ, Wallin EL, Bargar, JD, Faurie DK, 2012. Geochemical and Geophysical Changes during Ammonia Gas Treatment of Vadose Zone Sediments for Uranium Remediation. Vadose Zone Journal, 11, 4. doi: 10.2136/vzj2011.0158

Subtask 1.1.1: Characterization of New Uranium-Bearing Samples

Subtask 1.1.1: Introduction

The combination of unintended and intentional discharge of hazardous waste into the Hanford subsurface has resulted in the contamination of the central plateau vadose zone. A complicated effort to mitigate the impact of mobile radiochemical species (i.e.: uranium) on the ecosystem has focused primarily on sequestering the pollutants via in situ remediation amendments. The injection of reactive gases in particular has been favored for the treatment due to the advantages of limiting the addition of liquids into the subsurface, which could further mobilize the slow moving pore water contaminants. Among the most promising approaches to handling uranium in the vadose zone is the injection of ammonia gas (NH_3) to reduce the mobility of the contaminants by changing the chemistry of vadose zone (Szecsody et al., 2010).

Succinctly, the remediation technology is believed to function by injecting the reactive ammonia gas to raise the pH of the pore water, which resides in the interstitial space of the unsaturated vadose zone, to alkaline levels. This is thought to promote the partial dissolution of subsurface minerals. When the natural buffer capacity of the environment causes the re-establishment of natural pH conditions, the re-precipitation of mineral phases is thought to reduce the mobility of uranium phases, likely by physically containing them. Past studies by Pacific Northwest National Laboratory (PNNL) scientists have associated the use of this amendment with a reduction in uranium mobility on a laboratory scale (Szecsody et al., 2012).

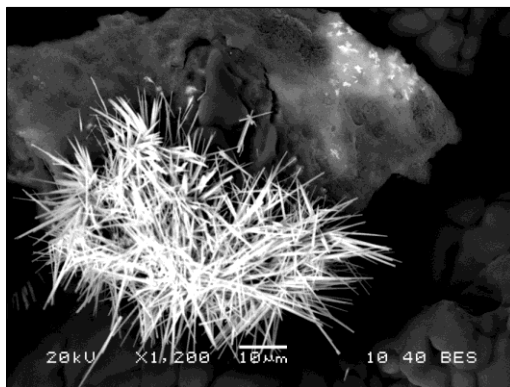


Figure 15. SEM image showing the crystalline uranium phases of interest

Prior studies made use of a combination of scanning electron microscopy with energy dispersive spectroscopy (SEM with EDS) and X-ray diffraction (XRD) analysis to attempt to determine the morphological and mineralogical characteristics of the uranium solid phases produced. The observation of crystal-like uranium phases (Figure 15) by SEM and EDS was used as criteria to select samples for XRD analysis. The diffraction analysis of those samples revealed potential matches for cejkaite ($\text{Na}_4(\text{UO}_2)(\text{CO}_3)_3$), though it is believed that the overwhelming presence of nitratine (NaNO_3) limited the ability to detect other mineral phases (Figure 16)(Lagos et al., 2013).

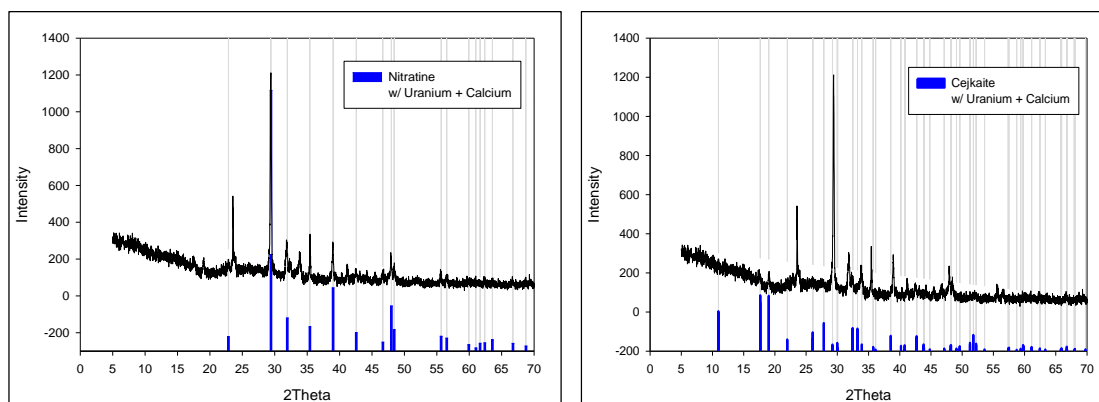


Figure 16. Comparisons of the XRD patterns for uranium bearing precipitates with nitratine (left) and cejkaite (right)

The results of this previous research directed the study towards increasing the uranium content in pore water solutions to increase the presence of the uranium phases in precipitates and prevent the analytical interference believed to be caused by excessive nitratine formation (Lagos et al., 2013). These modified sample preparation methods resulted in samples that showed uranium-rich phases, but did not show the crystal-like phases expected based on prior sample analysis. For this reason they were largely omitted from the additional ongoing sample analysis, though they will be revisited.

This report summarizes the ongoing investigation of solid samples produced with the application of the remediation technique to a synthetic pore water designed to be relevant to the Hanford 200 Area vadose zone conditions. Additional analytical approaches to conclusively characterize and identify the uranium phases being formed were planned and undertaken. These include the expansion of geochemical modeling ability, the modification of sample preparation methodology, and most significantly, the shift from XRD to transmission electron microscope (TEM) analysis for the purpose of selective area electron diffraction (SAED).

Subtask 1.1.1: Materials and Methods

The sample preparation methods for samples used in TEM analysis remain largely the same as has been described in prior studies (Lagos et al., 2013). The synthetic pore water solutions used were formulated using stock solutions of various salts and combined to achieve the final concentrations selected for said samples (Table 6). Initially, the KHCO_3 , Na_2SiO_3 , and $\text{Al}(\text{NO}_3)_3$ components were combined in a 50mL vial. From there, nitric acid is used to pH adjust the alkaline solution and reach the 7 – 8 range, which is representative of the pore water conditions in the Hanford vadose zone. At this point, the solutions are treated with ammonia gas until the system is within range of the desired final pH of 11. Immediately after ammonia gas treatment, the final components, CaCl_2 and $\text{UO}_2(\text{NO}_3)_2$, are added as small volumes of concentrated solutions to minimally effect total concentrations. After a 2 week reaction period, the solid precipitate phase and supernatant are separated and stored for analysis.

Table 6. Stock Solution & Synthetic Pore Water Concentrations for Sample Preparation

Stock Solution	Concentration (mM)		Synthetic Pore Water Concentrations (mM)	
CaCl₂·2H₂O	2500.00		5 – 10	
KHCO₃	400.00		50	
Na₂SiO₃·9H₂O	422.24		100	
Al(NO₃)₃	50.00		5	
UO₂(NO₃)₂·6H₂O	4.2	210.06	0.84 (200 ppm)	2.1 (500 ppm)
5% NH₃ in N₂ (g)	Bubbled into solution until pH ≈ 11			

TEM Sample Preparation & Analysis

For analysis using transmission electron microscopy, samples were required to be suspended in solution and deposited on copper TEM micro-grids. This sample preparation was preceded by a short extraction experiment in order to determine the suspending solution which would least effect the immobile uranium analytes.

Sample specimens were limited to those which were known to have shown uranium-bearing crystal phases (Figure 15) using scanning electron microscopy and energy dispersive spectroscopy. This decision ruled out the elevated uranium (500 ppm) samples, prepared using methods modified specifically to overcome the limitations associated with the low analyte content in sample analysis. Samples selected for TEM analysis were prepared by the approach reported in previously reported studies with constituent concentrations detailed in Table 7.

Table 7. Concentrations of Primary Constituents

[Si]	[Al ³⁺]	[Ca ²⁺]	[HCO ₃ ⁻]
100 mM	5 mM	5 & 10 mM	50 mM

The preparation of sample suspensions required the selection of a solution which would least interfere with the solid uranium phases being targeted by analysis. The solutions tested were suspensions of a sample known to contain solid uranium phases, based on SEM-EDS analysis, prepared in methanol, ethanol, and isopropanol. Because of the expected mobility of the uranium phases, a suspension was prepared using water to serve as a control group. It was decided that the most suitable criteria for comparing the suspensions would be the average amount of uranium extracted from solid sample phase, as detected by kinetic phosphorescence analyzer.

Suspensions were prepared with a 10-to-1 (mg/mL) solid-to-liquid ratio (Table 8) for the extraction experiments to ensure concentrations would be relative. The mixtures were vortexed individually over the course of a 2 minute extraction. From there, samples were weighed and centrifuged at 2500 rpm for two minutes to separate the liquid phase from the solid samples. The supernatant solutions were filtered before undergoing sample preparation procedures for KPA analysis.

Table 8. Extraction Experiment Solid-to-Liquid Ratios

Suspension Solutions	Mass Sample (mg)	Volume Solvent (mL)
DI Water (control)	23	2.3
Methanol	20	2.0
Ethanol	20	2.0
Isopropanol	22	2.2

The KPA analysis of the sample extracts showed that the ethanol and isopropanol suspensions removed negligible amounts from the uranium-bearing solid phases (Table 9). Based on this data, ethanol was selected over isopropanol for TEM suspensions due to incompatibility of the latter solvent with some lab materials.

Table 9. Uranium Content of Suspension Extractions

Extraction Solution	Uranium Concentration ($\mu\text{g/L}$)	
	100x Diluted	1000x Diluted
DI Water	301.79	21.524
Methanol	0.682	~0
Ethanol	0	0
Isopropanol	0	~0

Samples selected for TEM analysis were known to contain uranium-rich, crystal-like solids. Consistent throughout the makeup of those samples was the use of 200 ppm of uranium and 5-10 mM of calcium in the pore water solutions. Suspensions were initially prepared with the 10-to-1 solid-to-liquid ratios used in extraction experiments. The suspensions were agitated over the course of one hour in a Branson 2510 sonicator in order to disperse the solid particulates (Figure 17). Due to incomplete dispersion, samples were further diluted and sonicated for an additional hour. From these suspensions, a single drop was deposited onto copper TEM micro-grids coated with a carbon mesh. The prepared TEM samples were then allowed 24 hours to dry.

**Figure 17. TEM suspensions undergoing sonication to disperse solids**

For TEM imaging and selective area electron diffraction, the assistance of FIU's Advanced Materials Engineering Research Institute (AMERI) were employed. The facilities instrumentation included a Phillips CM-200 200 kV Transmission Electron Microscope though the system's Energy Dispersive Spectroscopy (EDS) unit was not available. Though the lack of EDS capability was considered a hindrance to effective characterization, the analysis went on with the intentions to work around the deficiency.

Geochemical Modeling for Speciation Prediction

To support the sample characterization data being collected in the lab, the details of the system components were input into prediction based geochemical equilibrium modeling software. The modeling software was used to attempt to simulate the changes that occur with the application of the remediation method to pore water solutions. The results of those predictions could be used to determine the likely mineral phases being formed, allowing them to be considered in ongoing characterization studies. Similarly, the likelihood of formation of a particular mineral phase could be tested under various simulated conditions.

Though geochemical modeling software has been used in past analysis, the variety and understanding of the software was increased with the assistance of colleagues at Pacific Northwest National Laboratory well versed in its application to environmental simulations. The two most recommended tools were Visual Minteq (VM), which has been used often in previous research, and Geochemist's Workbench (GW), which has not. Despite their many differences, it was thought that the similarities between the GW's React module and the VM interface were significant enough to allow for a steep learning curve (Figure 18).

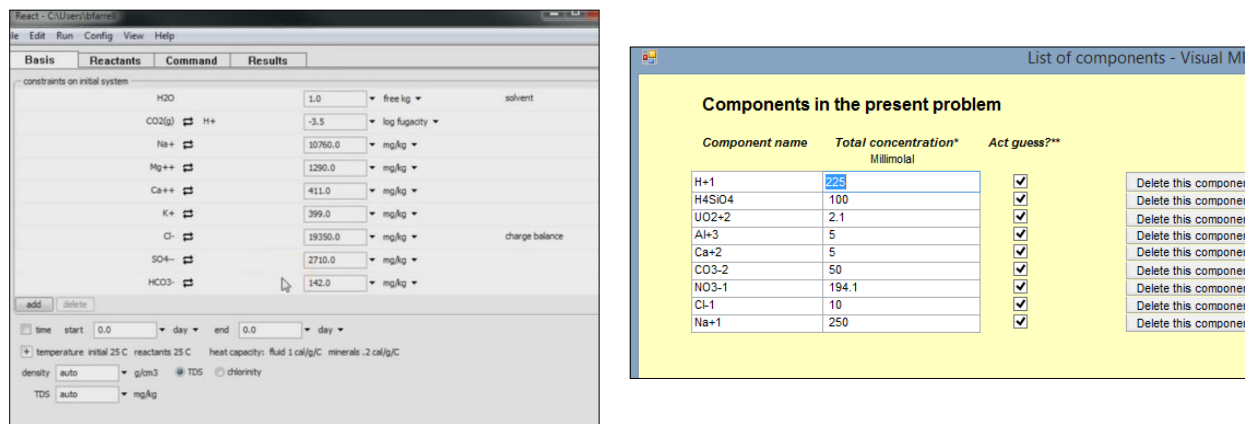


Figure 18. Example component input for geochemical modeling software

Subtask 1.1.1: Results and Discussion

Transmission Electron Microscopy for SAED Analysis

The sample extraction experiment was considered successful for determining the solvent (ethanol) which would least effect the uranium phase for suspension preparation. The TEM analysis of those samples was problematic in that few areas with clear diffraction patterns were detected. This is possibly related to the fact the instrument used did not have the ability to tilt and rotate the samples in order to optimize the angle of the incident electron beam. Though diffraction capable crystalline material was identified in the samples (Figure 19), there were occasions where the focus of the incident electron beam cause the material to either dislocate or shrink before diffraction could be done. The cause of this is unclear.

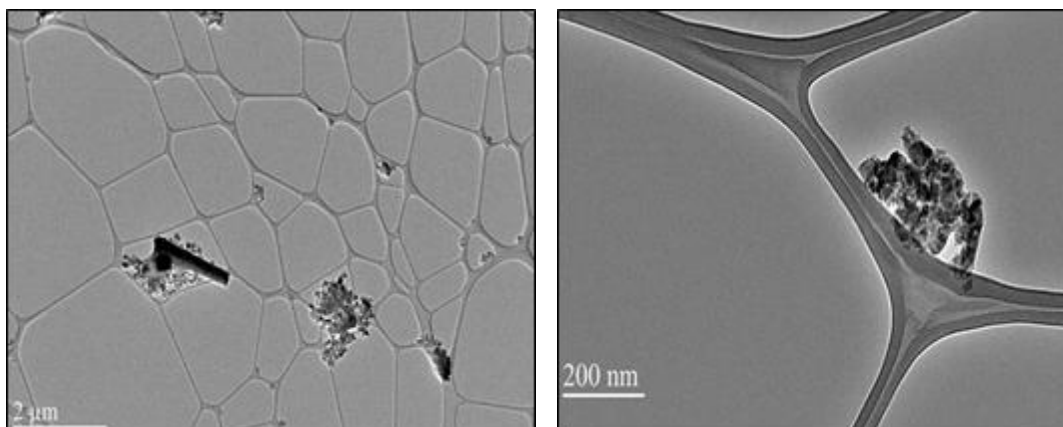


Figure 19. TEM images of sample fragments attached to carbon mesh of TEM micro-grid

Areas where crystalline lattices were detected were selected for electron diffraction. In the instances where the fragment did not dislodge from the mesh, diffraction patterns were captured (Figure 20). The pattern of rings, rather than a constellation-like pattern of discrete dots is used to classify the material as polycrystalline, rather than a single crystal of any type.

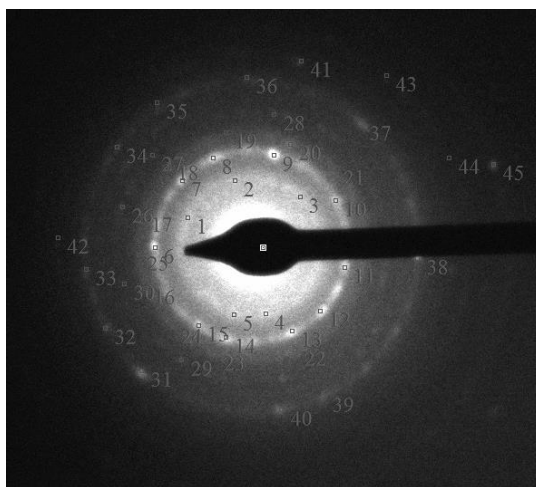


Figure 20. Selective area electron diffraction pattern for detected crystalline phase

Multiple points were measured from the center of the diffraction pattern to the fringe of each ring that encircled it. That data (Table 10) was used to calculate the d-spacings present for this diffraction pattern. Comparison to the diffraction information for most of the expected mineral phases showed no discernable match.

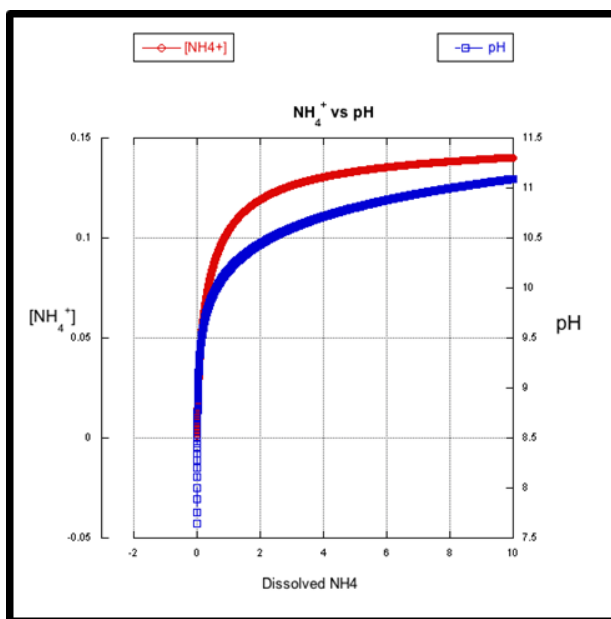
Table 10. Average d-spacings as determined by diffraction pattern analysis

Ring	Average d-Spacing (Å)
1	2.5832
2	1.9276
3	1.5561
4	1.2952
5	1.0810

This course of TEM analysis will continue with new samples modified to increase the yield of the uranium solid phase and minimize the presence or interfering minerals.

Geochemical Modeling

Simulations were run using both Visual Minteq and Geochemist's Workbench with mixed results. Despite the similar interfaces, the limited experience with GW resulted in several failed simulations and few successful ones. Visual Minteq was used to simulate several varying instances of the experimental system and evaluate associated speciation changes. Initially, the VM sweep function was used to prove that the pH of the system could be managed by the concentration of ammonium (NH_4^+) in solution (Figure 21). This was intended to simulate the effect of injecting reactive ammonia gas, rather than simply allowing the system to manipulate the pH. From there, further manipulations of the system used the change in ammonium concentration to manipulate the pH and observe the predicted chemical changes.

**Figure 21. Changes in pH associate with increasing dissolved NH_4^+**

Among the more interesting results simulated with this method was the impact of changing pH on the presence of uranyl carbonates in the system (Figure 22). With the increasing pH, we see the decrease of calcium uranyl carbonate ($\text{Ca}_2\text{UO}_2(\text{CO}_3)_3$) in the system with a proportional increase in $\text{CaUO}_2(\text{CO}_3)_3^{2+}$. As pH conditions approach 11, the concentrations of both calcium

bearing species begin to decrease while the relatively miniscule concentration of uranyl carbonate ions ($\text{UO}_2(\text{CO}_3)_3^{4+}$) in solution increase. This is consistent with that is expected of uranyl phases with the increasing pH conditions. It is hypothesized that as the pH returns to natural conditions (~ 8), the reverse would occur and uranyl carbonates would be the phases precipitating out of the solution.

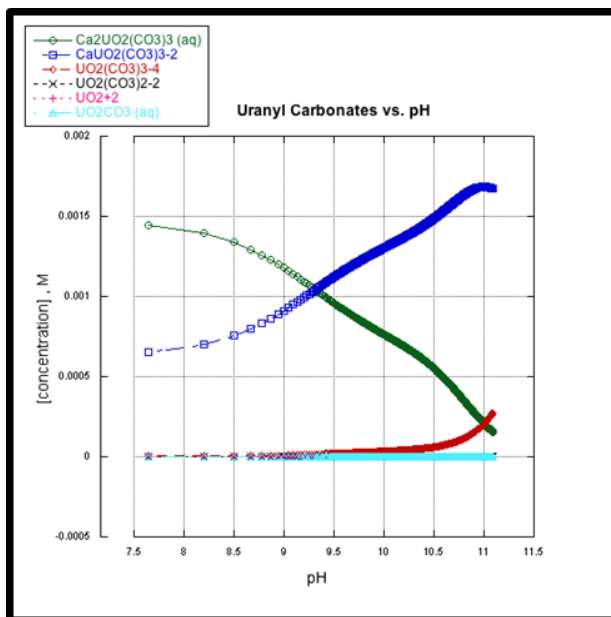


Figure 22. Speciation changes for uranyl-carbonate species with increasing pH (by NH_4 increase)

The produced speciation prediction models are severely hindered by the lack of thermodynamic data for the many other uranyl minerals capable of being formed. Specifically, the lack of information needed to confirm simulate the hypothesized formation of cejkaite ($\text{Na}_4(\text{UO}_2)(\text{CO}_3)_3$), which was detected in XRD analysis of samples.

Subtask 1.1.1: Future Work

The short extraction study will be repeated with additional replicates for statistical purposes. During this re-run, the mass of solid used will be increased and retained post-extraction for SEM-EDS analysis. This additional data will be useful for validating the analytical approach for publication.

It is strongly believed that the TEM analysis was hindered by limitations of the available instrumentation. The availability of EDS analysis to confirm that any crystalline phases being analyzed were in fact uranium bearing phases and the ability to vary the angle of the incident electron beam to maximize the potential of locating uranium crystalline phases are invaluable to the success of this analysis. For this reason, a proposal for experimental analysis using the advanced facilities of PNNL's Environmental Molecular Sciences Laboratory (EMSL) has been submitted for consideration. The proposed work would include the use of electron microprobe (EMP), focused ion beam (FIB), and high resolution transmission electron microscopy (TEM) analysis.

As proposed, the EMP analysis would be used to map and quantitatively determine elemental content, allowing for the estimation of a molecular formula. This would rely on using associations and ratios of elements present in high uranium areas. The focal point of the proposed work is the combination of FIB and TEM analysis. The ion milling function of FIB will be used to section off a uranium rich fragment from a sample greatly increasing the effectiveness of TEM selective electron diffraction.

Since highlighted geochemical modeling data was collected, expanded mineral libraries have been added to the system. Geochemical simulations of the experimental system will continue to be run using the new data made available. The new simulations will be compared to the findings of the data retrieved on completion of the proposed experimental analysis.

Subtask 1.1.1: Acknowledgements

Funding for this research was provided by the U. S. DOE cooperative agreement DE-EM0000598. We would like to acknowledge Mr. Tom Beasley from FIU/FCAEM for his assistance with SEM/EDS, Dr. Yusuf Emirov from FIU/AMERI for his assistance with TEM analysis, and Dr. Jim Szecsody from PNNL for his assistance with geochemical modeling software.

Subtask 1.1.1: References

- Lagos, L., Katsenovich, Y., Gudavalli, R., Cardona, C., Musaramthota, V., Sepulveda, P., et al. (2013). Year-end technical report - rapid deployment of engineered solutions for environmental problems at Hanford. Florida International University's Applied Research Center.
- Szecsody, J. E., Truex, M. J., Zhong, L., Johnson, T. C., Qafoku, N. P., Williams, M. D., et al. (2012). Geochemical and geophysical changes during ammonia gas treatment of vadose zone sediments for uranium remediation. *Vadose Zone Journal*, 11(4)
- Szecsody, J. E., Truex, M. J., Zhong, L., Williams, M. D., Resch, C. T., & McKinley, J. P. (2010). Remediation of uranium in the Hanford vadose zone using gas-transported reactants (PNNL-18879) Pacific Northwest National Laboratory.

Subtask 1.2: Investigation on Microbial Meta-Autunite Interactions - Effect of Bicarbonate

Task 1.2: Introduction

Uranium is a key soil and groundwater contaminant at many U.S. Department of Energy sites, serving a leading role in the nation's defense for over 50 years. Uranium contamination of soil and groundwater is of great environmental concern due to the toxicological properties of the uranyl species. The behavior of uranium and its mobility in the subsurface is affected by various factors such as porewater and groundwater chemical composition, soil mineralogy, and micro-organisms that thrive under these conditions. Uranium exists in four oxidation states but, under oxidizing conditions, it dominates as a highly soluble and stable uranyl ion, UO_2^{2+} . In neutral or basic pH conditions, uranium undergoes hydrolysis in aqueous solutions and can readily complex with a wide variety of ligands such as carbonate, nitrate and phosphate. In a bicarbonate-rich environment, carbonate anions are an important complexing agent for U(VI), and soluble uranyl-carbonate complexes are formed, such as negatively charged $\text{UO}_2(\text{CO}_3)_2^{2-}$ and $\text{UO}_2(\text{CO}_3)_3^{4-}$, as well as neutral complexes such as UO_2CO_3^0 (Bachmaf et al., 2008). The presence of carbonates clearly affects the dissolution of actinides and facilitates uranium desorption reactions from soil and sediments, thus increasing uranium mobility in natural waters (Langmuir, 1978). The above mentioned complexes have been identified in contaminated pore water at the Hanford Site, Washington State, and have been shown to inhibit the microbial reduction of U(VI) (Bernhard et al., 2001; Brooks et al., 2003).

The addition of tripolyphosphate amendments is one of the methods to decrease the concentration of soluble uranium in contaminated plumes. The introduction of sodium tripolyphosphate into uranium-bearing saturated porous media results in the formation of uranyl phosphate solid phases (autunite) of general formula $\{\text{X}_{1-2}[(\text{UO}_2)(\text{PO}_4)]_{2-1} \cdot n\text{H}_2\text{O}\}$, where X is a monovalent or divalent cation. The stability of the uranyl phosphate solids in the subsurface is a critical factor that allows for determining the long-term effectiveness of the sodium tripolyphosphate remediation strategy. The presence of soil bacteria can affect uranium mobility significantly. Bacteria, in an effort to obtain phosphorous, a vital nutrient for their metabolism, may dissolve uranyl-phosphate minerals, thus liberating uranium in the aqueous phase. In addition to the biological activity, the presence of bicarbonate ions seems to enhance the release of U(VI) into the aqueous phase (Gudavalli et al., 2013b). Natural systems are complex and their behavior is dictated by the synergistic and/or antagonistic effect of both biotic and physico-chemical factors.

The Columbia River, adjacent to the Hanford Site, exhibits large stage variations, causing fluctuations in the water table. These water table fluctuations and multiple rise-and-fall cycles in the river created an oxic-anoxic interface in this region. Previous assessments of Hanford sediment samples collected from this area noted a decline in cultivable aerobic bacteria and suggested the presence of facultative anaerobic bacteria (Lin et al., 2012). *Shewanella oneidensis* MRI is one of the most common bacterial groups found in Hanford sediment samples (Lin et al., 2012; Marshall et al., 2008). Therefore, understanding the role of facultative and anaerobic bacteria (e.g., *Shewanella*) as one of the factors affecting the stability of autunite solids is very important for designing a successful environmental remediation strategy.

The objective of this research is to investigate autunite dissolution in the oxygen-restricted conditions by focusing on the bacterial strains of *Shewanella Oneidensis MR1* sp. There have been a few studies on the microbial dissolution of autunite in the anaerobic conditions examining a dissimilatory metal-reducing bacteria (DMRB) (*Shewanella putrefaciens 200R*) (Smeaton et al., 2008) and *Shewanella oneidensis MR1* (Sheng & Fein, 2013; Sheng & Fein, 2014). Previous experiments with aerobic *Arthrobacter oxydans* strains illustrated a bio-enhanced release of U(VI) from natural Ca-autunite in the presence of various concentrations of bicarbonate. *Arthrobacter* strains, G968 and G975, which exhibited various degrees of tolerance to U(VI) toxicity, were able to bio-enhance the release of U(VI) from natural Ca-autunite at almost the same capacity (Katsenovich et al., 2012a). Previous research by Bencheikh-Latmani and Leckie (2003) and Katsenovich (Katsenovich et al., 2012b) has also suggested that uranyl-carbonate complexes formed in the solution do not strongly interact with the negatively charged bacterial surface, which in turn can mitigate U(VI) toxicity on cells.

Task 1.2: Materials and Methods

Bicarbonate media solution preparation

The media solution was prepared in 1 L of DIW buffered with 0.02M Na-Hepes buffer with pH adjusted to 7.1 with 0.1 mol/L HCl or NaOH. Sodium lactate ($C_3H_5NaO_3$, 60% w/w) was added to the solution with a concentration of 0.024 mol/L. The solution was divided into four 250-mL bottles and sterilized by autoclaving at 121°C, 15 psi for 15 min and cooled at room temperature. As the experiment is based on the investigation of bacteria interactions in the presence of different bicarbonate concentrations, potassium bicarbonate salt was added to the autoclaved bottles to obtain one bottle each of 3 mM, 5mM and 10 mM bicarbonate; the remaining bottle was kept bicarbonate free. This accounts for a total of four concentrations of bicarbonate for the experiment tested. Next, the solutions were filter-sterilized into other sterile 250-mL bottles. Finally, the sterile bottles were stored in the anaerobic chamber until the beginning of the experiment.

Shewanella Oneidensis MR1 culture growth conditions

Shewanella Oneidensis MR1 strains (Figure 23), was obtained from the Pacific Northwest National Laboratory (PNNL). Fresh culture was grown on sterile hard and liquid Luria-Bertani (LB) media prepared with 10.0 g of tryptone, 5.0 g of yeast extract, and 10.0 g of sodium chloride, with a pH of 7.0. Hard media required an addition of 15.0 g of agar.

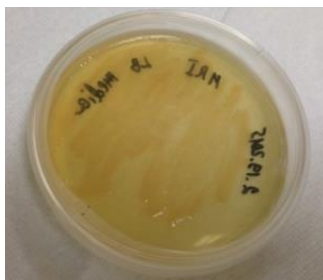


Figure 23. Petri dish with grown culture of *Shewanella oneidensis MR1*.

Fresh culture was grown in 15-mL tubes placed in the incubator for two days at 30°C, as shown in Figure 24:

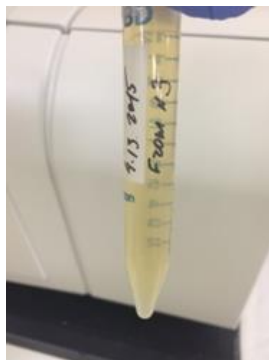


Figure 24. Fresh culture of *Shewanella oneidensis* MR1 grown in liquid LB media.

Bacterial cells were harvested in the late logarithmic phase of growth and cell density (cells/mL) was calculated with a glass hemocytometer (Fisher Scientific, Pittsburg, PA) to determine the concentration of a stock solution and estimate a desired volume (mL) of a bacterial suspension needed for the inoculation of each bottle. In addition, fresh bacterial culture was preserved in 25% glycerol at -80°C.

Sterile 100-mL serum bottles prepared in triplicate for each bicarbonate concentration tested were used as mixed bioreactors for experimentation. Each bottle contained 50 mL of sterile bicarbonate-bearing media buffered with 20 mM HEPES-Na and 90 mg of meta-autunite to provide a U(VI) concentration of 4.4 mmol/L. This concentration was used to compare results with previous data obtained in the autunite mineral dissolution experiments using *Arthrobacter* strains, G968 and G975 (Katsenovich et al., 2012a; Sepulveda, et al., 2015) and in the research conducted by Liu et al. on the dissolution of Na-boltwoodite in anaerobic conditions by *Shewanella oneidensis* strain MR-1 (Liu et al., 2007). After preparation, each bottle was crimp-sealed and left in the incubator shaker at 80 rpm with the temperature set at 20°C for the autunite equilibration with the bicarbonate-amended media solutions for about 30 days.

After autunite equilibration, when the dissolution was close to its solubility, the triplicate samples were inoculated with the desired volume of bacterial suspension to obtain an initial cell density of 10^6 cells/mL. In addition, abiotic control bottles were kept for each bicarbonate concentration and sampled in parallel with the experimental bottles. A total of 4 bottles per concentration with a final number of 16 bottles were prepared. All of the bottles were crimp-sealed to keep the cells under oxygen-restricted conditions and then placed in the incubator-shaker at 20°C (Figure 25).

To account for viable bacteria, a well-mixed homogeneous aliquot of 0.01 mL of the suspension from each biotic test bottle was uniformly spread on sterile LB-agar Petri plates. The inoculated plates were kept inverted in an incubator at 30°C. Viable microorganisms were calculated from the number of colony-forming units (CFU) found on a specific dilution. In addition, the agar plating was used to provide a quick visual check for contamination.



Figure 25. Experimental bottles placed in incubator-shaker at 20°C for autunite dissolution studies.

Sampling procedure and elemental analysis

1-mL sterile syringes (BD) were used to inject bacteria inoculum or extract liquid samples from the bottles. At certain time intervals dictated by the experimental schedule, aliquots of 0.2 mL were isolated from the supernatant solutions of the experimental and control bottles and filtered through 0.45 μm PTFE filters into a 20-mL scintillation vial for further uranium analysis by the kinetic phosphorescence analysis (KPA-11, Chemchek Instruments Inc.) instrument. The presence of organic content in the solutions can interfere with KPA measurements; hence, samples collected during the experiments were pre-processed by wet ashing followed by dry ashing procedures. A modified ashing technique described by Ejnik et al. (2000) was used for wet and dry ashing. Wet digestion was performed by the addition of 500 μL of concentrated nitric acid (HNO_3) and 500 μL of concentrated hydrogen peroxide (H_2O_2) to each vial; the vials were placed on a heating plate until full evaporation was achieved and a white solid residue was acquired. Occasionally, some samples turned yellow while ashing; 0.5 mL of peroxide was added to these samples and the process was continued until a white precipitate was obtained. The dry samples were placed in a furnace preheated to 450°C for 15 min and then allowed to cool at room temperature. Finally, precipitates obtained in the drying step were dissolved in 1 mL of 2 mol/L nitric acid and analyzed by means of the KPA instrument to determine uranium concentrations released into the aqueous phase as a function of time. In addition, calcium and phosphorous were determined by means of inductively coupled plasma – optical emission spectroscopy (ICP-OES 7300 Optima, Perkin Elmer) using calcium and phosphorous standards (Spex CertiPrep).

ANOVA statistics were used to examine the results on the release of U(VI) due to varying concentrations of bicarbonate ions. The significant levels were set at $\alpha = 0.05$.

Task 1.2: Results and Discussion

Autunite dissolution experiments

The results of U(VI) concentration in the aqueous phase as a function of time for each condition studied (0, 3, 5 and 10 mM HCO_3^-), prior to inoculation, are compiled in Table 11 and presented in Figure 26. Average values and relative standard deviations were calculated for the triplicate samples.

The data suggest that before the inoculation with bacteria, there was a significant amount of U(VI) released from autunite to the aqueous phase due to the presence of bicarbonate ions in the liquid media solution. Specifically, in the bicarbonate-free samples, the amount of U(VI) released into the supernatant was negligible; whereas, in samples amended with 3 mM, 5mM and 10 mM bicarbonate concentrations, U(VI) levels in the aqueous phase were found to be 2 ppm, 5 ppm and 10 ppm, respectively. These results are in agreement with the data analysis reported for the enhanced autunite dissolution in the presence of bicarbonates (Gudavalli et al., 2013b) and for the relatively fast extraction of uranium from contaminated soil (Mason et al., 1997).

Table 11. U(VI) Concentrations in the aqueous phase under all conditions studied

HCO₃ Concentration, (mM)	Time (days)	U(VI) Concentration, (ppb)
0	5	26.5 ± 2
	8	84.2 ± 31
	12	6.88 ± 9
	15	63.19 ± 18
	23	60.48 ± 6
	27	63.49 ± 36
3	5	723 ± 70
	8	2428 ± 800
	12	1791 ± 200
	15	2400 ± 705
	23	1432 ± 300
	27	1242 ± 300
5	5	2441 ± 400
	8	4771 ± 200
	12	4241 ± 700
	15	4429 ± 600
	23	4047 ± 300
	27	2995 ± 100
10	5	9238 ± 1300
	8	11089 ± 300
	12	10617 ± 1200
	15	10242 ± 1300
	23	11688 ± 400
	27	7080 ± 700

The results of uranium monitoring in the aqueous phase after inoculation with bacteria are presented in Figure 27 for 0 mM bicarbonate, Figure 28 for 3 mM HCO₃⁻ and Figure 29 for 5 mM HCO₃⁻ and 10 mM HCO₃⁻. In the case of 0 mM bicarbonate, a sharp decrease in uranium concentration was observed (Figure 27) in the first three days after bacterial inoculation, making U(VI) difficult to detect due to very low, close to the detection limit, concentrations.

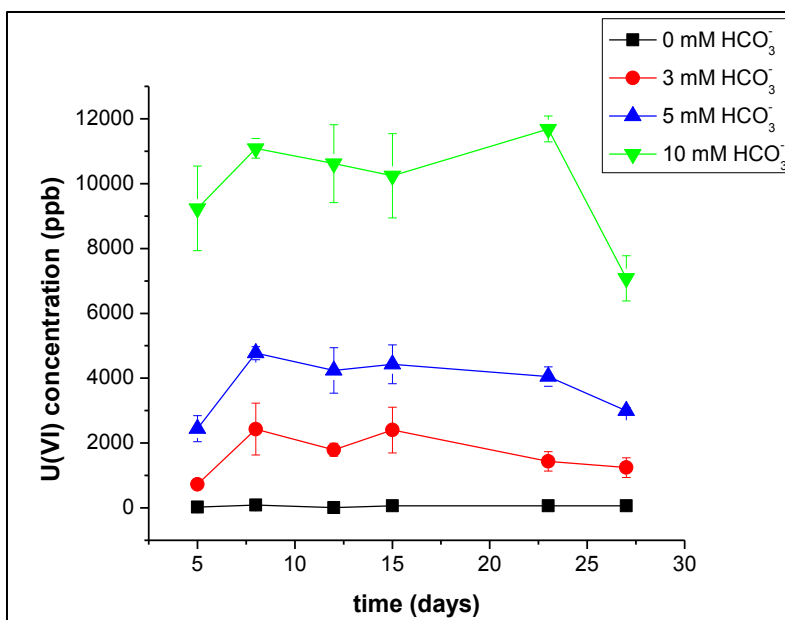


Figure 26. Concentration of U (VI) released from autunite to the aqueous phase before inoculation with *Shewanella oneidensis*.

Results also showed that after the first three days of sharp decrease, U(VI) concentrations began to slowly rebound. This is probably due to the lack of organic substrate that was consumed faster in the presence of the remaining oxygen, dissolved and present in the headspace of the oxygen-restricted bioreactors.

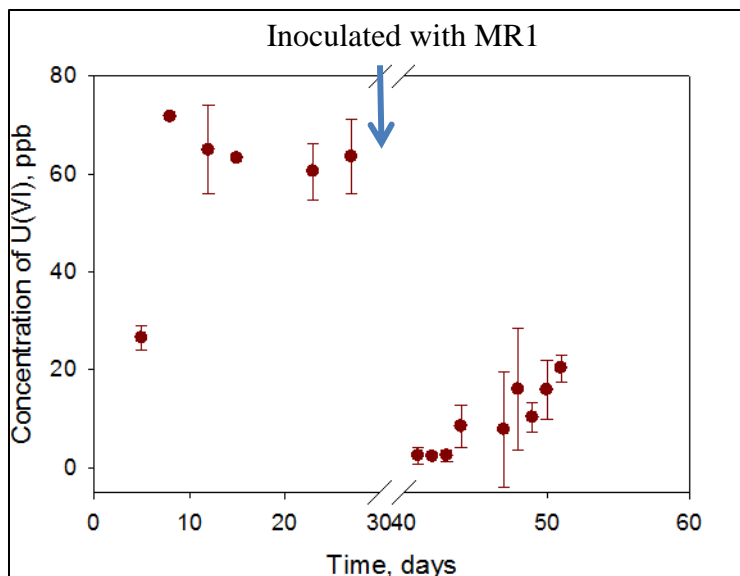


Figure 27. Uranium (VI) released into the aqueous phase as a function of time in bicarbonate-free solution.

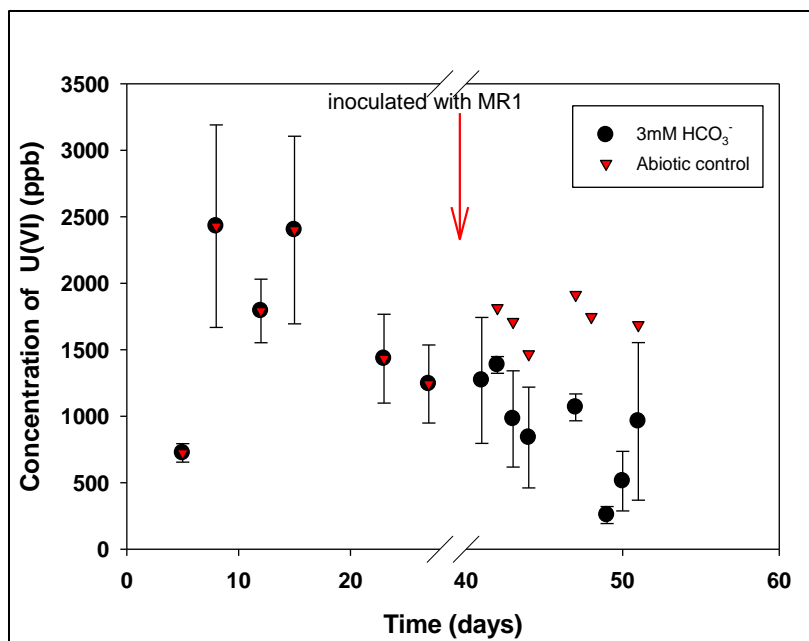


Figure 28. Uranium (VI) released into the aqueous phase as a function of time in 3 mM bicarbonate media solution.

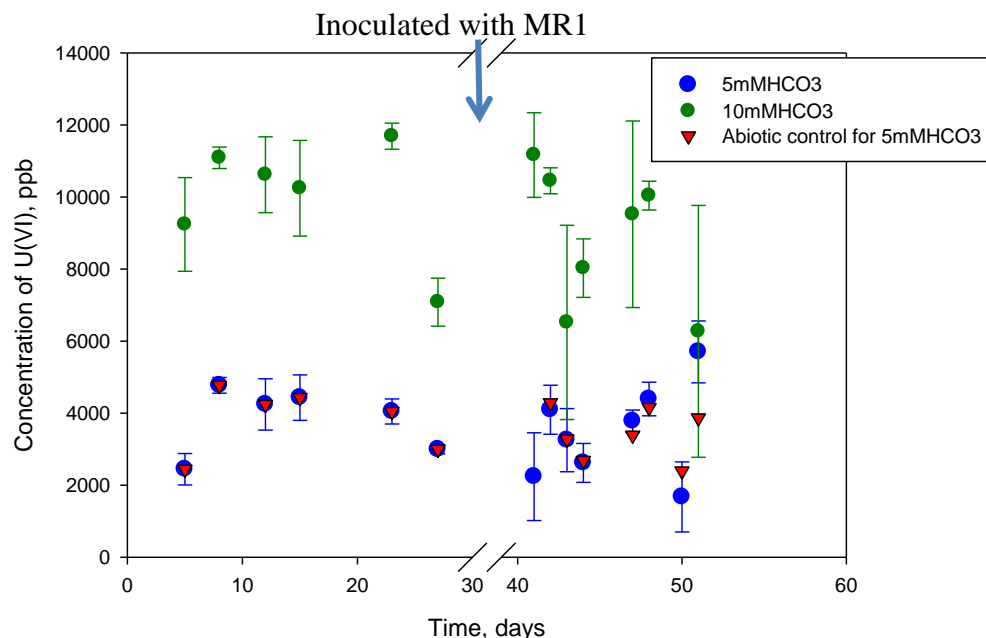


Figure 29. Uranium (VI) released in the aqueous phase as function of time under two different bicarbonate concentrations: 5 and 10 mM.

In the case of the samples amended with 5 and 10 mM bicarbonate, the data revealed no change in the U(VI) concentration before and after bacterial inoculation. On the other hand, it is clear that an increase in bicarbonate concentration leads to an increase in uranium release to the aqueous phase. This was expected since the uranium release from autunite is strongly influenced by the increase in bicarbonate concentrations, leading to the formation of aqueous uranyl bicarbonate complexes (Gudavalli et al., 2013b). Bicarbonate can promote mineral dissolution by fast binding to the autunite surface, followed by a slow detachment of the U(VI) carbonate species from the surface into solution (Gudavalli et al., 2013a).

Results obtained by means of ICP-OES are presented in Figure 30 and Figure 31 for calcium and phosphorous, respectively.

Phosphorous is released to the aqueous phase from phosphate-bearing minerals through microbial dissolution. The primary mechanisms of P solubilization are H^+ excretion, production of low molecular weight organic acid, and acid phosphatase biosynthesis (Behera et al., 2014). Furthermore, phosphorous is one of the major essential macronutrients for biological growth, playing a central role in the cellular activities for the synthesis of DNA, ATP, polyphosphates, and cell wall phospholipids (Hirota et al., 2010). In addition, speciation modeling conducted for the post-inoculation conditions predicts the formation of hydroxyl-apatite, which is a practically insoluble mineral. Therefore, a reduction in phosphorous levels after bacterial inoculation might have been expected. In addition, according to the statistical analysis by ANOVA, there is not a statistically significant difference ($P = 0.413$) between phosphorus concentrations detected after the bioreactors' bacteria inoculation, justifying that the levels of phosphorous detected in the aqueous phase are similar for all different bicarbonate concentrations tested. Bacterial inoculation incurred a slight decrease in calcium concentration, noted for all of the bicarbonate-

amended media. This decrease might be attributed to the formation of secondary minerals such as calcite and calcium phosphate. Similar to phosphorus, there is not a statistically significant difference ($P = 0.221$) for calcium concentrations measured in the media solutions after bacteria inoculation for any of the bicarbonate concentrations tested.

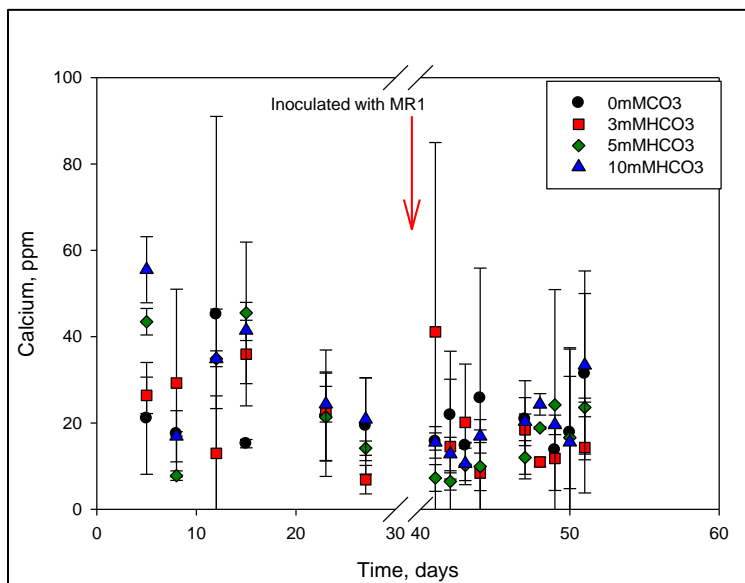


Figure 30. Concentration of calcium detected in the aqueous phase as a function of time in different bicarbonate concentrations: 0, 3, 5 and 10 mM.

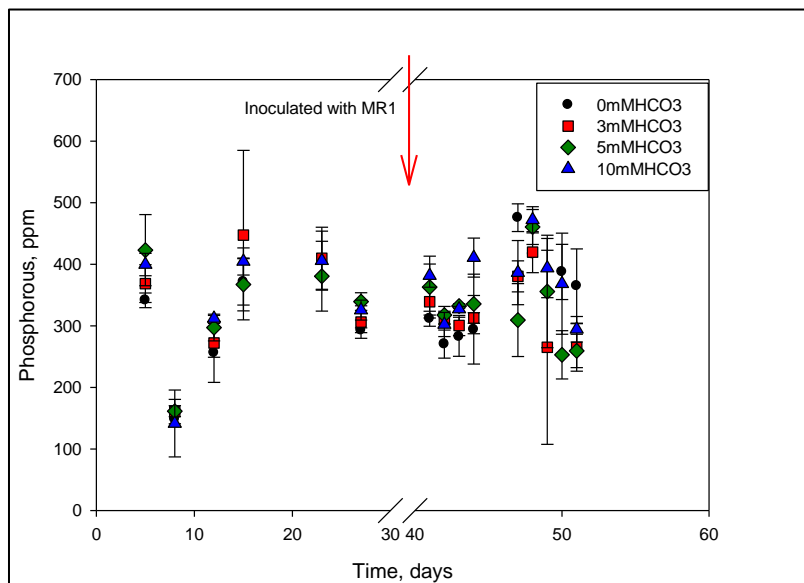


Figure 31. Concentration of phosphorous released in the aqueous phase as a function of time in different bicarbonate concentrations: 0, 3, 5 and 10 mM.

Agar plating

Agar plating was used to check for culture contamination with a visual inspection. For that, an aliquot of 0.01 mL was taken from each experimental bottle and spread on a sterile Petri dish

containing LB growth media prepared with agar. Figure 32 shows the expected colonies grown on hard media after inoculation with *Shewanella Oneidensis MRI*.

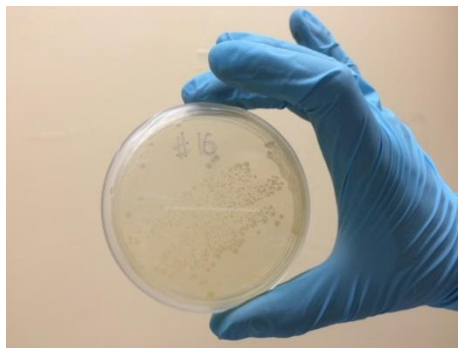


Figure 32. Bacterial growth in the sample amended with 10 mM and inoculated with bacteria.

At day 30, the experimental bottles were inoculated with facultative anaerobic bacteria; all control bottles were kept bacteria free. The sampling procedures were applied to all control and experimental bottles after inoculation with bacteria and uranium analysis was conducted on the collected samples via the KPA instrument.

Multiple sampling through septa resulted in contamination of some control bottles. Control samples were periodically prescreened under a light microscope and then examined by plating on the hard LB media. Abiotic control samples containing 0 mM and 10 mM of bicarbonate showed growth of microorganisms that suggest a contamination of the control bottles (Figure 33).

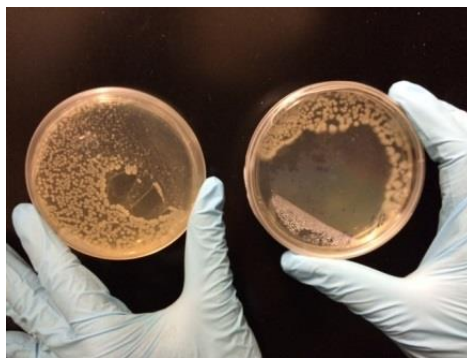


Figure 33. Bacterial contamination in the control samples with no-bicarbonate and amended with 10 mM bicarbonate.

On the other hand, the petri dishes inoculated from the control bottles amended with 3 mM and 5 mM of bicarbonate presented no evidence of bacterial contamination (Figure 34).

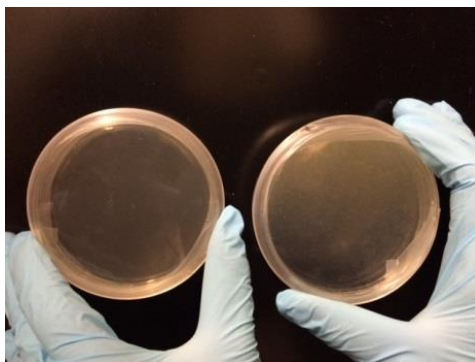


Figure 34. Clear plates with no evidence of contamination; samples were taken from control bottles amended with 3 mM and 5 mM of bicarbonate.

Preparations for the next round of dissolution experiments

The experiment is currently being replicated following the same experimental procedures as described above with two notable differences: the introduction of sacrificial vials for each experimental point (as opposed to sampling periodically from the same batch sample) in order to eliminate cross-contamination. Currently, FIU has completed preparations for the autunite dissolution experiments in the presence of anaerobic *Shewanella oneidensis* MR-1. To prevent microbial contamination during sampling events, the experiment is being conducted using sacrificial 20-mL glass scintillation vials. Each vial is filled with 18 mg of autunite powder to provide a final U(VI) concentration of 4.4 mmol/L, which is similar to concentrations used in the mixed bioreactors. All prepared glass vials with autunite were covered with plastic caps and autoclaved for 15 min at 121°C to ensure sterile conditions.

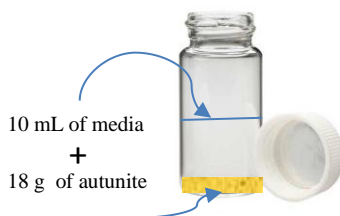


Figure 35. 20-mL glass scintillation vial prepared with media amended with KHCO_3 and autunite mineral.

The vials were amended with 10 mL of sterile media solution containing 0, 3, and 10 mM KHCO_3 . Each set, prepared using a specific bicarbonate concentration, includes duplicate sacrificial biotic vials and an abiotic control. Samples are being sacrificed at specific time intervals according to the sampling schedule. In addition, to allow the media solutions to equilibrate with the autunite, three abiotic samples were prepared at each bicarbonate concentration and sampled every 5 days before bacteria inoculation. The interval of time between sampling events after the media equilibrates with the autunite and bacteria inoculation is about 4-5 days, as shown in Figure 36. The total number of sacrificial vials for the duration of the experiment was calculated as 99.






























































































inoculation																																								
Sampling	Day 3			Day 7			Day 10			Day 14			Day 17			Day 21			Day 25			Day 25			Day 35			Day 39			Day 44			Day 50			Day 56			Tot
Abiotic																																								
Biotic	Duplicates																																							
																																								
# vials	1	1	1	1	1	1	1	1	1	3	3	3	3	3	3	3	3	3	3	3	3	3	3	3	3	3	3	3	3	3	3	3	3	3	3	3	99			
Legend																																								
0mM																																								
3mM																																								
10mM																																								

Figure 36. Sampling schedule before and after inoculation.

A media solution for the experiment was created by following the same method described in the “Bicarbonate media solution preparation” section. The bottles with the media solutions amended with bicarbonate were stored in an anaerobic chamber until initiation of the experiment (Figure 37). This experiment is still in progress and results will be presented in the next report.



Figure 37. Sacrificial vials inside the anaerobic glove box, prepared to conduct the autunite biodissolution experiment.

Collected samples will be evaluated for U(VI) content and concentrations of Ca and P through KPA. Cell density is being counted via hemocytometer and the viability of cells will be assessed by the Live/Dead fluorescent assay as complimentary qualitative and quantitative analysis. The Live/Dead fluorescent assay will be used to illustrate the effect of varying concentrations of bicarbonate ions on the viability of bacterial cells after exposure to uranium (Sepulveda et al., 2015). Imaging is widely used to provide information of the surface morphology. A scanning electron microscopy (SEM) instrument will also be used to produce images that may show the location of bacterial cells and adhesion to the autunite mineral.

The preliminary results obtained during preparation for the experiments using sacrificial vials are presented below.

Cells viability assays and protein analysis

In this round of experiments, additional analytical parameters are being introduced, such as cell protein analysis and cell viability via Live and Dead assay. For cell protein determination, a BCA (Pierce) protein analysis kit is being used. For the preliminary assessment of the protein kit, a fresh culture of facultative anaerobic bacteria *Shewanella Oneidensis MRI* was grown in two 15-mL tubes filled with LB liquid media. The tubes were placed in the incubator for two days at 30 °C. After two days, the tubes were centrifuged and the pellet was washed with deionized water and re-suspended in 1.5 mL of DIW water. The washing procedures were repeated twice. After washing, the cells were counted via hemocytometer and 1.2 mL from each vial was extracted into the 1.5-mL microcentrifuge tubes to be used for the bicinchoninic acid (BCA) protein assay. The BCA protein assay is based on the highly selective colorimetric detection of the cuprous cation (Cu^+) by bicinchoninic acid as a result of the reduction of Cu^{2+} to Cu^+ by protein in an alkaline medium. Cell density concentration in vial #1 was calculated as 884,210,526 cells/mL and in vial #2 as 877,419,355 cells/mL. Following the protocol procedures, the cells were lysed by boiling at 100 °C for 10 min and then cooled down on ice. The addition of an alkaline medium followed and the samples were placed in a water bath (30 °C) for 30 minutes (Figure 38). A calibration curve was prepared by using albumin as a standard (Figure 39) and the absorbance was measured at 562 nm spectrophotometrically. This protocol proved to be not sensitive enough, since the detection limit correlated to a cell density of 10^7 cells/mL (Figure 40).

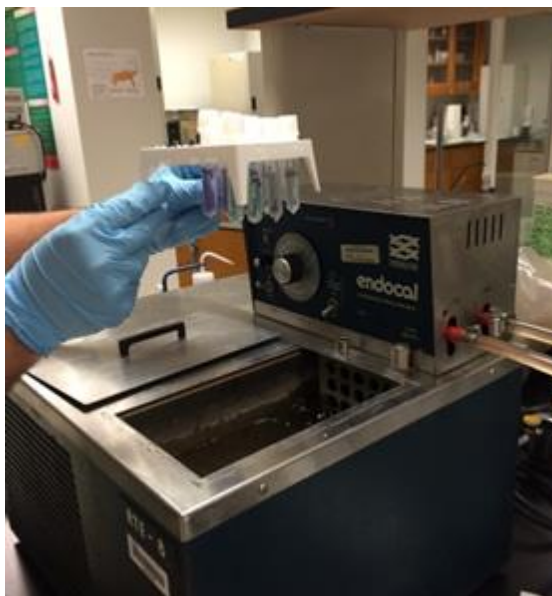


Figure 38. Water bath with dilutions for calibration curve.

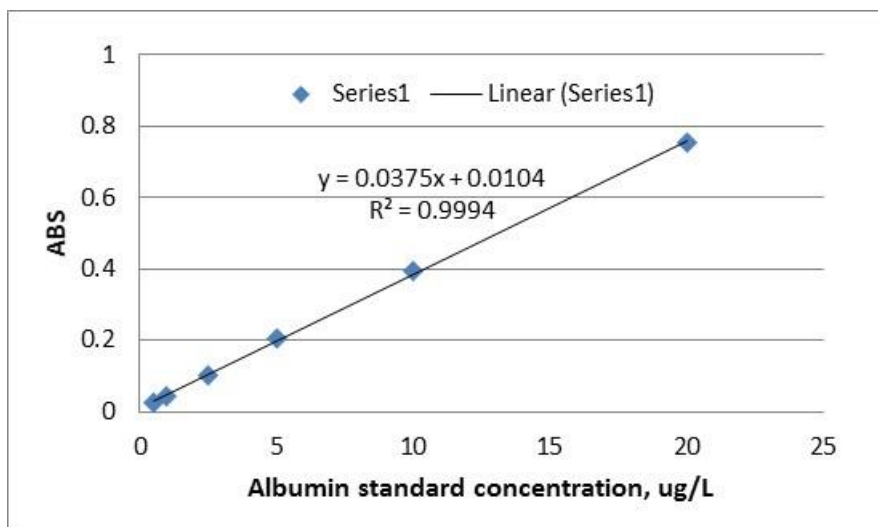


Figure 39. Calibration curve for protein analysis.

The protocol was amended and the samples remained in a water bath of 60 °C for 1h and the calibration curve and samples were re-evaluated. The amendment of the protocol yielded better results in terms of a lower detection limit ($10^{5.9}$ cell/mL) (Figure 41).

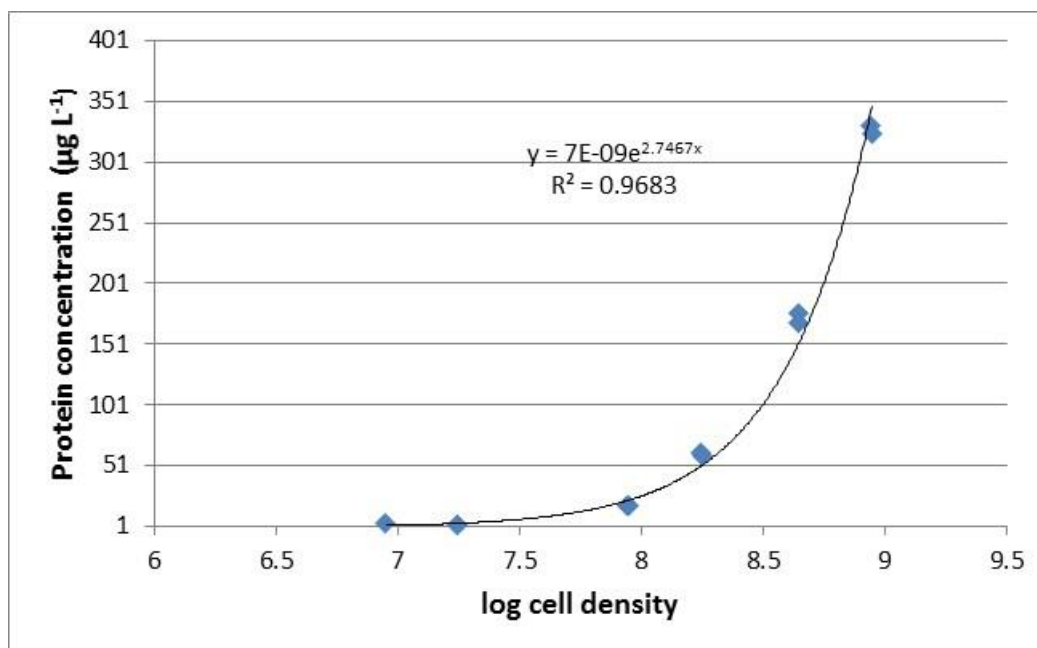


Figure 40. Correlation between cell density of *Shewanella oneidensis* MR1 and protein content.

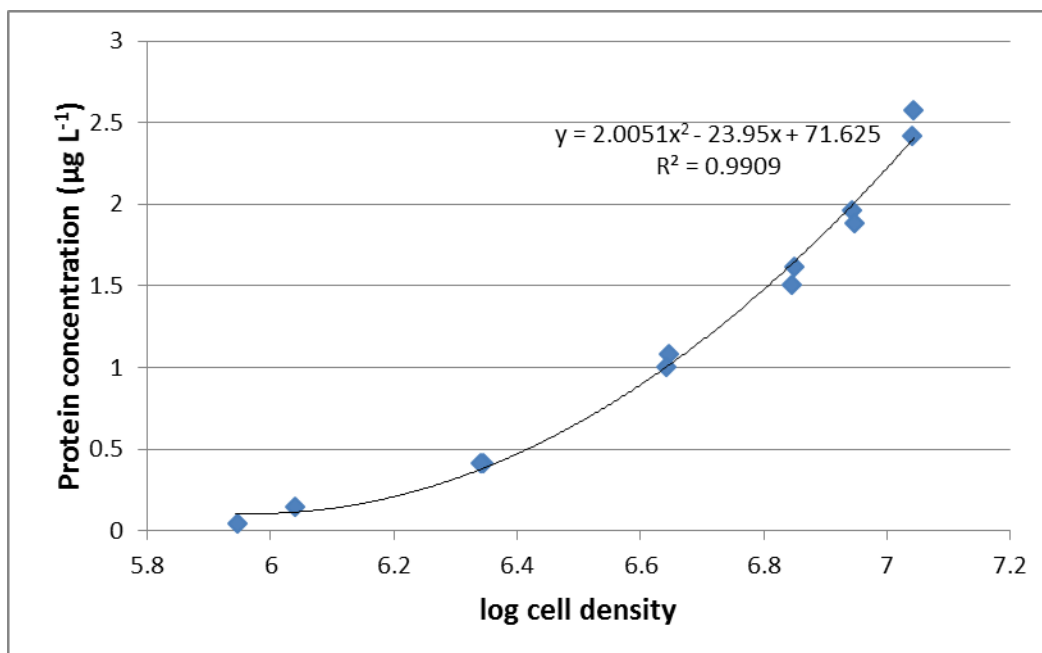


Figure 41. Correlation between cell density of *Shewanella oneidensis* MR1 and protein content based on amended protocol.

Fluorescent microscope

The technique of fluorescence microscopy is a useful tool for the identification of cells with its microscopic cellular components. Fluorescent optical imaging has many advantages that can support data analysis.

For this new round of experiments using sacrificial vials, estimates of bacterial cell wall integrity are planned, using the Live/Dead BacLight Bacterial Viability Kit (Molecular Probes, L-7012). This assay can illustrate the effect of varying concentrations of bicarbonate ions on the viability of bacterial cells after exposure to uranium. Preliminary experiments were focused on the preparation and microscopy analysis of uranium-free control alive and dead bacterial samples. Preparations for this assay included culturing cells in the LB media and then, after centrifugation, re-suspension of the cell pellet in 2 mL of the synthetic groundwater solution (SGW). Next, the cells were counted and diluted to log 6 cells/mL density in the suspension. The cell suspension prepared in SGW solution then was equally divided between two tubes. Samples prepared for killed bacteria were kept for 15 min in 15 mL of 70% isopropyl alcohol and then the pellets, after centrifugation, were re-suspended in 1 mL of SGW to wash out the alcohol solution. Both killed and alive samples were mixed with 3 µL of a dye mixture composed of SYTO 9 and propidium iodide from the LIVE/DEAD® BacLight Bacterial Viability Kit. Samples were incubated for 15 min in the dark and filtered through a black polycarbonate filter (Whatman #110656) via a vacuum filtration system. Samples were then washed with 1 mL of DIW water and placed on the slide with one drop of mounting oil. Samples were covered with the coverslip and observed via a fluorescence microscope DV Elite system. The results of the microscopy analysis suggested that more time is required to kill the bacteria in the preparation of a “dead” sample. FIU started preparation of new control Live/Dead samples following the same procedures, but keeping

bacteria overnight in the isopropyl alcohol solution for the preparation of a “dead” sample and then checking the sample under the light microscope.

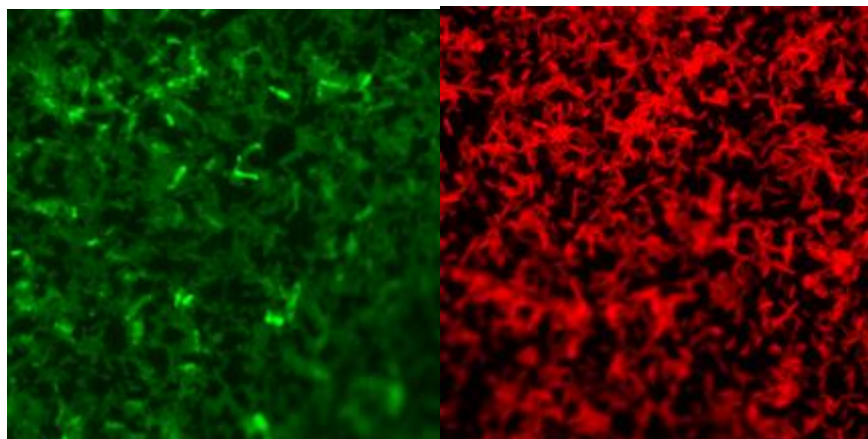


Figure 42. Image of live cells on the left and dead cells on the right.

Task 1.2: Future Work

The collected samples will be analyzed for U(VI) by means of KPA and Ca and P by means of ICP-OES. Metal analysis in the aqueous phase will be coupled with speciation modeling calculations in an effort to clarify the possible formation of secondary minerals as a result of autunite dissolution. Cell viability will be assessed by protein determination, observation with an optical microscope, counting of bacterial colonies in agar plates, and observation with a fluorescent microscope using a Live & Dead Assay kit. Cell morphology and surface elemental analysis will be investigated by means of SEM-EDS. Another experimental set will be conducted for the Na-synthetic autunite to compare results for U release with natural Ca-autunite.

Data analysis of anaerobic facultative bacteria and the interactions with bicarbonate ions will be compared with previous studies to draw conclusions and identify main differences to assure a long-term remediation strategy for U (VI) contained in soil and groundwater at the Hanford 300 Area.

Task 1.2: Acknowledgment

Funding for this research was provided by U.S. DOE cooperative agreement DE-EM0000598. We truly appreciate Dr. Brady Lee and Dr. Hope Lee from PNNL for their support of this research and providing us with the *Shewanella* culture.

Task 1.2: References

- Bachmaf, S., Planer-Friedrich, B., Merkel, B.J. 2008. Effect of sulfate, carbonate, and phosphate on the uranium(VI) sorption behavior onto bentonite. *Radiochimica Acta*, **96**(359-366).
- Behera, B.C., Singdevsachan, S.K., Mishra, R.R., Dutta, S.K., Thatoi, H.N. 2014. Diversity, mechanism and biotechnology of phosphate solubilising microorganism in mangrove—A review. *Biocatalysis and Agricultural Biotechnology*, **3**(2), 97-110.

- Bencheikh-Latmani, R., Leckie, J.O. 2003. Association of uranyl with the cell wall of *Pseudomonas fluorescens* inhibits metabolism. *Geochimica et Cosmochimica Acta*, **67**(21), 4057-4066.
- Bernhard, G., Geipel, G., Reich, T., Brendler, V., Amayri, S., Nitsche, H. 2001. Uranyl(VI) carbonate complex formation: Validation of the $\text{Ca}_2\text{UO}_2(\text{CO}_3)_3(\text{aq.})$ species. in: *Radiochimica Acta International journal for chemical aspects of nuclear science and technology*, Vol. 89, pp. 511.
- Brooks, S.C., Fredrickson, J.K., Carroll, S.L., Kennedy, D.W., Zachara, J.M., Plymale, A.E., Kelly, S.D., Kemner, K.M., Fendorf, S. 2003. Inhibition of Bacterial U(VI) Reduction by Calcium. *Environmental Science & Technology*, **37**(9), 1850-1858.
- Ejnik, J.W., Hamilton, M.M., Adams, P.R., Carmichael, A.J. 2000. Optimal sample preparation conditions for the determination of uranium in biological samples by kinetic phosphorescence analysis (KPA). *Journal of Pharmaceutical and Biomedical Analysis*, **24**(2), 227-235.
- Gudavalli, R.K.P., Katsenovich, Y., Wellman, D.M., Lagos, L., Tansel, B. 2013a. Quantification of kinetic rate law parameters for the dissolution of sodium meta-autunite as a function of aqueous bicarbonate concentration. *Environmental Chemistry*, **10**(6), 475-485.
- Gudavalli, R.K.P., Katsenovich, Y.P., Wellman, D.M., Idarraga, M., Lagos, L.E., Tansel, B. 2013b. Comparison of the kinetic rate law parameters for the dissolution of natural and synthetic autunite in the presence of aqueous bicarbonate ions. *Chemical Geology*, **351**, 299-309.
- Hirota, R., Kuroda, A., Kato, J., Ohtake, H. 2010. Bacterial phosphate metabolism and its application to phosphorus recovery and industrial bioprocesses. *Journal of Bioscience and Bioengineering*, **109**(5), 423-432.
- Katsenovich, Y., Carvajal, D., Guduru, R., Lagos, L., Li, C.-Z. 2012a. Assessment of the Resistance to Uranium (VI) Exposure by *Arthrobacter* sp. Isolated from Hanford Site Soil. *Geomicrobiology Journal*, **30**(2), 120-130.
- Katsenovich, Y.P., Carvajal, D.A., Wellman, D.M., Lagos, L.E. 2012b. Enhanced U(VI) release from autunite mineral by aerobic *Arthrobacter* sp. in the presence of aqueous bicarbonate. *Chemical Geology*, **308–309**, 1-9.
- Langmuir, D. 1978. Uranium solution- mineral equilibria at low temperatures with application to sedimentary ore deposits. *Geochimica et Cosmochimica Acta*, **42**, 547-569.
- Lin, X., Kennedy, D., Peacock, A., McKinley, J., Resch, C.T., Fredrickson, J., Konopka, A. 2012. Distribution of Microbial Biomass and Potential for Anaerobic Respiration in Hanford Site 300 Area Subsurface Sediment. *Applied and Environmental Microbiology*, **78**(3), 759-767.
- Liu, C., Jeon, B.-H., Zachara, J., Wang, Z. 2007. Influence of Calcium on Microbial Reduction of Solid Phase Uranium(VI). *Biotechnology and Bioengineering*, **97**(6), 1415-1422.
- Lüttge, A., Conrad, P.G. 2004. Direct Observation of Microbial Inhibition of Calcite Dissolution. *Applied and Environmental Microbiology*, **70**(3), 1627-1632.

- Marshall, M., Plymale, A., Kennedy, D., Shi, L., Wang, Z., Reed, S., Dohnalkova, A., Simonson, C., Liu, C., Saffarini, D., Romine, M., Zachara, J., Beliaev, A., Fredrickson, J. 2008. Hydrogenase- and outer membrane c-type cytochrome-facilitated reduction of technetium(VII) by *Shewanella oneidensis* MR-1. *Environmental Microbiology*, **10**(1), 125-136.
- Mason, C.F.V., Turney, W.R.J.R., Thomson, B.M., Lu, N., Longmire, P.A., Chisholm-Brause, C.J. 1997. Carbonate Leaching of Uranium from Contaminated Soils. *Environmental Science & Technology*, **31**(10), 2707-2711.
- Sheng, L., Fein, J.B. 2013. Uranium adsorption by *Shewanella oneidensis* MR-1 as a function of dissolved inorganic carbon concentration. *Chemical Geology*, **358**, 15-22.
- Sheng, L., Fein, J.B. 2014. Uranium reduction by *Shewanella oneidensis* MR-1 as a function of NaHCO₃ concentration: surface complexation control of reduction kinetics. *Environmental Science and Technology*, **1**(48), 3768-3775.
- Smeaton, C.M., Weisener, C.G., Burns, P.C., Fryer, B.J., Fowle, D.A. 2008. Bacterially enhanced dissolution of meta-autunite. *American mineralogist*, **93**, 1858-1864.

TASK 2.0: REMEDIATION RESEARCH AND TECHNICAL SUPPORT FOR SAVANNAH RIVER SITE

Subtask 2.1: Sodium Silicate Treatment For U(VI) Bearing Groundwater At F/H Area At Savannah River Site

Subtask 2.1: Introduction

The Savannah River Site (SRS) was established as one of the major sites for the production of materials related to the U.S. nuclear program during the early 1950s. An estimated 36 metric tons of plutonium were produced during the period 1953-1988. Since then, it has become a hazardous waste management facility responsible for nuclear storage and remediation of contaminated soil and groundwater from radionuclides. The groundwater at the F/H Area Seepage Basins Groundwater Operable Units at SRS was impacted by operations of the Hazardous Waste Management Facilities (HWMFs). Approximately 1.8 billion gallons (7.1 billion liters) and 1.6 billion gallons (6.0 billion liters) of low-level waste solutions have been received in the F and H areas, respectively, originating from the processing of uranium slugs and irradiated fuel at the separation facilities. The effluents were acidic (wastewater contaminated with nitric acid) and low-activity waste solutions containing a wide variety of radionuclides and dissolved metals. Waste solutions were transported approximately 3,000 feet from each processing area through underground vitrified clay pipes to the basins. After entering the basin, the wastewater was allowed to evaporate and to seep into the underlying soil. The purpose of the basins was to take advantage of the interaction with the basin soils to minimize the migration of contaminants to exposure points. Though the seepage basins essentially functioned as designed, the acidic nature of the basin influent caused mobilization of metals and radionuclides resulting in groundwater contaminant plumes.

Currently, more than 235 monitoring wells at the site are sampled for a variety of chemical and radioactive parameters. Groundwater monitoring results have indicated the presence of elevated levels of metals, radionuclides and nitrates. Significant chemical differences exist between the groundwater from the two areas. The F Area groundwater contains higher concentrations of dissolved metals than that in the H Area. The constituents of concern (COCs) associated with the F Area HWMF groundwater plume are tritium, uranium-238, iodine-129, strontium-90, curium-244, americium-241, technetium-99, cadmium, and aluminum. The COCs in H Area are tritium, strontium-90, and mercury.

To remove contaminants from polluted groundwater, pump-and-treat and re-inject systems were implemented. Downgrade groundwater within the system would be pumped up to a water treatment facility and then re-injected upgrade within the aquifer. This system was disconnected since the process incurred the risk of exposure to workers, generated a secondary waste stream that must be managed and was expensive, as well as time- and labor- intensive. In 2004, a funnel-and-gate process was implemented to carry out injections of alkaline solutions directly into the gates of the F-Area groundwater to raise pH levels. This approach allows for the creation of focused treatment zones and chemical stabilization of metals in those zones (*in situ* immobilization). Initial addition of sodium hydroxide revealed a decrease in uranium and strontium concentrations, but the concentration of iodine remained unaffected. Consequently, addition of carbonate solutions was investigated, but this solution eventually raised concerns about the re-mobilization of uranium previously contained within the treatment zone, due to the

formation of highly soluble uranium-carbonate complexes. Furthermore, a systematic re-injection of carbonate solution would be required for the sustainability of circumneutral pH values in the treatment zone.

FIU-ARC is conducting research for the replacement of injection of carbonate alkaline solutions with sodium silicate. Sodium silicate is an alkaline solution that is favorable because it is environmentally benign with moderate to low cost (Baehr & Koehl, 2007). The main objective of these studies was to assess whether sodium silicate has sufficient alkalinity to restore the natural pH of the groundwater. Silica solutions have an inherent $\text{pH} \leq 10$, which complies with the regulatory constraints of injecting solutions of high pH values into subsurface systems. The optimal levels of sodium silicate for the restoration of circumneutral conditions were investigated, taking into account silica solubility levels in order to avoid clogging of the aquifer's permeability. The degree of U(VI) immobilization as a consequence of pH elevation was examined as well.

SUBTASK 2.1: Materials and Methods

Soil samples and SRS synthetic groundwater

Soil samples from the SRS F/H Area were sieved and the fraction of mean diameter $0.18 < d < 2$ mm was used for all experiments. Soil samples were kept in a desiccator, which contains anhydrous calcium sulfate (Drierite, Drierite Company Inc).

Synthetic groundwater that mimics SRS groundwater characteristics was prepared according to the recipe by Storm and Kabak (Storm & Kaback, 1992) by dissolving 5.4771 g CaCl_2 , 1.0727 Na_2SO_4 , 3.0943 g MgCl_2 , 0.3997 KCl and 2.6528 NaCl in 1 L of deionized water (Barnstead NANOpure water purification system). 1 mL of the stock solution was diluted into 1 L of deionized water acidified to pH 3.5 to create the working solution. All reagents were of analytical grade. Sodium silicate solutions were created by dissolving specific amount of $\text{Na}_2\text{SiO}_3 \cdot 9\text{H}_2\text{O}$ (reagent grade, MP Biomedicals) in deionized water.

Experimental procedures

In the preliminary experiments, 400 mg of SRS soil (mean diameter $0.18 < d < 2$ mm) were mixed in a 50-mL propylene vial with 20 mL of SRS synthetic groundwater (triplicate samples) resulting in 20 g/L soil suspensions. Each sample was spiked with the appropriate volume from a freshly prepared sodium silicate solution (Fisher Scientific), with the exception of the control samples that contained only soil and SRS groundwater solution. The final sodium silicate concentration ranged from 10-80 mg L^{-1} . Vials were agitated on a platform shaker at 120 rpm for 72 h and pH readings were taken periodically in order to determine the range of sodium silicate concentrations prompting the pH increase to circumneutral conditions and the amount of time required for this process.

Subsequently, working solution aliquots were combined with appropriate volumes of concentrated uranium standard 997 mg L^{-1} (Spex CertiPrep) in order to provide a final uranium concentration equal to 0.5 mg L^{-1} . Sample preparation procedures were kept the same as described above: each sample was spiked with the appropriate volume of a freshly prepared concentrated sodium silicate solution and the vials were equilibrated at room temperature. At different time intervals, 0.15 mL aliquots were isolated from the supernatant without further

treatment. Additional aliquots of 0.5 mL were first filtered through a PTFE filter of pore diameter 0.45 μm and the filtrate was re-filtered through a PTFE filter of 0.2 μm pore diameter. 0.15 mL aliquots were isolated from each filtrate for elemental analysis. Both filtered and unfiltered aliquots were diluted 1:20 with 1% HNO_3 for uranium and iron analysis; separate aliquots were isolated for the determination of Si, which were diluted 1:20 with deionized water.

The purpose of the sequential filtrations was to determine the uranium association with different size fractions after the sodium silicate amendment to the aqueous phase. More specifically, by determining the residual U(VI) concentration in the supernatant in undisturbed (unfiltered) samples, the amount of uranium that has precipitated can be determined using Eq. 9.

$$\% \text{ U}_{\text{precipitated}} = [\text{U}]_{\text{init}} - [\text{U}]_{\text{resid.}} / [\text{U}]_{\text{init}} \times 100 \quad \text{Eq 9}$$

where $[\text{U}]_{\text{init}}$ is the initial uranium concentration in the sample (constant throughout the experiments and equal to 500 $\mu\text{g L}^{-1}$), and $[\text{U}]_{\text{resid}}$ is the residual uranium concentration ($\mu\text{g L}^{-1}$). Both concentrations were measured by means of KPA.

Sequential filtration allowed for determination of the size range of colloidal particles and the percentage of U(VI) associated with silica presumably present in the solution in a colloidal form. Particles of diameter $d > 0.45 \mu\text{m}$ were collected on the filter with pore size of 0.45 μm . Similarly, filtration with 0.2 μm is expected to reveal if uranium is associated with the formation of colloidal particles of average size between 0.2-0.45 μm . Uranium detected in the residual filtrate (resulted after filtration with 0.2 μm) is labeled as $\text{U}_{\text{soluble}}$, whereas uranium detected after the first filtration (0.45 μm) is a sum of soluble U(VI) and uranium associated with silica colloidal formations of average size between 0.2-0.45 μm (Figure 43).

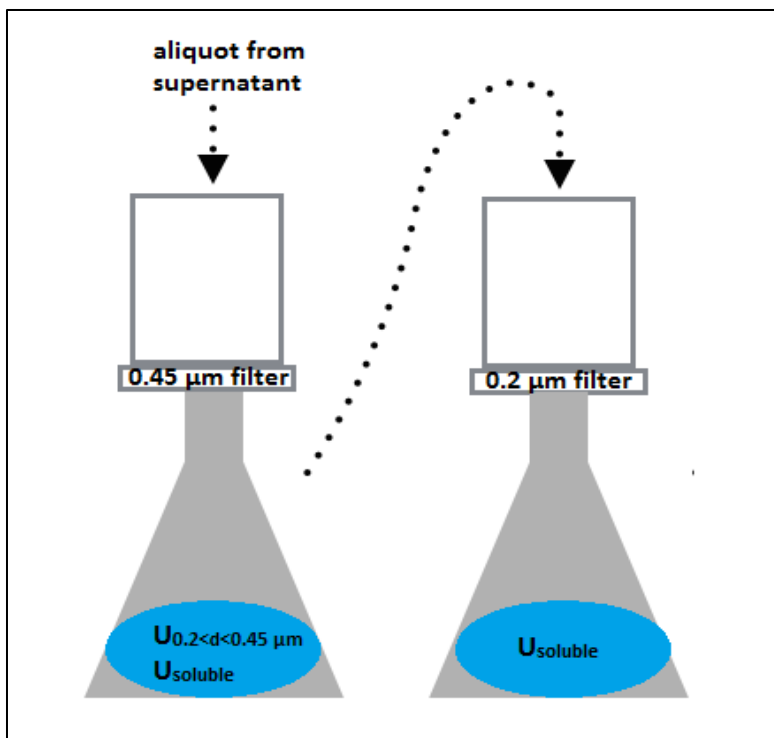


Figure 43. Schematic representation of sequential filtration experimental procedure.

The different fractions of uranium can be calculated by mass balance equation (Eq 10).

$$[U]_{init} = [U]_{precipitate} + [U]_{d > 0.45 \mu m} + [U]_{0.2 < d < 0.45 \mu m} + [U]_{soluble} \quad \text{Eq 10}$$

Elemental analysis

The residual uranium concentration in undisturbed and filtered samples was analyzed by means of kinetic phosphorescence analysis (KPA-11, Chemchek Instruments Inc.). Iron and silicon were determined by means of inductively coupled plasma - optical emission spectroscopy (ICP-OES 7300 Optima, Perkin Elmer).

The morphology and elemental composition of precipitates collected on the filters were investigated using scanning electron microscopy equipped with energy dispersive spectroscopy (SEM-EDS) at the Florida Center for Analytical Electron Microscopy located on the Florida International University Modesto A. Maidique Campus (MMC). The SEM system used was a JOEL-5910-LV with acceleration potentials ranging from 10 to 20 kV. EDS analysis was produced using an EDAX Sapphire detector with UTW Window controlled through Genesis software. Any required gold coating was done with an SPI-Module Control and Sputter unit for 2 minutes to produce a thin layer of gold. Filters were dried in a conventional oven at 30°C for a period of 5 days. This technique provided a better understanding of the morphology and elemental composition of silicate colloidal particles formed as a result of the sodium silicate addition.

Speciation modeling

Speciation calculations were performed with the aid of Hydrochemical Equilibrium-Constant Database (HYDRA) software and the speciation diagrams were plotted with MEDUSA software based on data exported by HYDRA software. HYDRA-MEDUSA software package was created by Ignasi Puigdomenech at School of Chemical Science and Engineering in the Royal Institute of Technology (KTH, Stockholm, Sweden) and can be found at: <https://www.kth.se/en/che/medusa>.

Subtask 2.1: Results and Discussion

Initial results - pH monitoring

The objective of the preliminary experiments was to determine the range of sodium silicate concentrations required for the pH to be elevated to circumneutral conditions and the amount of time needed for this process. The duration of the preliminary experiments for pH monitoring was 3 days (72 h). In these experiments, all samples contained only SRS synthetic groundwater (no uranium was introduced to the samples). The results are presented in Figure 44.

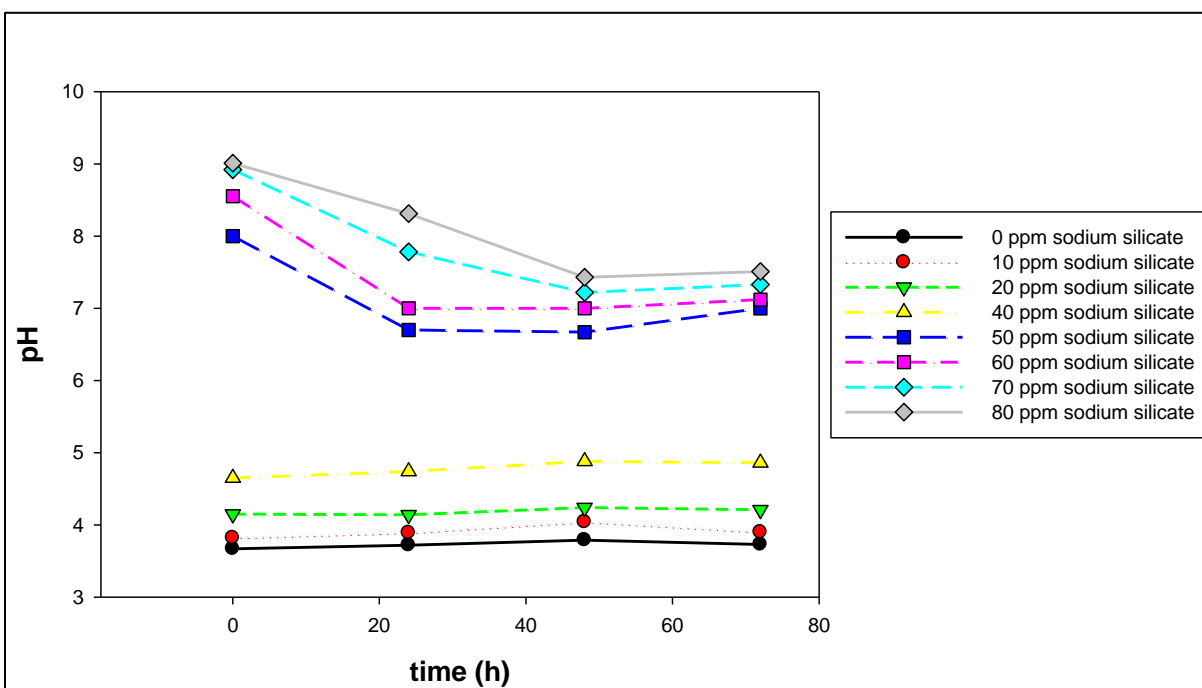


Figure 44. Monitoring of pH as a function of time for batch samples of SRS soil and synthetic groundwater.

As it can be seen in Figure 44, concentrations of sodium silicate higher than 50 mg L^{-1} increased the initial pH of 3.5 to values higher than 8 and then pH stabilizes at values ~ 7 for the next 3 days (72 hours). In comparison, sodium silicate concentrations lower than 50 mg L^{-1} do not achieve a significant increase in pH. Based on these results, the following experiments with uranium-bearing samples were performed using sodium silicate concentrations higher than 50 mg L^{-1} . These experiments also accounted for the percent of uranium removal from the aqueous phase. The preliminary pH monitoring experiments were the only experimental part that were not performed in triplicate, as their role was introductory in order to provide a general pH pattern in a wide range of sodium silicate concentrations.

Uranium removal studies

Based on the above discussion, it was decided to investigate uranium removal in the presence of sodium silicate at concentrations higher than 50 mg L^{-1} . In these experiments, SRS soil and synthetic groundwater were amended with 0.5 mg L^{-1} of U(VI) and sodium silicate concentrations ranging between $60\text{--}90 \text{ mg L}^{-1}$. Samples were prepared in triplicate and were brought in contact for a period of 3 days. Equilibrium pH and uranium concentrations were measured after three days.

The pH after a period of three days was found to be 5.15 ± 0.1 , 6.54 ± 0.06 , 7.14 ± 0.13 and 7.51 ± 0.38 for the samples amended with 60, 70, 80 and 90 mg L^{-1} of sodium silicate, respectively. It was noted that the addition of 60 mg L^{-1} sodium silicate did not manage to elevate pH values to the circumneutral level. Uranium removal studies revealed rather poor removal efficiency (20%) in samples spiked with 60 mg L^{-1} sodium silicate but significantly greater removal ($>50\%$) at higher sodium silicate concentrations after 3 days (Figure 45). The theoretical calculations showed that at pH 5.2, which is a pH value achieved by 60 mg L^{-1} of sodium silicate addition, the formation of solid phases of uranium hydroxides in the form of $\text{UO}_2(\text{OH})_2 \cdot \text{H}_2\text{O}$ was not anticipated. As suggested by the speciation modeling, uranium at this pH is expected to form mainly as soluble species UO_2^{2+} (40%) and UO_2OH^+ (40%), whereas in smaller percentages it is found as uranyl-silicate complex ($\text{UO}_2\text{HSiO}_3^+$). U(VI) was also predicted in hydrolyzed forms ($\text{UO}_2(\text{OH})_2^{2+}$ and $(\text{UO}_2)_3(\text{OH})_5^+$) and as carbonate complex (UO_2CO_3). Nevertheless, Krestou and Panias (Krestou & Panias, 2004) reported that at pH 5.2, 20% of U(VI) is found as $\text{UO}_2(\text{OH})_2$ (precipitate) for ionic strength equal to 0.001 M, an estimate which is closer to our experimental observations. Furthermore, in aqueous systems at equilibrium with atmospheric carbon dioxide, where atmospheric CO_2 is the only source of carbonates in the aqueous phase, soluble UO_2CO_3 is found in the aqueous phase (Rich, 2007; Taylor, 2015). On the other hand, in systems rich in carbonates due to geochemical conditions (e.g. dissolution of carbonaceous materials), rutherfordine (UO_2CO_3) was observed in the solid phase at pH range 4.5–6 (Krestou & Panias, 2004). SRS synthetic groundwater has low carbonate concentrations as the only carbonate source was atmospheric CO_2 .

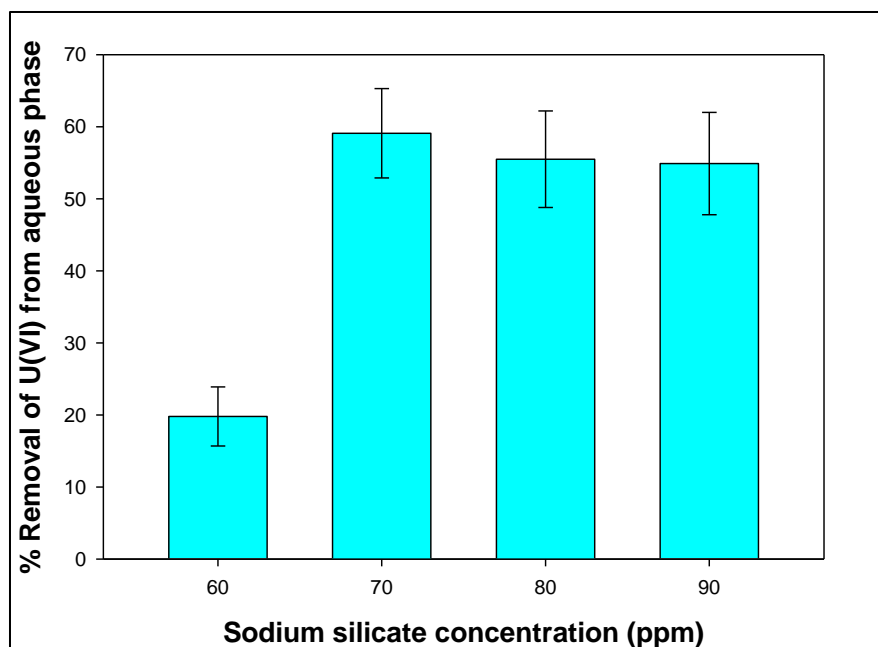


Figure 45. Percent removal of U(VI) from aqueous phase as a function of sodium silicate concentration added in the sample. Data were recorded after 3 days of equilibration

For concentrations of sodium silicate equal to or higher than 70 mg L^{-1} , pH stabilizes in the range of 6.8-7.1. In this pH region, according to the speciation diagram, U(VI) is predominantly found in the solid phase as $\text{UO}_2(\text{OH})_2 \cdot \text{H}_2\text{O}$ (65%), but coexists with soluble uranyl carbonato-hydroxo-U(VI) complex, $\text{UO}_2\text{CO}_3(\text{OH})_3^-$. In our experiments, precipitation was found to be 60%, which is in agreement with the theoretical calculations using speciation modeling. Finally, the removal of U(VI) from the aqueous phase was not affected by the increase in sodium silicate concentration introduced into solution. Speciation diagrams for 70, 80 and 90 mg L^{-1} sodium silicate amended solutions are not presented, because they do not differ from the one presented in Figure 46. In conclusion, concentrations equal to or higher than 70 mg L^{-1} of sodium silicate achieved the highest degree of U(VI) removal under the conditions studied.

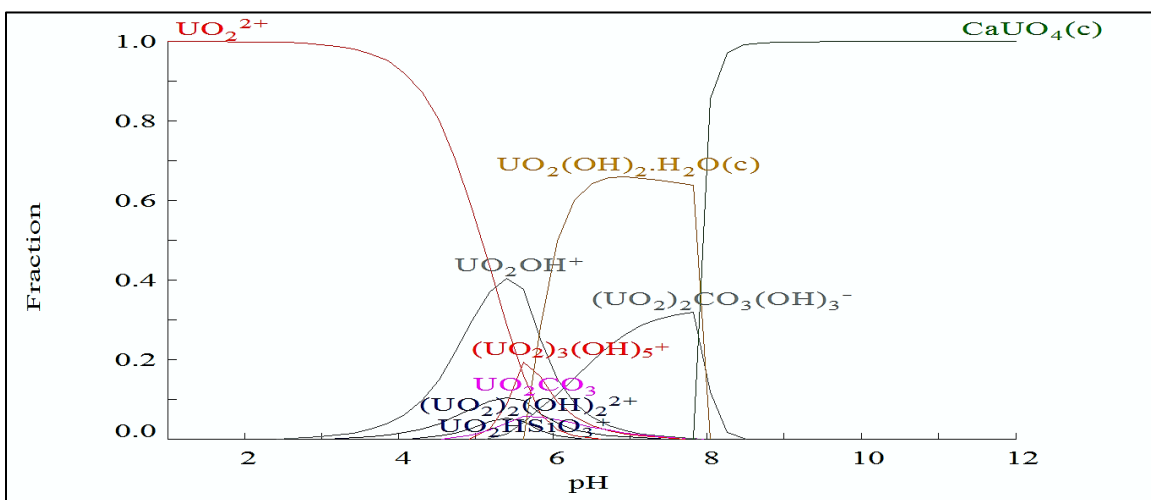


Figure 46. Speciation diagram for the conditions of Savannah River Site synthetic groundwater amended with 0.5 mg L⁻¹ U(VI) and 60 mg L⁻¹. The solubility of atmospheric CO₂ has been included. Note: “c” stands for crystalline

Studies of uranium in different phases

The results for uranium after sequential filtration with variable sodium silicate amendments are presented in Figure 47- Figure 49. Sequential filtration allows for the determination of the percentage of uranium associated with sodium silicate presumably present in the solution in a colloidal form, as explained above. Uranium based on the experimental set up can be associated with three different phases: precipitate ($U_{\text{precipitate}}$), colloidal ($U_{0.2 < d < 0.45 \mu\text{m}}$ and $U_{d > 0.45 \mu\text{m}}$) and soluble (U_{soluble}).

The experimental results indicated that the fractions of U(VI) remain stable within a period of 9 days. U(VI) fraction in the precipitate is ~60%, whereas ~20% is found in a colloidal form, as retained by a 0.45 μm filter (further discussion follows later) and 20-25% remains in soluble form, as passed through a 0.2 μm filter. Chemical analysis revealed that uranium does not associate with colloidal particles of mean diameter between $0.2 < d < 0.45 \mu\text{m}$, and this is why uranium fraction for $U_{0.2 < d < 0.45 \mu\text{m}}$ is absent in Figure 47- Figure 49.

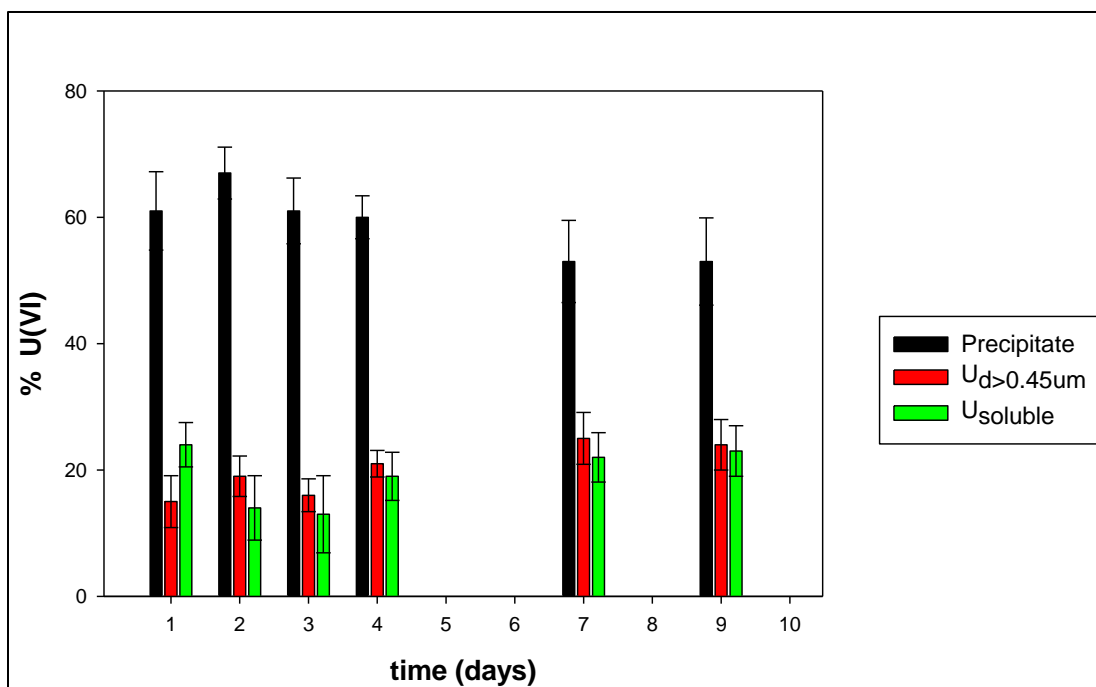


Figure 47. U(VI) distribution between different phases as a function of time for treatment with 70 ppm sodium silicate.

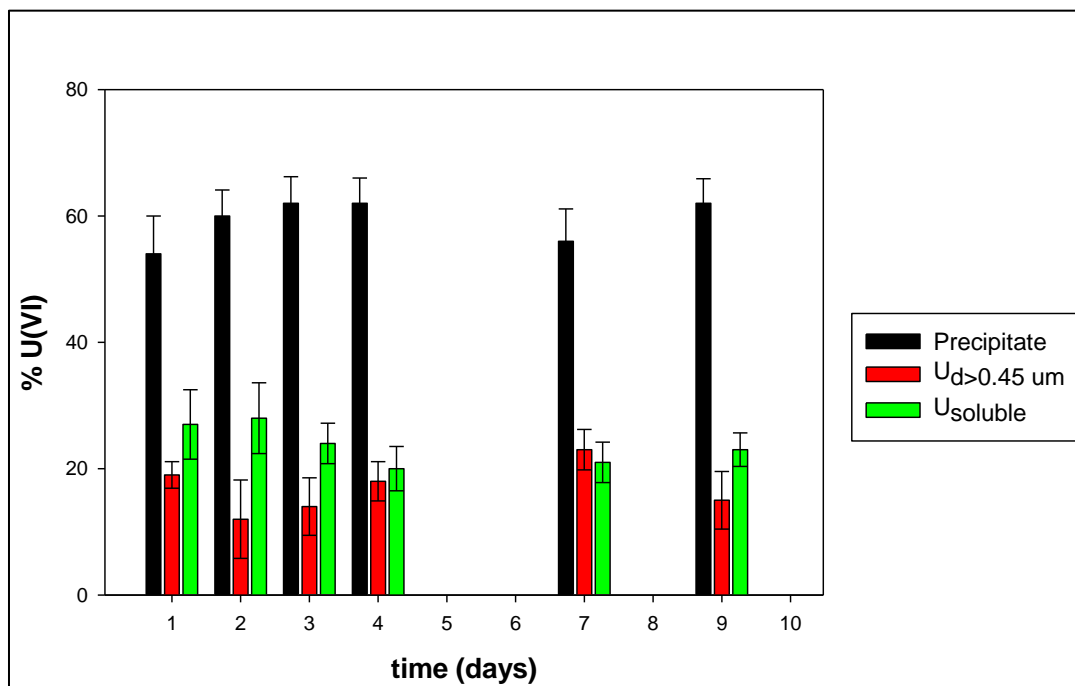


Figure 48. U(VI) distribution between different phases as a function of time for treatment with 80 ppm sodium silicate.

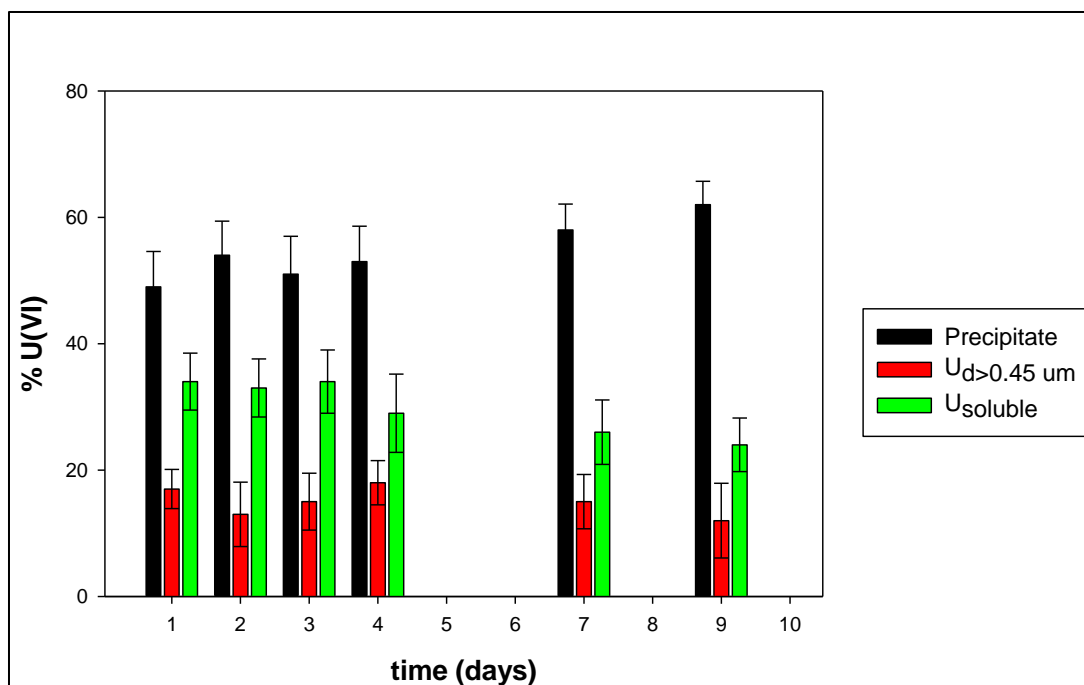


Figure 49. U(VI) distribution between different phases as a function of time for treatment with 90 ppm sodium silicate.

Table 12 presents the average values of uranium percentage by phase in samples amended with 70, 80 and 90 mg L⁻¹ of sodium silicate. Results denote that all sodium silicate concentrations tested have achieved the same degree of precipitation. Furthermore, uranium associated with silica presumably present in the supernatant solution in a colloidal form ($U_{d>0.45\mu m}$) and percentage of soluble uranium in the filtrate were found to be similar across all categories. In conclusion, 70 mg L⁻¹ of sodium silicate is the most fitting concentration under the conditions studied.

Table 12. Uranium distribution in different phases in samples amended with 70, 80 and 90 mg L⁻¹ sodium silicate for a 9 day period.

U(VI) phases	Sodium silicate		
	70 mg L ⁻¹	80 mg L ⁻¹	90 mg L ⁻¹
% Precipitate	59±5	59±4	55±5
% Colloidal ($U_{d>0.45\mu m}$)	20±4	17±4	15.5±3
% In Soluble phase	20±5	24±4	29±5

The monitoring of silica revealed that after 2 days of reaction time, less than 10% of the initial silica concentration added in the solution still remained in the aqueous phase (Figure 50). The percent removal of silica from the solution was found to be 93±2%, 94±2% and 92±1% for samples spiked with 70, 80 and 90 mg L⁻¹ of sodium silicate, respectively.

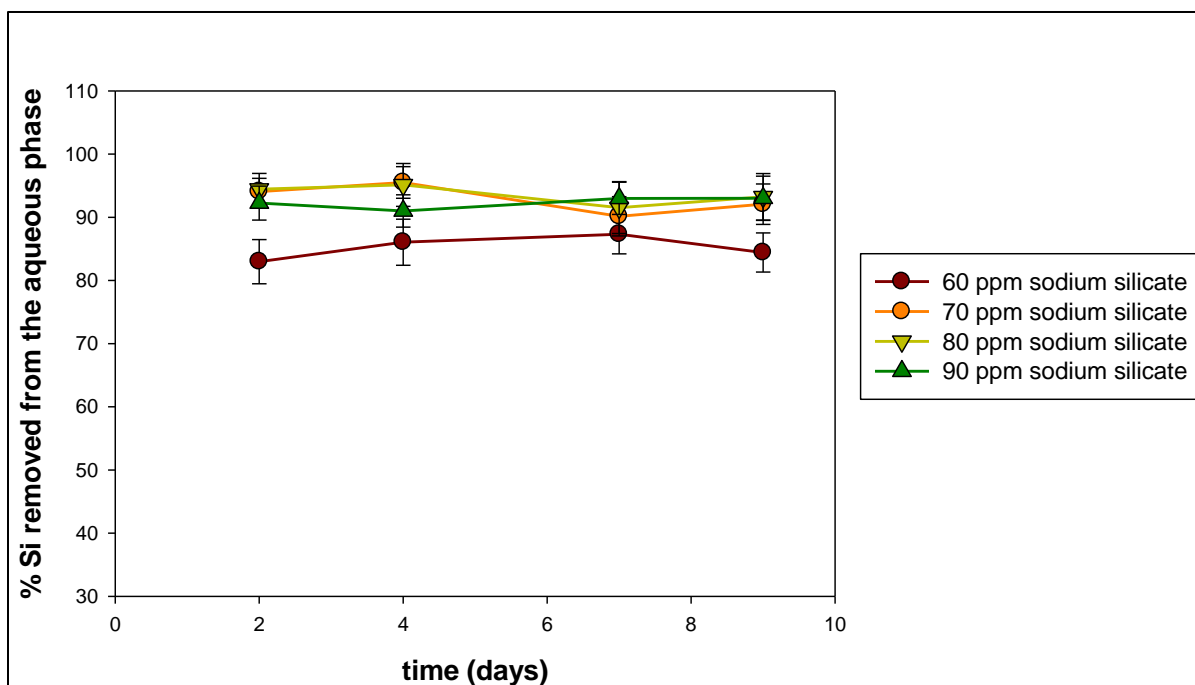


Figure 50. Percentage of Si removed from the aqueous phase as a function of time for treatment with different sodium silicate concentrations.

Sodium silicate solution chemistry is greatly affected by the pH. Acidic or alkaline conditions can affect equilibrium conditions of silicate solution polymerization reactions based on the following generalized scheme (Figure 51). Below pH 9, silica exists in anhydrous and hydrous amorphous Si phases that can contribute to the formation of colloidal particles of SiO_2 , which exist in equilibrium with silicic acid or $\text{Si}(\text{OH})_4$ (Iler, 1979). As pH decreases and the environment becomes more acidic, equilibrium is expected to shift to the right, favoring further polymerization of the colloidal species. On the other hand, silicic acid itself is better viewed as a complex hydrous polymer with variable Si, O and H composition and Si-O-Si connectivity (Falcone, 2006).

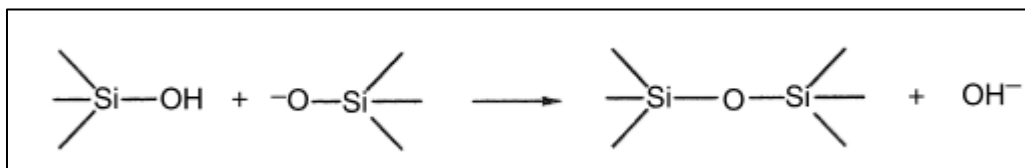


Figure 51. Schematic depiction of polymer equilibrium of silicate solutions.

Hence, the almost quantitative removal (~90%) of silica from the aqueous phase was expected due to the strongly acidic conditions of SRS synthetic groundwater.

The amount of iron detected in the supernatant for different sodium silicate concentrations added is presented in Figure 52. Iron is not a component of SRS synthetic groundwater and, therefore, its presence in the aqueous phase can be traced back to the soil's composition. Metal mobility depends on the interactions between the solid and liquid phase, which determine their partitioning (Carrillo-González et al., 2006) and pH is one of the main variables affecting these

phenomena. The composition of leachates from soils that comprise of primary silicates, such as quartz, includes iron, due to the primary silicate's frequent association with iron in geological formations (Sposito, 2008) and specifically in SRS soil (Dong et al., 2011). SRS soil from the F/H Area is comprised mostly of quartz with very small amounts of kaolinite and goethite (Dong et al., 2012). Hence, the change in pH, which is even more prominent in the initial stage (Figure 44) as a consequence of sodium silicate addition, is probably associated with the mobilization of iron from soil goethite minerals to the aqueous phase (McLean & Bledsoe, 1992).

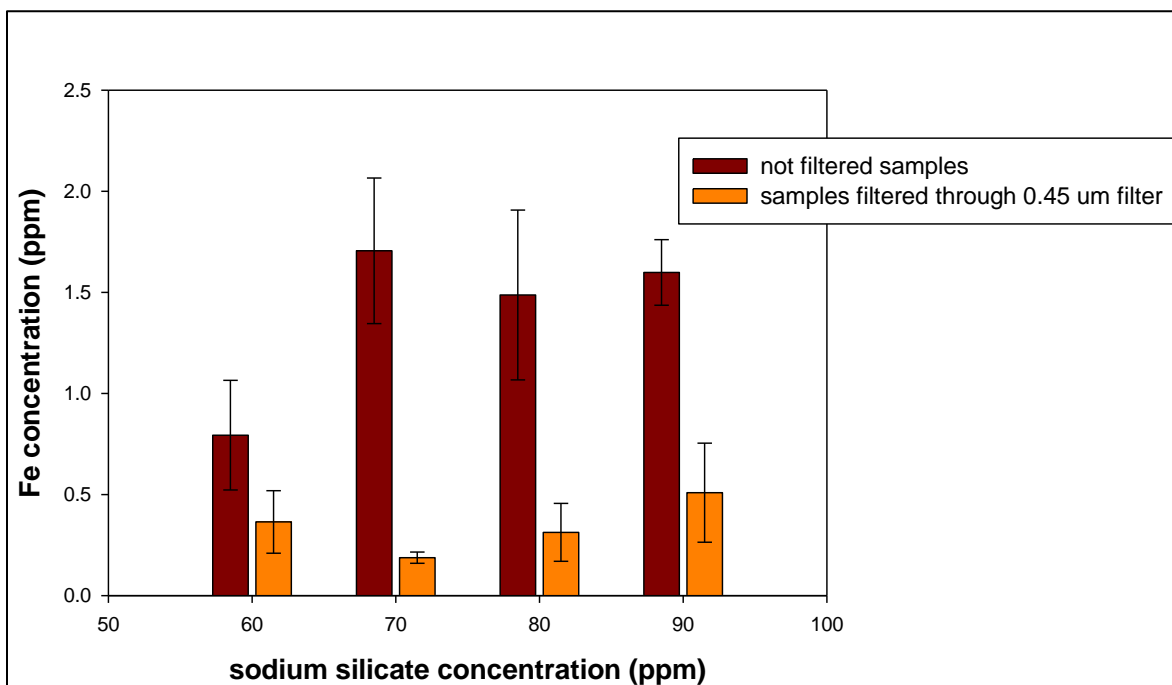


Figure 52. Iron concentration in the aqueous phase as a function of sodium silicate addition for unfiltered and filtered through 0.45µm filters samples.

There is a significant difference in the amount of iron detected in the aqueous phase between unfiltered and filtered samples. After filtration, the levels of iron in the aqueous phase are very low, in the range of 250-300 ppb. These values are comparable to those of the control samples (no addition of sodium silicate), which were approximately 180 ppb. Before filtration, the concentration of iron was approximately 1.8 ppm, a value which is roughly 6 times higher than the levels of iron after filtration and 9 times higher than the control samples. These results imply that the increase in iron concentration in the aqueous phase is associated with the addition of sodium silicate in the solution.

SEM/EDS analysis of filters

Analysis of the filters that have retained the colloidal particles (mean diameter larger than 0.45 µm) was performed by SEM-EDS in order to obtain a better understanding of the morphology and the elemental composition. As it can be seen in Figure 53, there are some amorphous particles “sitting” on top or incorporated in a “spongy” layer of smaller particles. The EDS analysis revealed that amorphous particles consist primarily of Si and O (Figure 54), while the “spongy” layer consists of Si with significant presence of Al (Figure 55). An overall elemental

composition of the sample revealed the presence of Fe, presumably associated with one or the other form (Figure 56).

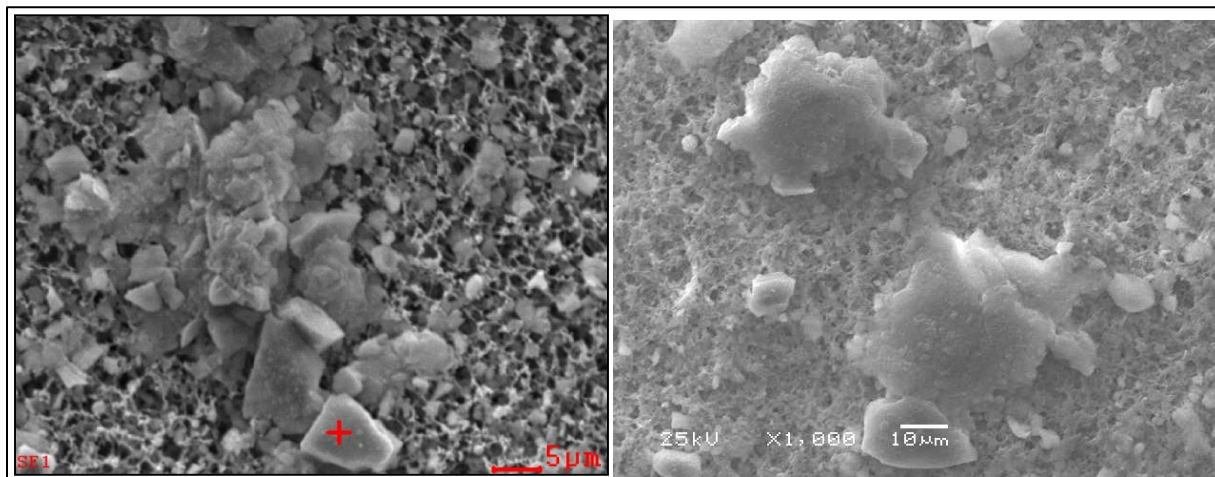


Figure 53. SEM images of the surface of 0.45 µm filters

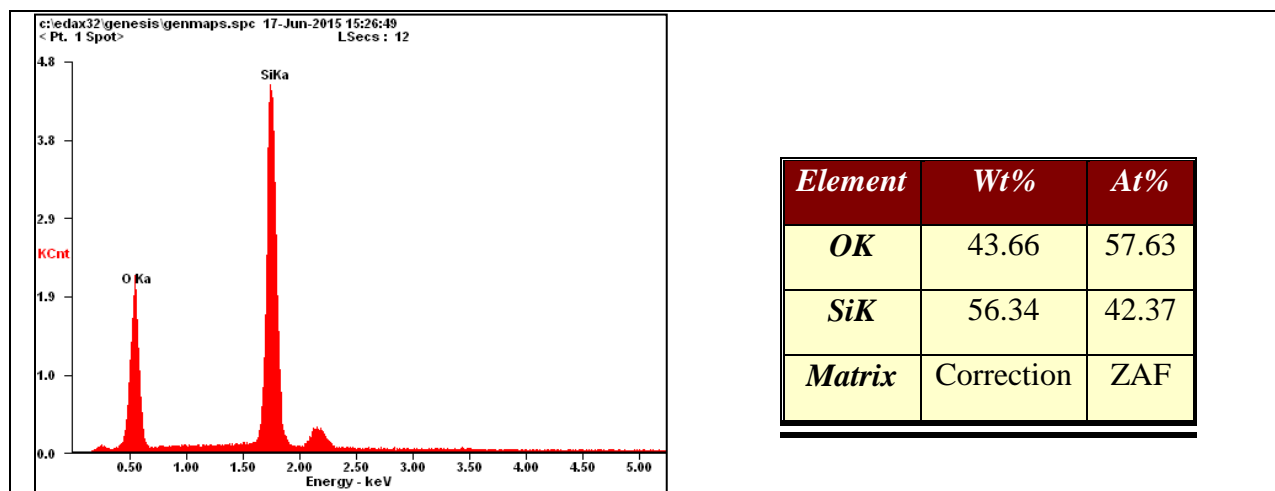


Figure 54. EDS spot analysis of the amorphous particle shown in Figure 53 on the left

The presence of Fe and Al can be clearly traced back to the soil composition, since there is no iron or aluminum present in the synthetic groundwater. Metal cations, such as Fe^{3+} and Al^{3+} , are sorbed on the surface of negatively charged colloidal silicate particles. The sorption of the cations results in charge neutralization and decrease of repulsion energy and subsequent destabilization of colloid particles (Iler, 1979; Shammass & Wang, 2015). This results in localized concentration of the metal ions near the siliceous surface (Ananthapadmanabhan & Somasundaran, 1985). This interaction decreases as the degree of polymerization decreases; hence, this phenomenon is more prominent in acidic environments where the degree of polymerization increases (Camenzuli et al., 2015; Falcone, 1982; Ortego et al., 1991).

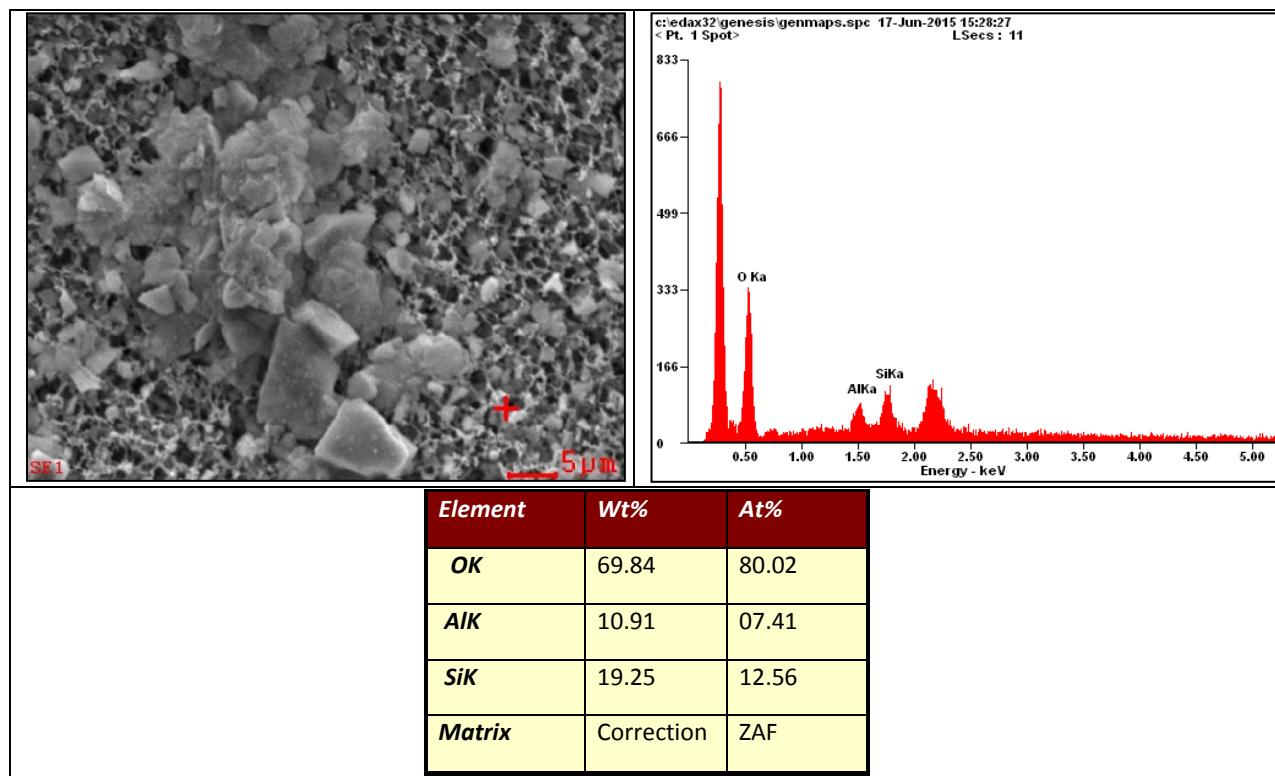


Figure 55. SEM/EDS analysis of the “spongy” background.

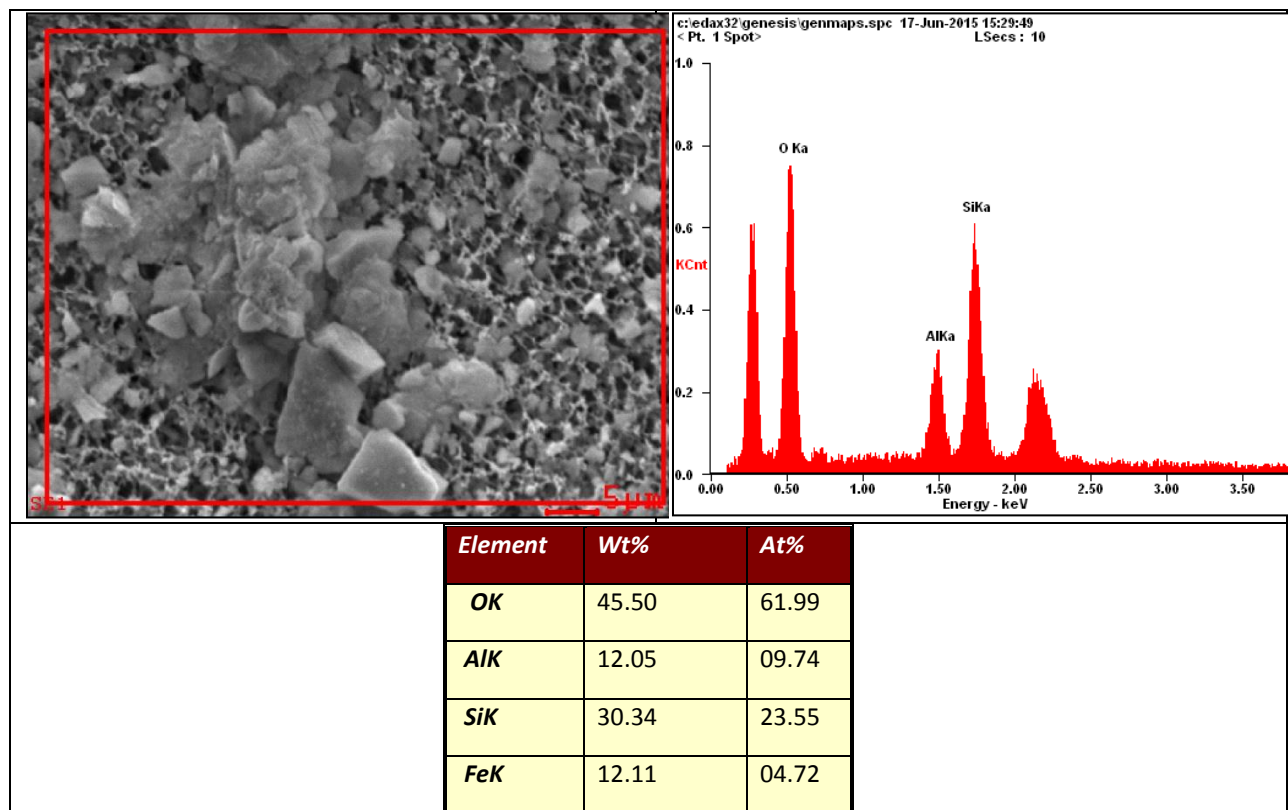


Figure 56. SEM/EDS area analysis, including the amorphous particles and the “spongy” layer (0.45 µm filters).

Uranium was not detected via EDS due to the low initial concentration (0.5ppm). It is estimated that ~20% of U(VI) is retained by the filter, which roughly translates to 100 ppb, which is lower than the detection limit of EDS. Uranium could be increased in future experiments to allow for detection by EDS. This will help to identify how uranium is associated with the amorphous formations observed on the filters.

The presence of amorphous particles with the diameter larger than $0.45\mu\text{m}$ comprised of Si (and possibly U), Fe and Al might justify the reduced mobility of sodium silicate through saturated sediments. It is possible that particle size might also contribute to their reduced mobility in the subsurface. Nevertheless, further consideration of the soil porosity is required.

The analysis of micro particles retained by the $0.2\mu\text{m}$ filters revealed the absence of a “spongy” layer and the existence of very few crystals, which comprised mostly of Al and O (Figure 57). There was no uranium detected in the chemical composition via EDS analysis, as expected, since there was no uranium detected via chemical analysis conducted during batch experiments.

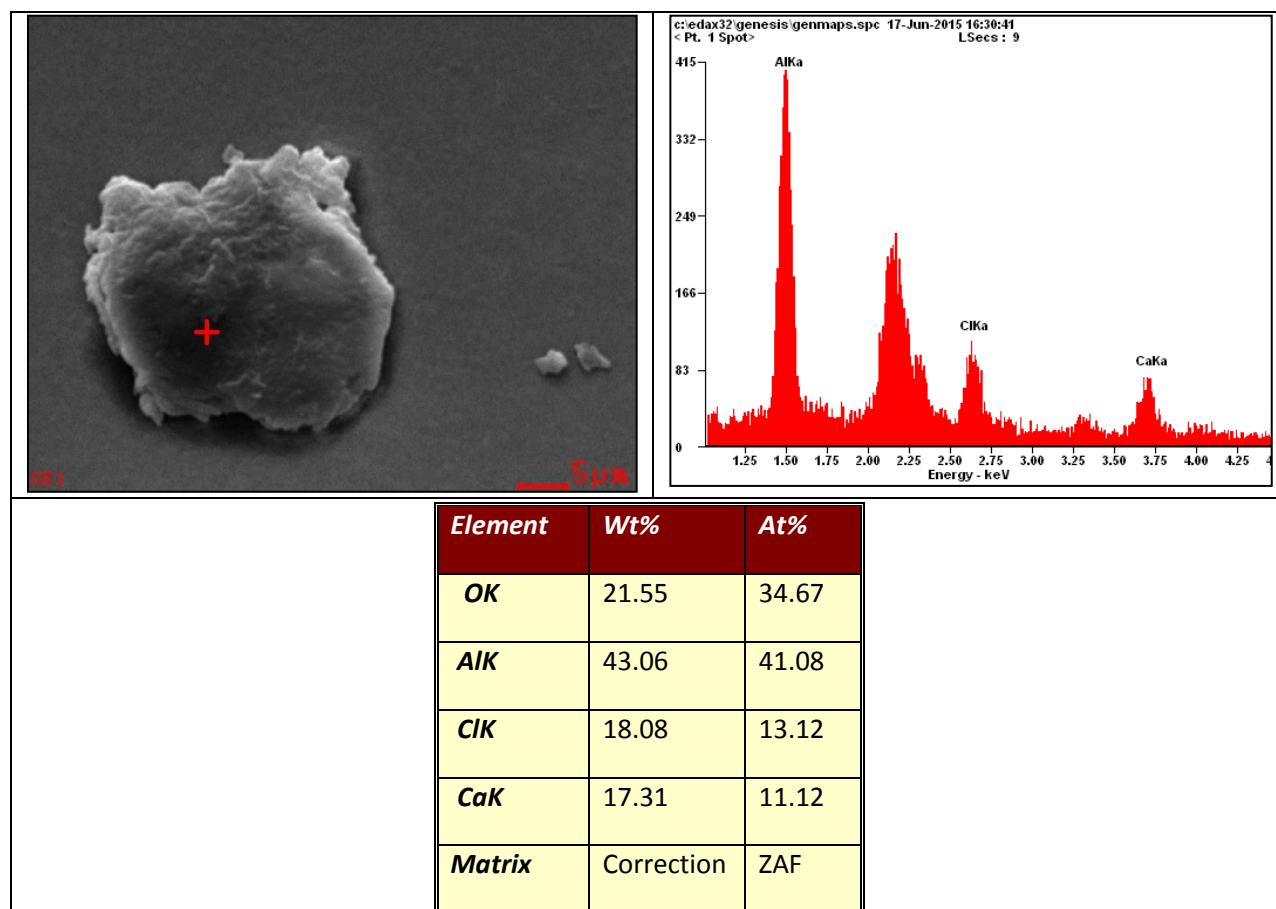


Figure 57. SEM image and EDS analysis of $0.2\mu\text{m}$ filter

Long-term pH sustainability

The optimization of sodium silicate concentration to elevate the pH to circumneutral conditions requires an assessment of whether or not the pH is stable over time. The ability of sodium silicate concentrations of 70, 80 and 90 mg L^{-1} to maintain a circumneutral pH for a longer period was

investigated (Figure 58). All previous experiments explored the increase of pH in a very short period of time (3 days) (Figure 44).

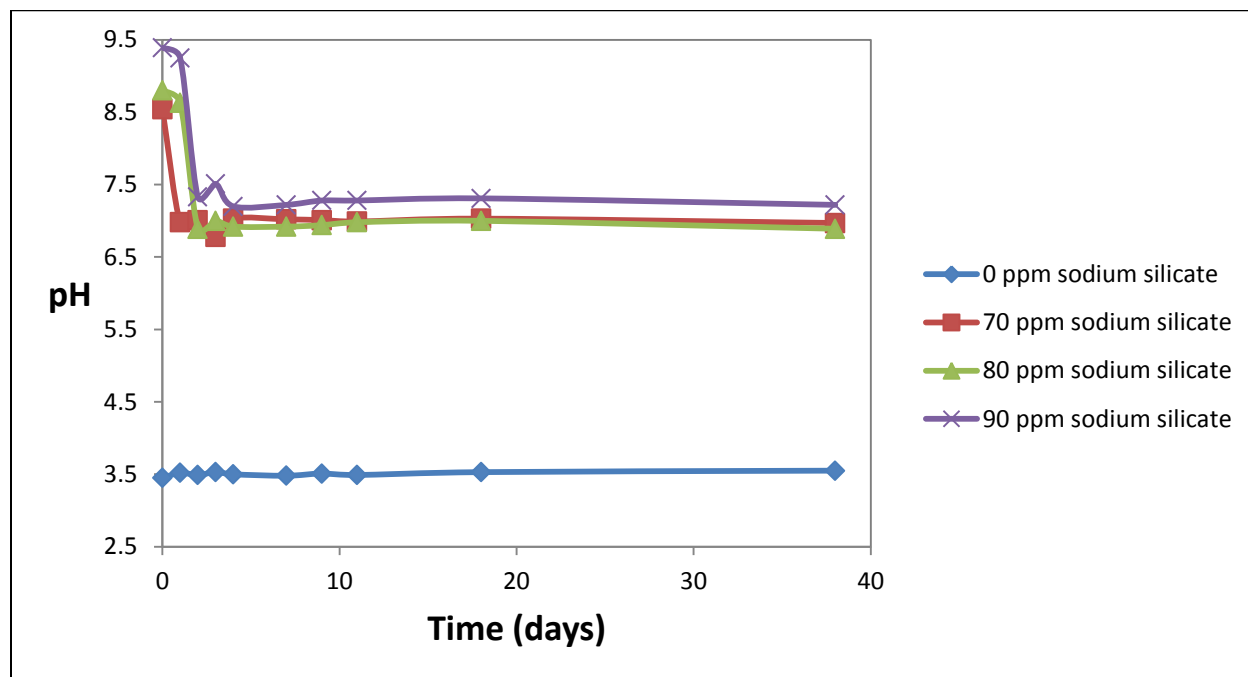


Figure 58. Monitoring of pH evolution for batch samples comprised of SRS soil and synthetic groundwater containing $0.5 \text{ mg L}^{-1} \text{ U(VI)}$, spiked with different sodium silicate concentrations

It is obvious that different concentrations of sodium silicate have the ability to elevate pH at different alkaline levels ranging from 8.5 to 9.5 (as shown in Figure 44) within the first 2-3 days, but eventually pH stabilized at ~ 7 for the remainder of the monitoring period of 40 days.

Subtask 2.1: Future Work

Future work will focus on the characterization of colloidal particles formed in the supernatant and the association of uranium with these particles. This will be achieved by following similar experimental procedures with the exception of using higher initial uranium concentrations. The increase in uranium concentration will lead to more accurate detection by SEM-EDS. Future studies will also focus on the stability of the sequestered uranium after sodium silicate applications. In addition, based on the charge properties of the sodium silicate particles and their ability to coagulate with metal cations, the potential application of the proposed technology will be evaluated in multi-metal systems (e.g., uranium and strontium).

Subtask 2.1: Acknowledgements

Funding for this research was provided by U.S. DOE cooperative agreement DE-EM0000598. We would like to thank Dr. Miles Denham from SRNL for the valuable suggestions and useful discussions on this research topic.

Subtask 2.1: References

- Ananthapadmanabhan, K.P., Somasundaran, P. 1985. Surface precipitation of inorganics and surfactants and its role in adsorption and flotation. *Colloids and Surfaces*, **13**, 151-167.
- Baehr, C.H., Koehl, W. 2007. Soluble silicates - highly versatile and safe. *International Journal of Applied Science*, **133**, 88-94.
- Camenzuli, D., Gore, D.B., Stark, S.C. 2015. Immobilisation of Metals in Contaminated Landfill Material Using Orthophosphate and Silica Amendments: A Pilot Study. *International Journal of Environmental Pollution and Remediation*, **3**, 27-32.
- Carrillo-González, R., Šimůnek, J., Sauvé, S., Adriano, D. 2006. Mechanisms and Pathways of Trace Element Mobility in Soils. in: *Advances in Agronomy*, Vol. Volume 91, Academic Press, pp. 111-178.
- Dong, W., Tokunaga, T.K., Davis, J.A., Wan, J. 2012. Uranium(VI) Adsorption and Surface Complexation Modeling onto Background Sediments from the F-Area Savannah River Site. *Environmental Science & Technology*, **46**(3), 1565-1571.
- Dong, W., Wan, J., Tokunaga, T.K., Denham, M., Davis, J., Hubbard, S.S. 2011. Surface Complexation Modeling of U(VI) Adsorption onto Savannah River Site Sediments. *AGU. American Geophysical Union*.
- Falcone, J.S. 1982. *Soluble Silicates*. American Chemical Society, Washington DC.
- Falcone, J.S. 2006. The uses of soluble silica. in: *Colloidal Silica. Fundamentals and Applications*, (Eds.) H.E. Bergna, W.O. Roberts, Taylor & Francis Group. Boca Raton.
- Iler, R.K. 1979. *The Chemistry of Silica: Solubility, Polymerization, Colloid and Surface Properties and Biochemistry*. John Wiley & Sons Inc., New York, USA.
- Krestou, A., Panias, D. 2004. Uranium (VI) speciation diagrams in the $\text{UO}_2^{2+}/\text{CO}_3^{2-}/\text{H}_2\text{O}$ system at 25°C. *The European Journal of Mineral Processing and Environmental Protection* **4**(2), 113-129.
- Ortego, J.D., Barroeta, Y., Cartledge, F.K., Akhter, H. 1991. Leaching effects on silicate polymerization. An FTIR and silicon-29 NMR study of lead and zinc in portland cement. *Environmental Science & Technology*, **25**(6), 1171-1174.
- Rich, R. 2007. *Inorganic Reactions in Water*. Springer-Verlag.
- Shammas, N.K., Wang, L.K. 2015. *Water Engineering: Hydraulics, Distribution and Treatment*. John Wiley & Sons Inc., Hoboken, New Jersey, USA.
- Sposito, G. 2008. *The chemistry of Soils*. Oxford University Press, Cary NC, USA.
- Storm, R.N., Kaback, D.S. 1992. SRP Baseline Hydrogeologic Investigation: Aquifer Characterization, Groundwater Geochemistry of the Savannah River Site and Vicinity (U). Westinghouse Savannah River Company, Savannah River Laboratory.
- Taylor, P.A. 2015. Physical, chemical and biological treatment of groundwater at contaminated nuclear and NORM sites. in: *Environmental Remediation and Restoration of Contaminated Nuclear and Norm Sites*, (Ed.) L. van Velzen, Woodhead Publishing.

Subtask 2.1.1: Carryover FIU's support for groundwater remediation at SRS F/H Area-Synergetic interactions between humic acid and colloidal silica for the removal of uranium

Subtask 2.1.1: Introduction

The Savannah River Site (SRS) was constructed during the 1950s and became one of the major producers of plutonium for the United States during the Cold War. Since the beginning of the environmental cleanup program in 1981, SRS has become a hazardous waste management facility. As a hazardous waste management facility, the site is responsible for storage of radioactive materials and remediation of soil and groundwater contaminated with radionuclides. During its production life, the F/H Area Seepage Basins received approximately 1.8 billion gallons of acidic waste containing radionuclides and dissolved heavy metals. This led to the unintentional creation of a highly contaminated groundwater plume at an acidic pH of 3-5.5. The acidity of the plume contributes to the mobility of several constituents of concern (COC) such as tritium, uranium-238, iodine-129, and strontium-90 for the F-Area plume and tritium, strontium-90 and mercury for the H-Area plume. This investigation will focus on uranium (VI).

Initially, removal of contaminant from the polluted groundwater was accomplished by a pump-and-treat and re-inject system constructed in 1997. Downgradient groundwater within the system was pumped to the water treatment facility and re-injected upgradient within the aquifer. The effectiveness and sustainability of this process diminished over time and it was discontinued in 2004. It was replaced with a funnel-and-gate process. This new process injects sodium hydroxide directly into the gates of the F-Area groundwater to effectively raise pH levels. By raising the pH of the groundwater, a treatment zone was created by reversing the acidic nature of the contaminated sediments and producing a negative charge on the surface of sediment particles, enhancing the adsorption of cationic contaminants. This process resulted in a decrease in the concentration of Sr and U; but led to an increase in iodine concentrations. The solution used for the injections contained a high carbonate alkalinity in order to overcome the surface acidic conditions and natural partitions in the groundwater system. To maintain the neutral pH in the treatment zone, systematic injections are required. Further, the continuous use of high concentrations of a carbonate solution to raise pH may re-mobilize uranium previously adsorbed within the treatment zone, although this has not been observed in monitoring data.

FIU-ARC is investigating interactions between U(VI) and colloidal silica and synergistic effects between humic acid (HA) and colloidal silica influencing the percent removal of U(VI). Humic substances (HS) are major components of soil organic matter with the ability to influence migration behavior and fate of heavy metals. Essentially, HS are polyfunctional organic macromolecules formed by the chemo-microbiological decomposition of biomass or dead organic matter. Being organic substances, HS are able to interact with both metal ions and organic compounds. Based on their solubility, HS are usually divided into three fractions (Chopping, et al. 1992). The three fractions are humin, humic acid and fulvic acid. Humin is insoluble at all pH values; HA represents the fraction which is soluble at pH greater than 3.5 and fulvic acid is soluble at all pH values.

Humic acid, which carries a large number of functional groups, provides an important function in ion exchange and as a metal complexing ligand with a high complexation capacity being able to affect the mobility of actinides in natural systems (Davis, 1982; Plancque et al., 2001). Various studies have suggested that the retention of U(VI) via sorption in the presence of HA is a

complex process due to HA forming organic coatings by sorbing on the surface of oxides and minerals, thus modifying the sorption capabilities of these metal ions (David, 1984; Zachara et al., 1994; Labonne-Wall et al., 1997; Perminova et al., 2002). The sorption of metal ions is expected to be enhanced at low pH and reduced at high alkaline pH (Ivanov et al., 2012). However, this sorption capacity is also affected by the concentration of HA in the system (Chen and Wang, 2007). The U(VI) sorption onto kaolinite is influenced by the pH, U(VI) concentration, presence of inorganic carbon species and naturally occurring HA. It has also been shown that U(VI) prefers to be adsorbed onto kaolinite as a uranyl-humate complex (Krepelova et al., 2007).

Silica, is the term applied to solid forms with the stoichiometric composition of SiO_2 ; silicas vary and are well-characterized by the Si-O bond lengths, Si-O-Si bond angle and Si-O bond coordination. The surface charge of silica is negative beyond pH 2 (Bergna, Roberts. 2006). Due to the negatively charged silica there are possible interactions with uranyl cations and positively charged U(VI) species.

This investigation analyzed any synergistic interactions between U(VI) ions, HA and colloidal silica under varying pH conditions from 3 to 8 and the presence of sediment collected from SRS FAW1. Multi-component batch systems were constructed to effectively analyze each of these parameters and their synergistic contributions to the removal of U(VI) from the aqueous phase.

Subtask 2.1.1: Materials and Methods

Materials

Sediment samples used in the experiments were collected at SRS from FAW1 at a depth of 70-90 feet and shipped to FIU-ARC. The sediment was sieved through 2 mm to remove gravel and larger sediment particles. Fumed colloidal silica, silicon (IV) oxide 99%, and humic acid sodium salt (50-60% as humic acid) were obtained from Fisher Scientific. Stocks of HA and Si were prepared in deionized water (DIW) at 2000 ppm and 100 ppm, respectively. A commercial 1000 ppm uranyl nitrate stock solution in 2% nitric acid (Fisher Scientific) was used as a source of U(VI).

Experimental Methods

Removal of U(VI) was studied through multi-component batch systems with a pH range from 3 to 8 in order to evaluate adsorption with respect to pH. Last year FIU/ARC investigated the synergetic effect of colloidal silica and HA on uranium removal by preparing seven batches with various combinations of Si and HA (Lagos, et al, 2014). This year experiments include additional controls (only soil and HA) to study the sorption behavior of uranium at a higher HA concentration (50 ppm). These results were compared to the data on the sorption behavior of U(VI) at a lower HA concentration (10 ppm) obtained last year. The following batches were prepared:

- Batch 2: Si (3.5 mM) + U(VI) (0.5 ppm) + HA (50 ppm), (no sediments)
- Batch 3: U(VI) (0.5 ppm) + HA (50 ppm), (no Si or sediments)
- Batch 5: Sediments + Si (3.5 mM) + U (VI) (0.5 ppm) + HA (50 ppm)
- Batch 6: Sediments + U(VI) (0.5 ppm) + HA (50 ppm), (no Si)

- Control: U(VI) (0.5 ppm), (no SI, HA, or sediment)

Further, the control samples were prepared in triplicate with DIW and 0.5 ppm U(VI) to account for any sorption between the uranium and the plastic vials. The resulting sample mixtures were spiked with uranium to yield a concentration within a solution matrix of ~0.5 ppm. Table 13 presents the amount of stock solutions needed to yield 50 ppm of HA, 3.5 mM of Si and 0.5 ppm of U(VI). Triplicate samples for each batch were prepared; uranium was added to each sample prior to adjusting the pH. The pH of the mixture was then adjusted to the required value using 0.01 M HCl or 0.1 M NaOH (Figure 59). Control samples were prepared in DIW amended with U(VI) at a concentration of 0.5 ppm U(VI) to test for U(VI) losses from the solutions due to sorption to the tube walls and caps. All volumes of solutions were prepared to initially have 20 mL of total volume in the sample tube. All control and experimental tubes were vortexed and then kept on the shaker at 100 rpm for 48 hours at room temperature.

Table 13. Experimental Matrix with Amount of Components

Batch #	Constituents					
	SiO ₂ ml	Humic Acid ml	Uranium U(VI) ml	Sediment mg	Water H ₂ O ml	Total Volume ml
Batch No. 2	2.1	10	0.01	0	7.89	20
Batch No. 3	0	10	0.01	0	9.99	20
Batch No. 5	2.1	10	0.01	400	7.89	20
Batch No. 6	0	10	0.01	400	9.99	20



Figure 59. Experimental setup.

Samples were shaken for 48 hr at 100 rpm and then centrifuged at 2700 rpm at 22°C for 30 minutes (Figure 60). After centrifuging the samples, two aliquots (filtered and unfiltered) were

prepared, filtered aliquots were by filtering supernatant solution using a 0.45 μ m PTFE syringe filter and unfiltered aliquots were prepared by simply taking supernatant solution. Aliquots were diluted for KPA (U(VI) analysis) and ICP-OES (Fe and Si analysis) by taking a 300 μ L and 500- μ L of filtered and unfiltered samples respectively for a 1:10 dilution in 1% HNO₃.



Figure 60. Shaker and centrifuge experimental setup.

Subtask 2.1.1: Results and Discussion

pH 3

Triplicate samples at pH 3 were analyzed with KPA to determine the uranium concentration. Percent uranium removal was calculated using the uranium concentration from the control samples and Table 14 shows the average U(VI) percent removal from the triplicate samples. The percent removal of uranium for batches 2 & 3 (with no sediment, 2 included Si while 3 did not) and batches 5 & 6 (amended with sediment, 5 included Si while 6 did not) ranged between 49-55% and a 79-84%, respectively. Solubility of HA is low at low pH while U(VI) is present as highly soluble uranyl ions (Krepelova, 2007a). Krepelova et al. (2007b) reported that HA enhances the U(VI) sediment uptake under acidic pH (<6) conditions and that U(VI) generally follows the sorption of HA in the presence of kaolinite. Further, the sorption/removal of HA under acidic pH creates more sorption sites for the uranium. The high percent removal of uranium can be attributed to the competition of solubilizing negative functional groups (deprotonated carboxyl groups) with hydrophobic groups; at low pH, the hydrophobic group is the stronger force causing aggregation/coagulation of the uranyl cations (Tipping, 2002). U(VI) interaction with silica colloids is found to be negligible as the average Si removal was $87.11 \pm 3.55\%$ and $84.38 \pm 0.15\%$ for batch 2 and 5, respectively. Batch 2 yielded significantly less U(VI) removal compared to batch 5 yet both have relatively similar Si removal. The presence of sediments increased the percent of U(VI) removal on average from 50% to 80%. The sediments provide significantly more sorption sites for U(VI) and the uranium cations are attracted to the negatively charged sediment particles, increasing the percent of U(VI) removal.

Table 14. Analytical Results for pH 3

Sample-Description, pH 3	U(VI) Avg Removal, %	Std Deviation	Si Avg Removal, %	Std Deviation	Fe, ppm	Std Deviation
Batch 2	55.17	4.00	87.11	3.55	No Sediment	
Batch 3	49.22	6.50	No Si	No Si	No Sediment	
Batch 5	83.83	1.97	84.38	0.15	0.31	0.02
Batch 6	79.16	2.90	No Si	No Si	0.37	0.07

pH 4

Resulting data for pH 4 was similar to that of pH 3, though showing slightly lower U(VI) removal for all batches. The samples prepared with sediments (batches 5 and 6) still provided a higher removal percentage than those without sediments, dropping from 70% removal with sediment to as low as 41% without sediment.

Table 15. Analytical Results for pH 4

Sample-Description, pH 4	U(VI) Avg Removal, %	Std Deviation	Si Avg Removal, %	Std Deviation	Fe, ppm	Std Deviation
Batch 2	53.2	3.93	82.4	1.27	No Sediment	
Batch 3	40.52	4.28	No Si	No Si	No Sediment	
Batch 5	65.36	2.39	85.61	1.65	0.3	0.06
Batch 6	70.06	0.42	No Si	No Si	0.41	0.02

pH 5 and 6

For batches at pH 5 and 6, the samples showed similar results. For batches 2 and 3, the U(VI) removal percentage gradually decreased with an increase in pH; the average uranium removal at pH 3 was observed as 53% and was reduced to the average removal value of 35% at pH 5 and 31% at pH 6. Similar trends were observed for batches 5 and 6; uranium removal decreased from 80% at pH 3 to 50% and 44% at pH 5 and 6, respectively. At these pH values, the number of uranyl cations in solution decreases, which ultimately limits the interactions between uranium and HA. Once the pH reaches 6, the dominant species in solution is $\text{UO}_2(\text{OH})\text{HA}(\text{I})$ with minimal presence of uranyl cations and $\text{UO}_2\text{HA}(\text{II})$ (Krepelova, 2007a). Similarly, due to the increased solubility of HA, fewer binding sites are available for interactions. Liao et al. (2013) reported that the coordination number between U(VI) and humic acid increases from 1:1 to 1:2 when pH increased from 3 to 6; the data obtained in these experiments supports this theory. The coordination number suggests the number of ligands attached to the central ion, showing that

greater amounts of HA is required to remove the same amount of U(VI). Similar to the lower pH results, the batches containing sediment showed higher uranium removal percentages compared to sediment-free batches.

Table 16. Analytical Results for pH 5

Sample-Description, pH 5	U(VI) Avg Removal, %	Std Deviation	Si Avg Removal, %	Std Deviation	Fe, ppm	Std Deviation
Batch 2	38.25	3.08	85.15	3.09	No Sediment	
Batch 3	32.98	4.12	No Si	No Si	No Sediment	
Batch 5	49.59	1.98	85.35	0.71	0.42	0.03
Batch 6	52.18	1.43	No Si	No Si	0.48	0.02

Table 17. Analytical Results for pH 6

Sample-Description, pH 6	U(VI) Avg Removal, %	Std Deviation	Si Avg Removal, %	Std Deviation	Fe, ppm	Std Deviation
Batch 2	30.87	5.66	77.71	4.96	No Sediment	
Batch 3	32.98	5.82	No Si	No Si	No Sediment	
Batch 5	43.08	0.94	84.14	1.75	0.48	0.03
Batch 6	45.82	0.84	No Si	No Si	0.59	0.07

pH 7

The neutral pH of 7 revealed the lowest percent uranium removal of all batches. Uranium removal for the sediment-free batches (batches 2 and 3) was at 19.5% and 21%, while sediment-containing samples yielded a higher removal at 39% and 45%, respectively for batches 5 and 6. By adding sediments into the solution, a ~50% increase in U(VI) removal is seen compared to samples without sediment.

Table 18. Analytical Results for pH 7

Sample-Description, pH 7	U(VI) Avg Removal, %	Std.	Si Avg Removal, %	Std Deviation	Fe, ppm	Std Deviation
Batch 2	19.51	3.64	75.67	4.02	No Sediment	
Batch 3	20.89	1.03	No Si	No Si	No Sediment	
Batch 5	39.26	1.91	84.2	0.97	0.48	0.03
Batch 6	44.80	1.66	No Si	No Si	0.68	0.18

pH 8

The pH 8 samples show a slight increase in percent removal of uranium compared to the values observed at neutral pH 7. Batches 2 and 3 resulted in a 46% and 34% removal, respectively, while batches 5 and 6 yielded 41.5% and 43.5% removal, respectively. The uranium removal observed at pH 8 seemed to not be affected by the presence of sediments. Tipping (2002) states that, at high pH, the proton-binding sites of HA molecules are sufficiently dissociated to carry any significant charge, thus reducing any binding potential. The major species expected is $(\text{UO}_2)_3(\text{OH})_8^{2-}$, a negatively charged complex that limits interaction with the dissociated functional groups of HA.

Table 19. Analytical Results for pH 8

Sample-Description, pH 8	U(VI) Avg Removal, %	Std Deviation	Si Avg Removal, %	Std Deviation	Fe, ppm	Std Deviation
Batch 2	46.14	2.62	68.66	4.23	No Sediment	
Batch 3	34.17	5.75	No Si	No Si	No Sediment	
Batch 5	41.57	0.54	83.57	0.5	0.46	0.03
Batch 6	43.52	1.34	No Si	No Si	0.58	0.03

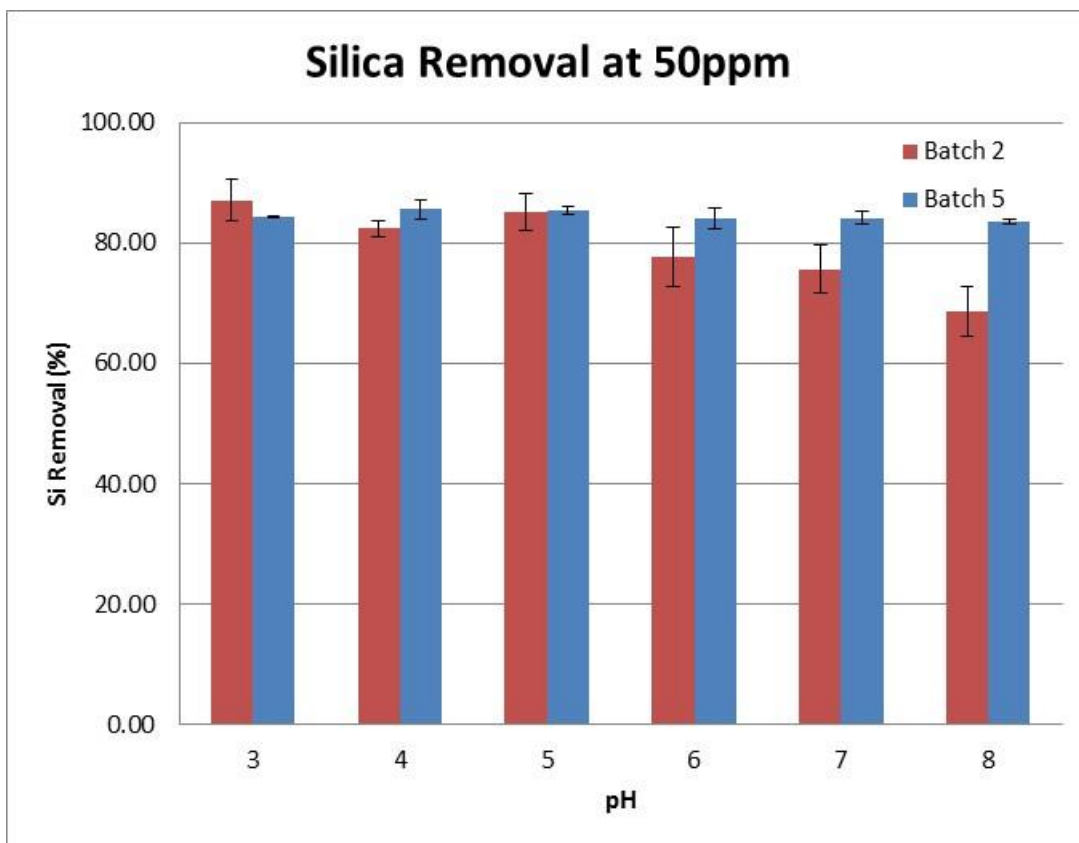


Figure 61. Silica removal at 50 ppm.

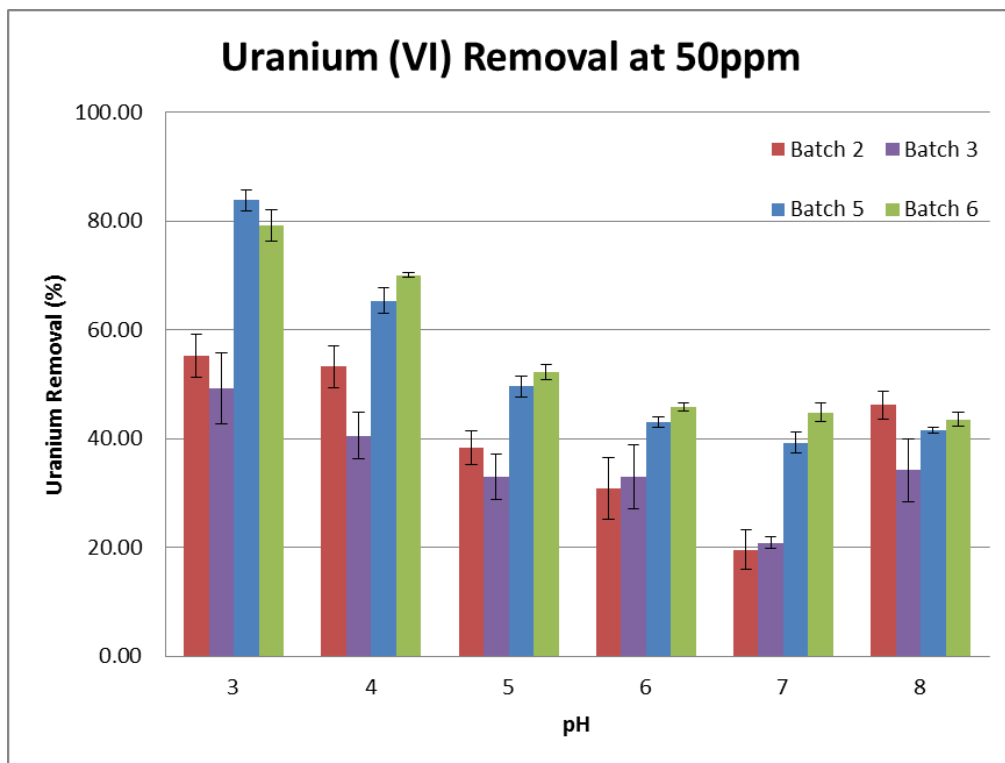


Figure 62. Uranium (VI) removal at 50 ppm HA.

The percent removal of U(VI) is directly influenced by the pH, HA and presence of sediments. Interactions of uranium with colloidal silica, HA, and sediment may be better explained by considering uranyl speciation at various pH conditions (see Table 20).

Table 20. Major Uranium species with respect to pH

pH	3	4	5	6	7	8
Uranyl Species	UO_2^{2+}	UO_2^{2+} $(\text{UO}_2)_2(\text{OH})_2^{2+}$	$(\text{UO}_2)_3(\text{OH})_5^+$ UO_2OH^+	$(\text{UO}_2)_3(\text{OH})_5^+$ UO_2OH^+	$(\text{UO}_2)_3(\text{OH})_5^+$ $(\text{UO}_2)_3(\text{OH})_7^+$	$(\text{UO}_2)_3(\text{OH})_8^{2-}$ $\text{UO}_2(\text{OH})_3^-$

At acidic pH, the uranyl cation is the dominant species. As pH increases, the dominant species becomes mononuclear and polynuclear hydrolyzed uranyl ions. As the pH reaches 8, the uranyl species changes from positively to negatively charged polynuclear complexes. At pH 4.5 and below, colloidal silica particles bear little negative surface charge; so, the positively charged uranyl complexes will have little interaction (Iler, 1975). At low pH, the presence of HA significantly increases uranium removal due to the functional groups available for interaction and binding. The removal of uranium increases with the addition of sediments due to the availability of more binding sites for the uranyl cations. As pH increases from 4 to 7, the removal decreases as the primary species is not the uranyl cation but rather hydrolyzed uranyl complexes. At this pH range, the coordination number increases (1:2), requiring more HA to remove the same amount of U(VI), unlike at an acidic pH where it is 1:1. Colloidal silica does not seem to have a significant effect, though Koopal et al. (1998) reported that HA could rapidly and strongly absorb onto the silica surface. If HA is absorbing to the silica, less removal of uranium will be observed from the limited binding sites.

Unfiltered 50 ppm Samples

For each sample, one aliquot (unfiltered) was pulled following the centrifuge step and an additional aliquot was pulled after filtering (filtered). The uranium (VI) removal for 50 ppm unfiltered samples (Figure 63) yielded a similar trend to that of the 50 ppm filtered samples; the highest removal exists at low pH with the overall removal decreasing and slightly leveling out by pH 8. A higher removal was seen for batches 5 and 6 (silica versus no silica) which are sediment bearing samples due to the increased availability of binding sites, with a high removal of 72% at pH 3 and a low of 33% at pH 8. The highest removal for Batches 2 and 3 was 45% at pH 3, decreasing to 18% by pH 8. The overall removal for U(VI) for the unfiltered samples was lower than the filtered. The highest removal reported for unfiltered samples was at pH 3 with 72% while for filtered samples at pH 3 the highest removal was 84%, both being sediment bearing samples; the lowest removal seen for unfiltered samples was at pH 8 with 18% while the lowest removal for filtered samples was 21% at pH 7. These values reinforce that the trend followed was similar on both occasions though slightly decreased for unfiltered samples. The filtration process would remove any semi-soluble components as well as adsorption to the filter may further decrease the U(VI) in suspension and thus decrease the removal rate compared to the unfiltered samples. There was a slight increase at pH 8 for the filtered samples for non-sediment bearing samples though this was not noted with the unfiltered samples.

Table 21. Uranium (VI) removal at 50 ppm HA.

50 PPM HA, unfiltered Samples						
Sample-Description, pH 3	U(VI) Avg Removal, %	Std Deviation	Si Avg Removal, %	Std Deviation	Fe, ppm	Std Deviation
Batch 2	31.80	4.57	94.55	1.00	No Sediment	
Batch 3	44.28	2.75	No Si	NA	No Sediment	
Batch 5	71.83	1.32	72.68	7.42	0.85	0.52
Batch 6	64.53	2.69	No Si	NA	0.62	0.06
Sample-Description, pH 4	U(VI) Avg Removal, %	Std Deviation	Si Avg Removal, %	Std Deviation	Fe, ppm	Std Deviation
Batch 2	44.98	0.50	88.92	1.37	No Sediment	
Batch 3	45.01	4.38	No Si	NA	No Sediment	
Batch 5	52.94	4.02	66.69	2.00	0.44	0.02
Batch 6	60.77	3.76	No Si	NA	0.51	0.07
Sample-Description, pH 5	U(VI) Avg Removal, %	Std Deviation	Si Avg Removal, %	Std Deviation	Fe, ppm	Std Deviation
Batch 2	37.55	1.66	84.02	0.29	No Sediment	
Batch 3	18.24	1.67	No Si	NA	No Sediment	
Batch 5	40.66	8.17	65.53	2.61	0.49	0.06
Batch 6	40.12	2.76	No Si	NA	0.43	0.03
Sample-Description, pH 6	U(VI) Avg Removal, %	Std Deviation	Si Avg Removal, %	Std Deviation	Fe, ppm	Std Deviation
Batch 2	28.27	6.27	76.77	1.86	No Sediment	
Batch 3	26.88	1.18	No Si	NA	No Sediment	
Batch 5	25.71	3.60	54.81	5.20	0.53	0.02
Batch 6	36.06	2.34	No Si	NA	0.44	0.02
Sample-Description, pH 7	U(VI) Avg Removal, %	Std Deviation	Si Avg Removal, %	Std Deviation	Fe, ppm	Std Deviation
Batch 2	22.92	7.99	60.24	4.40	No Sediment	
Batch 3	24.76	0.59	No Si	NA	No Sediment	
Batch 5	22.60	1.83	60.42	1.47	0.63	0.03
Batch 6	33.93	2.94	No Si	NA	0.55	0.04
Sample-Description, pH 8	U(VI) Avg Removal, %	Std Deviation	Si Avg Removal, %	Std Deviation	Fe, ppm	Std Deviation
Batch 2	21.40	0.12	44.04	14.01	No Sediment	
Batch 3	18.16	3.24	No Si	NA	No Sediment	
Batch 5	33.02	0.87	55.71	4.76	0.72	0.02
Batch 6	33.00	1.60	No Si	NA	0.59	0.05

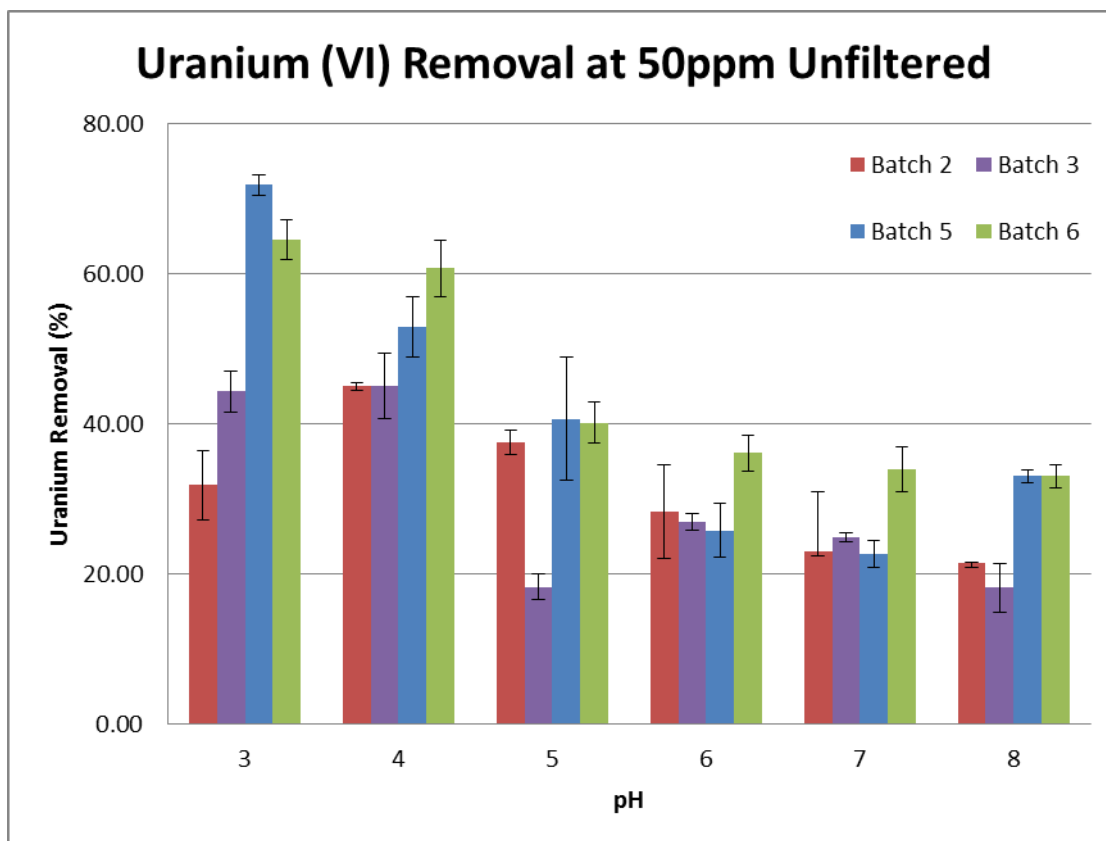


Figure 63. Uranium (VI) removal in unfiltered at 50 ppm HA.

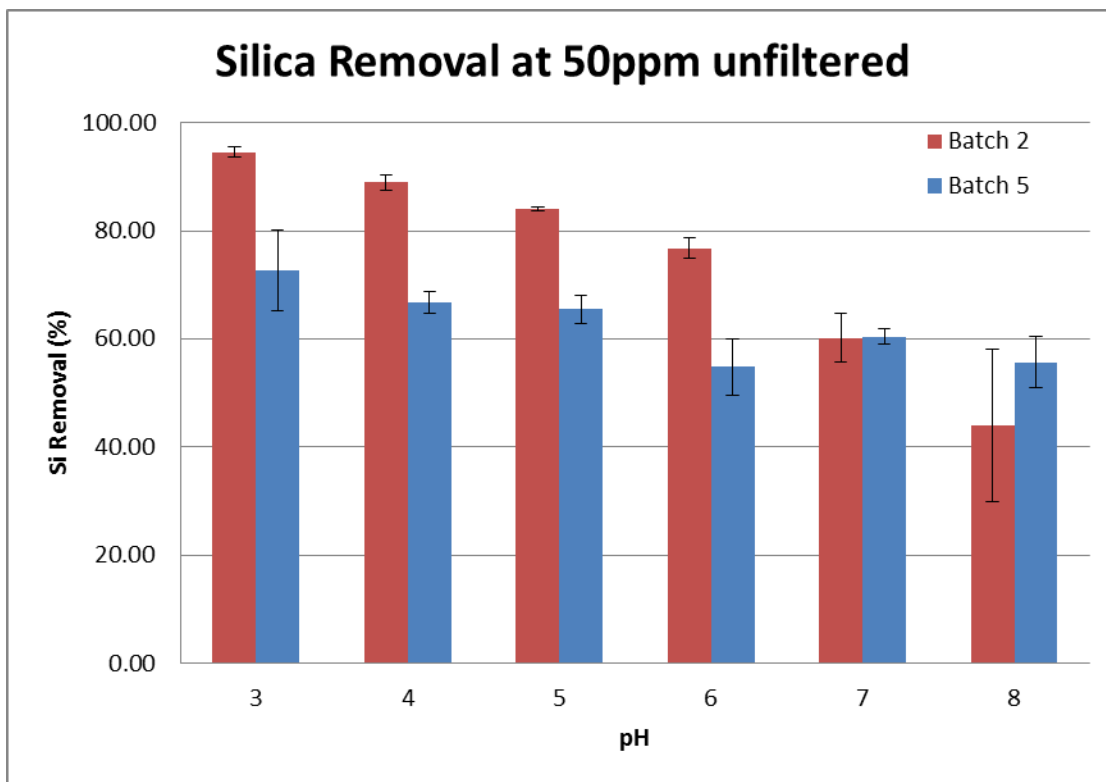


Figure 64. Uranium (VI) removal at 50 ppm HA Unfiltered.

Silica removal for unfiltered 50 ppm samples in Batches 2 and 3 gave a negative trend with the largest removal at pH 3 with 94.55% and decreasing towards pH 8 with 44.04% removal. This trend is unlike the filtered 50 ppm samples where removal of Si remained fairly constant for all batches with a slight deviation seen at pH 8. The non-sediment bearing samples, Batch 2, showed a higher removal than the sediment bearing samples, Batch 5, until an alkaline pH of 8.

Unfiltered 10 ppm Samples

Figure 6 represents the silica removal for the silica-containing batches (2 and 5) for the 10 ppm unfiltered samples. Silica removal averaged ~80% for sediment bearing samples, Batch 5, and for pH 3, 4 and 6 for Batch 2; at pH 5, 7 and 8, the removal was lower at ~50%. 50 ppm unfiltered samples showed similar results from Batch 2 at pH 3-6 though decreasing to 44% by pH 8; Batch 5 showed an overall lower removal of ~60%.

U(VI) removal for unfiltered samples showed distinct results; the 10 ppm HA solution showed significant removal at an alkaline pH, unlike the 50 ppm HA solution which shows a greater removal at acidic pH. It is postulated that 10 ppm HA is too low for significant interaction to occur, causing the uranium removal to be from the sediment present. However, further research is needed to test this hypothesis.

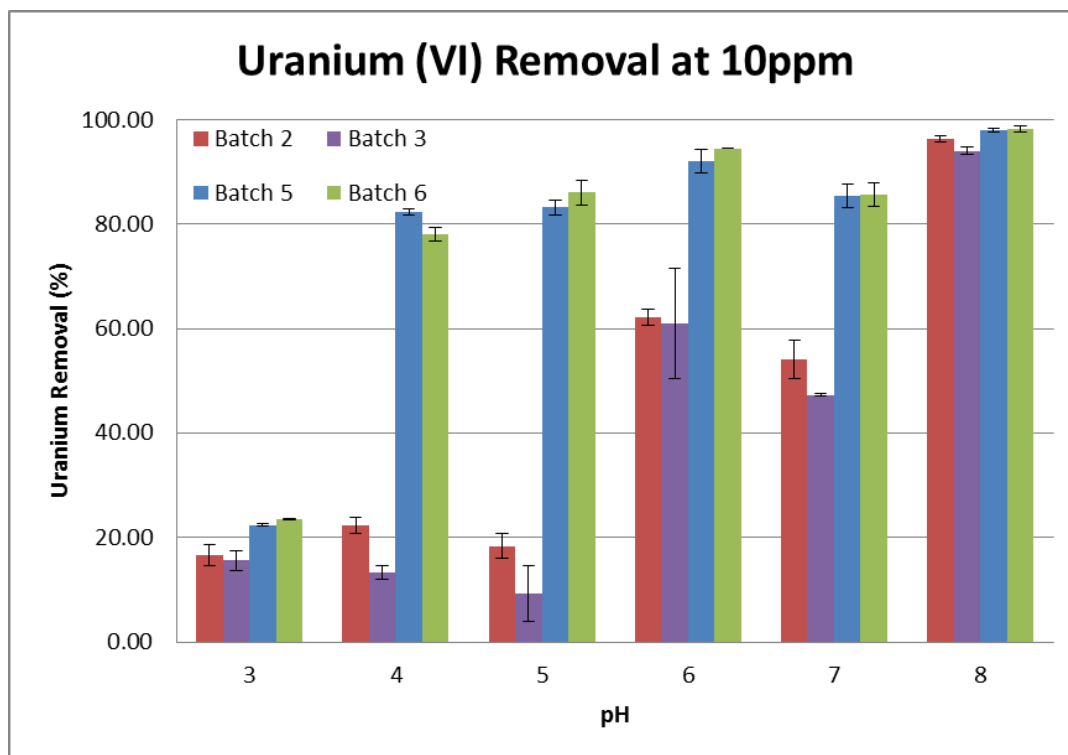


Figure 65. Uranium (VI) removal at 10 ppm HA Unfiltered.

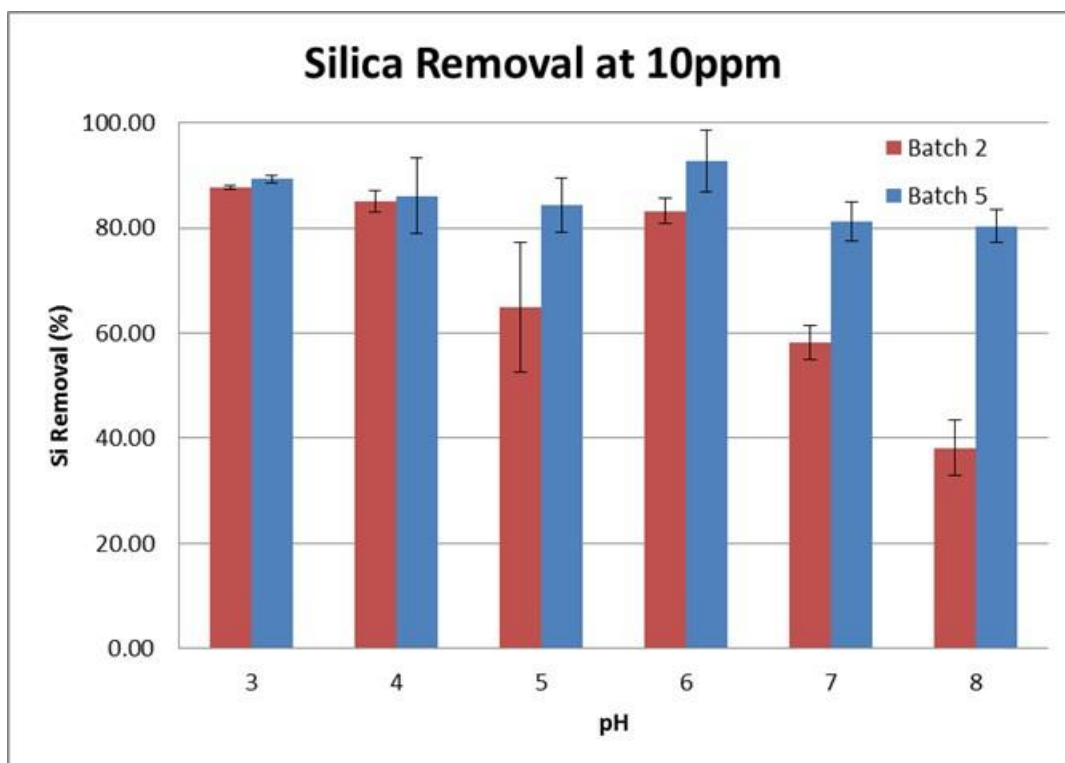


Figure 66. Uranium (VI) removal at 50 ppm HA Unfiltered.

Subtask 2.1.1: Future Work

Samples with an intermediate concentration of 30 ppm HA will be prepared and analyzed to determine if there are any significant trends between the 10 ppm and 50 ppm batches as well as whether the 10 ppm concentration is too low for an accurate representation for U(VI) removal.

Subtask 2.1.1: Acknowledgements

Funding for this research was provided by U.S. DOE cooperative agreement DE-EM0000598. We truly appreciate Dr. Miles Denham and Dr. Brian Looney from the SRNL for valuable inputs and support of this research.

Subtask 2.1.1: References

- Bergna, Horacio E., Roberts, William O., Colloidal Silica: Fundamentals and Applications, (Surfactant science series: v. 131)Chen, C., and X. Wang, 2007. Sorption of Th (IV) to silica as a function of pH, humic/fulvic acid, ionic strength, electrolyte type. *Applied Radiation and Isotopes* 65, 155-163.
- Choppin, G.R., 1992. The role of natural organics in radionuclide migration in natural aquifer systems. *Radiochim. Acta* 58/59, 113.
- Choppin, G.R., 1998. Humics and radionuclide migration. *Radiochim. Acta* 44/45, 23-28.
- Davis, J.A., 1982. Adsorption of natural dissolved organic matter at the oxide/water interface. *Geochim. Cosmochim. Acta* 46, 2381-2393.

- Davis, J.A., 1984. Complexation of trace metals by adsorbed natural organic matter. *Geochim. Cosmochim. Acta* 48, 679-691.
- Ivanov, P., Griffiths, T., Bryan, N.D., Bozhikov, G. and S. Dmitriev, 2012. The effect of humic acid on uranyl sorption onto bentonite at trace uranium levels. *J. Environ. Monit.*, 14, 2968-2975.
- Kerpelova, A., 2007. Influence of Humic Acid on the Sorption of Uranium(VI) and Americium(III) onto Kaolinite (Dissertation).
- Kerpelova, A., Brendler, V., Sachs, S., Baumann, N., Bernhard, G., 2007. U(VI)-Kaolinite Surface Complexation in Absence and Presence of Humic Acid Studied by TRLFS. *Environ. Sci. Technol.* 2007, 41, 6142-6147.
- Koopal, L.K., Y. Yang, A.J. Minnaard, P.L.M. Theunissen, W.H. Van Riemsdijk, 1998. Chemical immobilisation of humic acid on silica. *Colloids and Surfaces A: Physicochemical and Engineering Aspects* 141, 385-395.
- Labonne-Wall, N., Moulin, V., Vilarem, J.P., 1997. Retention properties of humic substances onto amorphous silica: consequences for the sorption of cations. *Radiochim. Acta*, 79, 37-49.
- Lagos, L., Katsenovich, P., Gudavalli, R., et al, 2014. Rapid Deployment of Engineered Solutions for Environmental Problems at Hanford. Yearend Technical Report, June 30, 2014, U.S. Department of Energy Office of Environmental Management Office of Science and Technology under Grant No. DE-EM0000598.
- Liao Jiali, Wen Wei, LI Bing, Yang Yuanyou, Zhang Dong, Kang Houjun, Yang Yong, Jin Jiannan, Liu Ning, 2013. Interaction between uranium and humic acid (II): complexation, precipitation and migration behavior of U(VI) in the presence of humic substances. *Nuclear Science and Techniques* 24, 030301
- Perminova, I.V., Hatfield, K., Hertkorn, N., 2002. Use of humic substances to remediate polluted environments: from theory to practice. In the proceedings of the NATO Advance Research Workshop, Springer, P.O Box 17, 3300 AA Dordrech, The Netherland.
- Plancque, G., Amekraz, B., Moulin, V., Toulhoat, P., Moulin, C., 2001. Molecular structure of fulvic acids by electrospray with quadrupole time-of-flight mass spectrometry. *Rapid Commun. Mass Spectrom.* 15, 827-835.
- Tipping, E., 2002. Cation Binding by Humic Substances. Vol. 12. Cambridge UP, p. 266.
- Wang, X. K.; Dong, W. M.; Dai, X. X.; Wang, A. X.; Du, J. Z.; Tao, Z. Y. 2000, Sorption and desorption of Eu and Yb on alumina: mechanisms and effect of fulvic acid. *Appl. Radiat. Isot.* 52, 165-173.
- Zachara, J.M., Resch, C.T., Smith, S.C., 1994. Influence of humic substances on Co^{2+} sorption by a subsurface mineral separate and its mineralogical components. *Geochim. Cosmochim. Acta* 58, 553-566.

Subtask 2.2: Monitoring of U (VI) Bioreduction after ARCADIS Demonstration at F-Area

Subtask 2.2: Introduction

In 2010, ARCADIS demonstrated the *in situ* injections of a carbohydrate substrate, molasses, to create reactive zones for uranium (VI) remediation via the enhanced anaerobic reductive precipitation (EARP) process at the F- Area of the Savannah River Site (SRS). The addition of the molasses substrate solution to groundwater produces anaerobic conditions that lead to uranium reduction and then precipitation as uranium (IV) due to the significantly decreased solubility of its +4 oxidation state. The SRS soil features very unique environmental conditions due to the naturally low alkalinity. A microcosm study, prepared with sieved SRS sediments, was designed to provide evidence for the capabilities of this remediation technology. The objective of the microcosm experiments was to replicate the anaerobic conditions created as a result of molasses injection performed by ARCADIS at SRS and investigate if any mineralogical changes could occur in the soil. Specifically, the study aimed to determine if forms of reduced iron such as siderite and pyrite would be created in the reducing conditions and their potential re-oxidation in sediments when oxidized conditions revert. These experiments also help to explain the types of reactions that occur in an anaerobic aquifer. However, the experiments conducted last year did not provide any evidence for the formation of siderite and pyrite forms in soil. The low soil pH and low groundwater concentrations of sulfate and bicarbonate to form ferrous carbonate or ferrous sulfide complexes are expected to be the major factors for the obtained results. In these experiments, the media solution was amended with molasses and sulfate to stimulate sulfate-reducing bacteria. The microbial reduction of sulfate produces hydrogen sulfide and releases HCO_3^- , resulting in an increase in alkalinity and pH. It was expected that in the anaerobic conditions, sulfate would be reduced to sulfide and bind to ferrous iron in order to create black precipitates of pyrite detectable by the XRD analysis. It was also expected that the increase in pH would cause the aqueous phase to become saturated with respect to FeCO_3 . This report presents experimental data collected from the beginning of FIU Year 5 on the sample pH evolution after molasses injection and XRD results to evaluate mineralogical changes that might occur in the anaerobic conditions. It would dictate if this technology is a viable option for uranium remediation under SRS conditions or not.

Subtask 2.2: Methodology

FIU received SRS F-Area sediments collected from a depth of 60-90 feet to be used in the microcosm experiments. To separate the fine and coarse fractions, the sediments were first ground using a mortar and pestle and then sieved through a No.80, 180 μm sieve (Figure 67). Sieving was a necessary step to remove large quartz particles which shield the finer fractions in XRD analysis.

For the microcosm experiment, 4 sets of samples were prepared in triplicate for a total of 12 samples. These samples were created in 50-mL polypropylene tubes and were treated using a basal medium solution augmented with sulfate and molasses (Figure 68). The basal medium solution consisted of (in g L⁻¹ deionized water): 1.5 NaHCO_3 , 0.2 NH_4Cl , 0.1 $\text{K}_2\text{HPO}_4 \cdot 3\text{H}_2\text{O}$, 0.055 KH_2PO_4 , 0.001 resazurin as a redox indicator, 0.039 $\text{Na}_2\text{S} \cdot 9\text{H}_2\text{O}$ as a sulfur source and reductant, and 0.1 $\text{MgCl}_2 \cdot 6\text{H}_2\text{O}$. In addition, 5 mL L⁻¹ trace metal solution was added. The trace metal solution consists of (in g L⁻¹): 0.005 $\text{FeCl}_2 \cdot 4\text{H}_2\text{O}$, 0.005 $\text{MnCl}_2 \cdot 4\text{H}_2\text{O}$, 0.001 $\text{CoCl}_2 \cdot 6\text{H}_2\text{O}$, 0.0006 H_3BO_3 , 0.0001 ZnCl_2 , 0.0001 $\text{NiCl}_2 \cdot 6\text{H}_2\text{O}$, 0.0001 $\text{Na}_2\text{MoO}_4 \cdot 2\text{H}_2\text{O}$, and 0.002 CaCl_2 .

2H₂O. The sulfate used for the augmented samples was from magnesium sulfate anhydrous (MgSO₄) and was combined with the basal medium solution to a concentration of 500 ppm. Sets 1 and 4 were inoculated with anaerobic sludge collected from the anaerobic digester of the Miami-Dade South wastewater treatment plant, in order to directly introduce anaerobic bacteria into half of the samples to give it a “jump start”.



Figure 67. No. 80, 180 μm sieve.

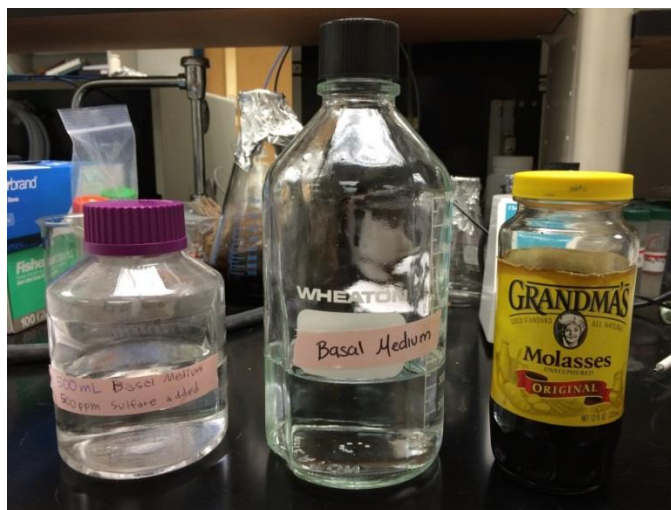


Figure 68. Basal medium with 500 ppm sulfate, basal medium, and molasses.

For the Batch 1 samples (Figure 69), Set 1 consisted of 20 mL of soil, 20 mL of basal medium, 500 ppm sulfate, 5-10% by weight molasses, and 5 mL of anaerobic bacteria. Set 2 consisted 20 mL of soil, 20 mL of basal medium, 500 ppm sulfate, and 5-10% by weight molasses. Set 3 consisted of 20 mL of soil, 20 mL of basal medium, and 5-10% by weight molasses. Set 4 consisted of 15 mL of soil, 15 mL of basal medium, 5-10% by weight molasses, and 5 mL of anaerobic bacteria. Set 4 was decreased to 15 mL of soil instead of 20 mL in order to conserve the SRS F-Area sediments for the next batch of microcosm samples. The components of each of the 4 sets from Batch 1 can be found in Table 22.



Figure 69. Batch 1 samples (12 bottles with orange caps).

Table 22. Batch 1 Sample Composition

Batch 1				
Sample Composition	Set #1	Set #2	Set #3	Set #4
Soil, mL	20	20	20	15
Basal Medium, mL	20	20	20	15
Sulfate, ppm	500	500	-	-
Molasses, % by weight	5-10%	5-10%	5-10%	5-10%
Anaerobic sludge, mL	0.5	-	-	0.5

It was observed that some of the original 12 samples, which were created and placed in the anaerobic chamber, were beginning to dry out. It was decided that a small amount of solution would be added to the samples. At week 6 of the experiment, two solutions were created for this purpose and added to the samples. Solution 1 consisted of 45 mL of basal medium and 7.1 g molasses (5% by weight). This solution was adjusted to a pH of 7.03 before it was added in the amount of 2 mL per sample to the set 3 and set 4 samples. Solution 2 consisted of 45 mL of basal medium augmented with 500 ppm of sulfate and 7.1 g molasses (5% by weight). This solution was adjusted to a pH of 6.99 before it was added in the amount of 2 mL per sample to the set 1 and set 2 samples.

During the monitoring of Batch 1 samples, a sharp decrease in the pH from week 1 to week 2 was noted and an investigation was conducted to determine the cause. It was concluded through a process of elimination that the addition of molasses led the drop in pH (Table 23). Prior to the molasses addition, the solutions exhibited more basic pH values ranging between 8.7-8.82. These values shifted significantly to below pH 5.0 after the molasses addition. It was noted that the

molasses solutions are acidic and, in addition, upon mixing with the solutions, triggers the fermentation process, resulting in a rapid drop in pH.

Table 23. pH Monitoring Data

Measured pH values			
Solution amended with 500 ppm sulfate, basal medium and molasses	Solution amended with basal medium and molasses	Basal medium solution	Solution amended with basal medium and 500 ppm of sulfate
4.85	4.57	8.7	8.82

In acidic conditions, carbonic acid is the most prevailing carbonate species, precluding the formation of any significant amount of bicarbonate HCO_3^- and carbonate CO_3^{2-} . In the open system, CO_2 can leave the solution, thus limiting any formation of siderite (FeCO_3) solid phases. Due to the acidic conditions within the samples from Batch 1, it was decided that a new set of samples would be created for Batch 2 (Figure 70) using the same basal-molasses solutions except that the pH was adjusted to a neutral level before the addition of any sediments. Sample 1 consisted of 12 mL of basal solution augmented with 500 ppm of sulfate, 0.75 grams of molasses (5-10% by weight), 12 mL of SRS F-Area sediments and 0.5 mL of anaerobic bacteria. Sample 2 consisted of 12 mL of basal solution augmented with 500 ppm of sulfate, 0.75 grams of molasses (5-10% by weight), and 12 mL of SRS F-Area sediments. Sample 3 consisted of 12 mL of basal solution, 0.75 grams of molasses (5-10% by weight), and 12 mL of SRS F-Area sediments. Sample 4 consisted of 12 mL of basal solution, 0.75 grams of molasses (5-10% by weight concentration), 12 mL of SRS F-Area sediments, and 0.5 mL of anaerobic bacteria. The components of the Batch 2 samples can be found in Table 24.

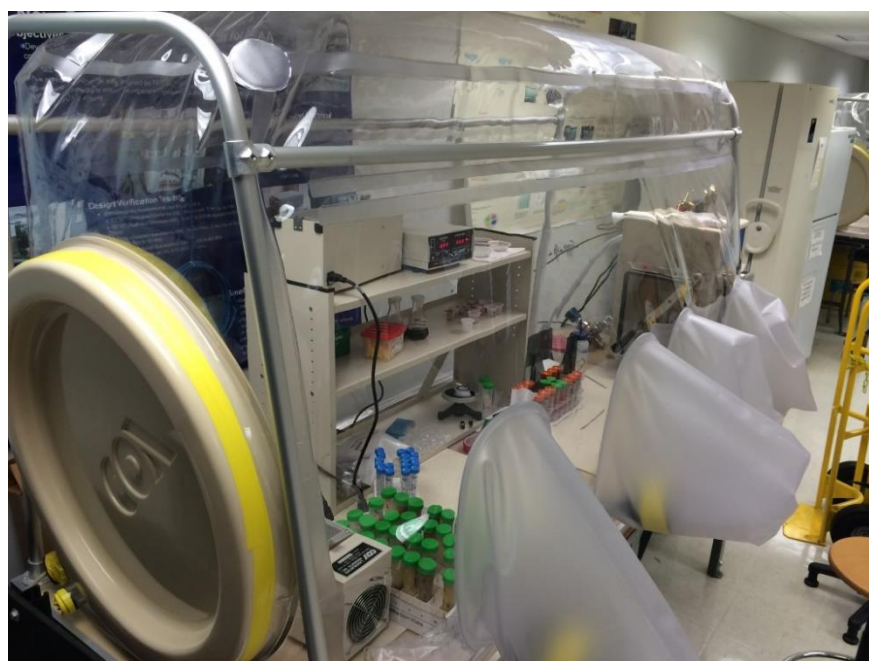


Figure 70. Microcosm Batch 2 samples.

Table 24. Batch 2 Samples Composition

Samples composition	Batch 2			
	Set #1	Set #2	Set #3	Set #4
Soil, mL	20	20	20	15
Basal Medium, mL	12	12	12	12
Sulfate, ppm	500	500	-	-
Molasses, % by weight	5-10%	5-10%	5-10%	5-10%
Anaerobic sludge, mL	0.5	-	-	0.5

To create anaerobic conditions necessary for the experiment, a vinyl anaerobic airlock chamber from COY Lab Products was used (Figure 71). The glove box was vacuumed and purged several times with pure nitrogen gas to establish anaerobic conditions, which were then confirmed by the oxygen gas analyzer. All experimental samples remained in the anaerobic chamber for the duration of the experiment. Oxygen levels were continuously monitored to ensure that no oxygen came into contact with the samples.

**Figure 71. Anaerobic chamber used for microcosm experiments.**

While the samples were in the anaerobic chamber, pH was monitored for both Batch 1 and Batch 2 experiments using a Eutech Instruments 200-Series pH meter and a Fisher Scientific Accumet pH electrode. The pH was measured at different intervals and the data are presented in the results section below.

Before creating any of the samples for the microcosm experiment, XRD analysis was conducted on the original sediments to obtain a reference for comparison. After the samples were created and given time to react in the anaerobic chamber, sub-samples were taken from both of the

microcosm experiments to be used for XRD analysis. For Batch 1, a small sub-sample was taken from each of the samples and combined to create a representative sample for each set, with a total of 4 sub-samples. Sub-samples from Batch 1 were taken at week 4 and week 8. From Batch 2, sub-samples were taken directly from each of the tubes for a total of 4 sub-samples. The Batch 2 sub-samples were taken after 4 weeks in the anaerobic chamber. Each of the sub-samples was placed individually onto an amorphous sample-holder (Figure 72) which was then placed into the XRD instrument.



Figure 72. Amorphous sample holder with F-Area sediment to be placed into XRD instrument.

X-ray diffraction analyses were performed using a Bruker 5000D XRD instrument (Figure 73) set to 35 kV and 40 mA. Diffraction patterns were obtained using a copper Cu K α radiation source ($\lambda=0.154056$ nm) with a tungsten filter. The XRD was programmed to run over a 2-theta (2θ) range from 3° to 70° with a 0.02° step size and 3 second counting per step. After experimental XRD patterns were received, these patterns were analyzed on SigmaPlot software and compared against known XRD patterns for siderite and pyrite.



Figure 73. Bruker 5000D XRD instrument.

ICP-OES analysis was conducted to find the ferrous iron concentration in the sub-samples. DI water was added to all of the samples in the amount of 5 mL and the samples were centrifuged in

tubes at 2700 rpm for 20 minutes. The supernatant was collected from each sample and filtered through a 45 um pore syringe filter. Standards were prepared for iron analysis with a calibration curve between 1 to 100 ppm. The supernatant was collected and diluted by a factor of 200 in Nitric Acid (HNO₃) 1%. Next, 3 mL of each of the diluted samples were placed into ICP tubes and ICP-OES analysis was conducted (Figure 74).

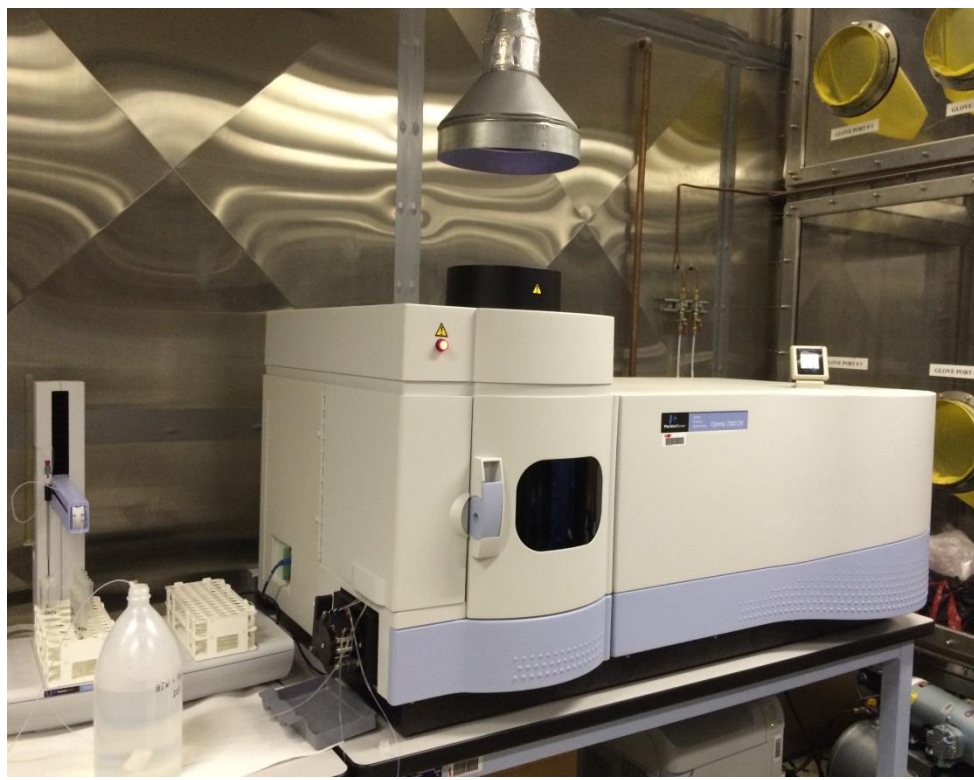


Figure 74. Perkin Elmer Optima 7300 ICP-OES.

Subtask 2.2: Results and Discussion

Batch 1 Results

In the Batch 1 microcosm study, there was no visible evidence of bacterial growth in any of the samples. In the samples that were amended with 0.5 mL of anaerobic bacteria, bubbles were observed in week 1 of the experiment but were not present in subsequent weeks. Small white patches of what appears to be fungal growth is present in some of the samples (Figure 75) but it appeared to be a random occurrence as it was not more common in any particular set. All samples including those augmented with sulfate were kept in the anaerobic glove box, making it difficult to detect the odor of possible hydrogen sulfide, an indication of the sulfate bioreduction process. Changes in the sulfate concentrations added to the initial solution and that remaining after keeping the samples under anaerobic conditions will be analyzed further to confirm that changes are due to bacterial activity.



Figure 75. Fungal growth in Batch 1 sample.

pH evolution

pH measurements suggested that almost all of the samples have followed a similar trend, with a decline in the pH value (Table 25 and Figure 76- Figure 79). This can be attributed to the fermentation process of molasses and the natural acidity of SRS soil used for the microcosm study. It was noted that samples amended with sulfates had slightly higher pH than sulfate-free samples. In addition, there was an increase in the pH of some of the samples from 11/30/2014 to 12/11/2014. This increase in the pH was caused by the addition of a pH-neutral solution to each of the samples to prevent them from drying out. By 12/11/2014, it was observed that the pH again dropped in almost all of the samples.

Table 25. Batch 1 Samples pH Evolution

Date	Set 1 (Basal Medium, Sulfate, Molasses, Bacteria)			Set 2 (Basal Medium, Sulfate, Molasses)			Set 3 (Basal Medium, Molasses)			Set 4 (Basal Medium, Molasses, Bacteria)		
	<i>pH</i> (1-1)	<i>pH</i> (1-2)	<i>pH</i> (1-3)	<i>pH</i> (2-1)	<i>pH</i> (2-2)	<i>pH</i> (2-3)	<i>pH</i> (3-1)	<i>pH</i> (3-2)	<i>pH</i> (3-3)	<i>pH</i> (4-1)	<i>pH</i> (4-2)	<i>pH</i> (4-3)
10/13/2014	5.95	5.95	5.95	5.95	5.95	5.9	5.55	5.76	5.81	5.95	5.95	5.95
10/21/2014	4.81	4.8	4.79	4.91	4.83	4.85	4.77	4.77	4.63	4.86	4.89	4.77
10/30/2014	4.82	4.63	4.34	4.85	4.86	4.83	4.86	4.89	4.8	4.93	4.87	4.33
11/30/2014	4.74	3.95	3.91	3.89	3.95	4.22	4.26	3.91	4.96	4.11	4.02	4.12
12/11/2014	4.73	3.94	3.9	4.01	4.04	4.35	4.39	4.22	5.29	4.37	4.31	4.4

Date	Set 1 (Basal Medium, Sulfate, Molasses, Bacteria)			Set 2 (Basal Medium, Sulfate, Molasses)			Set 3 (Basal Medium, Molasses)			Set 4 (Basal Medium, Molasses, Bacteria)		
	<i>pH</i> (1-1)	<i>pH</i> (1-2)	<i>pH</i> (1-3)	<i>pH</i> (2-1)	<i>pH</i> (2-2)	<i>pH</i> (2-3)	<i>pH</i> (3-1)	<i>pH</i> (3-2)	<i>pH</i> (3-3)	<i>pH</i> (4-1)	<i>pH</i> (4-2)	<i>pH</i> (4-3)
2014												
12/18/2014	4.87	4.01	3.95	3.87	3.91	4.06	3.91	3.86	4.74	3.94	3.88	3.97

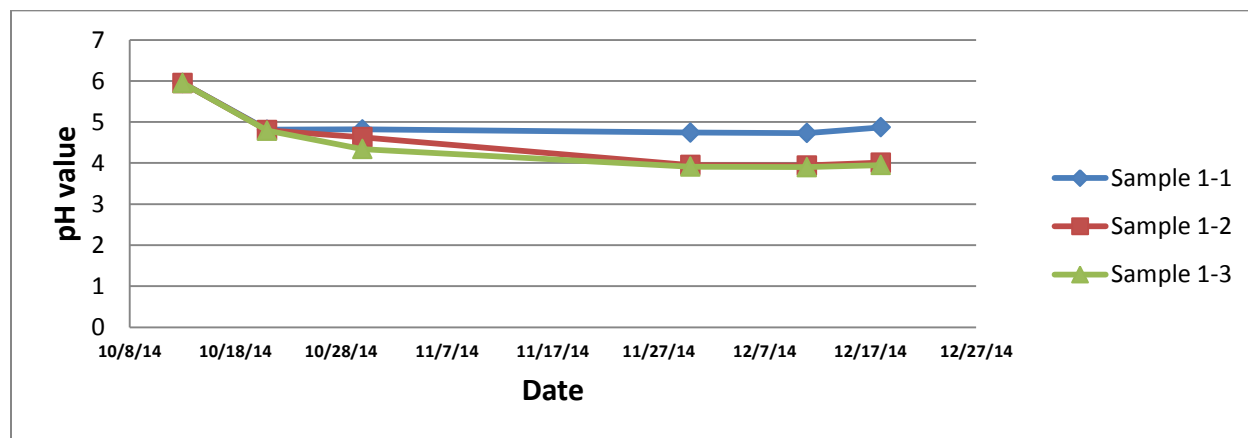


Figure 76. Batch 1, Set 1 pH evolution.

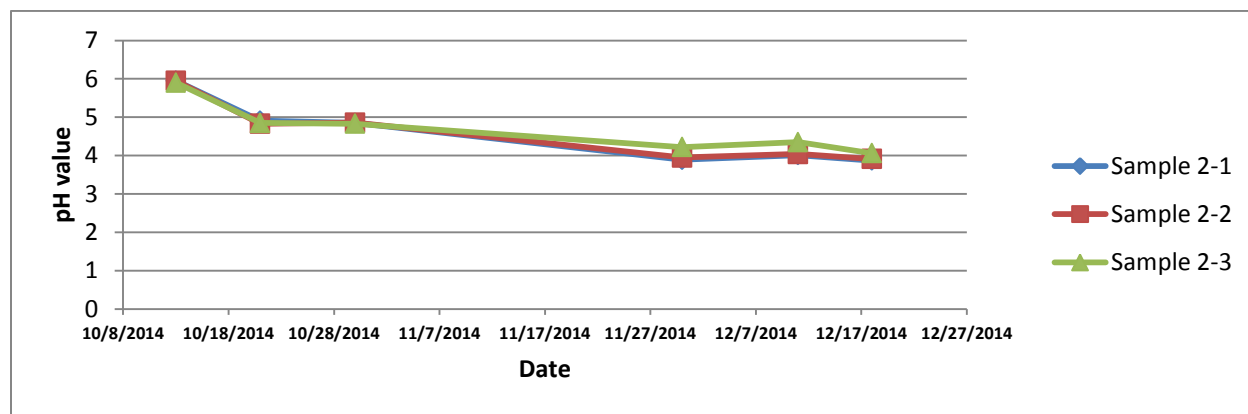


Figure 77. Batch 1, Set 2 pH evolution.

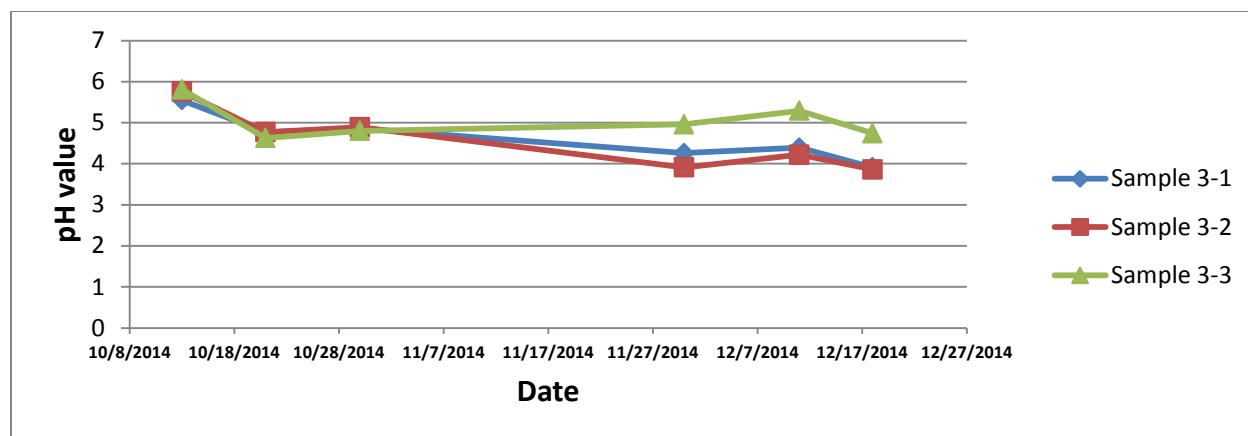


Figure 78. Batch 1, Set 3 pH evolution.

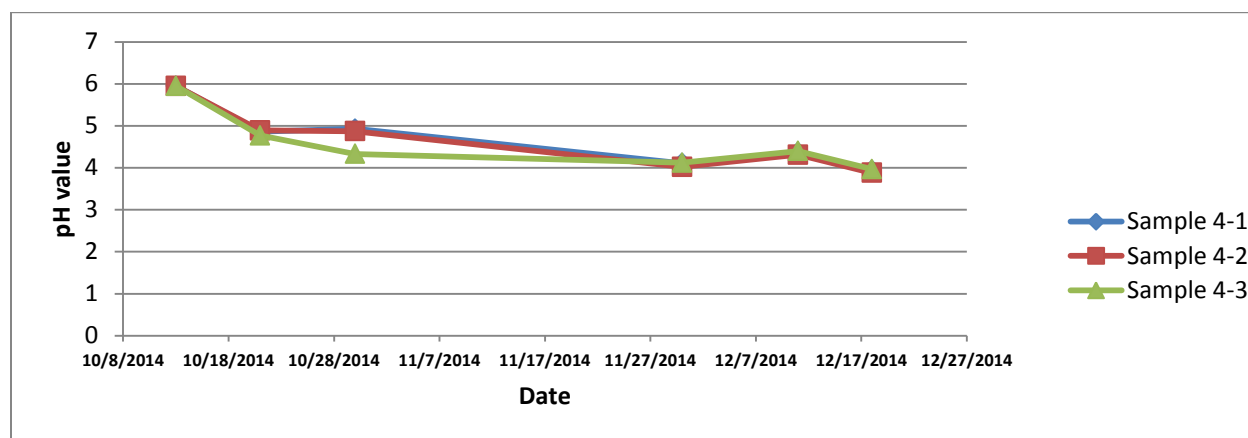


Figure 79. Batch 1, Set 4 pH evolution.

Batch 2 Results

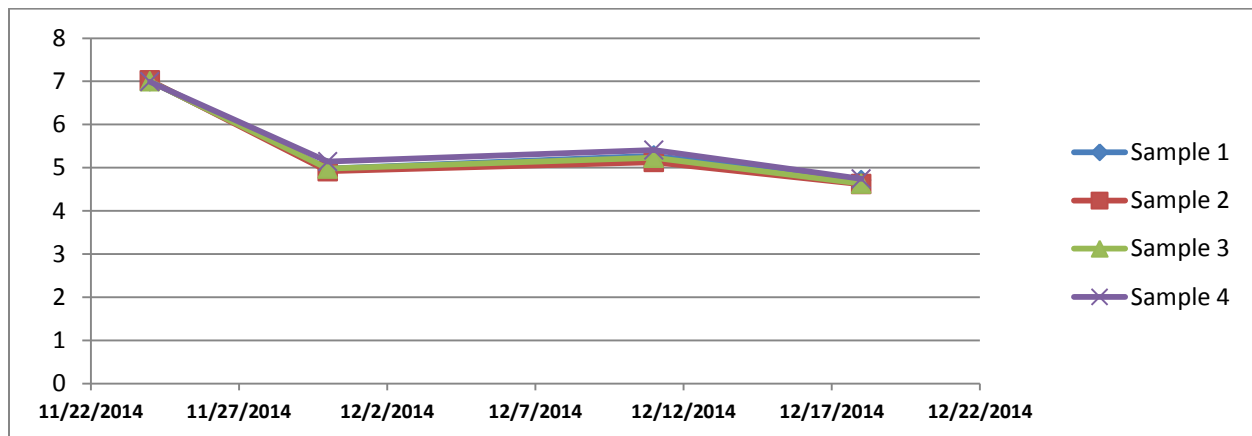
Batch 2 results were found to be similar to Batch 1 and the samples displayed no visible indications of anaerobic bacteria growth. Unlike Batch 1, there was no fungal growth in any of the samples. Any bubble formation in the samples that contained anaerobic bacteria was no longer present past the first week. The sulfate-augmented samples were kept in an anaerobic glove box, preventing the ability to detect any possible hydrogen sulfide odor.

pH evolution

Although Batch 2 was first pH-adjusted to pH 7 before the experiment began, the pH followed the same declining trend (Table 26, Figure 80) as observed in Batch 1. It was concluded that this was the natural condition within the samples and that the acidic state was inevitable. Sulfate-amended samples followed the same pH trend as samples without sulfate but had values slightly higher. It is believed that this was caused by the sulfate reduction in the amended tubes.

Table 26. Batch 2 Samples pH Evolution

Date	Measured pH values			
	Sample 1: Basal medium, 500 ppm sulfate, molasses, bacteria	Sample 2: Basal medium, 500 ppm sulfate, molasses	Sample 3: Basal medium, molasses	Sample 4: Basal medium, molasses, bacteria
11/24/2014	7	7.02	7	6.99
11/30/2014	4.98	4.92	4.98	5.14
12/11/2014	5.28	5.13	5.23	5.41
12/18/2014	4.71	4.62	4.63	4.74

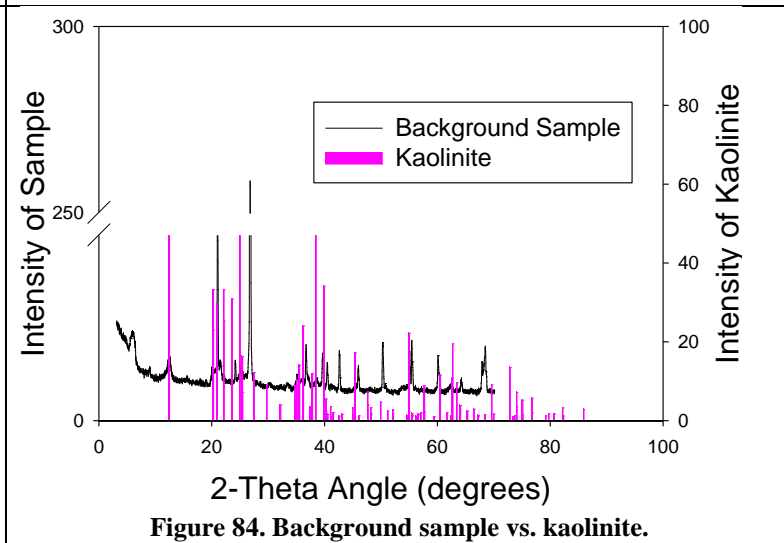
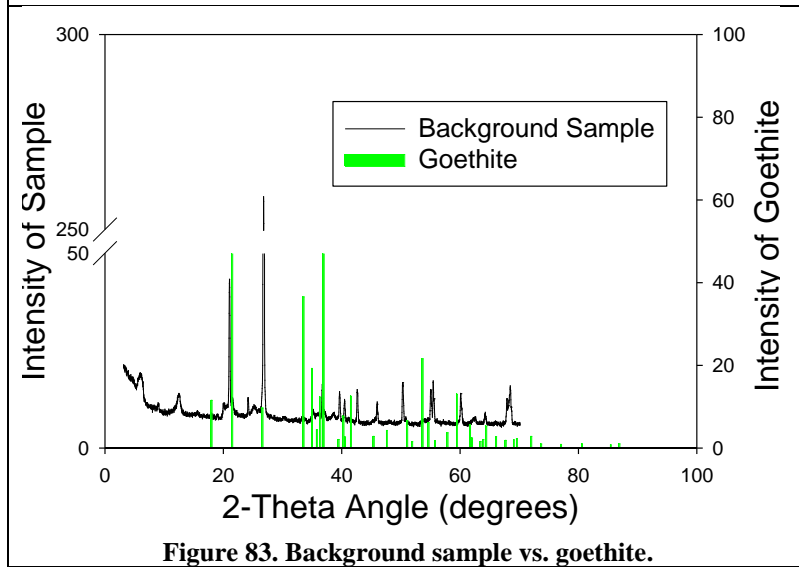
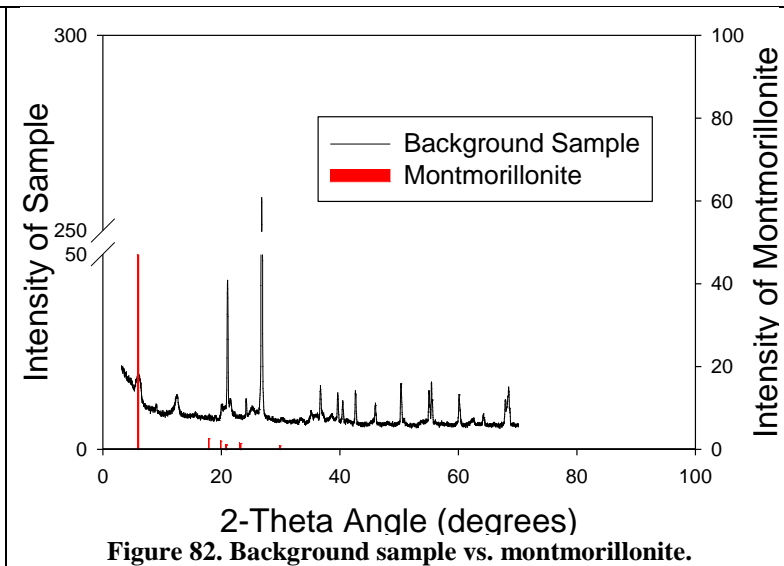
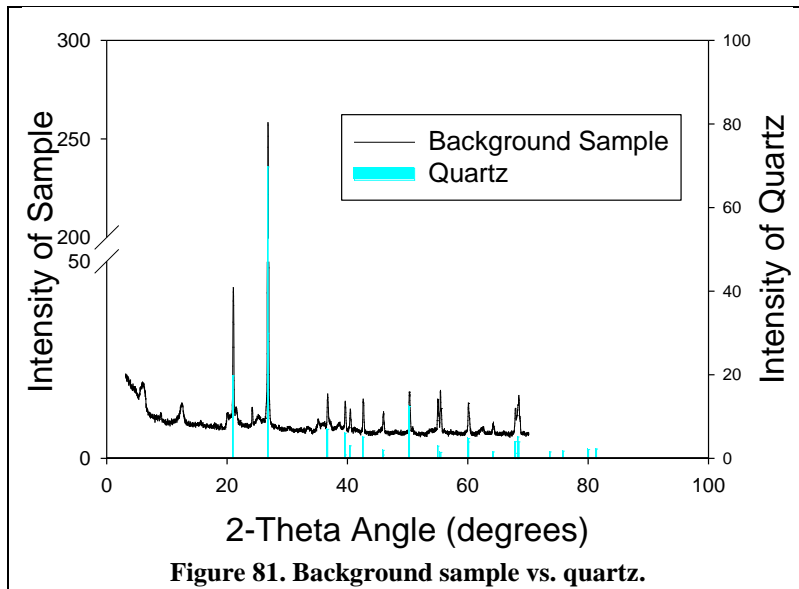
**Figure 80. Batch 2 samples pH evolution.**

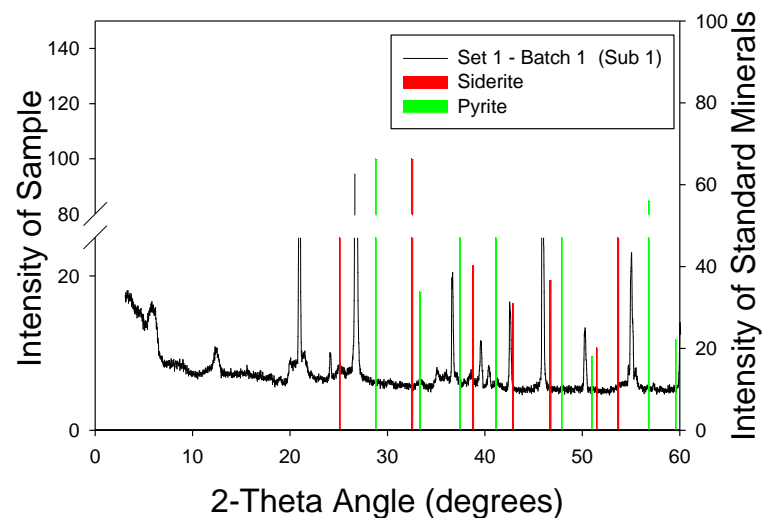
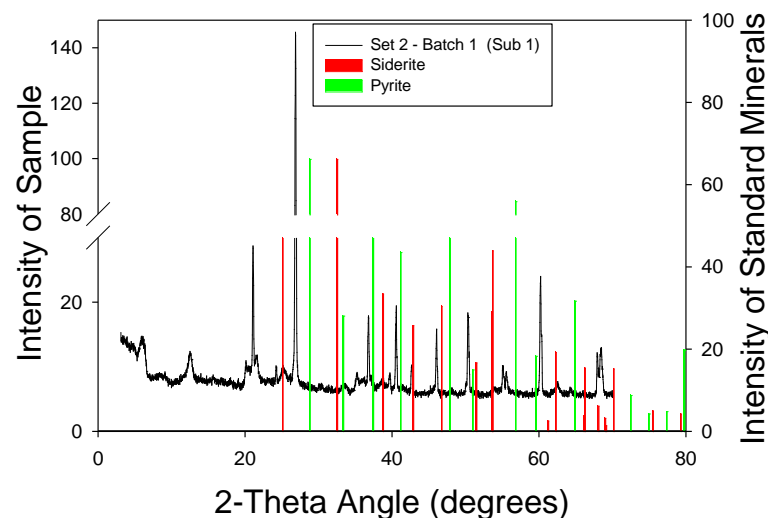
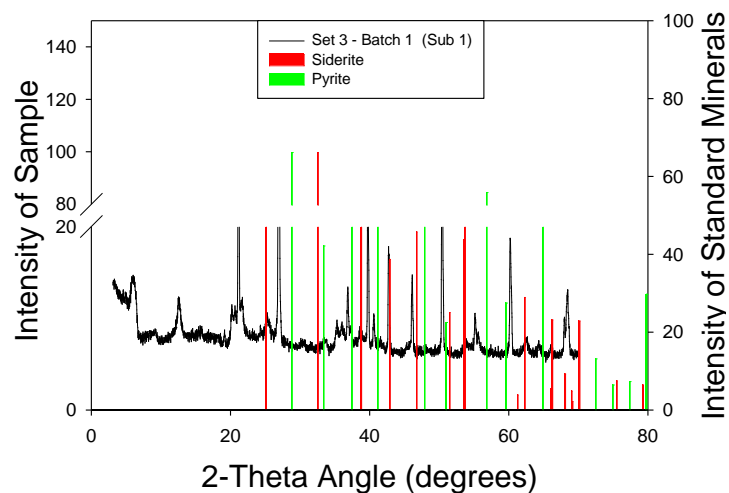
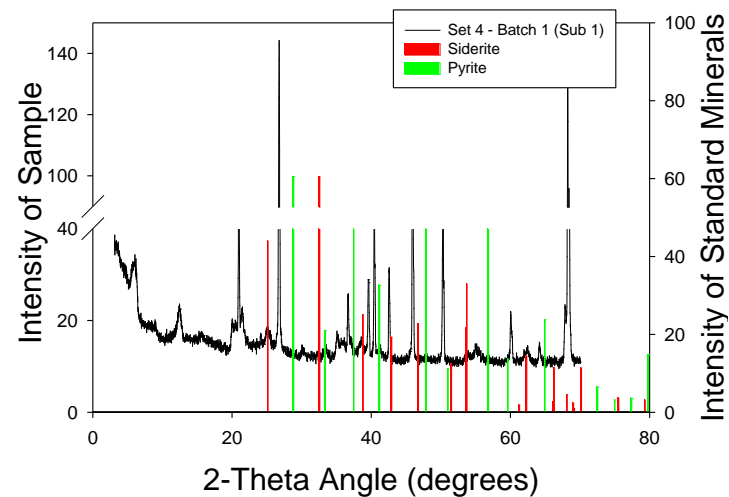
XRD Results

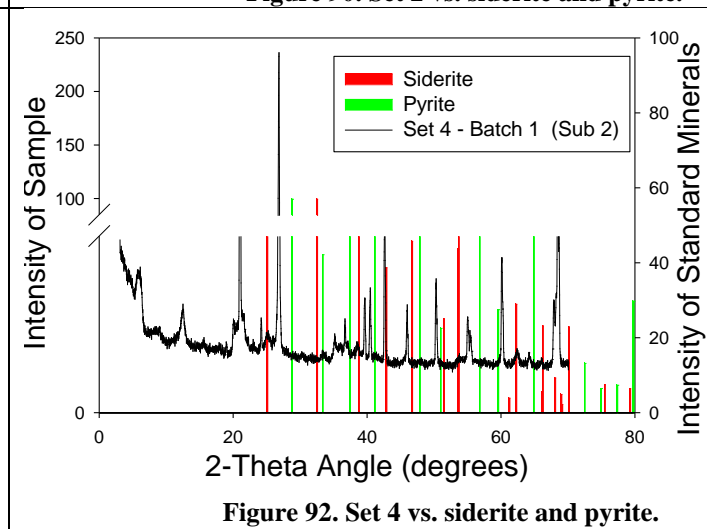
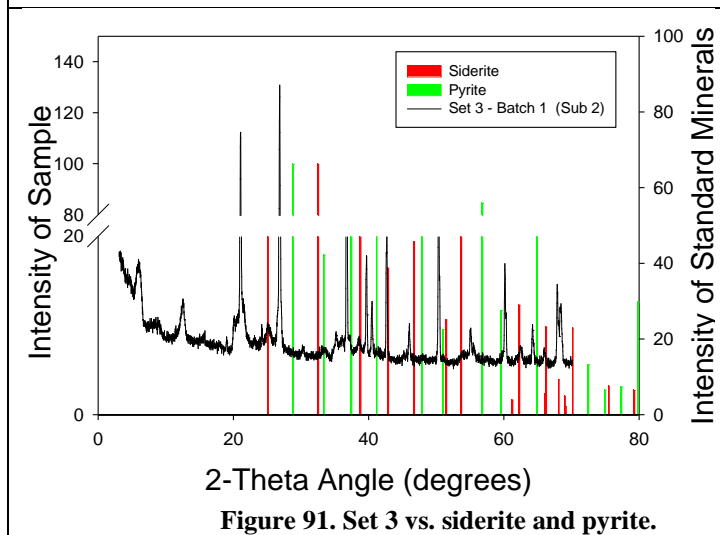
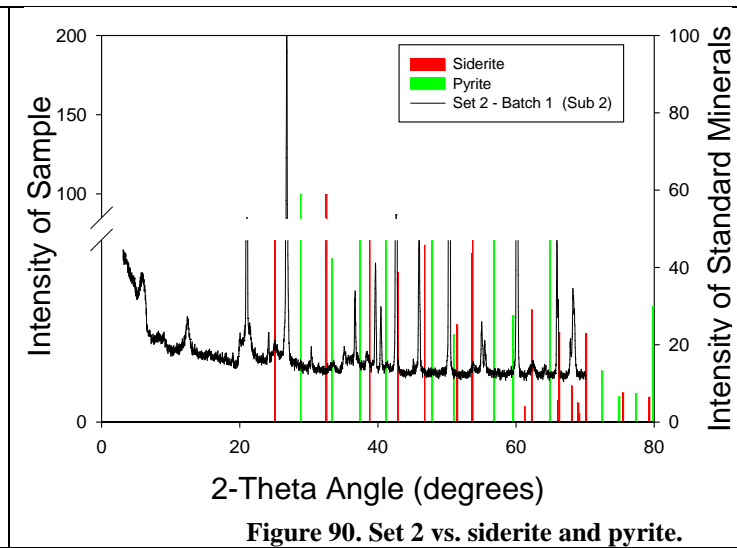
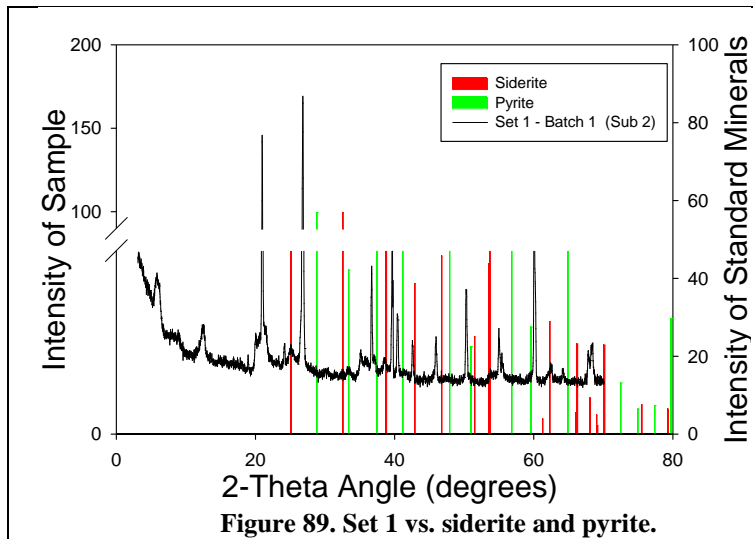
X-ray diffraction (XRD) analyses were conducted on fine clay fractions of previously collected soil samples to obtain a background reading before the beginning of the microcosm study. The results indicated that the sediments contained quartz, kaolinite, montmorillonite, and goethite (Figure 81-Figure 84). This analysis was also the determining factor in deciding the best grain size to sieve the sediments. Since quartz did not shield the other clay and iron-bearing minerals from being observed at 180 μ m, it was decided that this size sieve would be sufficient. The most prominent peak for quartz was observed at 2θ 26.65 degrees, montmorillonite at 5.89 degrees, goethite at 21.37 degrees, and kaolinite at 12.37 degrees.

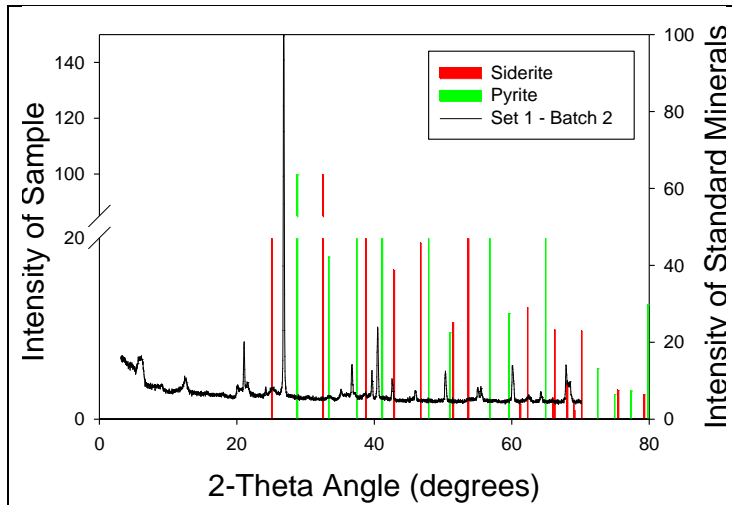
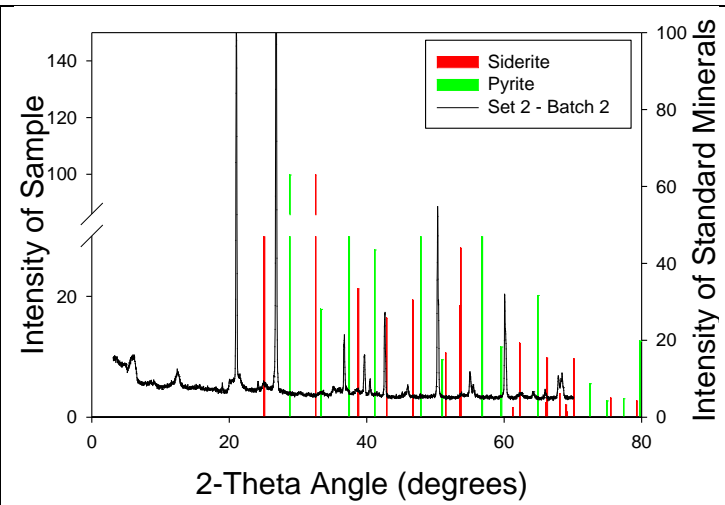
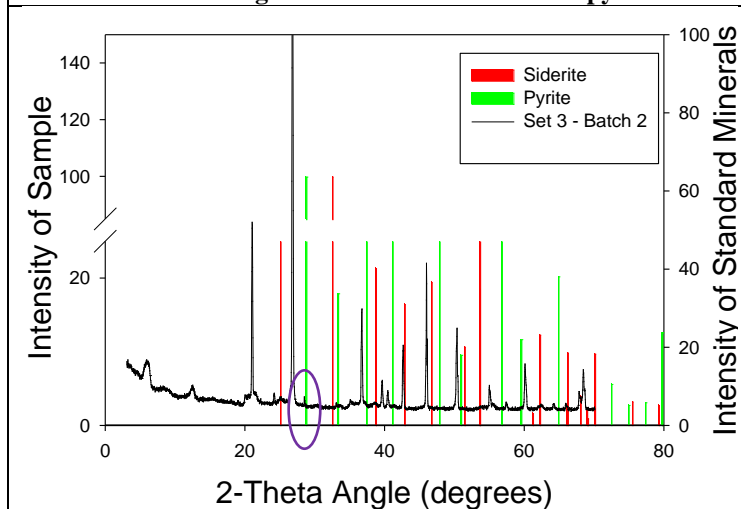
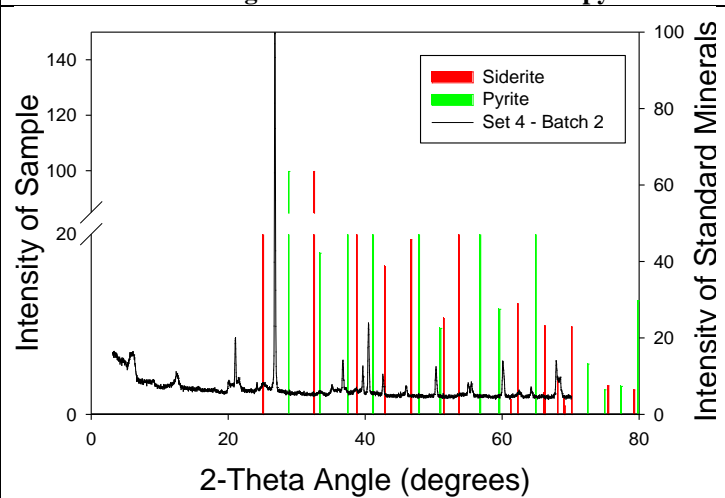
At week 4, a set of 4 sub-samples was obtained from Batch 1. These were analyzed via XRD and revealed no significant matches to siderite or pyrite when considering the angle and intensity of the most prominent peaks (Figure 85-Figure 88). The maximum intensity peaks for siderite occur at 32.49 2-theta value and for pyrite at 28.74 (100%) and 56.75 (84.7%) 2-theta values, respectively. It was noted that sub-sample 4 had a large peak around 700, which was not seen in the other sub-samples (Figure 88). At week 8, another set of sub-samples was taken, dried and then again analyzed via XRD. The unknown peak observed in sub-sample 4 was no longer present. It was concluded that this peak was not caused by the sediment and was an anomaly. Again there were no matches to siderite or pyrite in the week 8 XRD results (Figure 89-Figure 92). For Batch 2, XRD analysis was conducted at week 4. No matches to siderite or pyrite were observed in any of the Batch 2 sub-samples (Figure 93-Figure 96) except set 3 (Figure 95) where a tiny peak appeared at a 2-theta value of 28.74, which correlates with the maximum intensity peak for pyrite. We will continue monitoring the evolution of this peak in the next sampling events. All samples in both batches displayed nearly identical XRD patterns when compared against the original XRD pattern of the soil before the microcosm experiment began.

Background Sample



Batch 1/ Sub-Sampling 1**Figure 85. Set 1 vs. siderite and pyrite.****Figure 86. Set 2 vs. siderite and pyrite.****Figure 87. Set 3 vs. siderite and pyrite.****Figure 88. Set 4 vs. siderite and pyrite.**

Batch 1/ Sub-Sampling 2

Batch 2/ Sub-Sampling 1**Figure 93. Set 1 vs. siderite and pyrite.****Figure 94. Set 2 vs. siderite and pyrite.****Figure 95. Set 3 vs. siderite and pyrite.****Figure 96. Set 4 vs. siderite and pyrite.**

ICP-OES Results

The samples varied significantly in iron concentrations, with the greatest amount reaching 13312.80 ppb in Batch 1/ Set 1-2 (Table 27). It was noted that the Batch 1 samples containing the anaerobic bacteria (Sets 1 and 4) had the highest average iron concentrations in comparison to those which were not inoculated. It is believed that iron-reducing bacteria may have biodegraded molasses using ferric iron as a terminal electron acceptor which would explain the higher soluble ferrous iron concentrations in these samples. When comparing the samples without bacteria (Sets 2 and 3), it was observed that the ferrous iron concentration was almost identical. This suggests that the sulfide did not complex with the ferrous iron most likely due to the acidic conditions.

Overall, the Batch 2 samples had a lower average iron concentration (4522.52 ppb) in comparison to Batch 1 (6111.53 ppb) which is believed to have been caused by the formation of iron precipitates which may be too low in concentration to be detected via XRD. The lower average soluble iron concentration of Batch 2 is mainly due to Set 3 which had an uncharacteristically low iron value of 893.27 ppb; making it the lowest concentration from any of the Batch 1 or 2 samples. It was noted that as in Batch 1, the Batch 2 samples with the highest concentrations of iron were found in the samples inoculated with 5 mL of anaerobic bacteria (Sets 1 and 4).

The average ferrous iron concentration in the samples amended with sulfate for Batch 1 and Batch 2 combined was found to be 5726.535 ppb (Table 28). The average ferrous iron concentration in the samples which contained no sulfate for Batch 1 and Batch 2 combined was found to be 4907.5275 ppb. While it was expected that samples containing sulfate would have a lower ferrous iron concentration, it is believed that the acidic conditions hindered the formation of any iron-sulfide precipitates. The samples with sulfate had on average 14% more ferrous iron (822 ppb) than those without. This is most probably to have been caused by slight differences in the composition of the supernatant when it was collected from the microcosm tubes.

Table 27. ICP-OES Data for Batch 1 and Batch 2

Description	Fe Concentration (ppb)	
Batch 1 (Set 1-1) Amended with sulfate	1650.87	
Batch 1 (Set 1-2) Amended with sulfate	13312.80	Average
Batch 1 (Set1-3) Amended with sulfate	8462.03	7808.57
Batch 1 (Set 2-1) Amended with sulfate	4705.95	
Batch 1 (Set 2-2) Amended with sulfate	4757.76	Average
Batch 1 (Set 2-3) Amended with sulfate	5815.26	5092.99
Batch 1 (Set 3-1)	5730.32	
Batch 1 (Set 3-2)	4343.13	Average
Batch 1 (Set 3-3)	5349.70	5141.05
Batch 1 (Set 4-1)	5494.83	
Batch 1 (Set 4-2)	6118.96	Average
Batch 1 (Set4-3)	7596.79	6403.53
BATCH 1 Average	6111.53	
Batch 2 (Set 1) Amended with sulfate	5748.89	
Batch 2 (Set 2) Amended with sulfate	4255.69	
Batch 2 (Set 3)	893.27	Average
Batch 2 (Set 4)	7192.26	4522.52
BATCH 2 Average	4522.52	

Table 28. Average Fe concentration for Batch 1 and 2 Combined

Description	Fe Concentration (ppb)
Samples amended with sulfate	5726.535
Samples not amended with sulfate	4907.5275

Subtask 2.2: Future Work

FIU is currently working on the sulfate analysis via ion chromatograph and new data will be presented in the next monthly progress report. Due to no indication of bioreduction in the microcosm samples, the future work for the project, which included a re-oxygenation phase, will not be conducted. With the experience gained from this study, a new experiment may be conducted again at a later date. FIU will finalize the remaining sulfate analysis to justify the occurrence of the sulfate reduction process. FIU is also planning geochemical modeling studies

to investigate in the range of environmental conditions the formation of siderite and pyrite solid phases would occur.

Subtask 2.2: Acknowledgements

Funding for this research was provided by U.S. DOE cooperative agreement DE-EM0000598. We truly appreciate Dr. Miles Denham and Dr. Brian Looney from the SRNL for valuable inputs and support of this research. XRD analyses were conducted at FIU AMERI facilities.

Subtask 2.3: The Sorption Properties of the Humate Injected Into the Subsurface System

Subtask 2.3: Introduction

Savannah River Site (SRS), located 13 miles south of Aiken in South Carolina, was a defense nuclear processing facility owned by the U.S. government. During the Cold War, from 1953 to 1988, SRS produced a large amount of radioactive and hazardous acidic waste from the production of plutonium and irradiated fuel. The acidic waste solutions containing low-level radioactivity from numerous isotopes were discharged into a series of unlined seepage basins in the F/H Area. At that time, it was believed that most of the radionuclides present in the waste solution would bind to the soil, precluding the migration of the radionuclides. However, sufficient quantities of uranium isotopes, ^{129}I , ^{99}Tc , and tritium migrated into the groundwater, creating an acidic plume with a pH between 3 and 5.5. In an effort to remove the contaminants from the groundwater, pump-and-treat and re-inject systems were implemented in 1997. Downgradient contaminated groundwater was pumped up to a water treatment facility, treated to remove metals (through osmosis, precipitation/flocculation, and ion exchange), and then re-injected upgradient within the aquifer. The pump-and-treat water treatment unit eventually became less effective, generating large amounts of radioactive waste, and was very expensive to maintain, prompting research for new remedial alternatives. In 2004, the pump-and treat system was replaced by a funnel and gate system in order to create a treatment zone via injection of a solution mixture composed of two components, sodium hydroxide and carbonate. The injections were done directly into the gates of the F-Area groundwater to raise pH levels. The purpose of the treatment zone was to reverse the acidic nature of the contaminated sediments, thereby producing a more negative net charge on the surface of sediment particles and enhancing adsorption of cationic contaminants. This system of remediation required a systematic re-injection of the base to raise the pH to near neutral values. However, the continuous use of high concentrations of a carbonate solution to raise pH creates a concern of possible re-mobilization of uranium that was previously adsorbed within the treatment zone since U(VI) in the presence of bicarbonate ions forms soluble aqueous uranyl-carbonate complexes, though this has not been observed in monitoring data.

Savannah River National Laboratory (SRNL) has been testing an unrefined, low cost humic substance known as Huma-K as an amendment that can be injected into contaminant plumes to enhance sorption of uranium and Sr-90. The advantage of using an unrefined humic substance is that it is inexpensive and can be used for full scale deployment of remediation technologies.

Humic substances (Figure 97) are ubiquitous in the environment, occurring in all soils, waters, and sediments of the ecosphere. Humic substances consist of complex organic compounds formed by the decomposition of plant and animal tissue. This decomposition process is known as

humification, where the organic matter is transformed naturally into humic substances by microorganisms in the soil. Humic substances are divided into three main fractions: humic acid (HA), fulvic acid (FA), and humin. Their size, molecular weight, elemental composition, structure, and the number and position of functional groups vary.

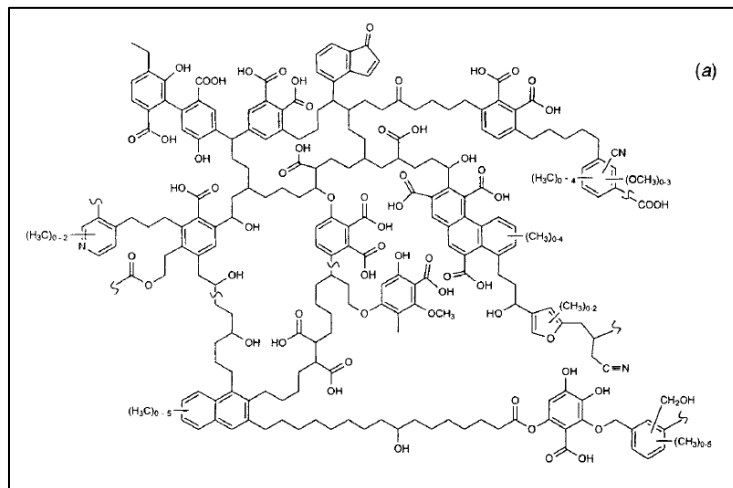


Figure 97. Soil humic acid structure proposed by Schulten and Schnitzer.

Studies show that HA is as an important ion exchange and metal-complexing ligand, carrying a large number of functional groups with high complexing capacity that can greatly affect the mobility behavior of actinides in natural systems (Davis, 1982; Choppin, 1998; Plancque et al., 2001). pH and concentration are the main factors affecting the formation of complexes between humic molecules and metals. It is generally considered that the sorption of metal ions on the mineral surfaces in the presence of HA is enhanced at low pH and reduced at high pH (Ivanov et al., 2012). Some studies have shown that U(VI) prefers to be adsorbed onto kaolinite as a uranyl-humate complex (Krepelova et al., 2007).

This study used Huma-K, an organic fertilizer used by farmers to stimulate plant growth and facilitate nutrient uptake. It is a water soluble potassium salt of humic and fulvic acids that comes from the alkaline extraction of leonardite (a low-rank coal). Leonardite has a very high content of humic substances due to decomposition by microorganisms. Also, compared to other sources of humic substances, leonardite has a higher humic/fulvic acid content. The extraction of humic/fulvic acid from leonardite is performed in water with the addition of potassium hydroxide (KOH), and the resulting liquid is dried to produce the amorphous crystalline black powder/shiny flakes as seen in Figure 98.



Figure 98. Huma-K black powder/shiny flakes.

Subtask 2.3: Methodology

Characterization of SRS sediments and Huma-K

A scanning electron microscope equipped with energy-dispersive X-ray spectroscopy (SEM/EDS) was used to investigate the surface morphology and elemental composition of SRS sediments from the F-Area. Elemental analysis was also performed for Huma-K. Both materials were placed on top of metal stubs and affixed with double-stick, carbon tape where they were coated with an electrical conductive material (gold/palladium) using a sputter coater, SPI-Module Control and Sputter unit, for 2 minutes to produce a thin layer of gold (Figure 99). After coating, the SRS sediment and Huma-K were analyzed by SEM/EDS for elemental analysis. The SEM system used was a JOEL-5910-LV with acceleration potentials ranging from 10 to 20 kV. EDS analysis was produced using an EDAX Sapphire detector with UTW Window controlled through Genesis software.



Figure 99. Samples coated with Gold/Palladium for SEM/EDS analysis

Potentiometric titrations of Huma-K and SRS sediments were performed in order to determine the point of zero charge and the protonation-deprotonation behavior of Huma-K and SRS sediments. The potentiometric titration consisted of placing a known amount of the material (Huma-K or SRS sediment) dissolved in 0.01 M NaNO_3 in a closed beaker. The setup is shown in Figure 100. The solution was stirred constantly and nitrogen was bubbled throughout in order to remove CO_2 and create an inert atmosphere. Once the pH of the solution containing the material was stable, NaOH was added to raise the pH to 11 in order to deprotonate the functional groups present in the material. Once the pH was stabilized again, the titration was started by adding small quantities of 0.01 M HNO_3 . After each addition of HNO_3 , the pH and the volume were recorded. The titration was ended at a pH around 3. In the case of the sediments, after the titration was finished, the supernatant was collected by vacuum filtration and titrated again. The purpose of titrating the supernatant was to estimate the functional groups that may have leached from the sediment and consumed hydrogen ions. In order to isolate the hydrogen ions consumed by the material, it was necessary to subtract a titration curve of the electrolyte (NaNO_3) from one of the material dissolved in the electrolyte using a data analysis software (OriginPro 8).



Figure 100. Setup for the Potentiometric Titration

For Fourier Transform Infrared (FTIR) analysis, a Perkin Elmer Spectrum 100 FT-IR Spectrometer coupled with an Attenuated Total Reflectance (ATR) was used to collect spectra from 4000 to 600 cm^{-1} . FTIR analysis can be used for the identification of minerals present in SRS sediments as well as the identification of the main functional groups present in the Huma-K. Before analysis, SRS sediments were sieved to a particle size $<63 \mu\text{m}$ in order to analyze the fine fraction which contains more clay. Also, the sample has to have a powder structure in order to generate a high quality spectrum. The $<63 \mu\text{m}$ collected fraction and the Huma-K were placed in an oven at 80°C for 48 hours to remove any adsorbed water. The samples were then stored in a desiccator until analysis. Huma-K had to be mixed with KBr (10 mg of sample with 150 mg KBr) and ground with a mortar and pestle to improve contact with the ATR crystal. Before the analysis, the ATR crystal of the FTIR was cleaned with ethanol, and the background was collected. A small amount sample was placed on top of the crystal. The pressure clamp was lowered and pressure was applied to ensure good contact between the sample and the crystal. After that, spectra were collected from 600 – 4000 cm^{-1} with 4 scans at a resolution of 4 cm^{-1} .

Sorption Experiment of Huma-K onto SRS sediments

Kinetic Experiment of Huma-K at pH 4

In this study, SRS sediments (FAW-1 70-90ft) collected from the F-Area were used for batch sorption experiments with a 20:1 liquid to soil ratio at ambient temperature (between 20 and 23 $^\circ\text{C}$).

First, the sediments were disaggregated with a mortar and pestle using minimal force in order to keep the original texture of the sediment. After disaggregation, SRS sediments were sieved to a particle size of $\leq 2 \text{ mm}$.

Several centrifuge tubes were prepared to contain the same amount of SRS sediments ($\sim 1 \text{ gram}$). A known concentration of Huma-K (50 ppm) was pipetted into each centrifuge tube. The pH was adjusted to pH 4 for all the samples by using either 0.1 M HCL or 0.1 M NaOH. DI water was added to a final volume of 20 mL in each tube. The samples were then placed on a shaker table. At predetermined time intervals, samples were withdrawn and centrifuged. The concentration of the supernatant was measured by UV-vis spectrophotometer at 254 nm wavelength and the amount of the adsorbed Huma-K at time t was calculated using the formula:

$$q_t = (C_i - C_t)V/w$$

Where:

q_t = amount of humate adsorbed to the sediments at time t

C_i = initial concentration of Huma – K

C_t = concentration of Huma – K at any time

V = total volume of solution used in the sample

w = weight of SRS sediment in the sample

Concentration Isotherms of Huma-K at pH 4

Concentration isotherms conducted as batch sorption experiments at pH 4 included the same amount of sediment in each of the centrifuge tubes, but the concentration of humate solution was varied in order to determine the maximum sorption capacity of the four types of sediment. The following concentrations (in ppm) were used: 10, 25, 50, 100, 150, 200, 250, 300, 350, 400, 450, and 500. The final volume for each of the samples was 20 mL. All the experiments were done in triplicate. First, a humate stock solution of 1000 ppm was prepared by dissolving 1000 mg in 1 liter of DI water. From this stock solution, all the concentrations were prepared.

To each centrifuge tube, 1 g of sediment was added. The appropriate volume of humate stock was pipetted into each centrifuge tube and DI water was added to a total volume of 19 mL, leaving 1 mL of volume for the pH adjustment. The pH was adjusted to 4 for all of the samples by using either 0.1 M HCl or 0.1 M NaOH. DI water was added for a final volume of 20 mL in each tube (Figure 101).

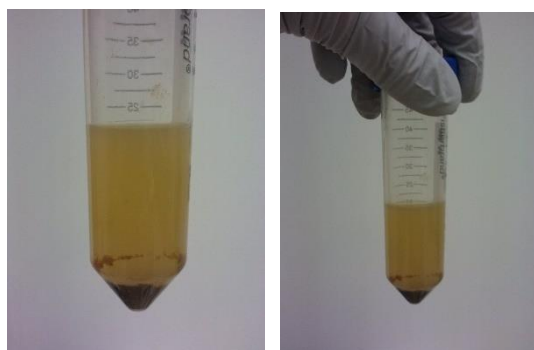


Figure 101. Centrifuge tube with sediment and humate solution

All the samples were vortex mixed and placed in a shaker table at 100 RPM until equilibrium was reached (time for equilibrium was previously determined in the kinetics experiments). The position of the centrifuge tubes was almost horizontal in order to maximize contact between the liquid and the sediment (Figure 102). After 24 hours, the samples were centrifuged at 2700 RPM (Figure 103) to separate the liquid solution from the sediment with the sorbed humate.



Figure 102. Shaker table with samples.



Figure 103. Samples centrifugation.

The liquid was analyzed using a Thermo Scientific Genesys 10S UV-Vis spectrophotometer (Figure 104). The analysis involved transferring 3 ml of the liquid sample to a quartz cuvette and placing the quartz cuvette in the spectrophotometer to measure the concentration of humate solution that was not sorbed by the sediment after equilibrium. The standard calibration curve and the measurements of the concentrations of the samples were done at a wavelength of 254 nm.



Figure 104. UV-Vis spectrophotometer.

Sorption Experiment of Huma-K at different pH values

In this experiment, a fixed concentration of 50 ppm was used to study the sorption behavior of Huma-K onto sediments at different pH values (from pH 4 to 9). The final volume for all the samples was 20 mL. All the experiments were done in triplicate.

To each centrifuge tube, 1 g of sediment was added. 50 ppm of Huma-K was pipetted into each centrifuge tube, and DI water was added for a total volume of 19 mL, leaving 1 mL of volume for the pH adjustment. The pH was adjusted to the desired value for all the samples by using either 0.1 M HCL or 0.1 M NaOH. DI water was added for a final volume of 20 mL in each tube.

All samples were vortex mixed, placed on a shaker table, and analyzed in the UV-Vis spectrophotometer using the same experimental procedure explained in the section: Sorption Experiment of Huma-K at pH 4.

Subtask 2.3: Results and Discussion

Characterization of SRS sediments and Huma-K

Scanning Electron Microscopy with Energy Dispersive X-Ray Spectroscopy (SEM/EDS)

Figure 105 presents the elemental analysis of Huma-K obtained by SEM/EDS. The elemental analysis of Huma-K shows that it contains K, C, O, Si, Ca, and Al. The K comes from treatment procedures to extract the humic substances from the coal leonardite by using KOH. C and O come from humic substances that are rich in aromatic rings, carboxyl groups, phenols, and aliphatic chains. Since Huma-K is an unrefined commercial product, it also contains impurities (mainly Si, Al, and Ca) that were present in Leonardite, and then were dissolved in the process of alkaline extraction. Gold and palladium comes from the coating of the sample.

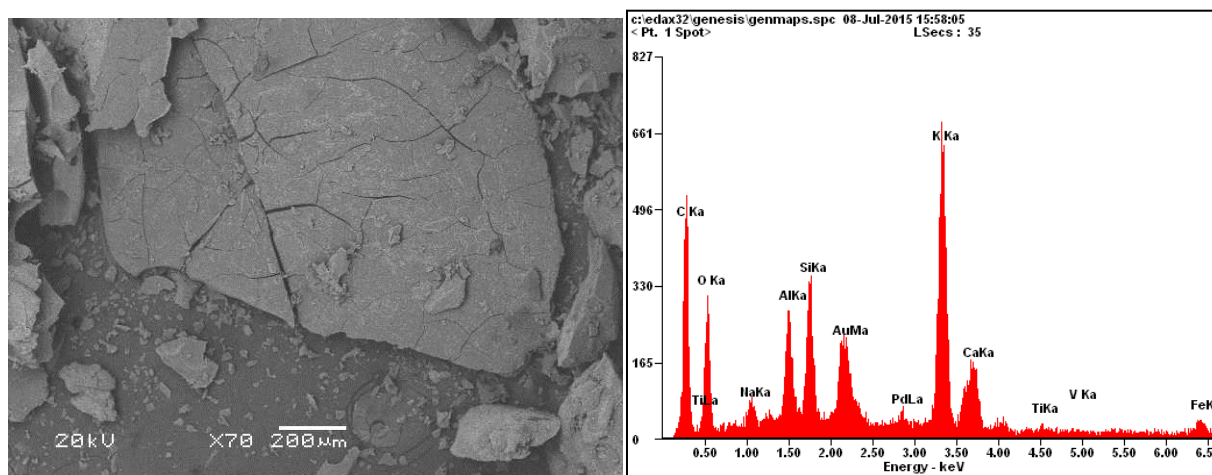


Figure 105. SEM Image and EDS Elemental Analysis of Huma-K

EDS analysis helped to carry out the elemental composition of the coarse and fine fraction of SRS sediments (Figure 106 and Figure 107). The elemental analysis shows that both the coarse and fine fraction have Si, Al, Fe, and Ti. The Si, Al, and Fe comes from the quartz, kaolinite, and goethite minerals present in SRS sediment. These minerals are characteristic of the F-Area based

on XRD analysis (Wan, 2011; Dong et al, 2014). Also, EDS analysis showed the presence of titanium, which is commonly found in sediments in the form of titanium oxide (TiO_2).

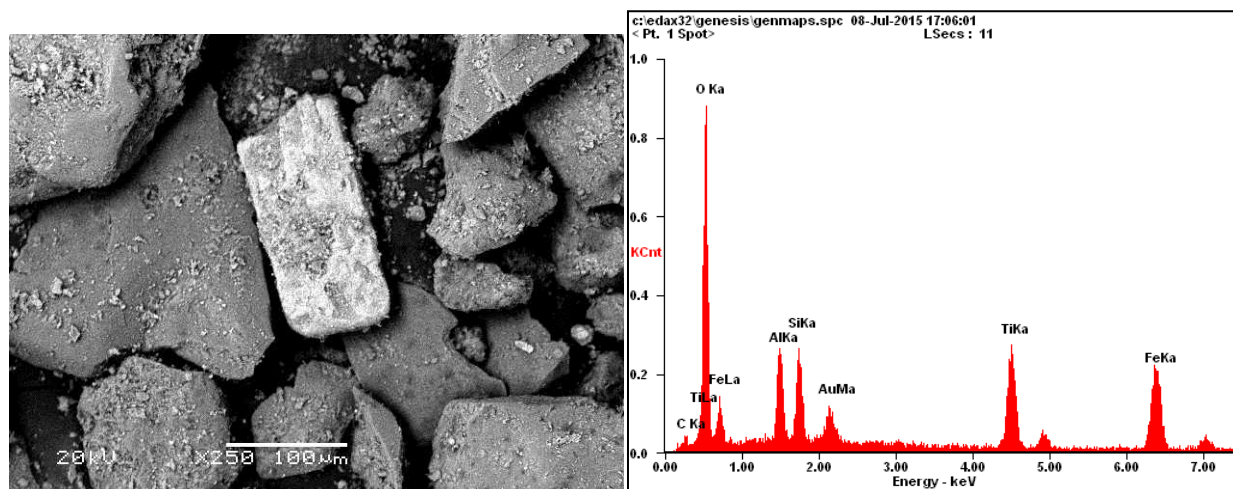


Figure 106. SEM Image and Elemental Analysis of SRS sediment coarse fraction via EDS

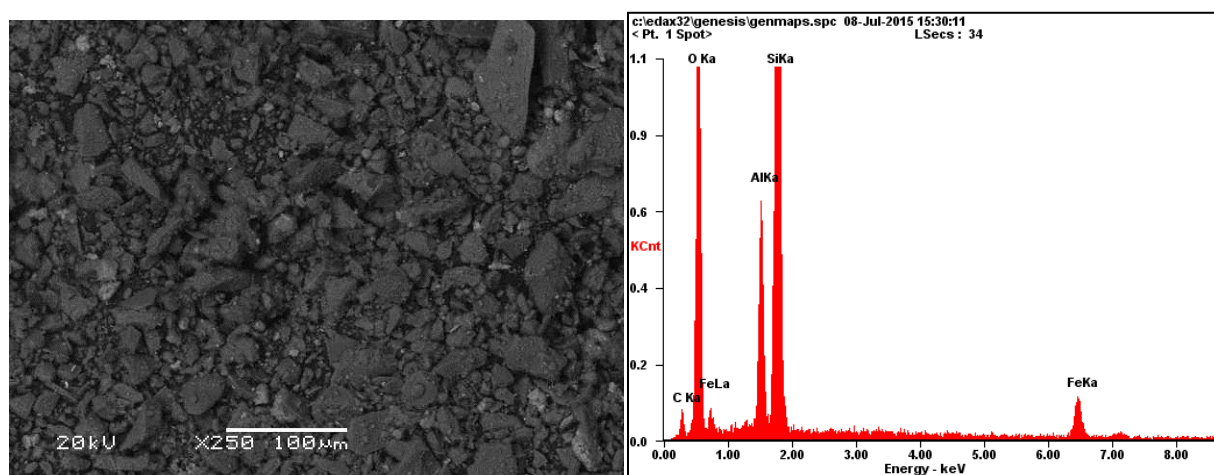


Figure 107. SEM Image and Elemental Analysis of SRS sediment fine fraction via EDS

Potentiometric Titrations

In the differential potentiometric titration curves, the protonation gradient $\frac{d[H^+_{cons,surf}]}{dpH}$ is used to determine the hydrogen consumption by the surface of a material as the pH in the solution is changed (Bourikas et al., 2005). At the beginning of the titration, most of the hydrogen ions are going to be consumed by the hydroxyl ions present in solution because they are in excess. As the pH is decreased with each addition of acid, the hydrogen ions are consumed not only by the hydroxyl ions in the solution but also by the surface sites of the material neutralizing the charges at that pH range. This consumption of hydrogen ions by the material is seen in the differential potentiometric titration curve as a reverse peak. As the surface site of the material begins protonating, the reverse peak is formed because the protonation gradient increases, taking its maximum at a pH value where half of the surface sites have been protonated (Bourikas et al.,

2005). The maximum of the reverse peak corresponds to the pK values of the surface sites present in the material that have acid/base properties that can be ionized (Bourikas et al., 2006). As the titration continues, the protonation gradient decreases until the protonation of the surface sites of the material have been completed (Bourikas et al., 2005).

With the differential potentiometric titration, it is possible to determine protonation/deprotonation behavior of the functional groups present in the Huma-K which will play an important role in the sorption process onto SRS sediments and formation of complexes with uranium. Figure 108 below shows the differential potentiometric titration curve of Huma-K (500 mg).

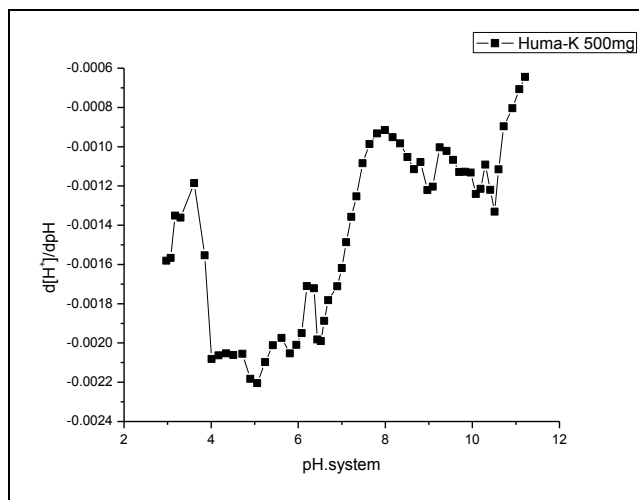


Figure 108. Differential potentiometric curve of Huma-K

Humic substances are complex organic molecules characterized by their molecular heterogeneity, complexity, and variable molecular size (Ghabbour et al., 2001). Humic substances possess many different functional groups (carboxyl, phenol, aliphatic acids, etc) arranged in a manner that can be protonated and deprotonated. These functional groups will have different pKa values. For instance, the presence of aliphatic acid (pKa = 4.8), aromatic acids (pKa = 4.2), or the combination of two acidic functional group in the aromatic ring with pKa values of 2.9 and 4.4 has been found in aquatic humic substances (Thurman et al., 1985). Also, other pKa values reported for humic and fulvic acid are for carboxylic acid pKa values between 4 and 6 and for phenolic groups between 9 and 11 (Stumm et al., 1996). The differential potentiometric titration result of the Huma-K shows that, between pH 4 and 6, there is a high hydrogen consumption. This is possibly due to the presence of a carboxyl group arranged in different configuration present in the humic and fulvic molecules of the Huma-K. There is probably also the presence of carbonate ions based on two peaks seen at pH 6.5 and 10.5. These two peaks could correspond to HCO_3^- (pKa = 6.3) and CO_3^{2-} (pKa = 10.33), respectively.

The differential potentiometric titration curves of SRS sediments (1gr) were prepared and compared with a quartz sand standard (Ottawa Sand Standard 20-30 Mesh) from Fisher Scientific. By comparing both materials, it can be seen that the differential potentiometric titration curve of SRS sediment is very similar to the quartz sand standard. This means that SRS sediments have a protonation/deprotonation behavior similar to quartz minerals. A study based on the surface acidity of quartz reported that silanol groups in quartz can be divided into three

groups based on their pKa values: the SiOH group with a pKa of 4.8, the Si(OH)₂ group with a pKa between 8.5 and 9.3, and the Si(OH)(O⁻) group with a pKa above 11 (Liu et al., 2014). Other studies have reported similar pKa values (4.5 and 8.5) for the acid /base behavior of silica interaction with water (Liu, 2014; Ong et al., 1992). Our results show that the SRS sediment and the quartz standard have pKa values of 4.5, 3.5, and three around 4.2. These pKa values may belong to the SiOH group based on the pKa values reported by other studies mentioned above.

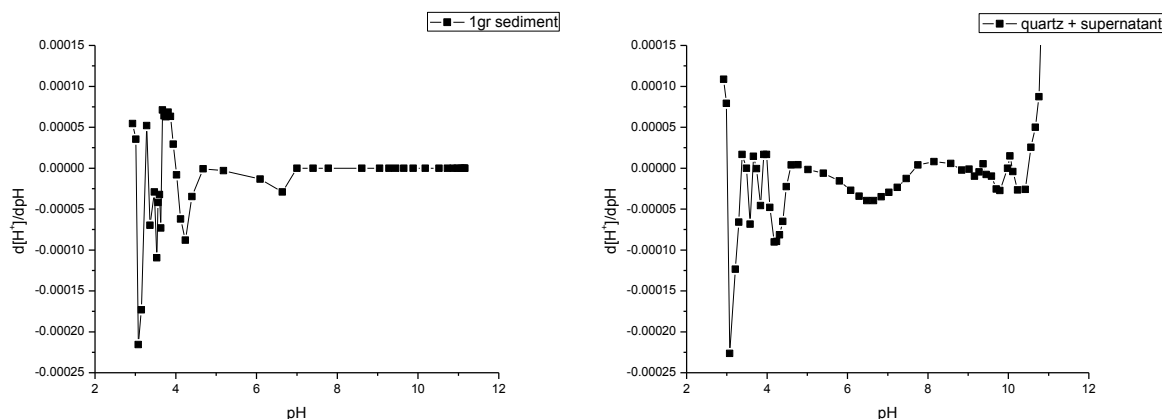


Figure 109. Differential potentiometric curve of SRS sediments and Quartz sand standard

Fourier Transform Infrared Spectroscopy

The FTIR spectrum of Huma-K (Figure 110) shows a broad peak at 3391 cm^{-1} . This peak is attributed to the O-H and N-H stretching of different sources such as alcohols, phenols, amines, or amides that usually appear in the $3400\text{--}3000\text{ cm}^{-1}$ region (Giovanela et al., 2004). The peak at 2925 cm^{-1} is attributed to the aliphatic C-H stretching of the methyl and methylene group that appears around 2926 and 2855 cm^{-1} (Giovanela, 2010; Giovanela et al., 2004). One of the main important peaks in the spectrum of humic substances is the peak at 1700 cm^{-1} which corresponds to the C=O stretching of the carboxylic acid (COOH). If the carboxylic acid functional groups present in the humic substances are in the form of carboxylate ion (COO⁻) or have formed a complex with a metal ion, the peak at 1700 cm^{-1} disappears and two new peaks will appear at about 1600 cm^{-1} and 1380 cm^{-1} for the symmetric and antisymmetric stretching vibration of the COO⁻ group (Erdogan et al., 2007). In the spectrum of Huma-K, a peak is not seen at 1700 cm^{-1} but rather two peaks at 1567 and 1383 cm^{-1} . This means that the carboxylic acid groups present in the Huma-K are in their salt form (COO⁻). Since the humic substances of the Huma-K were extracted from leonardite using an alkaline solution (potassium hydroxide), all the carboxyl groups are mostly in their dissociated form (COO⁻). The last peaks of the spectrum at 1029 and 914 cm^{-1} are attributed to the C-O and C-C stretching vibration of sugars which appear at 1105 , 1032 , 1010 and 913 cm^{-1} (Berthelin et al., 2012).

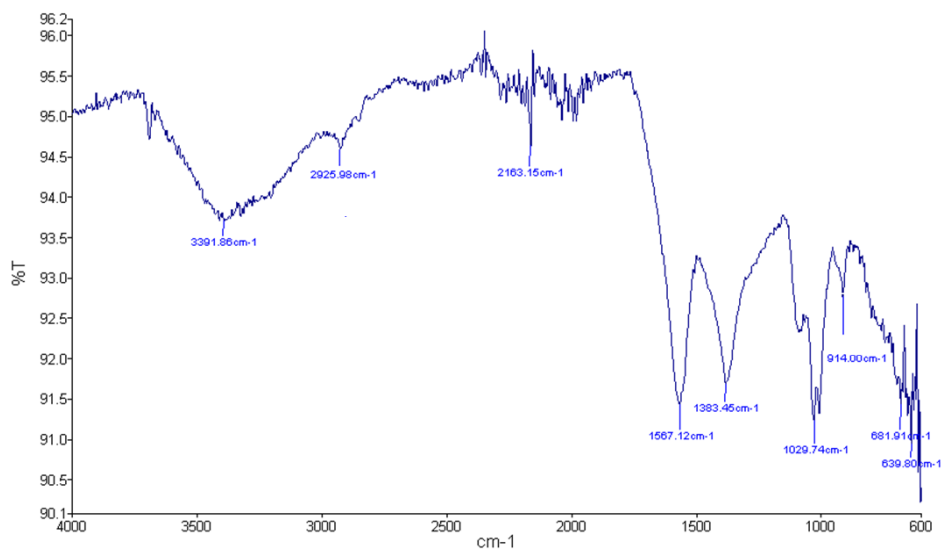


Figure 110. FTIR spectrum of Huma-K

Below is the FTIR spectrum of the SRS sediment fine fraction (less than 63 μm) and kaolinite.

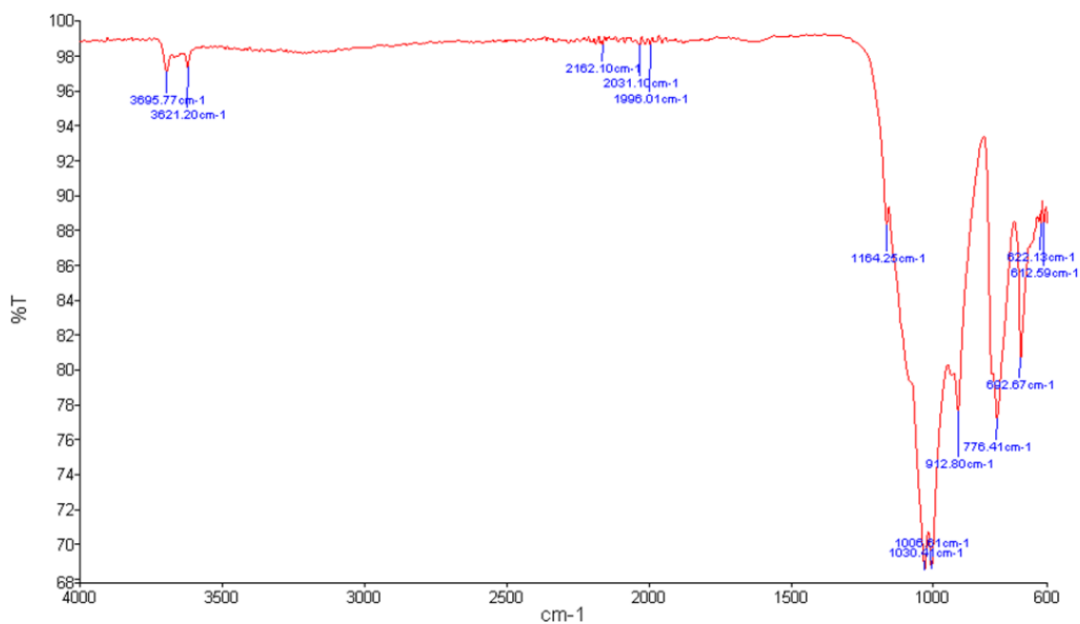


Figure 111. FTIR spectrum of SRS sediment fine fraction

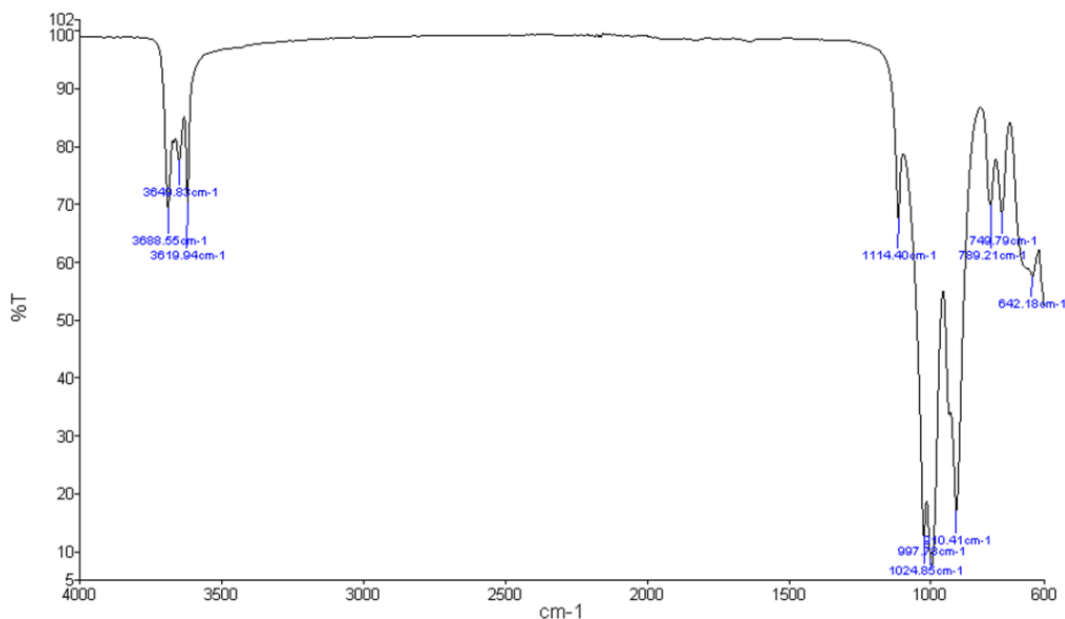


Figure 112. FTIR spectrum of Kaolinite

An FTIR spectrum of the coarse fraction was attempted but did not show prominent peaks due to the whole FTIR crystal area not being completely covered by bulky sediments. The SRS sediments had to be sieved to a particle size less than 63 μm in order to have a fine powder structure so the whole area of the crystal of the FTIR make contact with the sample. Also, the spectrum of pure kaolinite (aluminum silicate powder obtained from Alfa Aesar) was collected because it is one of the main minerals present in the F-Area sediments (Figure 112). As it can be seen, both spectra look very similar. Kaolinite has a distinctive pattern in the 3000 region (Müller et al., 2014). This unique pattern of kaolinite is seen by four peaks. The 3695, 3670, and 3650 cm^{-1} are attributed to the stretching vibration of the surface hydroxyl groups while the peak at 3620 cm^{-1} belongs to the inner-surface OH group stretching vibration (Djomgoue, 2013; Müller et al., 2014). The spectrum of the SRS sediment shows only two peaks (3695 and 3621 cm^{-1}) for that region. It is likely that the other two peaks are not present because they do not have a high intensity. Kaolinite and SRS sediment have a shoulder of absorption band at 1114 cm^{-1} and 1164 cm^{-1} , respectively, and this is attributed to the Si-O stretching. The peaks seen at 1030 and 1006 cm^{-1} for SRS sediments are close to the values for the in-plane Si-O stretching of the kaolinite (1024 and 997 cm^{-1}). Another characteristic peak found in SRS sediment at 912 cm^{-1} corresponds to the OH bending vibration of the inner surface OH groups in kaolinite which appears at 913 cm^{-1} (Vaculíková et al., 2011). In addition to the peaks identified as kaolinite, there are two peaks at 776 cm^{-1} and 692 cm^{-1} in the SRS sediment spectrum that could belong to quartz. The peak at 776 cm^{-1} may belong to both quartz and kaolinite and can be attributed to the Si-O symmetrical stretching vibration. The peak at 692 cm^{-1} is very close to the value reported for quartz at 695 cm^{-1} and belongs to the Si-O symmetrical bending vibration. To sum up, the FTIR spectrum of the SRS sediment fine fraction shows characteristic peaks that belong to the kaolinite and quartz minerals.

Sorption Experiment of Huma-K onto SRS sediments

Preliminary experiments were conducted to obtain a spectrum of Huma-K at different concentrations in order to detect possible sources of interference in the measurement of concentrations of Huma-K using a UV-vis spectrophotometer. The spectra of Huma-K with different concentrations is shown in Figure 16. It is clearly seen that some interferences appeared at 250 ppm and higher concentrations. The reason for that is that, at high concentrations, the distance between molecules become smaller; so, the charge distribution is affected, altering the molecules ability to absorb a specific wavelength. This outcome can affect the linear relationship between sample concentrations and absorbance (Beer's Law). For that reason, a standard calibration curve up to 100 ppm was created. Samples that contain concentrations higher than 100 ppm will be diluted so that they can be in the range of the standard calibration curve.

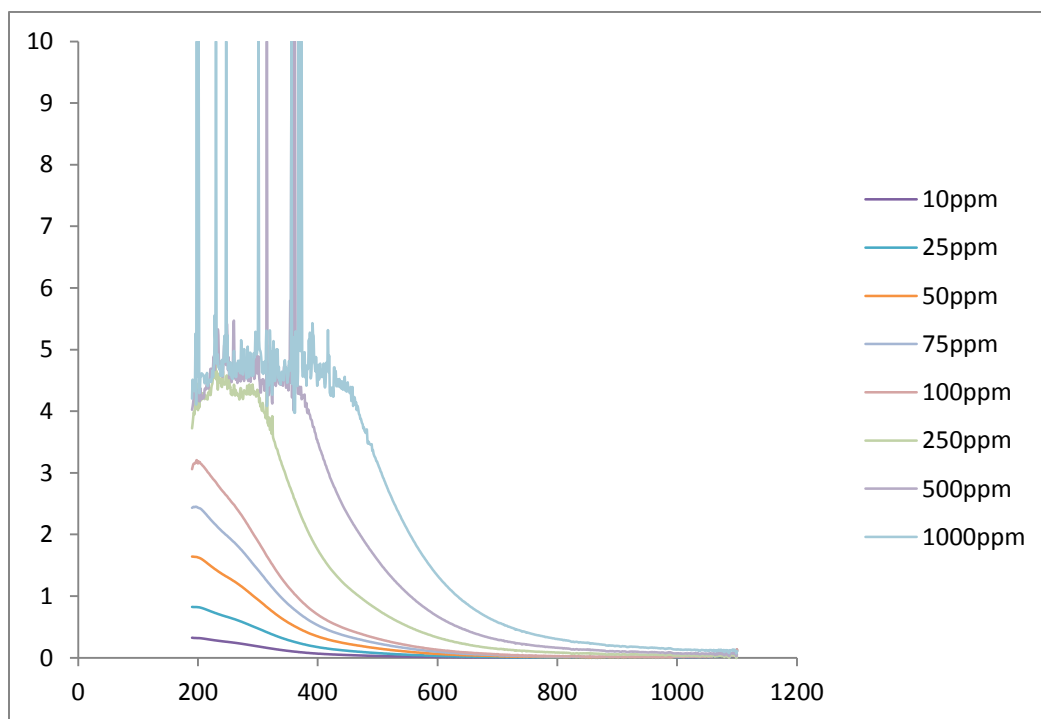


Figure 113. Spectra of Huma-K.

Kinetic experiments offer valuable information about the rate of the reaction and the reaction mechanism involved in the process. The kinetic experiments showed that sorption of Huma-K onto SRS sediments reaches a plateau at 4 days (96 hours) (Figure 114). After 4 days, no more humic molecules can be sorbed to the sediments possibly because the humic molecules have occupied all available binding sites on the sediment particles.

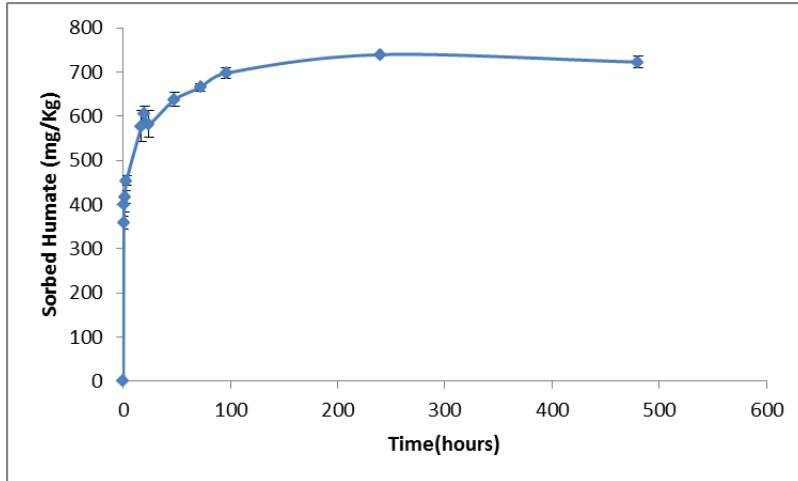


Figure 114. Kinetic Experiment of Huma-K.

With the data obtained from the adsorption kinetics, the sorption and diffusion processes can be calculated by using the mathematical kinetic models (1, 3) shown in Table 29.

Table 29. Kinetic Order Reaction Models

Kinetic model	Equation	Linear equation	Rate constant	Amount adsorbed at equilibrium	Plot	R ²
First-order	$q_t = q_e e^{-k_1 t}$	$\ln[q_t] = \ln[q_e] - k_1 t$	$K_1 = 1.1 \times 10^{-3}$	$q_e = 508.2$	$\ln[q_t] \text{ vs. } t$	0.3682
Pseudo first-order	$q_t = q_e (1 - \exp^{-k_{1p} t})$	$\log(q_e - q_t) = \log(q_e) - \frac{k_{1p} t}{2.303}$	$K_{1p} = 9 \times 10^{-3}$	$q_e = 178.2$	$\log(q_e - q_t) \text{ vs. } t$	0.4797
Second-order	$q_t = \frac{q_e}{1 + q_e k_2 t}$	$\frac{1}{q_t} = \frac{1}{q_e} + k_2 t$	$K_2 = -2 \times 10^{-6}$	$q_e = 500$	$\frac{1}{q_t} \text{ vs. } t$	0.3161
Pseudo second-order	$\frac{dq}{dt} = k_{2p} (q_e - q_t)^2$	$\frac{t}{q_t} = \frac{1}{k_{2p} q_e^2} + \frac{1}{q_e} t$	$K_{2p} = 4.26 \times 10^{-4}$	$q_e = 714.3$	$\frac{t}{q_t} \text{ vs. } t$	0.9995

Where:

q_t = amount of Huma – K sorbed at any time $\left(\frac{mg}{kg}\right)$

q_e = amount of Huma – K sorbed at equilibrium $\left(\frac{mg}{kg}\right)$

K_1 = first order rate constant (hour^{-1})

K_{1p} = pseudo first order rate constant (hour^{-1})

K_2 = second order rate constant $\left(\frac{kg}{mg \text{ hour}}\right)$

K_{2p} = pseudo second order rate constant $\left(\frac{kg}{mg \text{ hour}}\right)$

The model that best fit to the experimental data of the kinetic experiment is the pseudo second order model with a correlation coefficient R^2 of 0.9995. Other kinetic studies of humic acid adsorbed on kaolinite and hematite showed that kinetics follow a pseudo second order reaction (Shaker et al., 2012). In the pseudo first order kinetic model, it is assumed that one molecule will occupy one binding site at the surface while in the pseudo second order reaction one molecule will occupy two binding sites (Rudzinski, 2006; Liu, 2008). Also, the pseudo second order model assumes that two reactions are happening. One of the two reactions in the pseudo second order model proceeds to achieve equilibrium very fast. The rate of the other reaction is significantly slower, taking longer periods of time. These two reactions can occur in series or in parallel (Anagnostopoulos, 2012; Khanmbhaty, 2009). In the case of Huma-K, it could be assumed that there are two types of reactions (fast and slow). An example of a fast sorption reaction is adsorption through electrostatic attraction and inner sphere complexation (Strawn et al., 2000). Carboxyl groups from humic molecules tend to be negatively charged and can be attracted electrostatically to the positive charges developed at the surface of the sediment particles in the fast reaction. Examples of a slow sorption reaction can be slow interparticle diffusion, formation of precipitates on surfaces, and adsorption on sites that have a large activation energy (Strawn et al., 2000). At low pH values, humic molecules have less charge, so they can agglomerate and precipitate. The results from the adsorption of Huma-K at different pH values in Figure 20 show that there is a precipitation besides sorption at low pH values. This precipitation could be attributed to the slow reaction that is happening from the pseudo second order kinetic model.

In summary, sorption of Huma-K onto SRS sediments appears to follow a two-site sorption model. First, humic molecules will occupy the binding sites at the mineral surfaces. Then, as the concentration is increased, humic molecules will interact with the already bound humic molecules in the sediments and with themselves to form agglomerates followed by precipitation. In the sorption of Huma-K at different pH values, it was demonstrated that the precipitation of Huma-K increased at low pH values and sorption and precipitation decreased as the pH increased. Kinetics experiments of Huma-K showed that the rate of the reaction follows a pseudo second order.

From the results of the sorption experiment of Huma-K at pH 4 (Figure 115), it can be seen that sorption of Huma-K onto sediments follows a Langmuir isotherm up to 250 ppm. This means that a plateau is reached because all the binding sites of the minerals surface have been occupied and no more sorption can occur. It was noticed that after the 250 ppm (from 300 to 500 ppm), the sorption of Huma-K was increased. It is likely that there is another mechanism of interaction besides sorption between Huma-K and the sediments. According to Da Costa Saab et al. (2010), it was shown by using atomic fluorescence microscope imaging that aquatic fulvic acid at low pH values (pH 3) formed agglomerates at the surface of a mica sheet due to most of the fulvic molecules being uncharged. In our case, Huma-K contains both humic and fulvic acids. Since humic molecules are mostly uncharged at low pH values, they will agglomerate at the surface of the SRS sediments. Also, aggregation is related to the degree of hydrophobicity which is an important feature of humic molecules. Balnois et al. (1999) studied the agglomeration of a hydrophilic humic acid from the Suwannee River and a peat humic acid on a surface of a muscovite mica. Balnois et al. (1999) showed that, between pH values of 3 and 10, no aggregates were formed for the hydrophilic Suwannee humic, but peat humic acid, which is more hydrophobic, did form aggregates at pH values less than 5. From this, it can be assumed that the

humic molecules in Huma-K have a more hydrophobic character and formed aggregates at the surface of SRS sediments at low pH values.

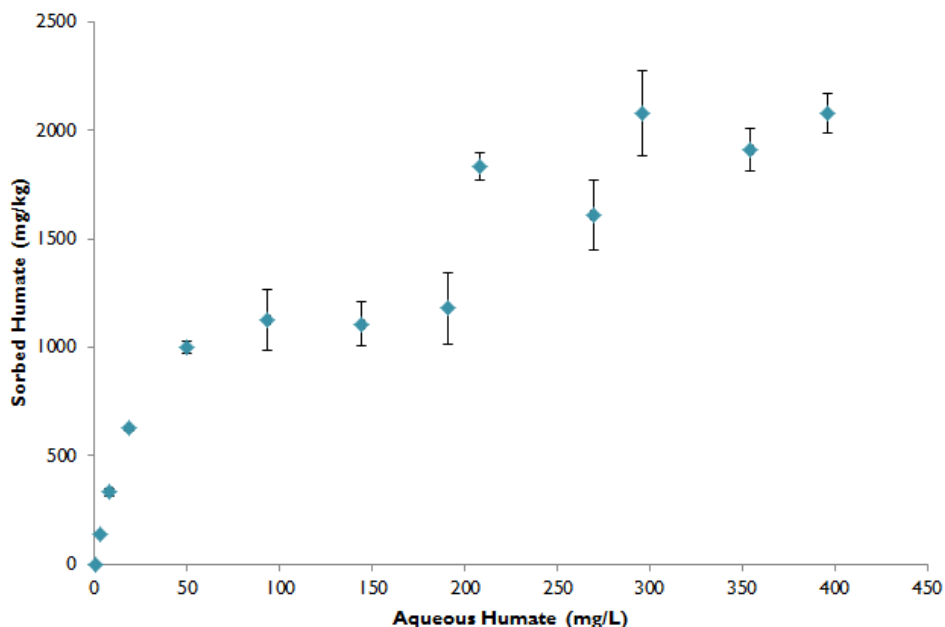


Figure 115. Sorption Experiment of Huma-K at pH 4.

Figure 116 shows the results of the sorption experiment of Huma-K (50 ppm) at different pH values. The blue bars correspond to the total removal of Huma-K in the presence of sediments. The yellow bars correspond to the removal of Huma-K due to precipitation without sediment. The red bar is assumed to be the sorption of Huma-K calculated from the difference between the total removal with sediments minus precipitation. The highest percentage of Huma-K sorbed to the sediments was noted at pH 4 (62.8%). When the pH is increased, the sorption was observed to decrease. At pH 7, only 6% of Huma-K was sorbed to the sediments. Beyond pH 7, no further significant adsorption was noted. One possible explanation for these findings is that, as the pH is increased, sediments become more negatively charged, as does humic molecules. The sorption is decreased due to the electrostatic repulsion between the humic molecules and sediments. The increase of pH diminishes sorption of humic molecules to the sediments. Also, it was studied to determine if precipitation of Huma-K contributes to its removal. The results show that, at pH 4, Huma-K forms precipitates, but as the pH is increased, it becomes more soluble, decreasing the precipitation. There was a minimum of precipitation at pH 6 and, beyond that pH, there was no precipitation (Figure 20).

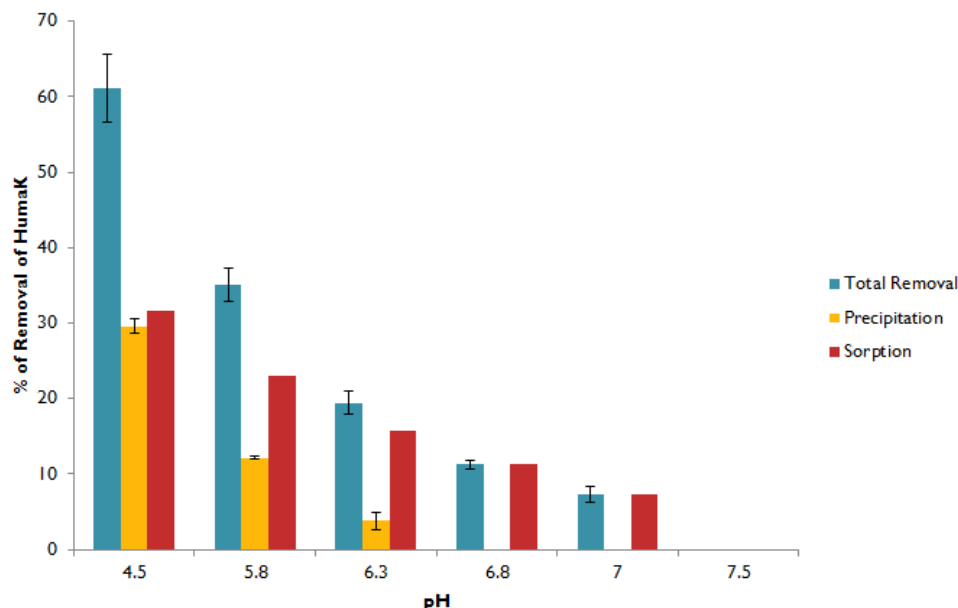


Figure 116. Sorption Experiment of Huma-K at different pH values.

Subtask 2.3: Future Work

Future work will focus on the batch experiments, exploring desorption of Huma-K from SRS sediments and studying the effect of initial Huma-K concentration, pH, and the presence of ions common in SRS groundwater such as NO_3^- , Ca^{+2} , Na^+ , etc. Also, FTIR analysis of Huma-K sorbed to SRS sediments will be performed to elucidate which functional groups play a role in the sorption process.

Subtask 2.3: Acknowledgements

Funding for this research was provided by U.S. DOE cooperative agreement DE-EM0000598. We truly appreciate Dr. Miles Denham and Dr. Brian Looney from the SRNL for their valuable contributions and support of this research.

Subtask 2.3: References

- Chen, Y., Senesi, N., Schnitzer. (1977). Information provided on humic substances by E_4/E_6 ratios. *Soil Science Society of America*. **41**: 352-358.
- Balcke, G., Kulikova, N., Hesse, S., Kopinke, F., Perminova, I., Frimmel, F. (2002). Adsorption of humic substances onto kaolin clay Related to their structural features. *Soil Science Society of America*. **66**: 1805-1812.
- Janot, N., Reiller, P., Zheng, X., Croué, J., Benedetti, M. (2012). Characterization of humic acid reactivity modifications due to adsorption onto $\alpha\text{-Al}_2\text{O}_3$. *Water Research*. **46**: 731-740.
- Wan, J., Dong, W., Tokunaga, T. (2011). Method to attenuate U (VI) mobility in acidic waste plumes using humic acids. *Environmental Science and Technology*. **45**: 2331-2337.
- Fein, J., Boily, J., Güçlü, K., Kaulbach, E. (1999). Experimental study of humic acid adsorption onto bacteria and Al-oxide mineral surfaces. *Chemical Geology*. **162**: 33-45.

- Illés, E., Tombácz, E. (2004). The role of variable surface charge and surface complexation in the adsorption of humic acid on magnetite. *Colloids and Surfaces A: Physicochem. Eng. Aspects.* **230**: 99-109.
- Vieyra, F., Palazzi, V., Sanchez de Pinto, M., Borsarelli, C. (2009). Combined UV-vis absorbance and fluorescence properties of extracted humic substances-like for characterization of composting evolution of domestic solid wastes. *Geoderma.* **151**: 61-67.
- Gan, D., Kotob, S. Walia, D. (2007). Evaluation of a spectrophotometric method for practical and cost effective quantification of fulvic acid. *Annals of environmental Science.* **1**: 11-15.
- Benedetti, M., Van Riemsdijk, W., Koopal, L. (1996). Humic substances considered as a heterogeneous donnan gel phase. *Environmental Science and Technology.* **30**: 1805-1813.
- Fuentes, M., González-Gaitano, G., García-Mina, J. (2006). The usefulness of UV-visible and fluorescence spectroscopies to study the chemical nature for humic substances from soils and composts. *Organic Geochemistry.* **37**: 1949-1959.
- Choppin, G.R., 1992. The role of natural organics in radionuclide migration in natural aquifer systems. *Radiochim. Acta* 58/59, 113.
- Choppin, G.R., 1998. Humics and radionuclide migration. *Radiochim. Acta* 44/45, 23-28.
- Davis, J.A., 1982. Adsorption of natural dissolved organic matter at the oxide/water interface. *Geochim. Cosmochim. Acta* 46, 2381-2393.
- Davis, J.A., 1984. Complexation of trace metals by adsorbed natural organic matter. *Geochim. Cosmochim. Acta* 48, 679-691.
- Dong, W., Tokunaga, T. K., Davis, J.A., Wan, J., 2011. Uranium(VI) Adsorption and Surface Complexation Modeling onto Background Sediments from the F-Area Savannah River Site. *Environmental Science & Technology*
- Fairhurst, A. J.; Warwick, P.; Richardson, S. 1995. The influence of humic acid on the sorption of europium onto inorganic colloids as a function of pH. *Colloids Surf., A*, 99, 187-199.
- Ivanov, P., Griffiths, T., Bryan, N.D., Bozhikov, G. and S. Dmitriev, 2012. The effect of humic acid on uranyl sorption onto bentonite at trace uranium levels. *J. Environ. Monit.*, 14, 2968 - 2975.
- Krepelova, A., Brendler, V., Sachs, S., Baumann, N., Bernhard, G., 2007. U(VI)-Kaolinite Surface Complexation in Absence and Presence of Humic Acid Studied by TRLFS. *Environ. Sci. Technol.* 2007, 41, 6142-6147.
- Labonne-Wall, N., Moulin, V., Vilarem, J.P., 1997. Retention properties of humic substances onto amorphous silica: consequences for the sorption of cations. *Radiochim. Acta*, 79, 37-49.
- Murphy, R. J., Lenhart J. J. and B. D. Honeyman, The sorption of Th(IV) and U(VI) to hematite in the presence of natural organic matter, *Colloids Surf., A*, 1999, 157, 47.
- Perminova, I.V, Hatfield, K., Hertkorn, N., 2002. Use of humic substances to remediate polluted environments: from theory to practice. In the proceedings of the NATO Advance Research Workshop, Springer, P.O Box 17, 3300 AA Dordrech, The Netherland.

- Plancque, G., Amekraz, B., Moulin, V., Toulhoat, P., Moulin, C., 2001. Molecular structure of fulvic acids by electrospray with quadrupole time-of-flight mass spectrometry. *Rapid Commun. Mass Spectrom.* 15, 827-835.
- Shmeide, K., Pompe, S., Bubner, M., Bernhard G. and H. Nitsche, 2000. Uranium(VI) sorption onto phyllite and selected minerals in the presence of humic acid, *Radiochim. Acta*, 88, 723
- Zachara, J.M., Resch, C.T., Smith, S.C., 1994. Influence of humic substances on Co^{2+} sorption by a subsurface mineral separate and its mineralogical components. *Geochim. Cosmochim. Acta* 58, 553-566.
- Liao Jiali, Wen Wei, LI Bing, Yang Yuanyou, Zhang Dong, Kang Houjun, Yang Yong, Jin Jiannan, Liu Ning, 2013. Interaction between uranium and humic acid (II): complexation, precipitation and migration behavior of U(VI) in the presence of humic substances. *Nuclear Science and Techniques* 24, 030301
- L.K. Koopal, Y. Yang, A.J. Minnaard, P.L.M. Theunissen, W.H. Van Riemsdijk, 1998. Chemical immobilization of humic acid on silica. *Colloids and Surfaces A: Physicochemical and Engineering Aspects* 141, 385-395.
- Wang, J., Dong, W., Tokunaga, T, 2011. Method to Attenuate U(VI) Mobility in Acidic Waste Plumes Using Humic Acids. *Environ. Sci. Technol.* 45, 2331-2337.
- Tinnacher, R., Nico, P., Davis, J., Honeyman, 2013. Effects of Fulvic Acid on Uranium(VI) Sorption Kinetics. *Environ. Sci. Technol.* 47, 6214-6222.
- Shaker, A., Komy, Z., Heggy, S, El-Sayed, M. (2012). Kinetic Study for Adsorption Humic Acid on Soil Minerals. *J. Phys. Chem. A*. 116: 10889-10896.
- Anagnostopoulos, V., Manariotis, I., Karapanagioti, H., Chrysikopoulos, C. (2012). Removal of mercury from aqueous solutions by malt spent rootlets. *Chemical Engineering Journal*. 213: 135-141.
- Khambhaty, Y., Mody, K., Basha, S., Jha, B. (2009). Kinetics, equilibrium and thermodynamic studies on biosorption of hexavalent chromium by dead fungal biomass of marine *Aspergillus niger*. *Chemical Engineering Journal*. 145: 489-495.
- Kumar, K. (2006). Linear and non-linear regression analysis for the sorption kinetics of methylene blue onto activated carbon. *Journal of Hazardous Material*. B137: 1538-1544.
- Hameed, B., Mahmoud, D., Ahmad, A. 2008. Equilibrium modeling and kinetic studies on the adsorption of basic dye by a low-cost adsorbent: Coconut (*Cocos nucifera* bunch waste. *Journal of Hazardous Materials*. 158: 65-72.
- Qiu, H., LV, L., Pan, B., Zhang, Q., Zhang, W., Zhang, Q. 2009. Critical review in adsorption kinetic models. *Journal of Zhejiang University*. 10(5): 716-724.
- Rudzinski, W., Plazinski, W. 2006. Kinetics of Solute Adsorption at Solid/Solution Interfaces: A Theoretical Development of the Empirical Pseudo-First and Pseudo-Second Order Kinetic Rate Equations, Based on Applying the Statistical Rate Theory of Interfacial Transport. *J. Phys. Chem. B*. 110: 16514-16525.
- Liu, Y., Liu, Y. 2008. Biosorption isotherms, kinetics and thermodynamics. *Separation and Purification Technology*. 61: 229-242.

Aguayo-Villarreal, I., Bonilla-Petriciolet, A., Hernández-Montoya, V., Montes-Morán, M., Reynel-Avila, H. 2011. Batch and column studies of Zn^{2+} removal from aqueous solution using chicken feathers as sorbents. *Chemical Engineering Journal*. 167: 67-76.

Rajamohan, N., Rajasimman, M., Rajeshkannan, R., Saravanan, V. 2014. Equilibrium, kinetic and thermodynamic studies on the removal of Aluminum by modified *Eucalyptus camaldulensis* barks. *Alexandria Engineering Journal*. 53: 409-415.

Strawn, D., Sparks, D. (2000). Effects of Soil Organic Matter on the Kinetics and Mechanisms of Pb(II) Sorption and Desorption in Soil. *Soil Sci. Soc. Am. J.* 64: 144-156.

Da Costa Saab, S., Carvalho, E., Bernardes Filho, R., de Moura, M., Martin-Neto, L., Mattoso, L. (2010). pH effect in aquatic fulvic acid from a Brazilian river. *J. Braz. Chem. Soc.* 21: 1490-1496.

Balnois, E., Wilkinson, K., Lead, J., Buffle, J. (1999). Atomic force microscopy of humic substances: effect of pH and ionic strength. *Environ. Sci. Technol.* 33: 3911-3917.

Bourikas, K., Kordulis, C., Lycourghiotis, A. (2006). How metal (hydr)oxides are protonated in aqueous media: The $(n + 1)$ rule and the role of the interfacial potential. *Journal of Colloid and Interface Science*. 296: 389-395.

Vakros, J., Kordulis, C., Lycourghiotis, A. (2002). Potentiometric mass titrations: a quick scan determining the point of zero charge. *Chem. Commun.* 1980-1981.

Appel, C., Ma, L., Rhue, R., Kennelley, E. (2003). Point of zero charge determination in soils and minerals via traditional methods and detection of electroacoustic mobility. *Geoderma*. 113:77-93.

Bourikas, K., Kordulis, C., Lycourghiotis, A. (2005). Differential Potentiometric Titration: Development of a Methodology for Determining the point of Zero Charge of Metal (Hydr)oxide by One Titration Curve. *Environ. Sci. Technol.* 39: 4100-4108.

Bourikas, K., Vakros, J., Kordulis, C., Lycourghiotis, A. (2003). Potentiometric Mass Titrations: Experimental and Theoretical Establishment of a New Technique for Determining the Point of Zero Charge (PZC) of Metal (Hydr)Oxides. *J. Phys. Chem. B.* 107: 9441-9451.

Prélot, B., Charmas, R., Zarzycki, P., Thomas, F., Vllieras, F., Piasecki, W, Rudziński, W. (2002). Application of the Theoretical 1-pK Approach to Analyzing Proton Adsorption Isotherm Derivatives on Heterogeneous Oxide Surfaces. *J. Phys. Chem. B.* 106: 13280-13286.

Bourikas, K., Kordulis, C., Lycourghiotis, A. (2006). The mechanism of the protonation of metal (hydr)oxides in aqueous solutions studied for various interfacial/surface ionization models and physicochemical parameters: A critical review and a novel approach. *Advances in Colloid and Interface Science*. 121: 111-130.

Anagnostopoulos, V., Koutsoukos, P., Symeopoulos, B. (2015). Removal of U(VI) from Aquatic Systems, Using Winery By-Products as Biosorbents: Equilibrium, Kinetic, and Speciation Studies. *Water Air Soil Pollut.* 226: 107.

Klucakova, M., Kolajova, R. (2014). Dissociation ability of humic acids: Spectroscopic determination of pKa and comparison with multi-step mechanism. *Reactive and Functional Polymers*. 78: 1-6.

E. A. Ghabbour and G. Davies , Eds., *Humic Substances: Structures, Models and Functions*, Royal Society of Chemistry, Cambridge, 2001, p. 26.

Thurman, E. M. *Organic Geochemistry of Natural Waters*. Dordrecht: M. Nijhoff, 1985, p. 90.

Stumm, Werner, and James J. Morgan. *Aquatic Chemistry: Chemical Equilibria and Rates in Natural Waters*. New York: Wiley, 1996, p. 141.

Liu, X., Cheng, J., Lu, X., Wang, R. (2014). Surface acidity of quartz: understanding the crystallographic control. *Phys. Chem. Chem. Phys.* 16: 26909-26916.

Leung, K., Nielsen, I., Criscenti, L. (2009). Elucidating the Bimodal Acid-Base Behavior of the Water-Silica Interface from First Principles. *J. AM. CHEM. SOC.* 131: 18358-18365.

Ong, S., Zhao, X., Eissenthal, K. (1992). Polarization of water molecules at a charged interface: second harmonic studies of the silica/water interface. *Chemical Physics Letters*. 191: 327-335.

Wan, J., Dong, W., Tokunaga, T. (2011). Method to Attenuate U(VI) Mobility in Acidic Waste Plumes Using Humic Acids. *Environ. Sci. Technol.* 45(6): 2331-2337.

Dong, W., Wan, J. (2014). Additive Surface Complexation Modeling of Uranium(VI) Adsorption onto Quartz-Sand Dominated Sediments. *Environ. Sci. Technol.* 48: 6569-6577.

Giovanela, M., Crespo, J.S., Antunes, M., Adamatti, D.S., Fernandes, A.N., Barison, A., da Silva, C.W.P., Guegan, R., Motelica-Heino, M., Sierra, M.M.D. (2010). Chemical and spectroscopic characterization of humic acids extracted from the bottom sediments of a Brazilian subtropical microbasin. *Journal of Molecular Structure*. 981: 111-119.

Giovanela, M., Parlanti, E., Soriano-Sierra, E.J. Soldi, M.S., Sierra, M.M.D. (2004). Elemental compositions, FT-IR spectra and thermal behavior of sedimentary fulvic and humic acids from aquatic and terrestrial environments. *Geochemical Journal*. 38: 255-264.

Erdogan, S., Baysal, A., Akba, O., Hamamci, H. (2007). Interaction of Metals with Humic Acid Isolated from Oxidized Coal. *Polish J. of Environ. Stud.* 16(5): 671-675.

Jacques Berthelin, P.M. Huang, J-M. Bollag, Francis Andreux. *Effect of Mineral-Organic-Microorganism Interactions on Soil and Freshwater Environments*. Springer Science & Business Media, 2012, p. 136.

Madejová, J., Komadel, P. (2001). Baseline studies of the clay minerals society source clays: infrared methods. *Clays and Clay Minerals*. 49: 410-432.

Djomgoue, P., Njopwouo, D. (2013). FT-IR Spectroscopy Applied for Surface Clays Characterization. *Journal of Surface Engineered Materials and Advanced Technology*. 3: 275-282.

Palayangoda, S., Nguyen, Q. (2012). An ATR-FTIR procedure for quantitative analysis of mineral constituents and kerogen in oil shale. *Oil Shale*. 29: 344-356.

Müller, C., Pejčić, B., Esteban, L., Piane, C., Raven, M., Mizaikoff, B. (2014). Infrared Attenuated Total Reflectance Spectroscopy: An Innovative Strategy for Analyzing Mineral Components in Energy Relevant Systems. *Sci. Rep.*

Müller, C., Molinelli, A., Karlowatz, M., Aleksandrov, A., Orlando, T., Mizaikoff, B. (2012). Infrared Attenuated Total Reflection Spectroscopy of Quartz and Silica Micro- and Nanoparticulate Films. *J. Phys. Chem. C*. 116: 37-43.

Vaculíková, L., Plevová, E., Vallová, S., Koutník, I. (2011). Characterization and differentiation of kaolinites from selected Czech deposits using infrared spectroscopy and differential thermal analysis. *Acta Geodyn. Geomaster*. 8: 59-67.

Balan, E., Lazzeri, M., Saitta, M., Allard, T., Fuchs, Y., Mauri, F. (2005). First-principles study of OH-stretching modes in kaolinite, dickite, and nacrite. *American Mineralogist*. 90: 50-60.

Saikia, B., Parthasarathy, G., Sarmah, N. (2008). Fourier transform infrared spectroscopic estimation of crystallinity in SiO₂ based rocks. *Bull. Mater. Sci.* 31: 775-779.

TASK 3.0: EVALUATION OF AMMONIA FATE AND BIOLOGICAL CONTRIBUTIONS DURING AND AFTER AMMONIA INJECTION FOR URANIUM TREATMENT

Task 3.1: Investigation on NH₃ Partitioning In Bicarbonate-Bearing Media

Task 3.1: Introduction

The following experiments are part of a broader investigation into NH₃ gas (g) partitioning and its effects on the subsurface sediments and uranium geochemistry. The Hanford reservation plans to use NH₃(g) injection for remediation of uranium. The porewater pH increase caused by injection is expected to lead to dissolution of sediments (i.e. silicates), which will then precipitate uranium as the water returns to the natural pH. The goal of this work is to elucidate the partitioning of NH₃(g) in solutions pertinent to the Hanford groundwater and porewaters. Initial experiments were carried out at variable bicarbonate concentrations as this is a major component of the site's natural waters. Further discussion of previous work by PNNL and Hanford, ammonia chemistry, and experimental methods for future work is included in the literature review attached (Appendix A).

Task 3.1: Current Experimental Protocol

Experimental Methodology

Experiments include step injections of NH₃ as gas (g) (5% NH₃/95% N₂) via a syringe and syringe pump (Kloehn Las Vegas, NV, operated via Hyperterminal software) into solutions with variable bicarbonate (0 - 100 mM) with 100 mL of solution in 150 mL Pyrex beakers open to the atmosphere with a stirrer (Orion Star series, 096019). Continuous measurement of pH, temperature and conductivity (μS/cm) are conducted throughout and aliquots are removed are removed for measurement of total NH₃/NH₄⁺ by ammonia gas-sensing electrode (Orion 9512BNWP). Samples are acidified with H₂SO₄ (1 mL concentrated H₂SO₄ per 50 mL of sample) and refrigerated until analysis. Upon analysis, a pH and ISA adjusting solution (2 mL per 100 mL of sample) is added to raise the pH to 11 and adjust ionic strength (Orion 951211). It contains a blue dye indicator to ensure that the appropriate pH is reached for the electrode to function properly.

Statistical Analysis

Data is shown as an average and standard deviation of triplicate experiments (i.e., each bicarbonate concentration was run three times). A comparison of the average for triplicate measurements of aqueous NH₃ and pH for variable bicarbonate concentration was conducted through Tukey's comparison method by calculating 95% confidence intervals as outlined by Berthouex and Brown (Berthouex and Brown, 1994). Two averages (with each average being based on triplicate experiments at the same bicarbonate concentration) are compared against each other at a 95% confidence interval and the method allows for comparison of multiple treatments. However, it must be noted that all data points could not be compared as samples for NH₃ concentration were often pulled for analysis at different time points (i.e. amounts of NH₃ injected, comparisons applicable for 1, 5, 9 and 20 mL of NH₃ (g) injected as summarized in the supplemental data (Appendix B)). In addition, a power law regression was fit to each of the

datasets comparing the volume of $\text{NH}_3(\text{g})$ injected versus aqueous NH_3 concentration to estimate a 95% confidence interval for the datasets using Sigmaplot software. However, this is not included as the error predicted was similar (although slightly greater) to that predicted with the standard deviation of triplicate measurements.

Geochemical Modeling

Simple speciation models were developed using Visual Minteq and PHREEQC software and are discussed in subsequent sections. The Visual Minteq models assume a constant ionic strength. However, the ammonia concentration reached as high as 31 mM during the experiments. Because the ionic strength is changing throughout the experiments, these models should only be used for qualitative comparison. Future experiments will be completed at a constant ionic strength to simplify modeling for this purpose and to simplify the system by making this variable constant throughout the experimental sets. PHREEQC was used to theoretically estimate the conductivity in samples based on major ions present for comparison with conductivity measurements gathered throughout experiments.

Task 3.1: Discussion

Data comparing the injection volume versus pH and conductivity for 3 mM, 30 mM, 60 mM, and 100 mM HCO_3^- solutions (Figure 117 - Figure 118) shows that the presence of bicarbonate significantly increases the buffering capacity of the solutions and leads to a requirement of significantly more $\text{NH}_3(\text{g})$ to reach the target pH for remediation purposes.

Conductivity

As shown in Figure 117, the conductivity is increasing with respect to the amount of $\text{NH}_3(\text{g})$ injected and with respect to the initial bicarbonate concentration. The bicarbonate concentrations appear to follow an approximately linear increase with respect to volume injected based on Figure 119 - Figure 120. However, the slope of a linear fit of the 100 mM solution is more than twice that of the 3 mM solution. Further, normalization by change in conductivity ($\Delta\text{cond} = C_t - C_0$) shows a greater increase in conductivity throughout the experiment at greater bicarbonate concentrations. While it is expected that the initial conductivity would be different as these are not at constant ionic strength, they should be increasing similarly unless there are other changes occurring within this open system. It is possible that the bicarbonate has an effect on sorption of other gases from the open system in these experiments. In order to further understand the relationship between conductivity and injected ammonia, future experiments will be conducted at constant ionic strength (~ 0.15 M, as adjusted using NaCl). Further, modeling using PHREEQC (Figure 121) shows that theoretical predictions of conductivity based on the major ions present predict a similar conductivity and trend but are continuously lower than measured values. Although it is possible that our model is missing a factor leading to under prediction of conductivity, it must be noted that laboratory water quality fell below optimum resistivity during these experiments as discussed below and could also be a contributing factor in the higher than predicted conductivity measurements.

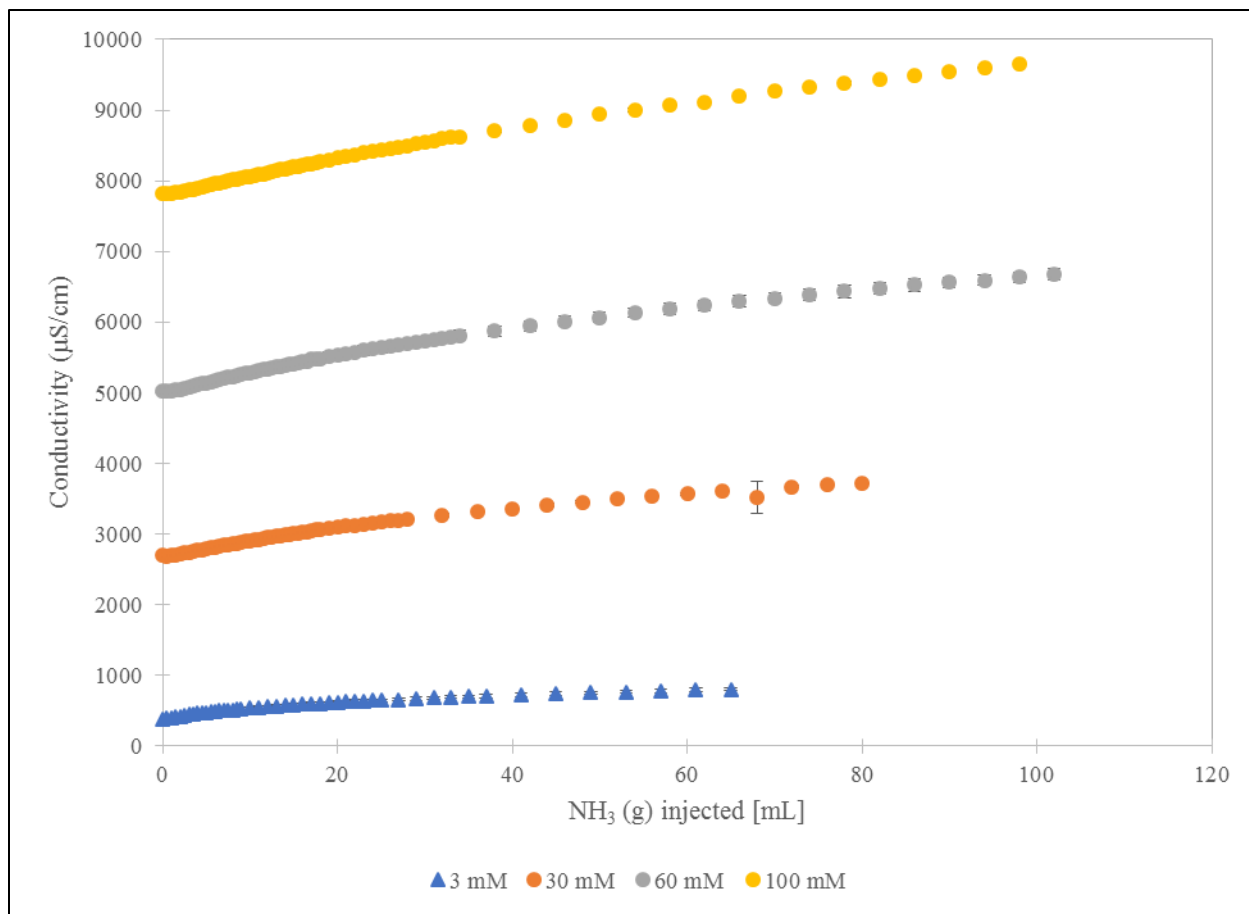


Figure 117. Comparison of triplicate measurements of conductivity changes in 3 mM, 30 mM, 60 mM and 100 mM HCO_3^- solutions with respect to the volume of NH_3 gas injected

Note: error bars are based on one standard deviation of measurements from triplicate experiments at each bicarbonate concentration.

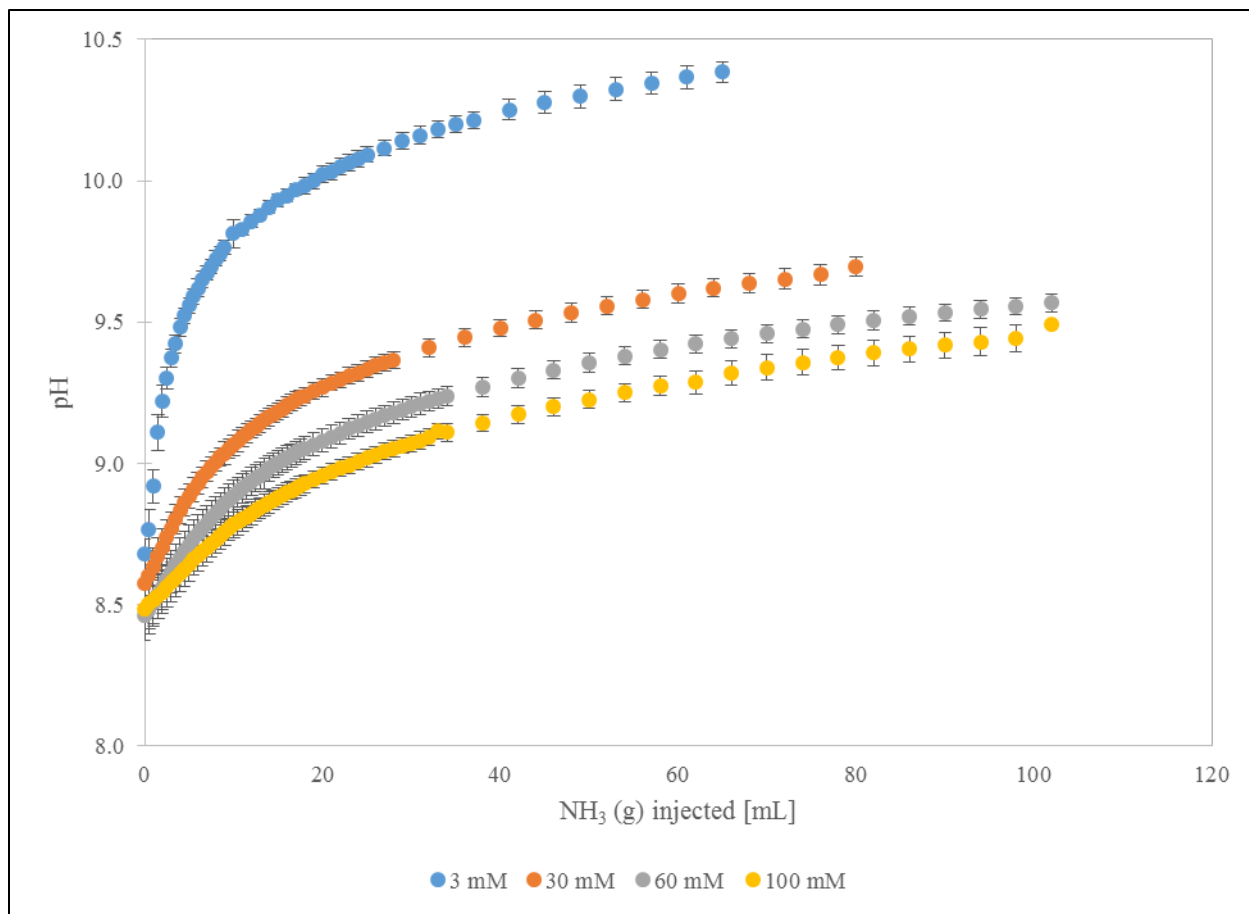


Figure 118. Comparison of triplicate measurements of pH in 3 mM, 30 mM, 60 mM and 100 mM HCO_3^- solutions with respect to the volume of NH_3 gas injected

Note: error bars are based on one standard deviation of measurements from triplicate experiments at each bicarbonate concentration

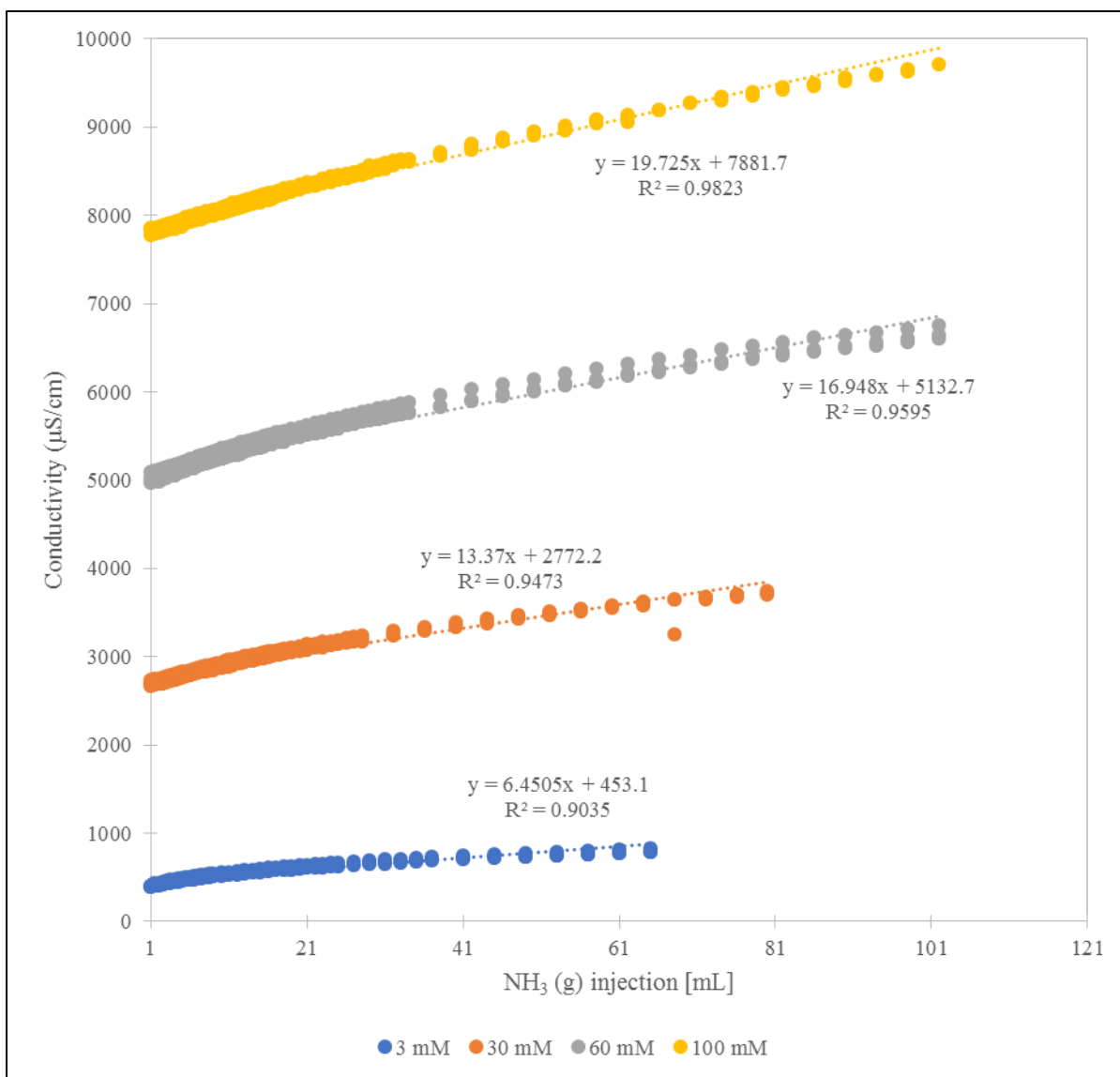


Figure 119. Comparison of the conductivity (μS/cm) with respect to injection volume of NH₃ (g) for variable bicarbonate suspensions with a linear fit including data from triplicate experiments for each bicarbonate concentration

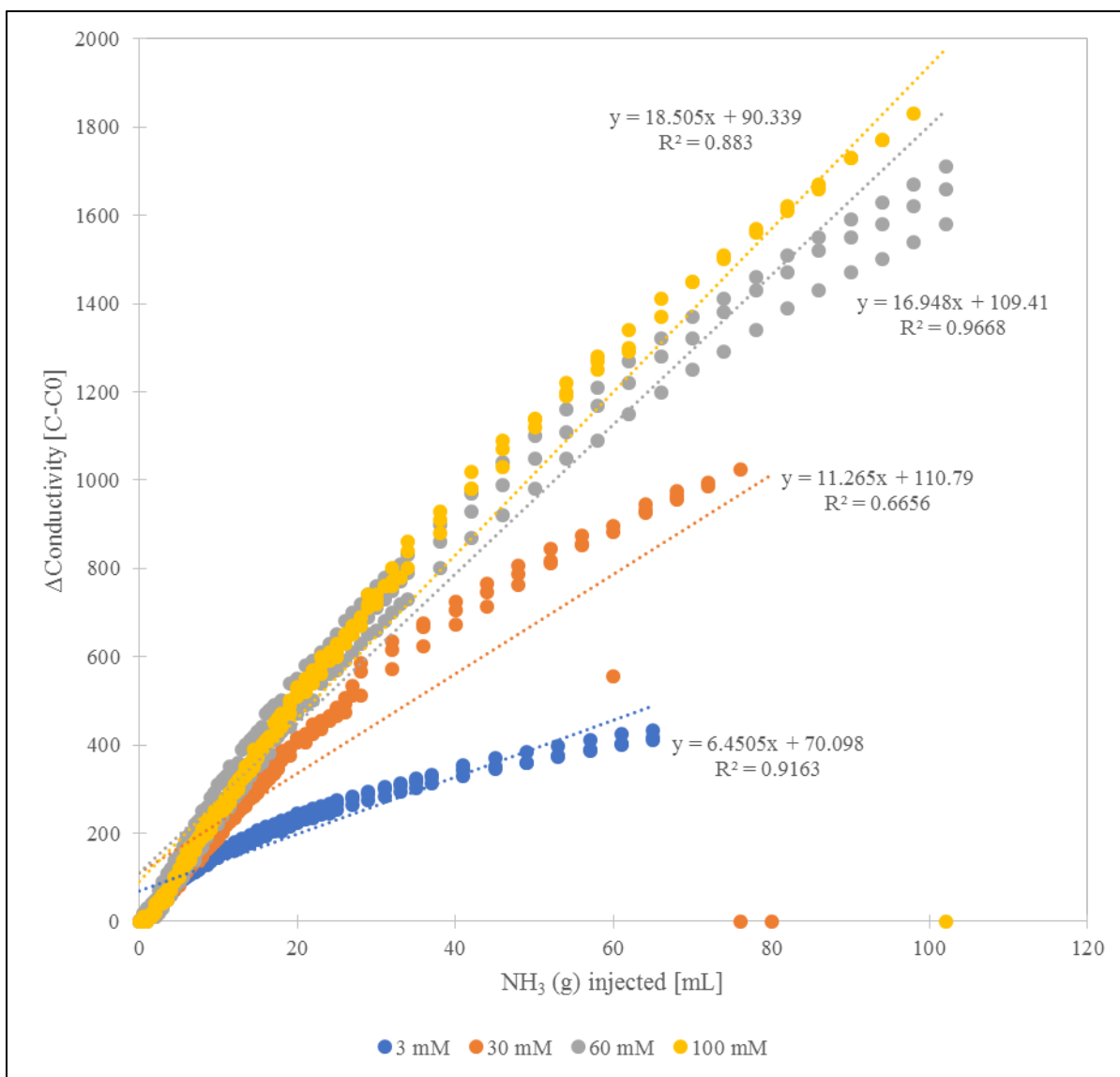


Figure 120. Comparison of the change in conductivity ($\mu\text{S/cm}$) with respect to injection volume of NH_3 (g) for variable bicarbonate suspensions with a linear fit for each dataset (including triplicate experiments)

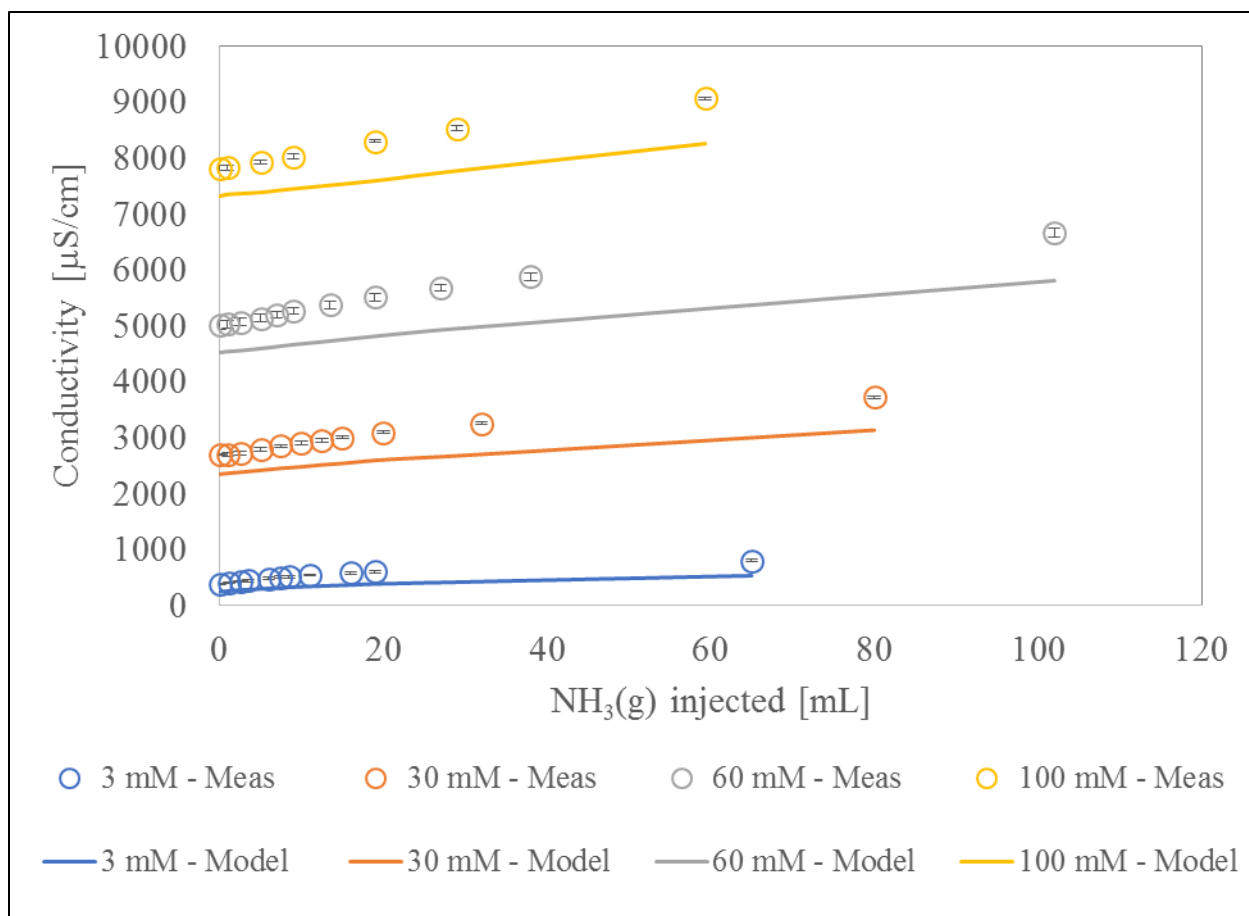


Figure 121. Comparison of measured (*open circles*) conductivity ($\mu\text{S}/\text{cm}$) with respect to injection volume of $\text{NH}_3(\text{g})$ for variable bicarbonate suspensions with a model prediction from PHREEQC software (USGS, *lines*) with error bars based on triplicate experiments

Buffering Capacity

Figure 118 shows a comparison of pH versus amount of $\text{NH}_3(\text{g})$ injected into 100 mL of 3 mM, 30 mM, 60 mM, and 100 mM HCO_3^- solutions. Table 30 below lists the average initial pH for each HCO_3^- concentration. However, modeling in Visual Minteq of the initial pH for a closed and open system (to atmospheric CO_2) (Figure 122), are not representative of the initial pH of the actual system. This is indicative that the system is (a) not reaching equilibrium for an open or closed system (it would be expected to be equilibrium for a closed system as water was degassed by bubbling $\text{N}_2(\text{g})$ and vigorously mixing for over an hour) or (b) there is a component in the water that the model is not capturing. Because samples were left to equilibrate for at least three days at temperature before experiments were begun, option 'b' is the most likely. The water purification in the laboratory was checked for quality and it was determined that all filters needed to be changed. Further, resistivity was $\sim 0.9 \text{ M-ohm}$ and distilled deionized water is generally expected to have a resistivity of $> 18 \text{ M-ohm}$. In addition, the pH electrode was calibrated at pH 4.01, 7 and 10.01 prior to each use with a slope of $> 96\%$ for each use; therefore, these measurements are expected to be accurate. It is most likely that water quality issues contributed to the discrepancies between models and experimental measurements.

Figure 123 - Figure 124 represent the aqueous NH_3 in mol/L with respect to volume injected and pH, respectively. It is notable that the difference in pH for the 3 mM HCO_3^- are statistically different with respect to all other HCO_3^- concentrations after injection of 1 mL, 5 mL, 9 mL and 20 mL of $\text{NH}_3(\text{g})$ (Tables B5-8 in the supplemental data (Appendix B)). In addition, after injection of 20 mL of $\text{NH}_3(\text{g})$, the average difference in pH for all of the HCO_3^- concentrations is significantly different. This is due to the buffering capacity of HCO_3^- . To reach a pH of greater than 10.0, at least 10 mL of NH_3 gas must be injected for 100 mL of 3 mM HCO_3^- solutions at $\sim 21^\circ\text{C}$. However, greater than 50 mL of $\text{NH}_3(\text{g})$ is required to reach a pH of just 9.5 with 100 mM HCO_3^- . The theoretical buffering capacity (in mol/L-pH unit) is compared for pure water versus the variable HCO_3^- solutions at the initial pH in Table 30. It is important to note that at the highest concentration of bicarbonate, the buffering capacity is nearly three orders of magnitude greater than that of pure water. As an example, the initial pH of the 3 mM HCO_3^- system is 8.68 ± 0.05 . The theoretical buffering capacity for a 3 mM versus 100 mM HCO_3^- solution at this initial pH is 1.91×10^{-4} and 6.01×10^{-3} mol/L per pH unit. This means that the solution must reach a concentration of 3.48×10^{-4} or 1.09×10^{-2} mol/L of strong base just to reach pH 10.5 for a 3 and 100 mM HCO_3^- solution, respectively. Further, $\text{NH}_3(\text{g})$ acts as a weak base and significantly more will be required to raise the pH as the pH increases due to the logarithmic relationship between pH and OH^- concentrations and the changes in speciation of $\text{NH}_3/\text{NH}_4^+$ with pH (Figure 125 for an open system and Figure 126 for a closed system). Therefore, almost two orders of magnitude more $\text{NH}_3(\text{g})$ will be required to reach the target pH in these systems.

Table 30. Theoretical buffering capacity (in mol/L per pH unit of change) for variable bicarbonate solutions based on initial experiment pH

Initial pH	Total HCO_3^- (mol/L)	Buffering Capacity (mol/L per pH unit)	
		HCO_3^- soln	Pure H_2O
8.681	0.003	1.91E-04	1.11E-05
8.574	0.03	1.57E-03	8.64E-06
8.463	0.06	2.81E-03	6.70E-06
8.463	0.1	4.68E-03	6.70E-06

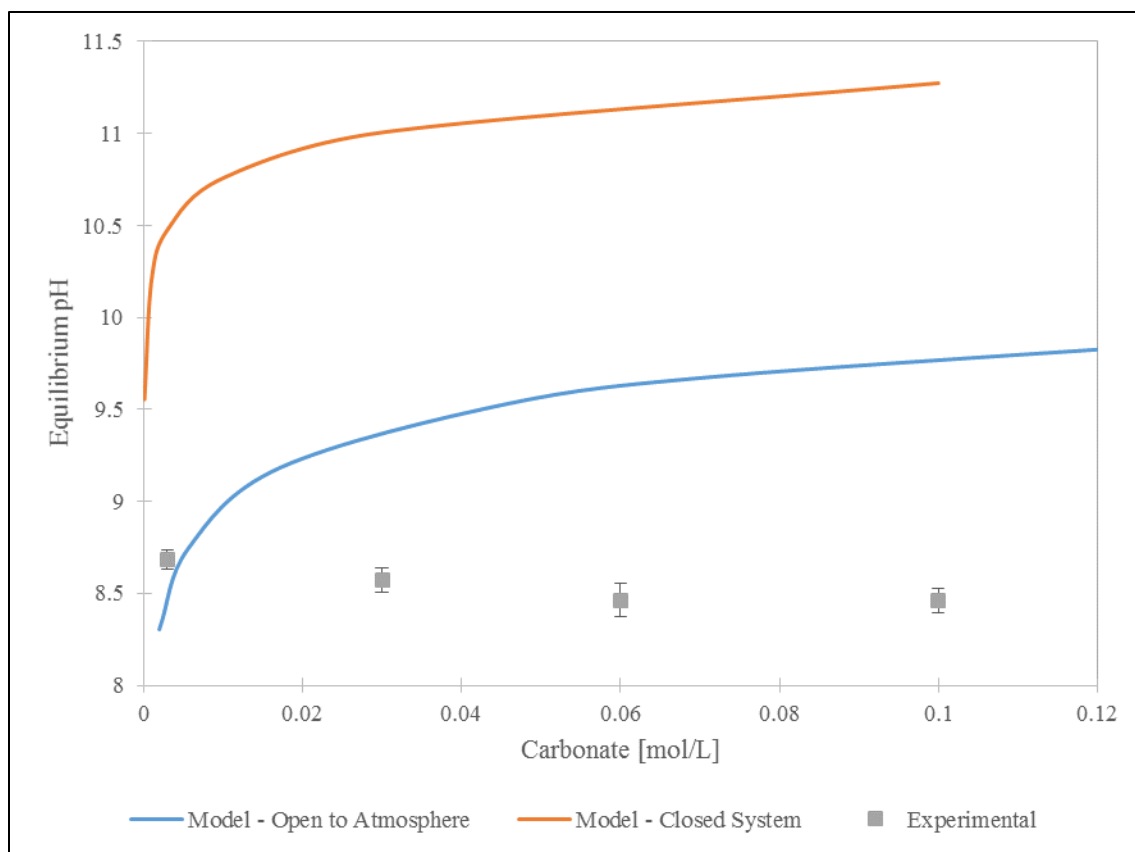


Figure 122. Comparison of initial, experimental pH in triplicate experiments at 3 mM, 30 mM, 60 mM and 100 mM HCO_3^- concentration to equilibrium pH of open and closed HCO_3^- systems at constant ionic strength (0.2 M) via Visual Minteq.

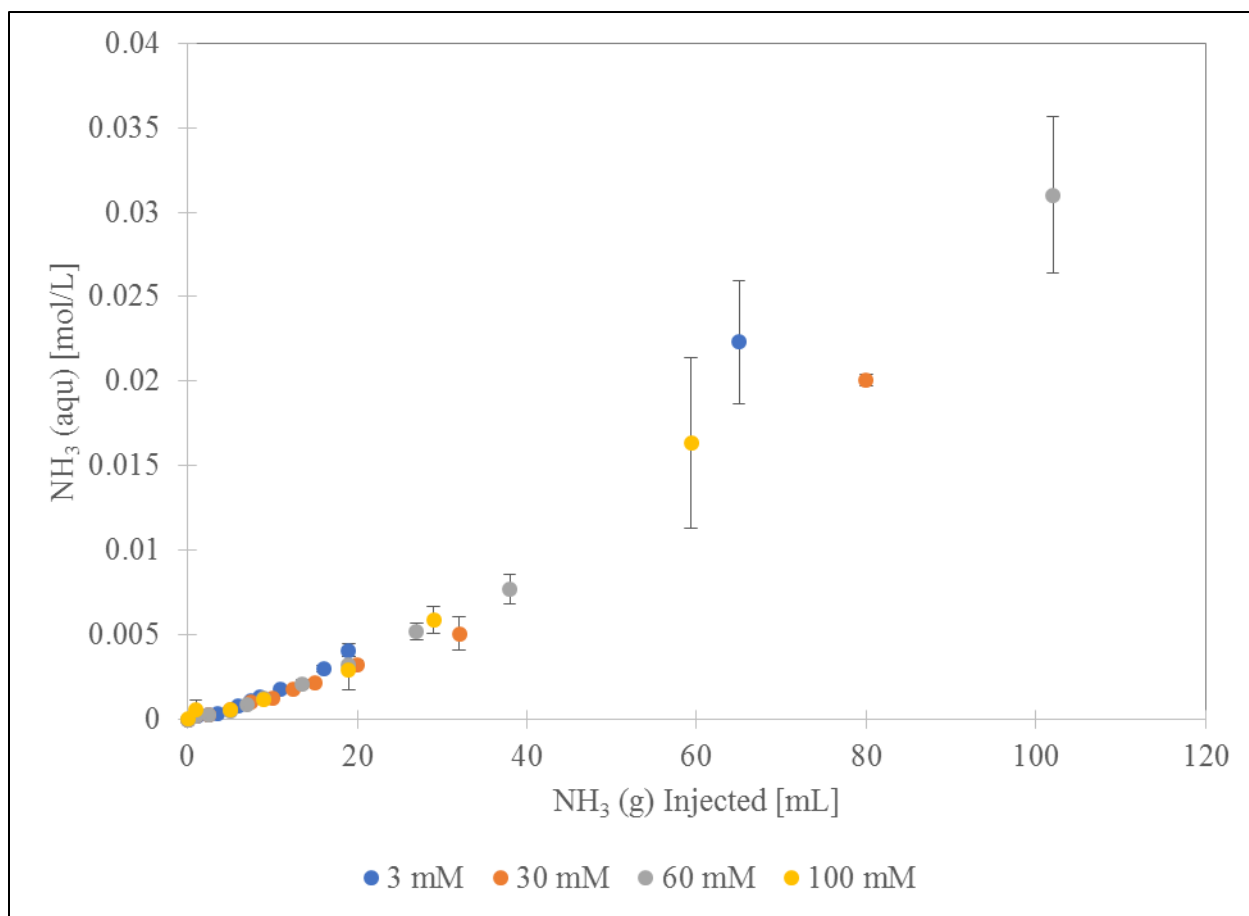


Figure 123. Comparison of triplicate experiments injecting NH₃ gas into 3 mM, 30 mM, 60 mM, and 100 mM HCO₃⁻ solutions versus aqueous NH₃ in mol/L incorporated into the sample versus injection gas volume

Note: error bars represent the standard deviation of measurements from triplicate experiments at each bicarbonate concentration

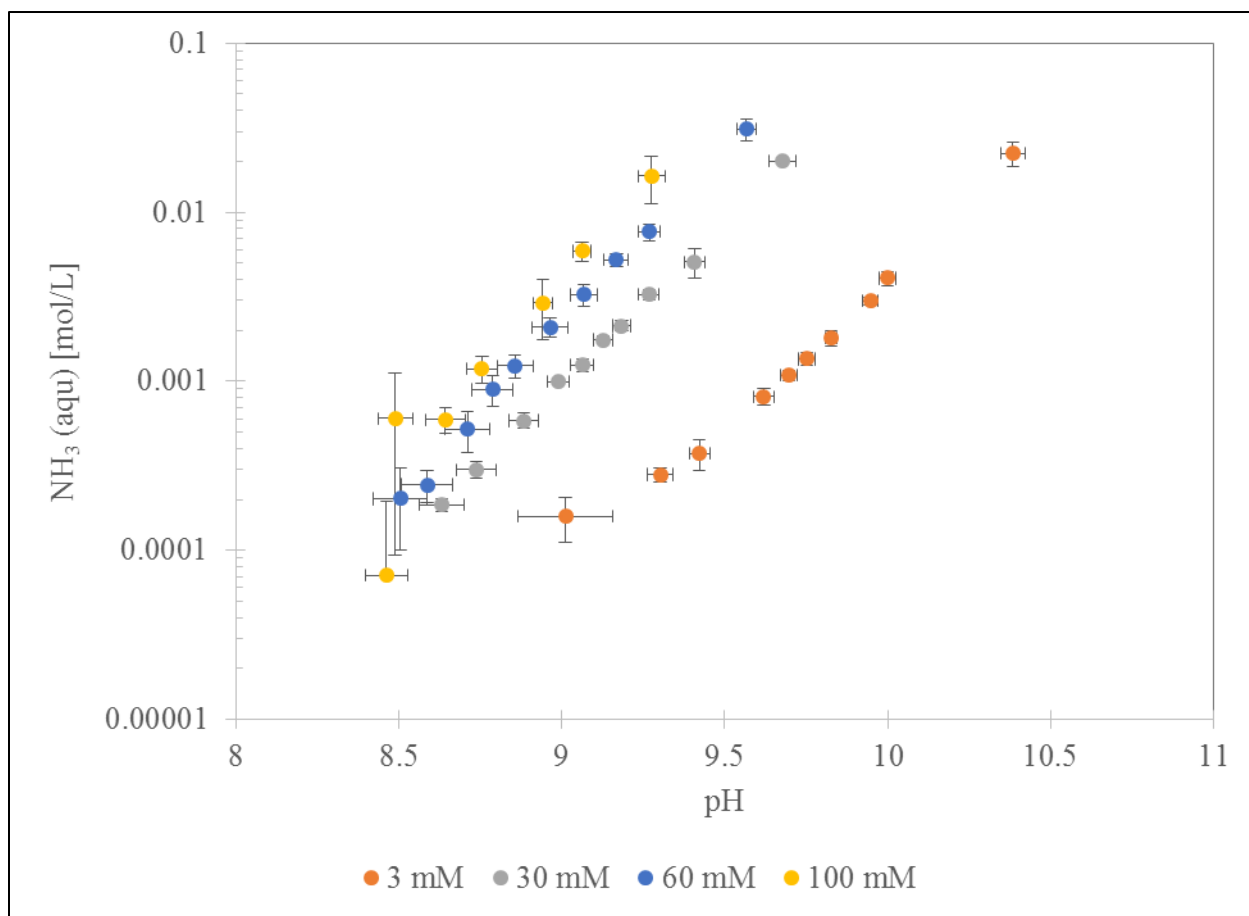


Figure 124. Comparison of triplicate experiments injecting NH_3 gas into 3 mM, 30 mM, 60 mM and 100 mM HCO_3^- solutions versus aqueous NH_3 in mol/L incorporated into the sample versus pH

Note: the aqueous NH_3 concentration is on a LOG scale and error bars represent standard deviation of measurements from triplicate experiments for each bicarbonate concentration

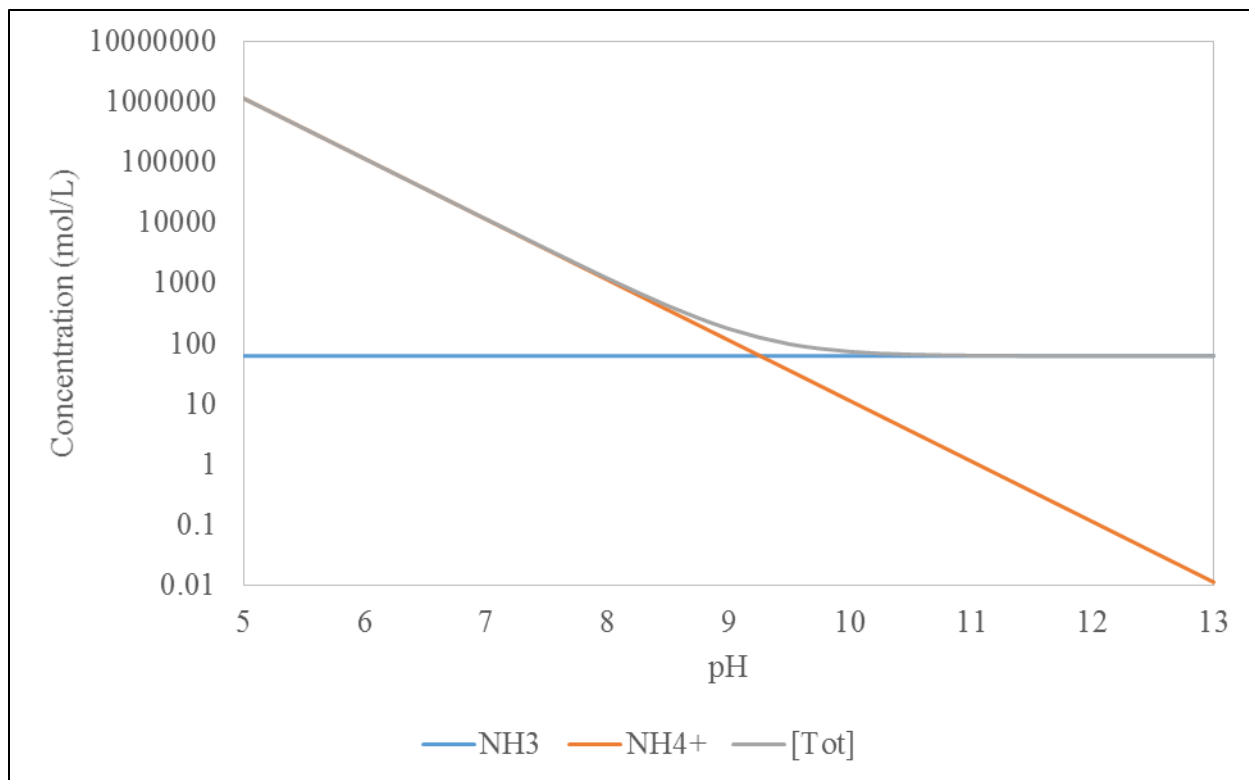


Figure 125. Ammonium (NH_3) and ammonia (NH_4^+) concentrations in pure/dilute H_2O at 25°C and gas partial pressure of 1 atm partial pressure of $\text{NH}_3(\text{g})$ with respect to pH for a system open to the gas phase

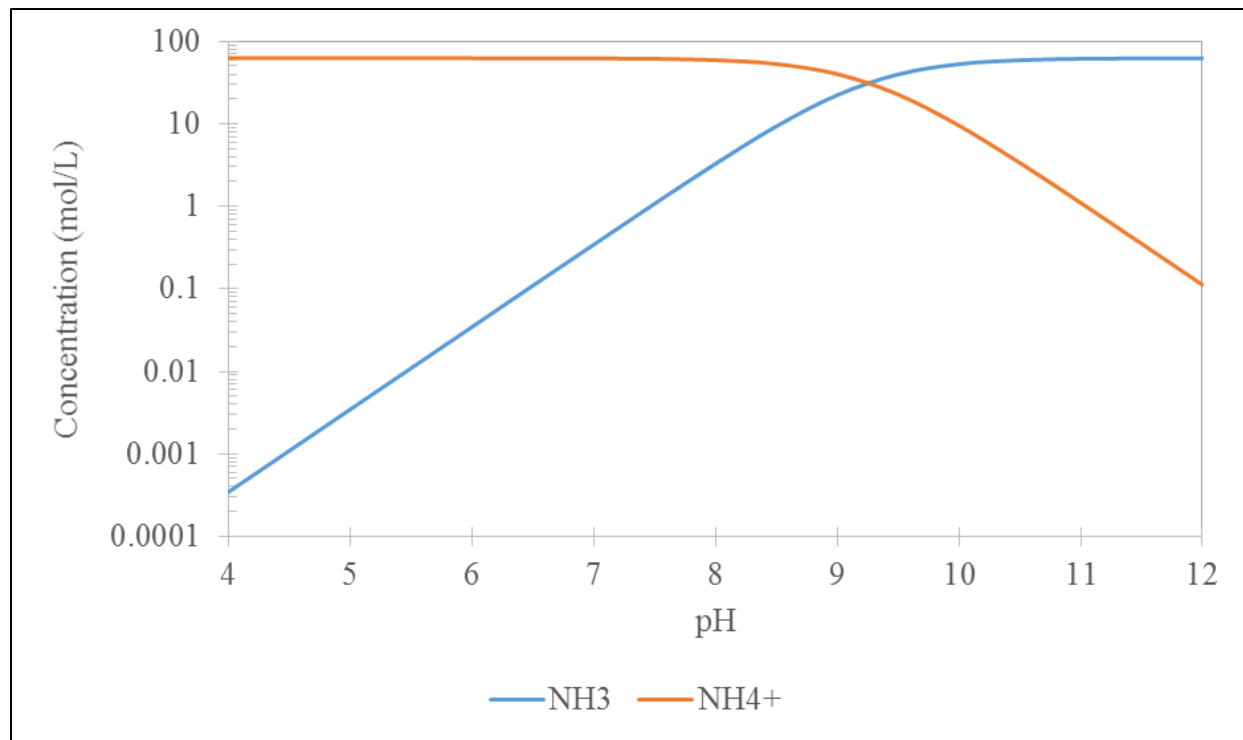


Figure 126. Ammonium (NH_3) and ammonia (NH_4^+) concentrations in pure/dilute H_2O at 25°C with respect to pH for a closed system

Total Aqueous $\text{NH}_3/\text{NH}_4^+$

Figure 124 - Figure 125 represent graphs of total aqueous NH_3 incorporated into solutions with respect to volume of $\text{NH}_3(\text{g})$ injected and pH, respectively, for variable bicarbonate concentrations (3 mM, 30 mM, 60 mM and 100 mM HCO_3^-). While a comparison of aqueous concentration versus pH results in very different results as discussed above in the buffering capacity discussion, the concentrations are not significantly different at different HCO_3^- concentrations with respect to volume injected as shown in Figure 122. Further, the results are not statistically different as shown in Figure 123 with standard deviations and based on statistical testing described previously. Results for aqueous NH_3 were not statistically different at a 95% confidence level with the exception of 60 and 100 mM HCO_3^- after 20 mL of $\text{NH}_3(\text{g})$ had been injected. The results are tabulated for a comparison of 1 mL, 5 mL, 9 mL and 20 mL of $\text{NH}_3(\text{g})$ injected in Tables B1-4 of the supplemental data (Appendix B). However, it is also apparent based on a mass balance of total aqueous NH_3 (in mg) divided by total injected NH_3 (in mg) (in Figure 127), that the gas phase does not have sufficient time to equilibrate with the solution based on the current setup (because $\text{NH}_3(\text{g})$ is very soluble in suspension it is expected that most of the gas will partition to the aqueous phase at equilibrium and based on the observation that the fraction partitioning is changing with injected volume). Further, the changes with respect to volume injected are similar (although with significant scatter as shown by standard deviation error bars), therefore, we must conclude that the variable bicarbonate concentrations do not have a significant effect on the rate of partitioning of $\text{NH}_3(\text{g})$ in this experiment. However, these results cannot be used to draw conclusions about the effects that variable bicarbonate concentrations will have on equilibrium partitioning coefficients (Henry's law constants) as they do not appear to reach equilibrium. In addition, to allow for direct comparison of injected gaseous and aqueous NH_3 partitioned with respect to bicarbonate concentrations, future experiments will be conducted at a constant ionic strength to allow for fewer variables changing with respect to time.

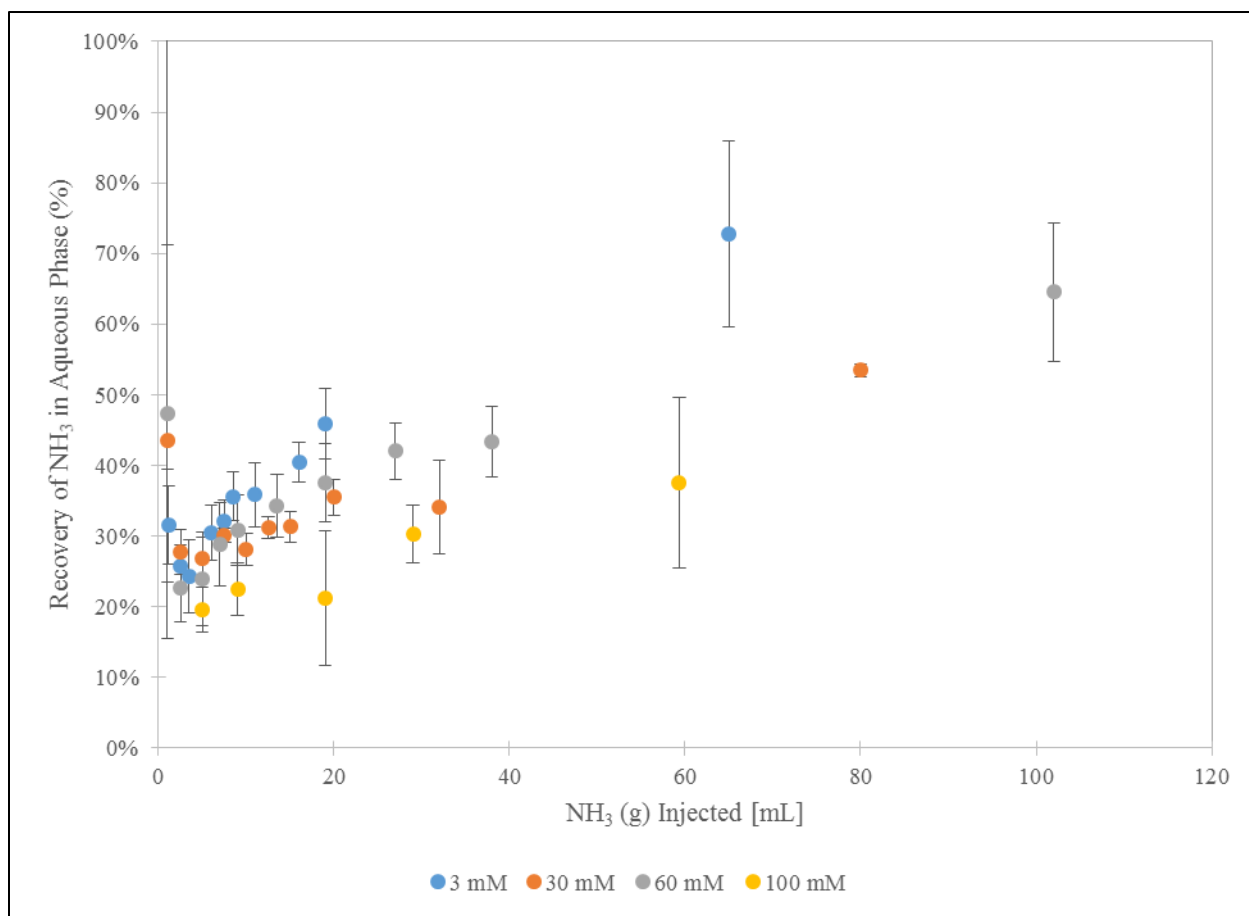


Figure 127. Comparison of recovery of NH₃ in the aqueous phase with respect to total gas mass injected, Note: one outlier is not shown

Important Takeaways

The equilibrium partitioning may or may not be different with the variable bicarbonate solutions, but the rate of incorporation of NH₃(g) into these open beaker systems is not statistically different with respect to bicarbonate concentration. However, buffering capacity will have a significant impact on the amount of NH₃(g) required for this remediation technique. Further alterations in the experimental design may be helpful in further elucidating the effect of variable bicarbonate concentrations on equilibrium NH₃(g) partitioning and are described briefly below in the Future Work and in depth in the literature review in Appendix A.

Task 3.1: Future Work

At ARC, we are planning to gather data to define the partitioning of NH₃(g) to the aqueous phase (and later including the solid soil phases and uranium) to better understand the NH₃(g) injection remediation technology being considered. There are two different experimental plans under consideration: (1) batch experiments or (2) NH₃(g) stripping experiments in a bubble column setup. Each has pros and cons as described below and within the literature review in Appendix A. Either of these experiments would allow for determination of Henry's law constants under variable conditions including temperature and bicarbonate concentration. In addition, speciation

modeling will be used to support analytical data and make predictions of species that cannot be quantified.

Batch Experiments

Batch equilibrium experiments will be completed for determination of Henry's constants and possibly kinetic rates of partitioning with variable HCO_3^- from 0 – 100 mM, constant ionic strength of ~0.15 M (as adjusted by addition of NaCl), variable temperature, variable gas to liquid ratios, variable NH_3 concentrations, and pH 12. A pH of 12 was chosen to simplify the system as 99.8% of total $\text{NH}_3/\text{NH}_4^+$ in the aqueous phase is present as NH_3 as shown by the speciation diagram (Figure 125). Further, addition of piperidine, bicarbonate, phosphate and ammonium hydroxide buffers were considered based on theoretical calculations. However, the natural buffering capacity of H_2O at pH 12 was deemed sufficient based on target NH_3 concentrations. These experiments will begin with aqueous $\text{NH}_3/\text{NH}_4^+$ based on the addition of NH_4Cl or NH_4OH as a liquid. While the aqueous to gas phase ratios for the batch experiments have yet to be chosen, it must be noted that these experiments may require a large gas to liquid volume ratio to have a measureable change in the aqueous phase due to the high solubility of the experiments (i.e. very little NH_3 will be expected to partition to the gas phase at equilibrium due to the high aqueous solubility so there will need to be a sufficient gas volume to result in a measureable change in the aqueous phase). However, it will be simple to include soils in these systems at a later date. Saturated soil experiments will include uranium to allow for investigation of the partitioning of both U and NH_3 simultaneously. These experiments could also be designed as sacrificial samples to estimate the kinetic rates of partitioning if deemed useful.

Stripping in a Bubble Column

In this process, NH_3 is stripped from the aqueous phase by injection of an inert gas (such as N_2) under constant pressure with a diagram of the experimental setup shown below as used by Lee *et al.* and Mackay in Figure 128 (Mackay, Shiu *et al.* 1979, Lee, Mukherjee *et al.* 2013). The method as used by Lee *et al.* allows for determination of both Henry's law constant and the hydrolysis loss rate and requires only relative concentrations of the solute in the gas phase with respect to time based on Eqn. 1 where C_0 and C_t are the concentration of solute in the gas phase at equilibrium and at time, t , after equilibrium, respectively, k is the first order hydrolysis loss rate (sec⁻¹), Φ is the gas flow rate, V is the volume, T is the temperature and R is the ideal gas law constant.

$$\ln \frac{C_{0,g}}{C_{t,g}} = \left[\frac{\Phi}{H_{cp}RTV} + k \right] \times t \quad \text{Eqn. 1}$$

Whereas the method outlined by Mackay is used only to determine Henry's constant based on measurements of the aqueous phase as described by equation 2.

$$\ln \frac{C_{t,aqu}}{C_{0,aqu}} = - \left[\frac{H_{cp}\Phi}{RTV} \right] \times t \quad \text{Eqn. 2}$$

A peristaltic pump (Masterflex digital L/S with size 14 tubing pump head) will be used for these experiments, replacing the syringe pump used previously for step injection experiments to allow

for correlation of flow rate and time. Future issues may arise with the experimental setup as pH, conductivity and temperature may not be monitored regularly during the experiment. In addition, the current capabilities at ARC would need to be modified to allow for appropriate mixing for experiments with Hanford soil present. The aqueous phase would also be difficult to measure as the column would need to be opened with the current setup (Figure 129). However, gas phase measurements could be monitored through the use of acid traps followed by measurement with the aqueous solutions with the gas sensing electrode or colorimetric method. Further work is in progress to find a more suitable experimental setup.

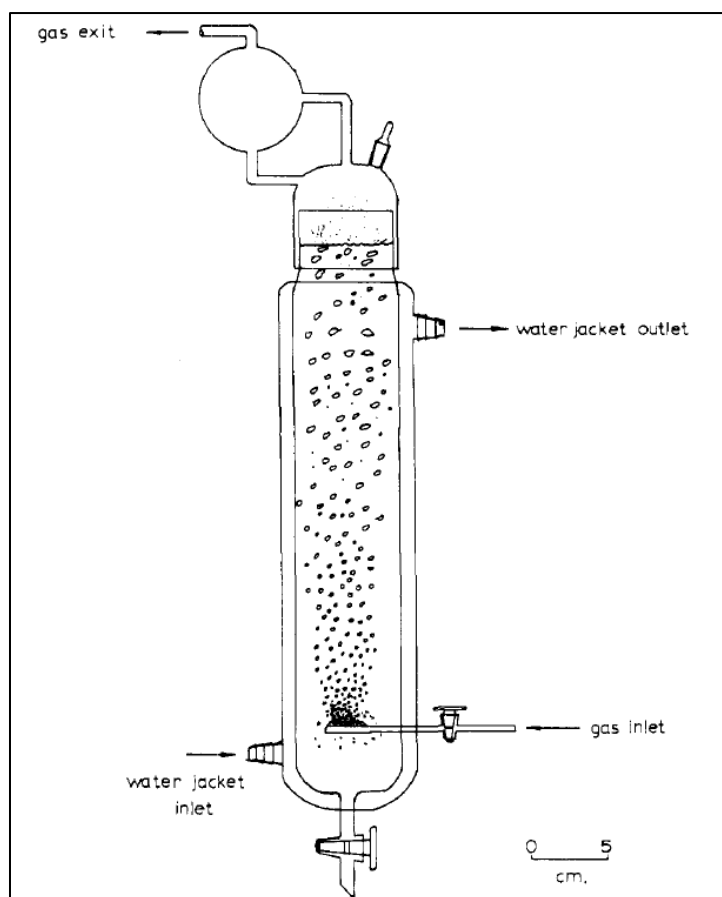


Figure 128. Diagram of apparatus used for experiments described by Mackay, Note: previous equipment was utilized in experiments by Lee et al. (Mackay 1979, Lee, Mukherjee et al. 2013)



Figure 129. Proposed equipment for the experimental setup of the $\text{NH}_3(\text{g})$ stripping experiments (Pyrex 31760-BO)

Task 3.1: References

- Berthouex, P. M. and L. C. Brown (1994). Multiple Paired Comparisons of k Averages. Statistics for Environmental Engineers. Boca Raton, Florida, CRC Press: 123-128.
- Lee, S.-H., S. Mukherjee, B. Brewer, R. Ryan, H. Yu and M. Gangoda (2013). "A Laboratory Experiment To Measure Henry's Law Constants of Volatile Organic Compounds with a Bubble Column and a Gas Chromatography Flame Ionization Detector (GC-FID)." Journal of Chemical Education 90(4): 495-499.
- Mackay, D. (1979). "FINDING FUGACITY FEASIBLE." Environmental Science & Technology 13(10): 1218-1223.
- Mackay, D., W. Y. Shiu and R. P. Sutherland (1979). "DETERMINATION OF AIR-WATER HENRYS LAW CONSTANTS FOR HYDROPHOBIC POLLUTANTS." Environmental Science & Technology 13(3): 333-337.

APPENDICES

The following documents are available at the DOE Research website for the Cooperative Agreement between the U.S. Department of Energy Office of Environmental Management and the Applied Research Center at Florida International University: <http://doeresearch.fiu.edu>

1. Project Technical Plan, Project 2: Rapid Deployment of Engineered Solutions to Environmental Problems, June 2014.
2. FIU Research Review Presentation, Rapid Deployment of Engineered Solutions to Environmental Problems, March 2015

The following documents are included in this report as separate attachments:

1. Appendix A - Literature review
2. Appendix B - Supplemental data